Passive Acoustic Monitoring for Marine Mammals in the Western Atlantic April 2016 – June 2017

Macey A. Rafter, Kaitlin E. Frasier, Bruce J. Thayre, Morgan A. Ziegenhorn, Rebecca Cohen, Erin O'Neill, Sean M.Wiggins, Simone Baumann-Pickering, John A. Hildebrand

Marine Physical Laboratory, Scripps Institution of Oceanography
University of California San Diego, La Jolla, CA 92037

Danielle M. Cholewiak, Sofie M. Van Parijs

NOAA NMFS Northeast Fisheries Science Center, Protected Species Branch,
Woods Hole, Massachusetts 02543

Bottlenose Dolphin, Photo Credit: Jennifer Trickey

MPL TECHNICAL MEMORANDUM #632

September 2018

Suggested Citation

Rafter, M.A., Frasier, K.E., Thayre, B.J., Ziegenhorn, M.A., Cohen, R., O'Neill, E., Wiggins, S.M., Baumann-Pickering, S., Hildebrand, J.A. Cholewiak, D.M., Van Parijs, S.M. Passive Acoustic Monitoring for Marine Mammals in the Western Atlantic April 2016 – June 2017. Final Report. Marine Physical Laboratory Technical Memorandum 632 September 2018.

Funding provided under the Cooperative Institute for Marine Ecosystems and Climate, NOAA Award: NA10OAR4320156 from the Northeast Fisheries Science Center, under sponsorship of Sofie Van Parjis.

Table of Contents

Executive Summary

Passive acoustic monitoring was conducted in the Western Atlantic (WAT) from April 2016 to June 2017. High-frequency Acoustic Recording Packages (HARPs) were deployed at eight offshore locations: Heezen Canyon (site HZ) at 850 m depth, Oceanographer Canyon (site OC) at 1100 m depth, Nantucket Canyon (site NC) at 980 m depth, Babylon Canyon (site BC) at 1000 m depth, Wilmington Canyon (site WC) at 1000 m depth, Gulf Stream (site GS) at 953 m depth, Blake Plateau (site BP) at 945 m depth, and Blake Spur (site BS) at 1005 m depth.

The HARPs recorded underwater sounds between 10 Hz and 100 kHz. Data analysis consisted of analyst scans of long-term spectral averages (LTSAs) and spectrograms, and automated computer algorithm detection when possible. One frequency band was analyzed for the ambient soundscape between 10-10,000 Hz. Two frequency bands were analyzed for marine mammal vocalizations and anthropogenic sounds: (1) Mid-frequency, between 10-5,000 Hz, and (2) High-frequency, between 1-100 kHz. No analysis was conducted for low frequency marine mammal vocalizations, such as those expected from mysticete whales.

Echolocation clicks from eight known odontocete species were detected: Cuvier's beaked whale, Gervais' beaked whale, Sowerby's beaked whale, True's beaked whale, Blainville's beaked whale, sperm whales, *Kogia* spp., and Risso's dolphins. Eight distinct click types that are not yet assigned to a species were also detected. Detections of Cuvier's beaked whales occurred at all eight sites but were highest at site WC. Gervais' beaked whale detections were highest at site GS and BP. Sowerby's beaked whale detections were highest at site HZ and WC with lower numbers at other sites. True's beaked whale detections were highest at site NC. Blainville's beaked whale detections were highest at site BS. Sperm whale clicks were detected at all eight sites throughout the recording period and had high numbers at sites NC, HZ, and BC. *Kogia* spp. echolocation clicks were detected in the highest numbers at site BS. Risso's dolphin click detections peaked in May 2016 and May 2017 at sites NC, WC, BC, and GS.

The ambient soundscape was dominated by anthropogenic sounds, primarily ship traffic and seismic exploration between 10-100 Hz at all sites. Between 100-1000 Hz the ambient soundscape was primarily a function of wind and sea state. A seasonal fin whale pattern is seen at all sites during winter months. Broadband ship sounds were detected the most at site WC and BC. Airgun detections peaked during the summer months of 2016 across all sites, and were detected in the lowest numbers at site OC. Other anthropogenic sounds, such as echosounders, were detected at all eight sites; whereas, explosions were detected at four sites. Echosounder detections were highest at site WC. There were 48 explosions detected throughout the recording period, at sites NC, WC, BC, and BP.

Project Background

In April 2015, a passive acoustic monitoring effort was initiated offshore of the northeast United States, in the Western Atlantic (WAT) with support from the National Oceanic and Atmospheric Administration (NOAA), Northeast Fisheries Science Center (NEFSC). The goal of this effort was to characterize vocalizations of marine mammal species recorded in the area and to determine their seasonal presence. This report documents the analysis of sounds recorded by High-Frequency Acoustic Recording Packages (HARPs) from eight sites: Heezen Canyon (site HZ), Oceanographer Canyon (site OC), Nantucket Canyon (site NC), Babylon Canyon (site BC), Wilmington Canyon (site WC), Gulf Stream (site GS), Blake Plateau (site BP), and Blake Spur (site BS) (Figure 1). All eight recording periods ranged from April 2016 to June 2017. These sites are all located on the continental slope at water depths of 845-1100 m.

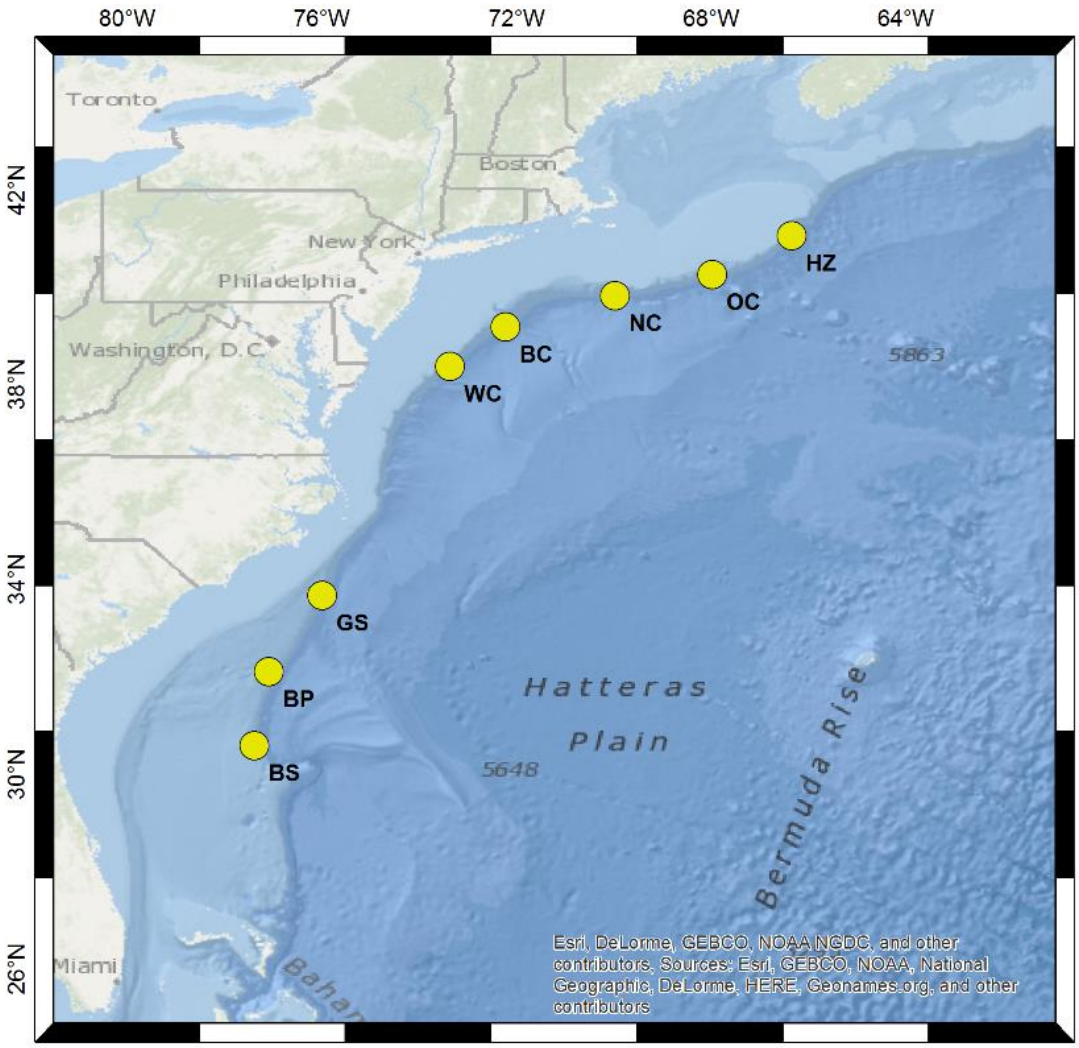

Figure 1. Location of High-frequency Acoustic Recording Packages (HARPs) as yellow circles at site HZ (depth 845 m), site OC (depth 1100 m), site NC (depth 977 m), site BC (depth 1000 m), site WC (depth 1000 m), site GS (depth 953 m), site BP (depth 945 m), and site BS (depth 1005 m).

Methods

High-Frequency Recording Package

HARPs are autonomous underwater acoustic recording devices that, dependent on configuration, can record sounds over a bandwidth from 10 Hz up to 160 kHz and are capable of approximately one year of continuous recording. The HARPs at sites HZ, OC, NC, BC, WC, GS, BP, and BS were deployed in mooring configurations with the hydrophones suspended approximately 20 m above the seafloor. Each HARP hydrophone was calibrated in the laboratory to provide quantitative analysis of the received sound field. Representative data loggers and hydrophones have been also calibrated at the Navy's TRANSDEC facility in the past to verify the laboratory calibrations (Wiggins and Hildebrand, 2007).

Data Collected

Eight HARPs were deployed from April 2016 to June 2017 at sites HZ, OC, NC, BC, WC, GS, BP, and BS. The instruments recorded continuously at 200 kHz to provide 100 kHz of effective bandwidth from 389 to 435 days (Table 1).

Table 1. Passive acoustic monitoring in the Western Atlantic from April 2016 – June 2017.

Deployment Name	Latitude (W)	Longitude (E)	Depth (m)	Start Date	End Date	Recording Duration	
						(Days)	(Hours)
HZ 02	41° 03.71	66° 21.10	845	4/22/2016	6/19/2017	422	10,140
OC 02	40° 15.80	67° 59.17	1110	4/24/2016	5/18/2017	389	9,336
NC 02	39° 49.95	69° 58.93	977	4/21/2016	5/24/2017	397	9,549
BC 01	39° 11.46	72° 13.72	1000	4/20/2016	6/10/2017	416	9,988
WC 01	38° 22.45	73° 22.24	1000	4/20/2016	6/29/2017	435	10,454
GS 01	33° 39.94	76° 00.01	953	4/29/2016	6/27/2017	424	10,195
BP 01	32° 06.36	77° 05.66	945	4/28/2016	6/27/2017	424	10,192
BS 01	30° 35.03	77° 23.44	1005	4/27/2016	6/26/2017	424	10,197

Ambient Soundscape

Ocean ambient sound pressure levels tend to decrease as frequency increases (Wenz, 1962). While baleen whales and anthropogenic sources, such as large ships and airguns, often dominate the ambient soundscape below 100 Hz (Sirovic *et al*., 2004; McDonald *et al*., 2006; Wiggins *et al*., 2016), wind causes increased sound pressure levels from 200 Hz to 20 kHz (Knudsen *et al*., 1948). To analyze the ambient soundscape, data were decimated by a factor of 100 to provide an effective bandwidth of 10 Hz to 1 kHz. LTSAs were then constructed with 1 Hz frequency and 5 s temporal resolution. To determine low-frequency ambient sound levels, daily spectra were computed by averaging five, 5 s sound pressure spectrum levels calculated from each 75 s acoustic record. System self-noise was excluded from these averages. Additionally, daily averaged sound pressure spectrum levels in 1-Hz bins were concatenated to produce long-term spectrograms for each site.

Data Analysis

The data analysis process is described below in terms of the low-frequency ambient soundscape, major classes of marine mammal calls and anthropogenic sounds in the WAT region, and the procedures used to detect them. For efficiency, the analysis for marine mammal calls and anthropogenic sounds were divided into two frequency bands: (1) Mid-frequency, 10-5,000 Hz, and (2) High-frequency, 1-100 kHz, where the full (high-frequency) band recordings were decimated by a factor of 20 to provide the mid-frequency band data. Analysis of the low-frequency band for marine mammal calls was not within the scope of this report.

To visualize the sound recordings, sound pressure level spectra were calculated for all recordings using a time average of 5 seconds and two frequency bin sizes (10, 100 Hz, for mid- and high-frequency band analysis, respectively). These spectra were arranged into Long-Term Spectral Averages (LTSAs) which were visually examined by analysts as a means to detect marine mammal and anthropogenic sounds. LTSAs were analyst-scanned in source-specific frequency bands and using automatic detection algorithms (described below). During visual analysis, when a sound of interest was identified but its origin was unclear, the corresponding waveform or spectrogram was examined further to classify the sounds to source (e.g. species and anthropogenic). Signal classification was carried out by comparison to known source-specific spectral and temporal characteristics.

Each band was analyzed for the sounds of an appropriate subset of species or anthropogenic sources. Nearby shipping, explosions, and airguns were categorized as mid-frequency. Echosounders, dolphin clicks, *Kogia* spp., sperm whale clicks, and beaked whale pulses were categorized as high-frequency.

We summarize and characterize sounds detected at sites HZ, OC, NC, BC, WC, GS, BP, and BS. The seasonal occurrence and relative abundance for calls of different species and for anthropogenic sounds were identified in the acoustic recordings.

Odontocetes

Odontocetes (toothed whales) with sounds in the high-frequency range and possibly found in the Western Atlantic region include Atlantic white-sided dolphins (*Lagenorhynchus acutus*), shortbeaked common dolphins (*Delphinus delphis*), Atlantic spotted dolphins (*Stenella frontalis*), Clymene dolphins (*S. clymene*), striped dolphins (*S. coeruleoalba*), Risso's dolphins (*Grampus griseus*), bottlenose dolphins (*Tursiops truncatus*), rough-toothed dolphins (*Steno bredanensis*), false killer whales (*Pseudorca crassidens*), short-finned pilot whales (*Globicephala macrorhynchus*), long-finned pilot whales (*G. melas*), killer whales (*Orcinus orca*), sperm whales (*Physeter macrocephalus*), dwarf sperm whales (*Kogia sima*), pygmy sperm whales (*K. breviceps*), Northern bottlenose dolphins (*Hyperoodon ampullatus*), Cuvier's beaked whales (*Ziphius cavirostris*), Gervais' beaked whales (*Mesoplodon europaeus*), Blainville's beaked whales (*M. densirostris*), Sowerby's beaked whales (*M. bidens*), and True's beaked whale (*M. mirus*).

Odontocete sounds can be categorized as echolocation clicks, burst pulses, or whistles. Echolocation clicks are broadband impulses with peak energy between 5 and 150 kHz, dependent upon the species. Buzz or burst pulses are rapidly repeated clicks that have a creak or buzz-like sound quality; they are generally lower in frequency than echolocation clicks. Dolphin whistles are tonal calls predominantly between 1 and 20 kHz that vary in frequency content, their degree of frequency modulation, as well as duration. These signals are easily detectable in an LTSA as well as the spectrogram (Figure 2). Echolocation clicks were analyzed as a proxy for odontocete presence because they are currently the most promising call type for species classification in the region. Further analysis might identify distinguishing whistle or burst pulse characteristics.

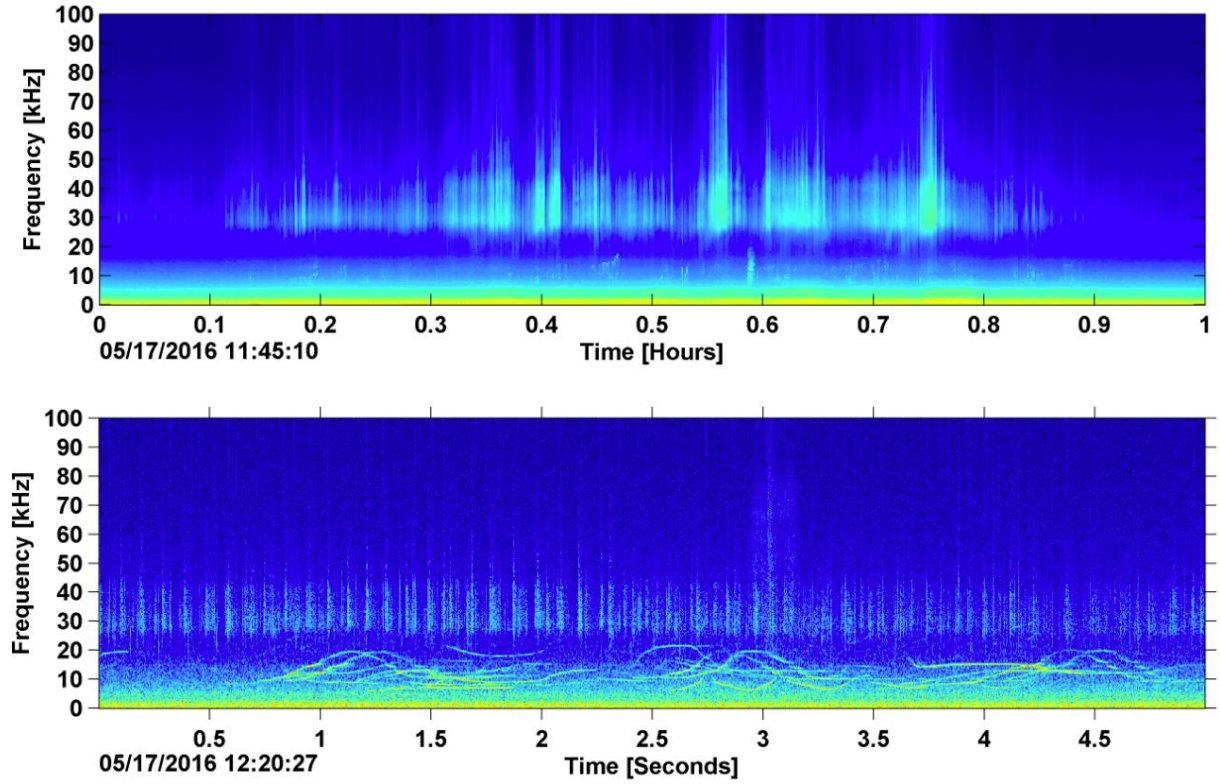

Figure 2. Generic example demonstrating odontocete signal types, in a LTSA (top) and spectrogram (bottom).

Click Classification

Odontocete echolocation clicks were detected automatically using an energy detector with a minimum received level threshold of 120 dBpp re: 1 μPa (Roch *et al.*, 2011; Frasier, 2015).

Dominant click types and false positive categories at these sites were identified automatically by dividing detections into successive five-minute windows and determining the impulse signal categories in each window. An automated clustering algorithm was then used to identify recurrent types based on spectral features and inter-click interval (ICI) distributions at each site (Frasier *et al.*, 2017). Common click types were manually aggregated across all eight sites to form classification training and testing sets for 20 signal types including 17 odontocete signals and three sources of false positives. Click types were attributed to a specific species if known (e.g. beaked whales and Risso's dolphin) or assigned a number if species was unknown. A deep neural network was trained to classify these signal types with 98% classification accuracy on a balanced test set. This trained network was used to classify all five minute windows across all sites. Classifications were retained if classification certainty exceeded 99% and the classified bin contained at least 50 clicks. Bins containing fewer than 50 detections were ignored. Bins with less than 99% classification certainty were classified as "Unidentified Odontocete". This conservative classification strategy was used to minimize misclassifications. Classifier confusion is expected to be highest between sperm whales and ship noise, and possibly between True's and Gervais' beaked whale signals. Further manual verification could be used to improve classification accuracy in the future. Patterns at sites with very low reported encounter rates for a particular species should be interpreted with caution prior to manual verification.

Beaked Whales

Beaked whales can be identified acoustically by their echolocation signals (Baumann-Pickering *et al.*, 2014). These signals are frequency-modulated (FM) upsweep pulses, which appear to be species specific and distinguishable by their spectral and temporal features. Identifiable signals are described for all beaked whales known to occur in the region, namely Blainville's, Cuvier's, Gervais', Sowerby's, and True's beaked whales, and Northern bottlenose whales. Beaked whale FM pulses were detected with an automated process.

Blainville's Beaked Whales

Blainville's beaked whale echolocation signals are polycyclic, with a characteristic frequency modulated upsweep, peak frequency around 34 kHz (Figure 4) and inter-pulse interval (IPI) of about 280 ms (Johnson *et al.*, 2006; Baumann-Pickering *et al.*, 2013). A bimodal ICI pattern was found in this dataset, with peaks at 225 and 335 ms. Blainville's FM pulses are also distinguishable in the spectral domain by their sharp energy onset around 25 kHz with only a small energy peak at around 22 kHz (Figure 3).

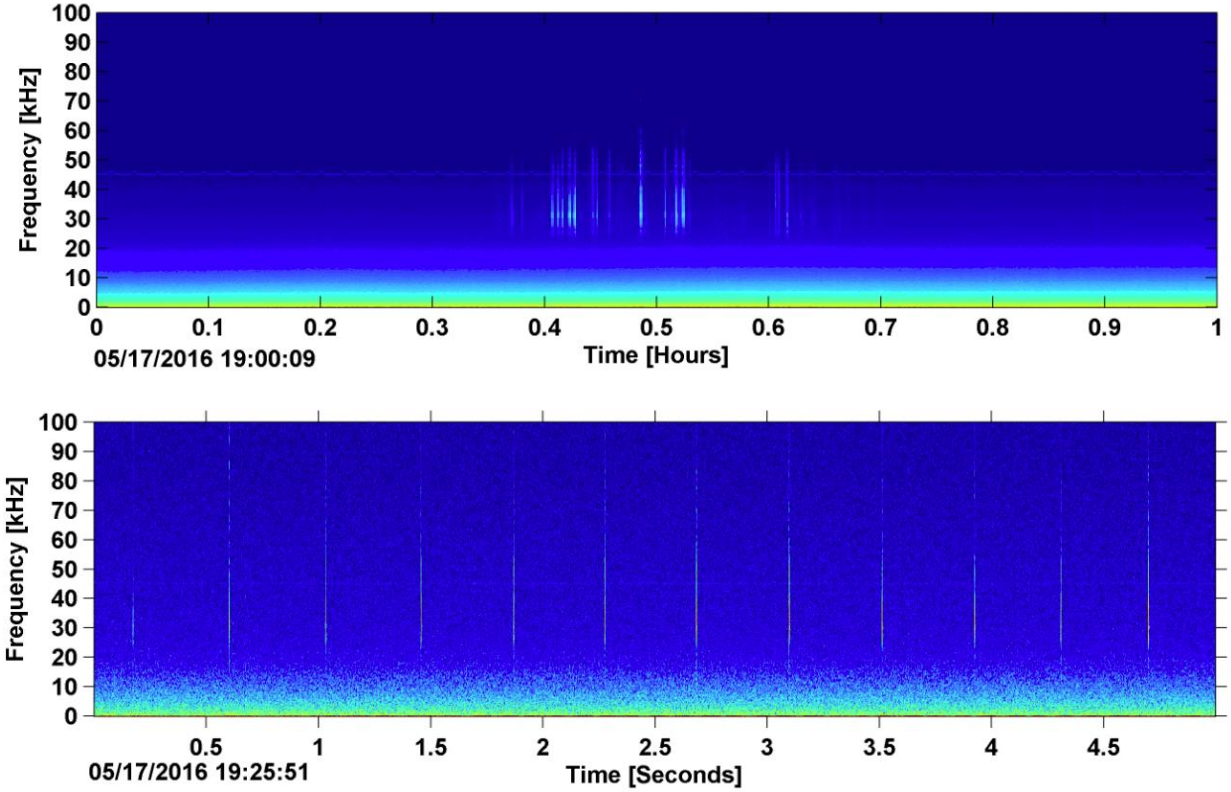

Figure 3. Blainville's beaked whale echolocation clicks in LTSA (top) and spectrogram (bottom) recorded at Site BS, May 2016.

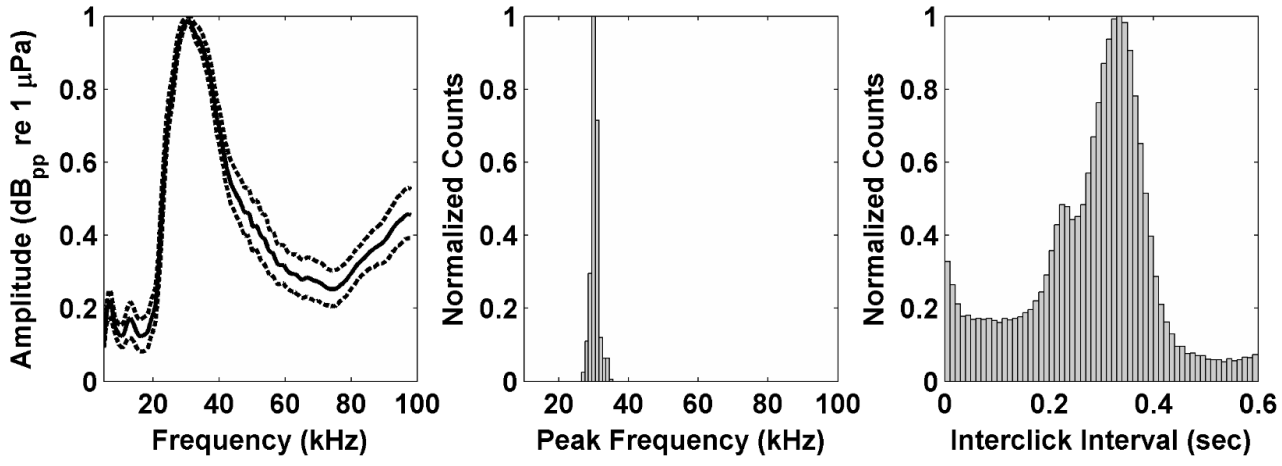

Figure 4. Left: Mean frequency spectrum of Blainville's beaked whale echolocation clicks (solid line) and 25th and 75th percentiles (dashed lines); Center: Distribution of click peak frequencies with peak near the Nyquist frequency (100 kHz); Right: Distribution of inter-click-intervals.

Cuvier's Beaked Whales

Cuvier's beaked whale echolocation signals are polycyclic, with a characteristic FM pulse upsweep, peak frequency around 40 kHz (Figure 5), and uniform inter-pulse interval of about 0.5 s (Johnson *et al*., 2004; Zimmer *et al*., 2005). An additional feature that helps with the identification of Cuvier's FM pulses is that they have two characteristic spectral peaks around 17 and 23 kHz.

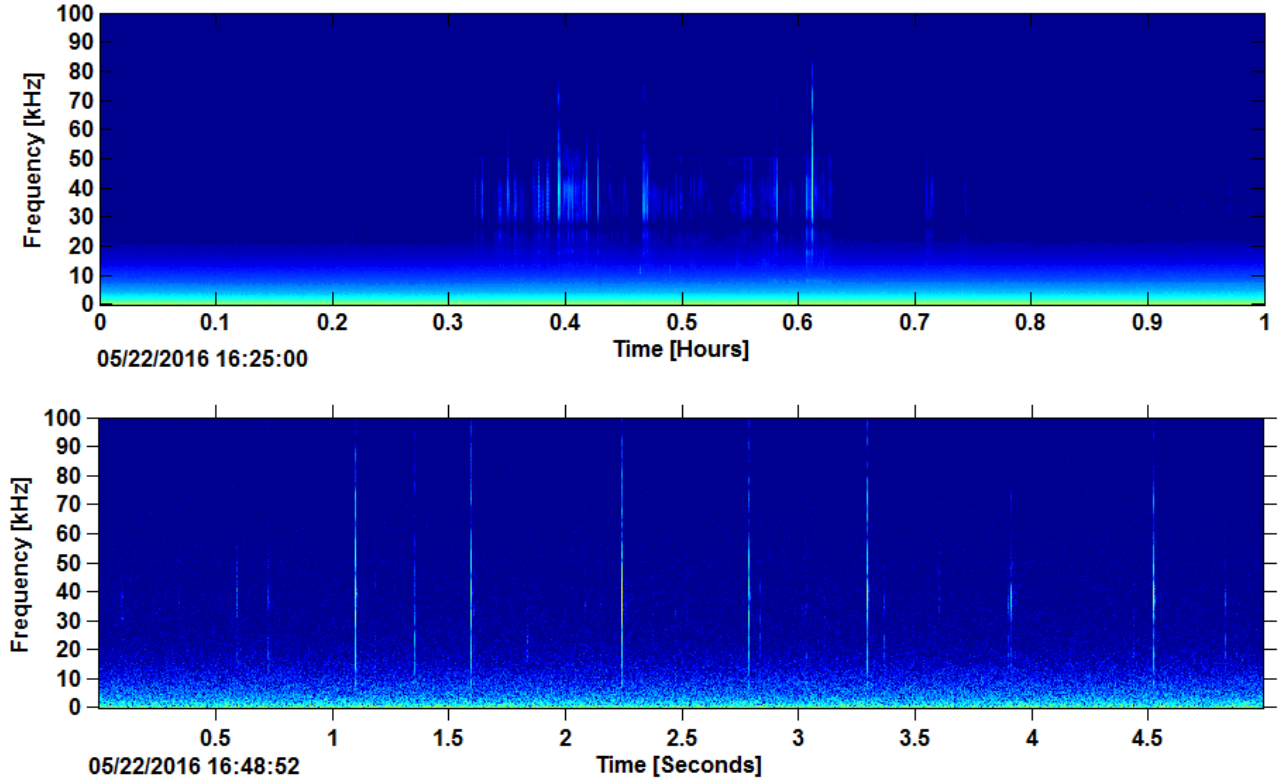

Figure 5. Cuvier's beaked whale echolocation clicks in LTSA (top) and spectrogram (bottom) recorded at site WC, May 2016.

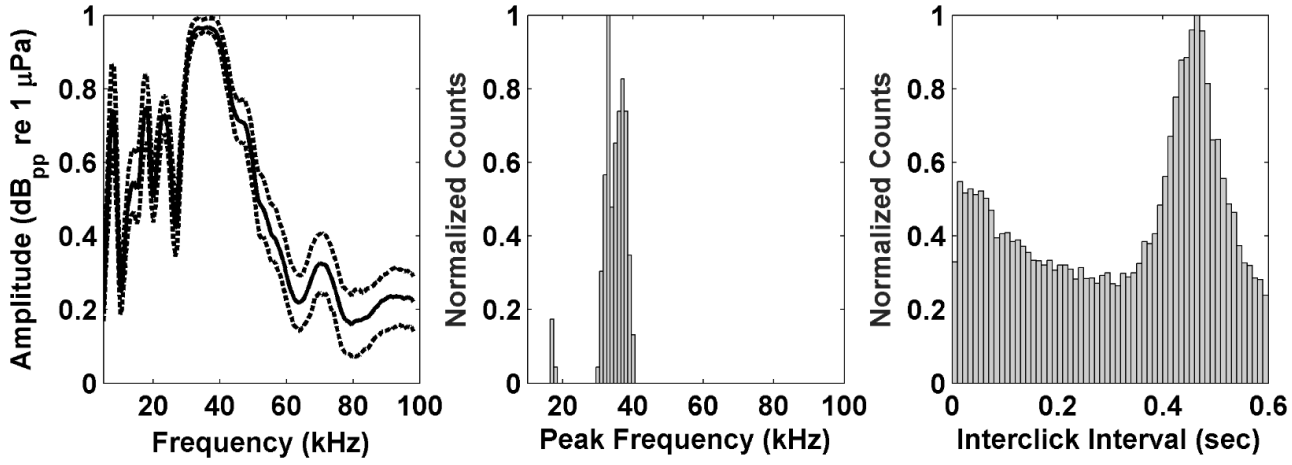

Figure 6. Left: Mean frequency spectrum of Cuvier's beaked whale echolocation clicks (solid line) and 25th and 75th percentiles (dashed lines); Center: Distribution of click peak frequencies with peak near the Nyquist frequency (100 kHz); Right: Distribution of inter-click-intervals.

Gervais' Beaked Whales

Gervais' beaked whale signals have energy concentrated in the 30-50 kHz band (Gillespie *et al*., 2009), with a peak at 44 kHz (Baumann-Pickering *et al*., 2013). While Gervais' beaked whale signals are similar to those of Cuvier's and Blainville's beaked whales, the Gervais' beaked whale FM pulses are at a slightly higher frequency than those of the other two species. Similarly, Gervais' beaked whale FM pulses sweep up in frequency (Figure 7). The IPI for Gervais' beaked whale signals is typically around 275 ms (Baumann-Pickering *et al*., 2013).

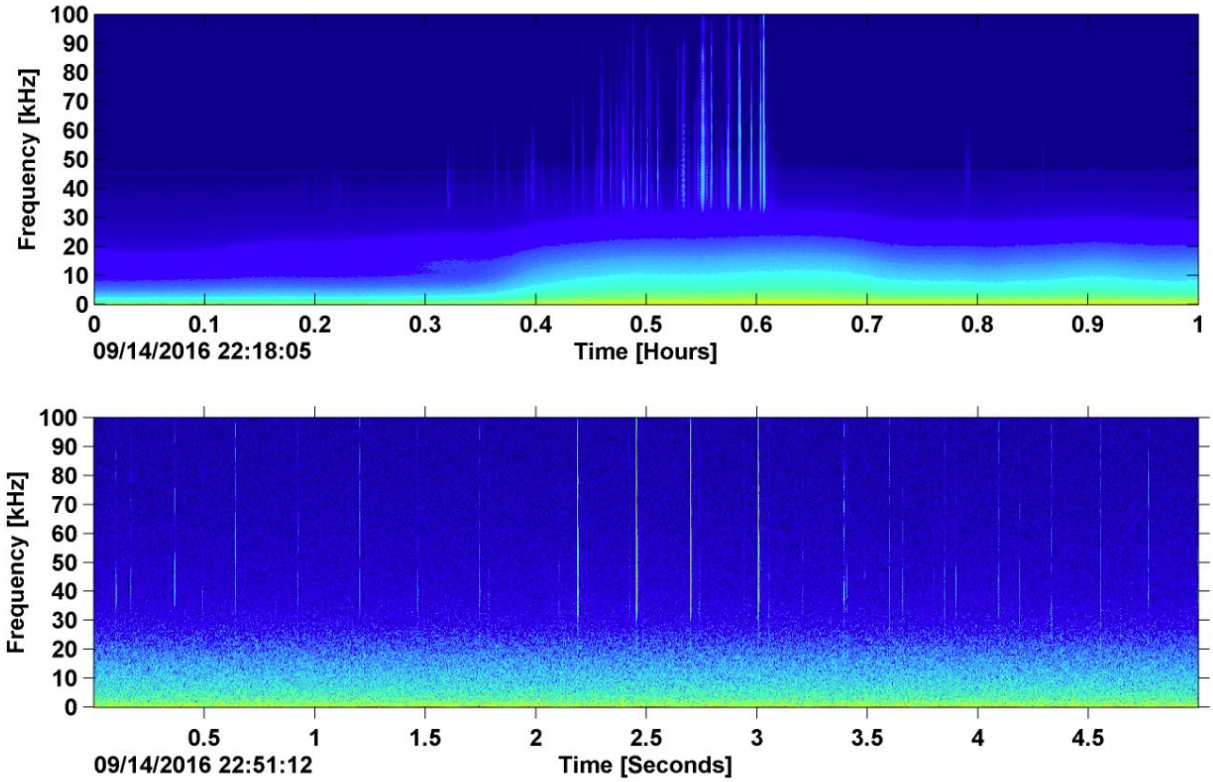

Figure 7. Gervais' beaked whale echolocation clicks in LTSA (top) and spectrogram (bottom) recorded at site BS, September 2016.

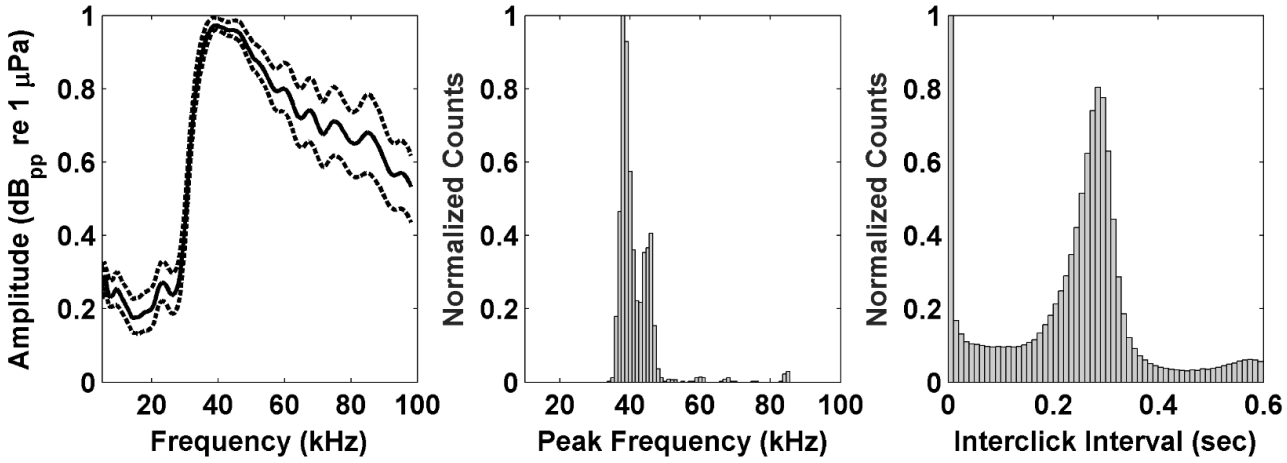

Figure 8. Left: Mean frequency spectrum of Gervais' beaked whale echolocation clicks (solid line) and 25th and 75th percentiles (dashed lines); Center: Distribution of click peak frequencies with peak near the Nyquist frequency (100 kHz); Right: Distribution of inter-click-intervals.

Sowerby's Beaked Whales

Sowerby's beaked whale echolocation signals have energy concentrated in the 50 – 95 kHz band, with a peak at 67 kHz (Figure 9). Sowerby's beaked whale signals have a characteristic FM upsweep, and are distinguishable from other co-occurring beaked whale signal types by their higher frequency content and a relatively short inter-pulse interval of around 150 ms (Cholewiak *et al.*, 2013).

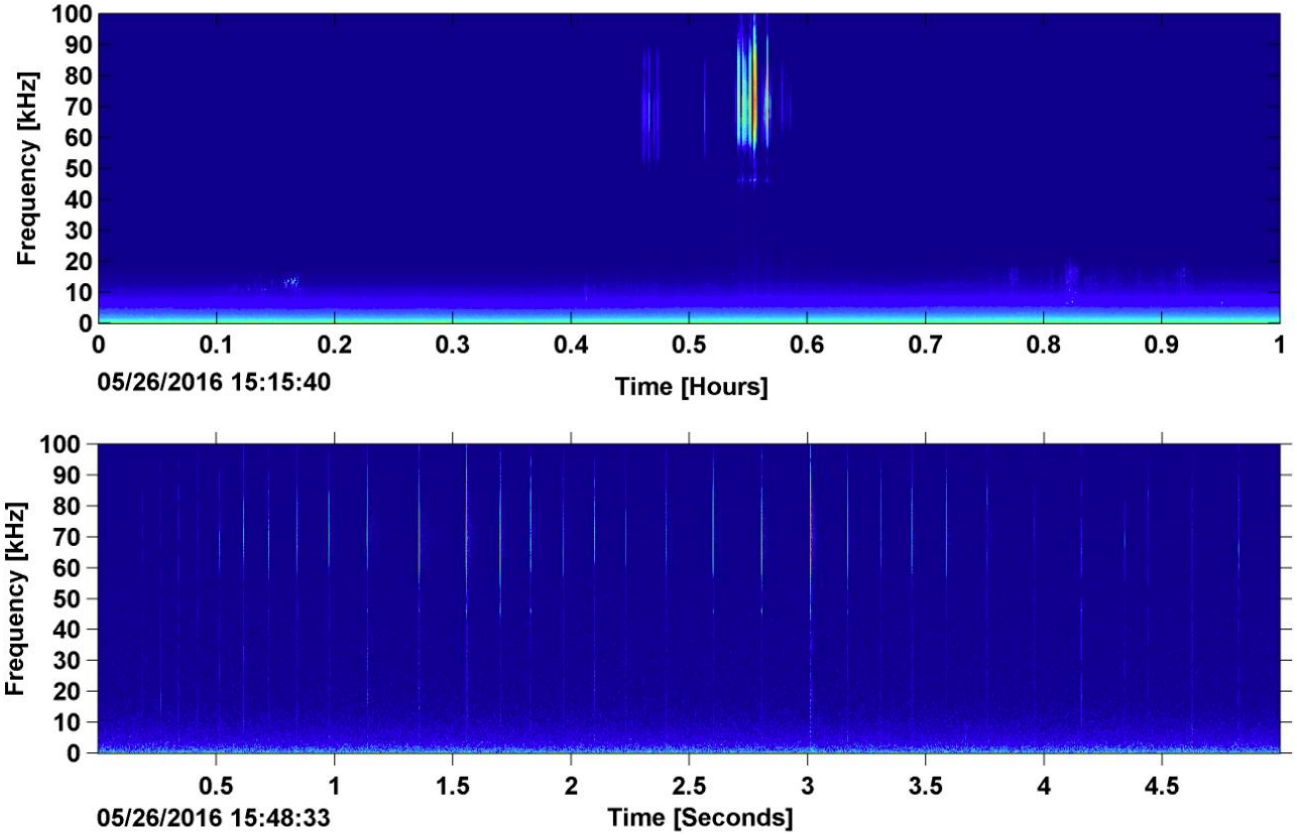

Figure 9. Sowerby's beaked whale echolocation clicks in LTSA (top) and spectrogram (bottom) recorded at site WC, May 2016.

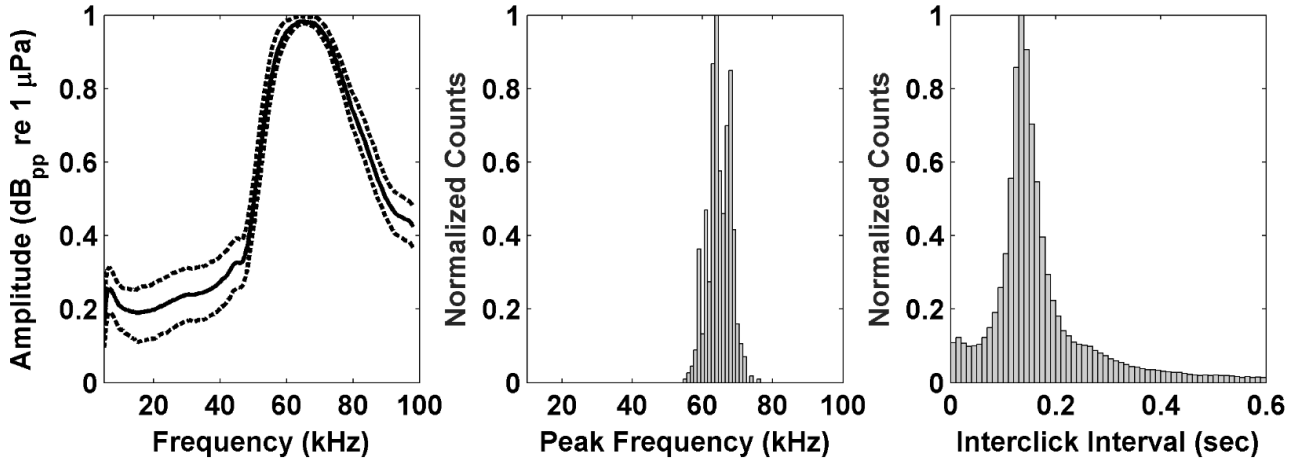

Figure 10. Left: Mean frequency spectrum of Sowerby's beaked whale echolocation clicks (solid line) and 25th and 75th percentiles (dashed lines); Center: Distribution of click peak frequencies with peak near the Nyquist frequency (100 kHz); Right: Distribution of inter-click-intervals.

True's Beaked Whale

True's beaked whale echolocation signals are FM upsweep pulses, with peak frequency around 46 kHz and an inter-pulse interval of about 180 ms (Figure 12). The spectral features of True's beaked whale FM pulses closely resemble those produced by Gervais' beaked whales, and acoustic discrimination between these two species remains challenging (DeAngelis *et al*., submitted).

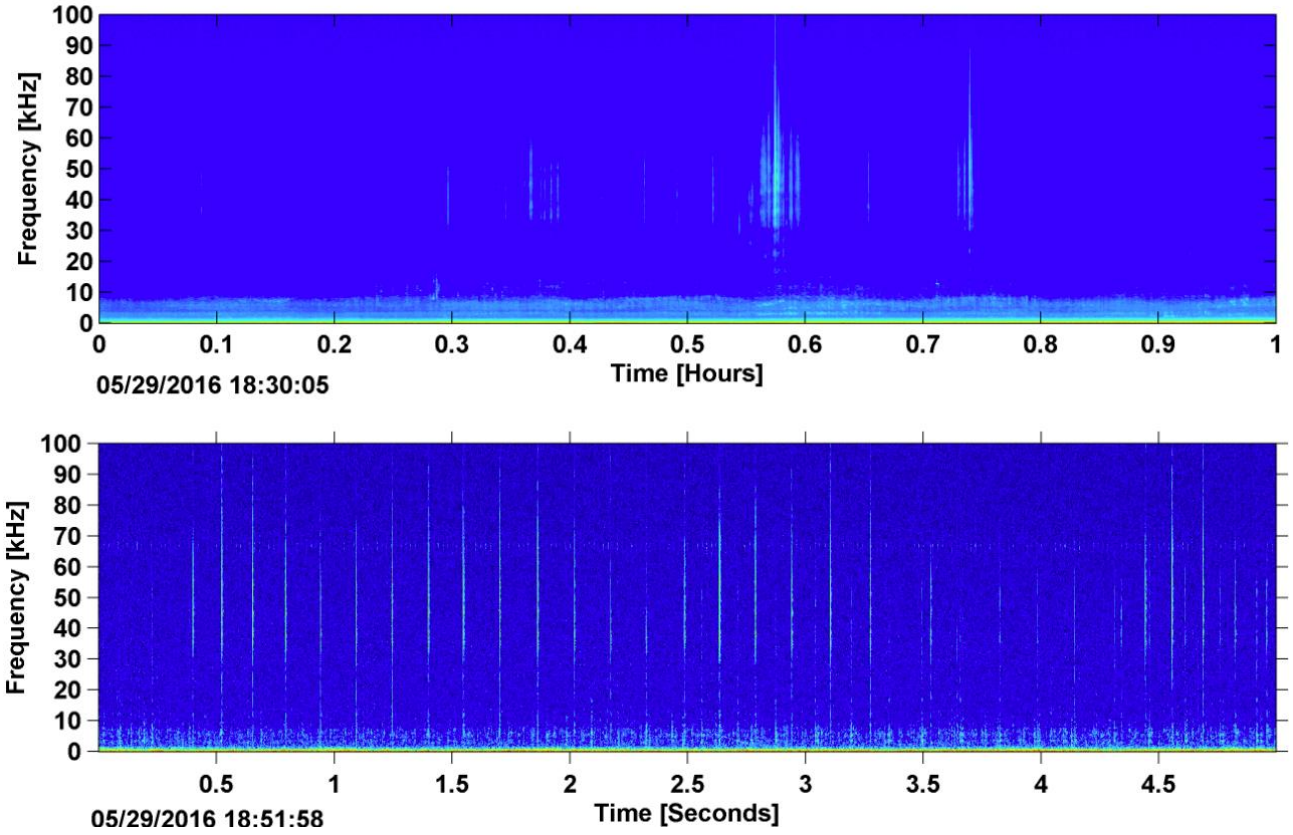

Figure 11. True's beaked whale echolocation clicks in LTSA (top) and spectrogram (bottom) recorded at site NC, May 2016.

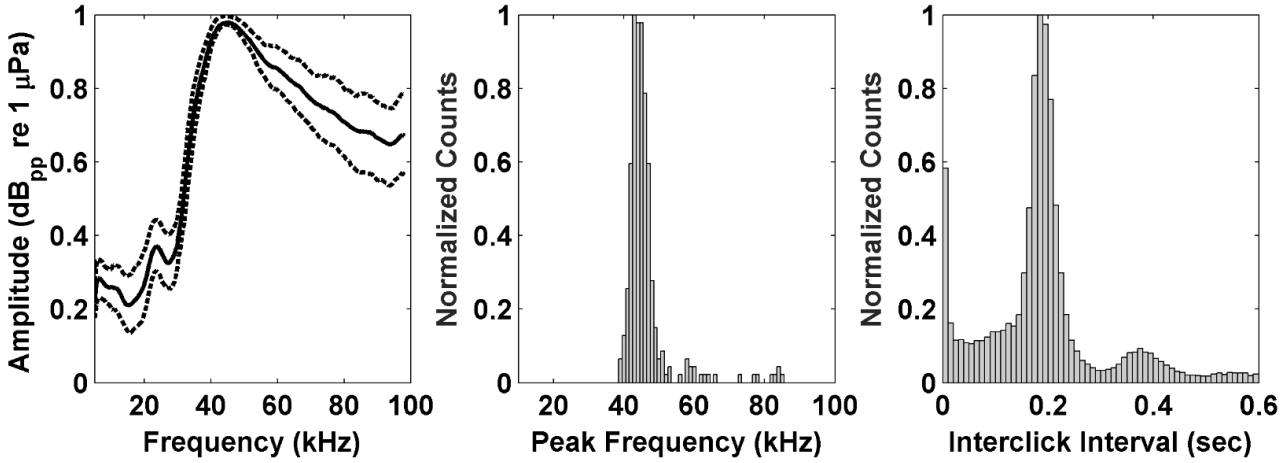

Figure 12. Left: Mean frequency spectrum of True's beaked whale echolocation clicks (solid line) and 25th and 75th percentiles (dashed lines); Center: Distribution of click peak frequencies with peak near the Nyquist frequency (100 kHz); Right: Distribution of inter-click-intervals.

Sperm Whales

Sperm whale clicks contain energy from 2-20 kHz, with the majority of energy between 10-15 kHz (Møhl *et al.*, 2003) (Figure 13). Regular clicks, observed during foraging dives, demonstrate an ICI from 0.25-2s (Goold and Jones, 1995; Madsen *et al.*, 2002a). Short bursts of closely spaced clicks called creaks are observed during foraging dives and are believed to indicate a predation attempt (Watwood *et al.*, 2006). Slow clicks are used only by males and are more intense than regular clicks with long inter-click intervals (Madsen *et al.*, 2002b). Codas are stereotyped sequences of clicks which are less intense and contain lower peak frequencies than regular clicks (Watkins and Schevill, 1977). Effort was not expended to denote whether sperm whale detections were codas, regular or slow clicks.

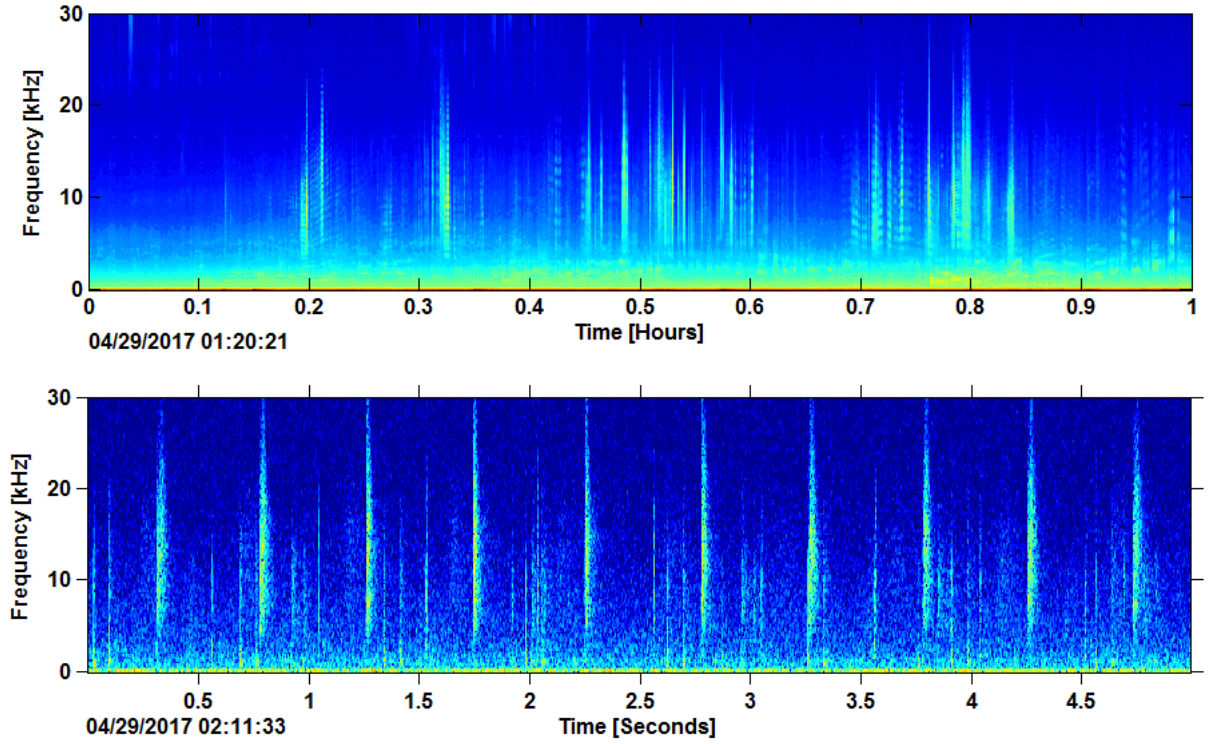

Figure 13. Sperm whale clicks in LTSA (top) and spectrogram (bottom) recorded at site NC, April 2017.

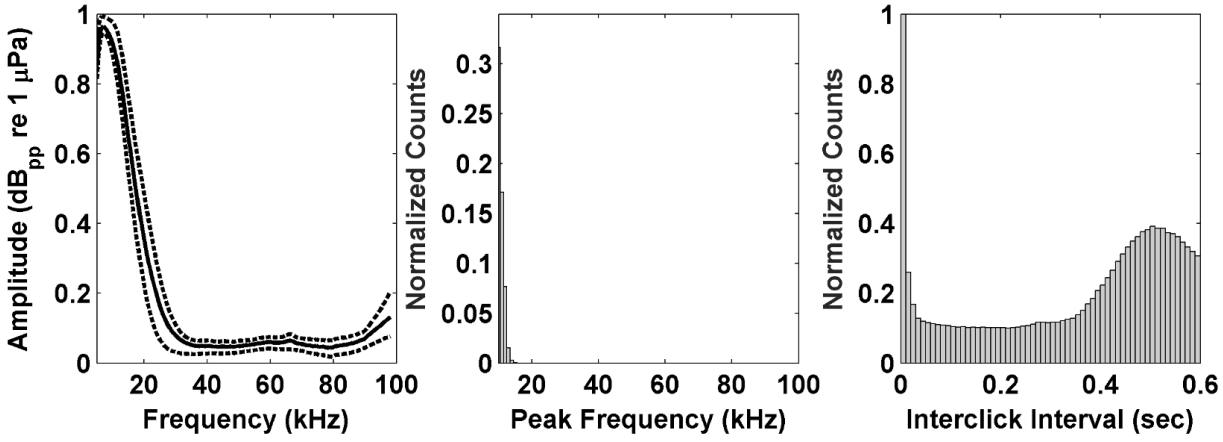

Figure 14. Left: Mean frequency spectrum of sperm whale clicks (solid line) and 25th and 75th percentiles (dashed lines); Center: Distribution of click peak frequencies with peak near the Nyquist frequency (100 kHz); Right: Distribution of inter-click-intervals.

***Kogia* spp.**

Dwarf and pygmy sperm whales emit echolocation signals which have peak energy at frequencies near 130 kHz (Au, 1993). While this is above the upper frequency band recorded by the HARP during these deployments, energy from *Kogia* clicks can be recorded within the 100 kHz HARP bandwidth (Figure 15). The observed signal may result both from the low-frequency tail of the *Kogia* echolocation click spectra, and from aliasing of energy from above the Nyquist frequency of 100 kHz (Figure 16).

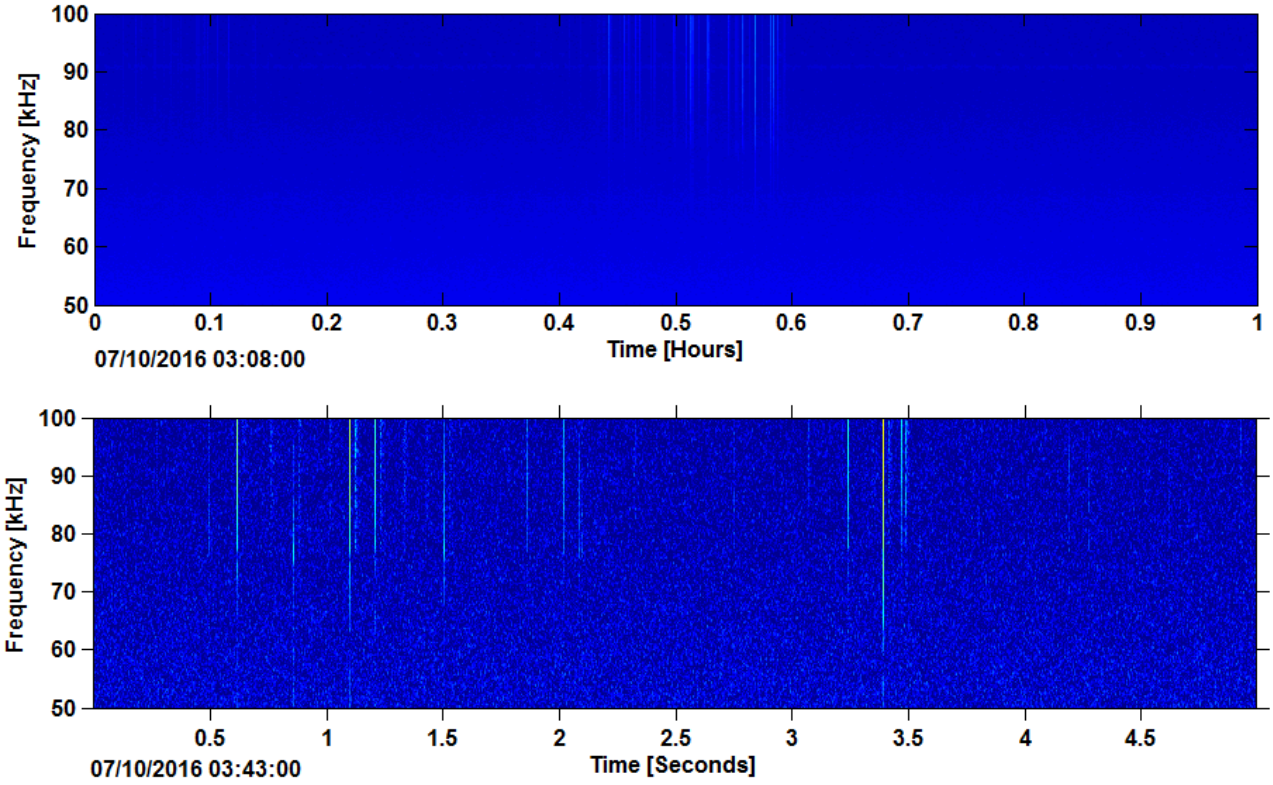

Figure 15. Kogia spp. clicks in LTSA (top) and spectrogram (bottom) recorded at site BS, July 2016.

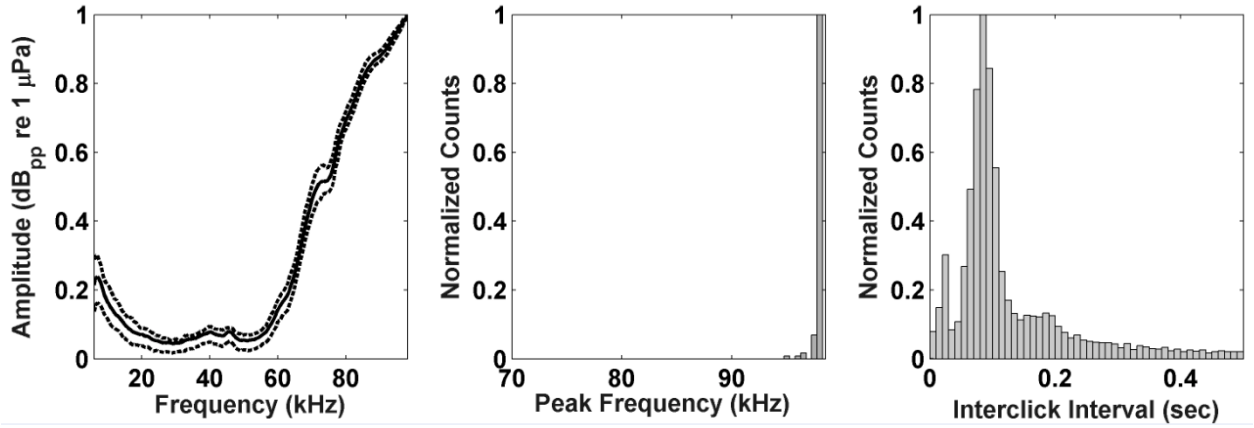

Figure 16. Left: Mean frequency spectrum of Kogia spp. clicks (solid line) and 25th and 75th percentiles (dashed lines); Center: Distribution of click peak frequencies with peak near the Nyquist frequency (100 kHz); Right: Distribution of inter-click-intervals.

Delphinid Click Types

At least eight delphinid click types were identified and labeled click type 2 – 10 and Risso's from across the eight sites. Some reported click types may contain multiple subtypes. Further analysis will be required to refine click types and reduce classification confusion between similar types.

Risso's Dolphin

Risso's dolphin clicks (Figure 17) have frequency peaks at approximately 22, 26, and 33 kHz. These clicks have a modal ICI of approximately 150 ms (Figure 18). Past studies have shown that spectral properties of Risso's dolphin clicks have slight variations with geographic region (Soldevilla *et al*.), although the multiple sharp frequency peaks and average ICI found at these North-Western Atlantic sites are similar to what has been found elsewhere.

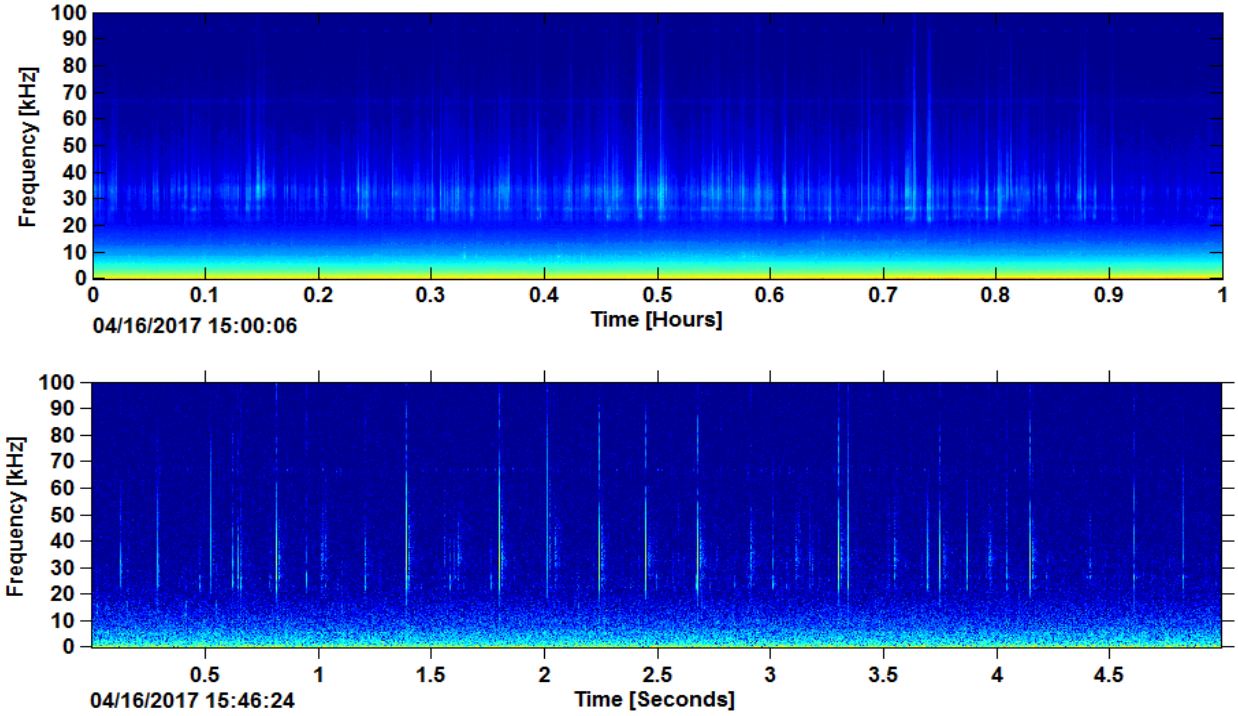

Figure 17. Risso's dolphin clicks in LTSA (top) and spectrogram (bottom) recorded at site NC, April 2017.

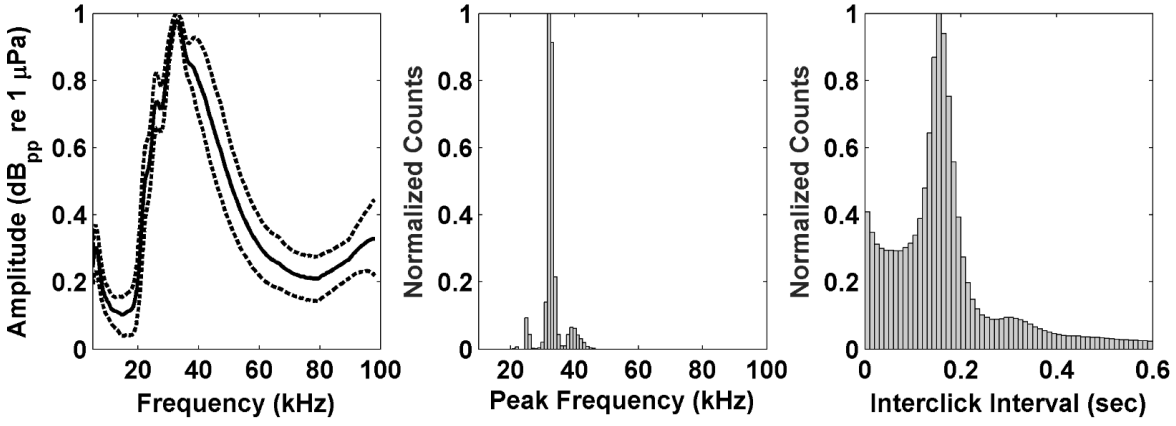

Figure 18. Left: Mean frequency spectrum of Risso's dolphin click cluster (solid line) and 25th and 75th percentiles (dashed lines); Center: Distribution of click cluster peak frequencies with primary peak at 33 kHz; Right: Distribution of inter click intervals within cluster with modal peak at 0.15 seconds.

Click Type 2

Click type 2 clicks (Figure 19) have a narrow spectral peak at 22 kHz and a broad peak from 32 to 43 kHz. These clicks have a modal ICI of approximately 130 ms (Figure 20).

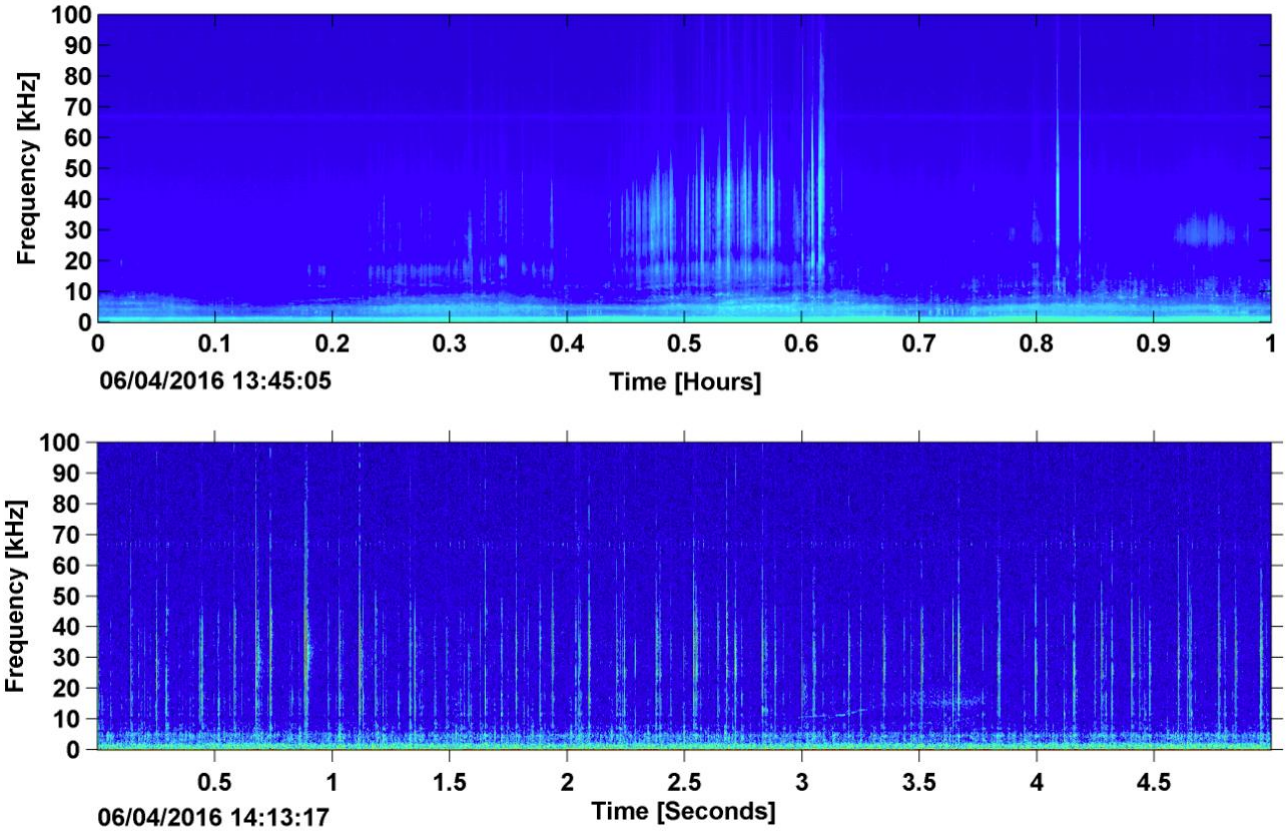

Figure 19. Click type 2 clicks in LTSA (top) and spectrogram (bottom) recorded at site NC, June 2016.

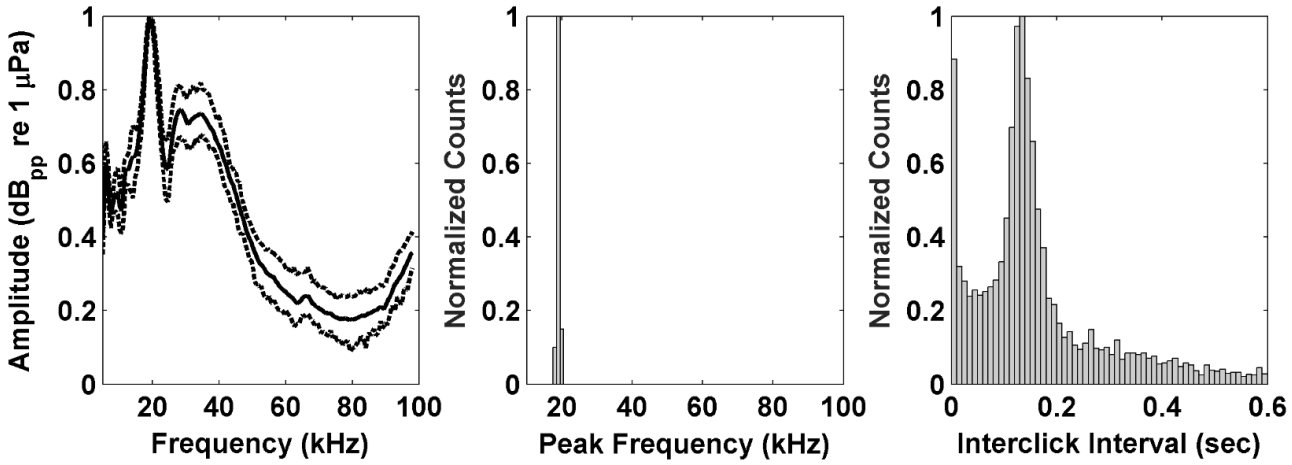

Figure 20. Figure 16. Left: Mean normalized received sound pressure spectrum level of click type 2 cluster (solid line) with 25th and 75th percentiles (dashed lines); Center: Distribution of click cluster peak frequencies with a peak at 22 kHz; Right: Distribution of inter-click-intervals within cluster with modal peak at 130 ms.

Click Type 3

Click type 3 clicks (Figure 21) have a peak frequency of approximately 32 kHz, and a modal ICI of 65 ms (Figure 22).

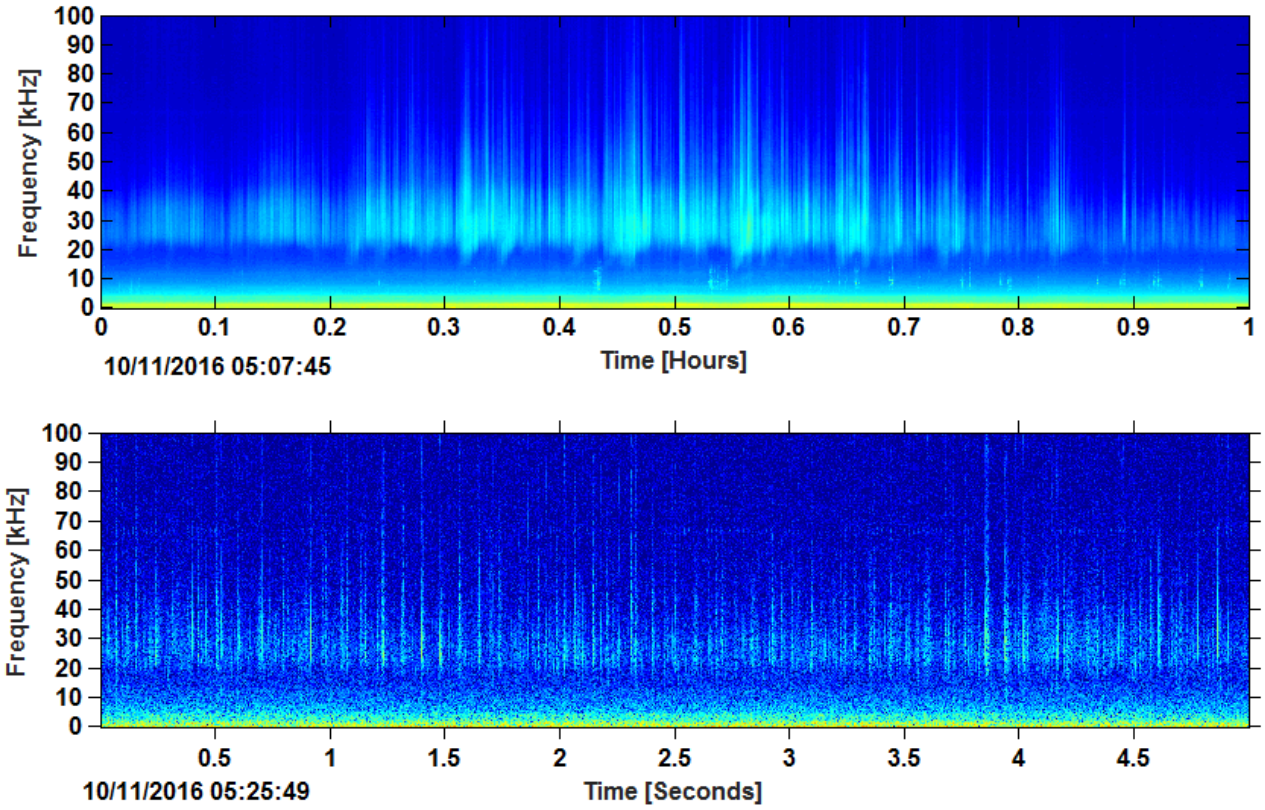

Figure 21. Click type 3 clicks in LTSA (top) and spectrogram (bottom) recorded at site NC, October 2016.

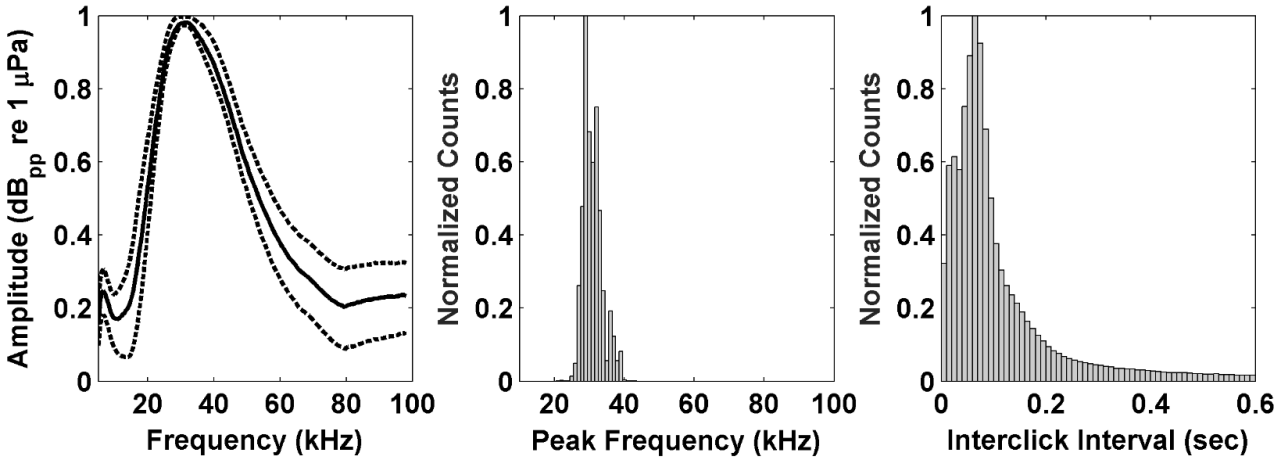

Figure 22. Left: Mean normalized received sound pressure spectrum level of click type 3 cluster (solid line) with 25th and 75th percentiles (dashed lines); Center: Distribution of click cluster peak frequencies with a peak at 32 kHz; Right: Distribution of inter-click-intervals within cluster with modal peak at 65 ms.

Click Type 4 / 6

Click types 4 & 6 from the previous report were not consistently distinguishable across all sites and have been combined due to their similarities in interclick interval and spectra. The combined click types 4 / 6 (
Figure 23) have a peak frequency of approximately 19 kHz, and a modal ICI of 145 ms (Figure 24).

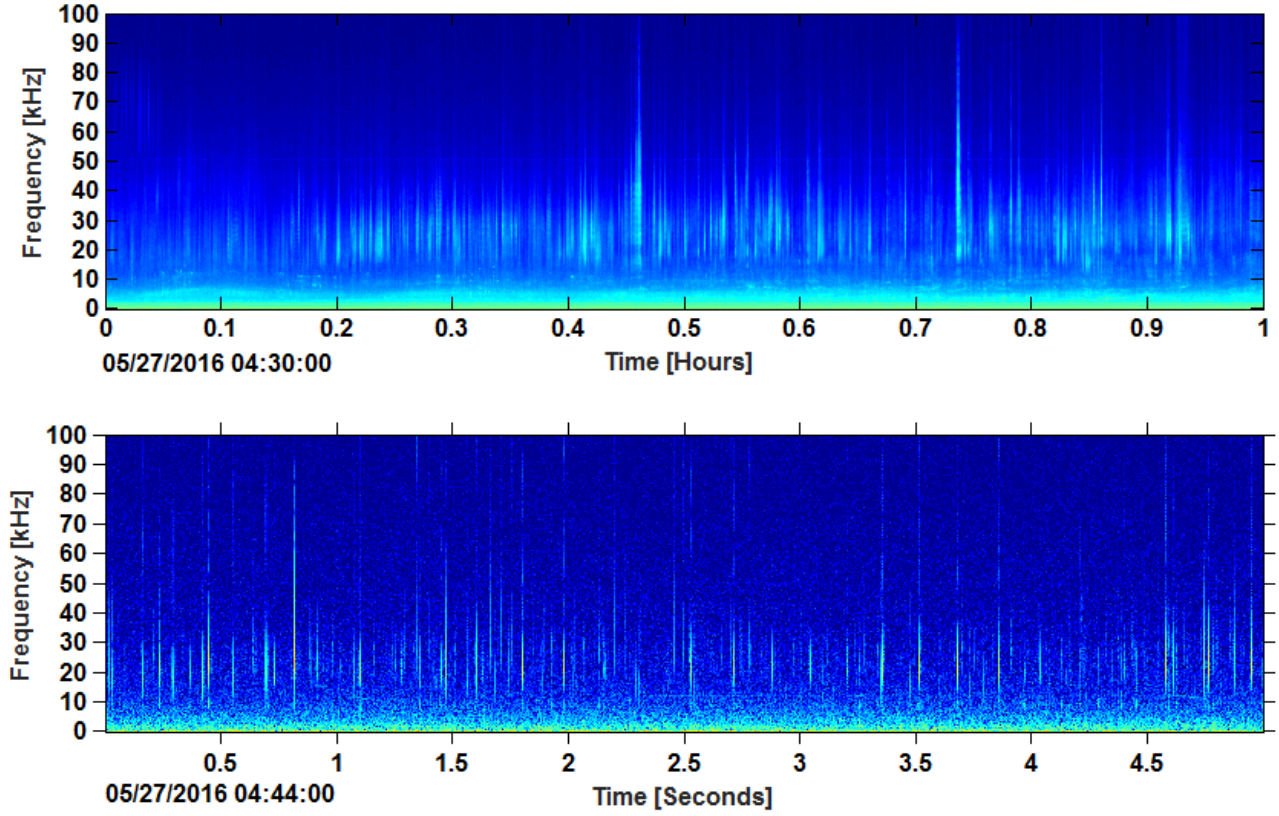

Figure 23. Click type 4 / 6 clicks in LTSA (top) and spectrogram (bottom) recorded at site WC, May 2016.

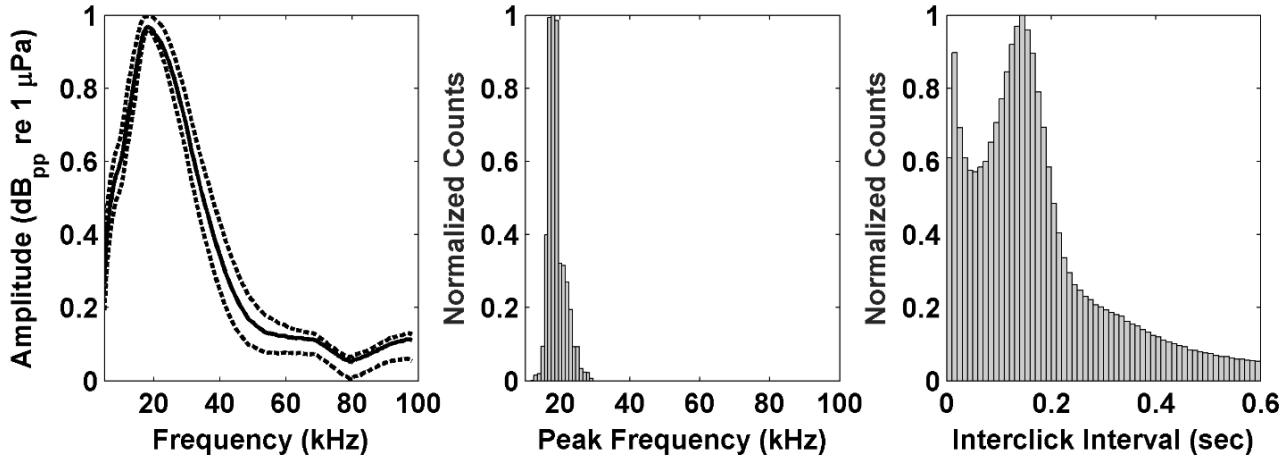

Figure 24. Left: Mean normalized received sound pressure spectrum level of click type 4 / 6 cluster (solid line) with 25th and 75th percentiles (dashed lines); Center: Distribution of click cluster peak frequencies with a peak at 19 kHz; Right: Distribution of inter-click-intervals within cluster with modal peak at 145 ms.

Click Type 5

Click type 5 clicks (Figure 25) have a main peak frequency between 34 and 51 kHz, and two minor spectral peaks at 19 and 27 kHz. This click type has a modal ICI of 65 ms (Figure 26).

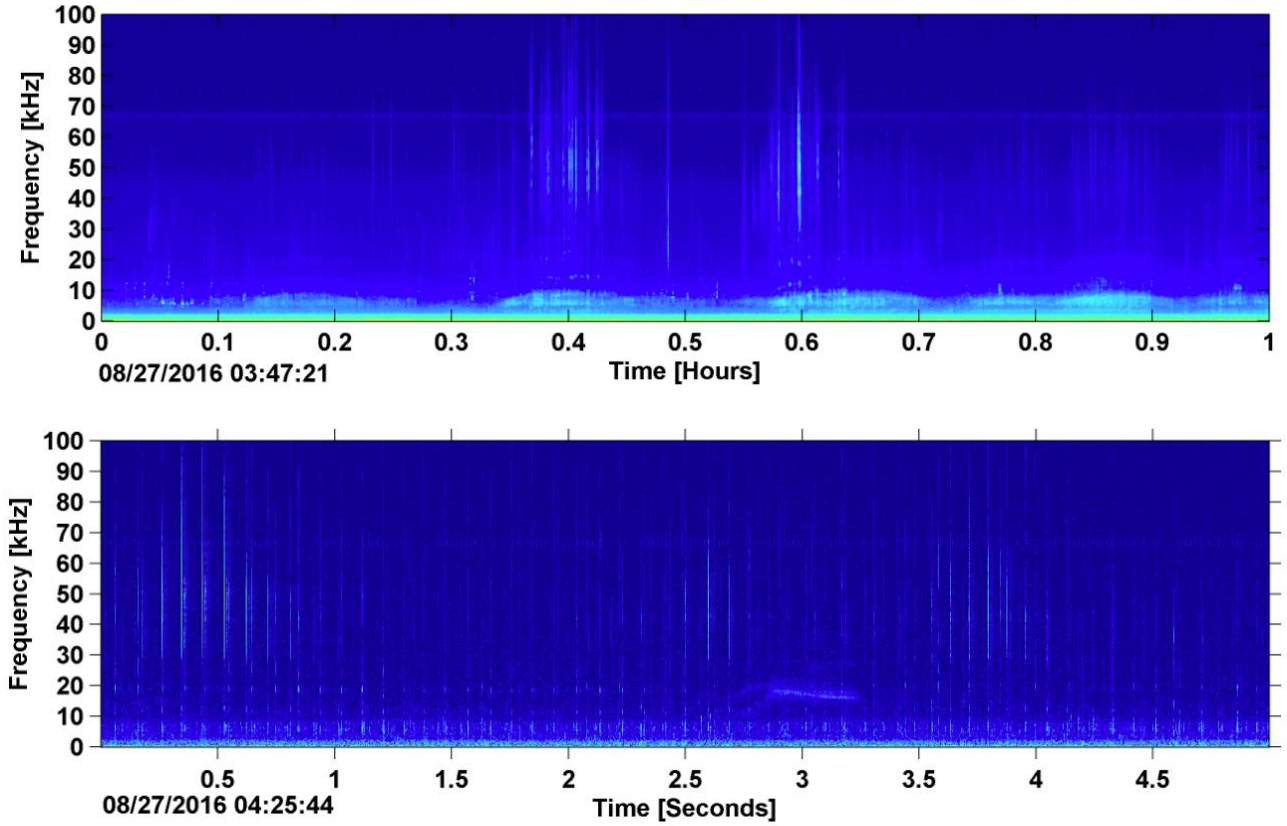

Figure 25. Click type 5 clicks in LTSA (top) and spectrogram (bottom) recorded at site NC, August 2016.

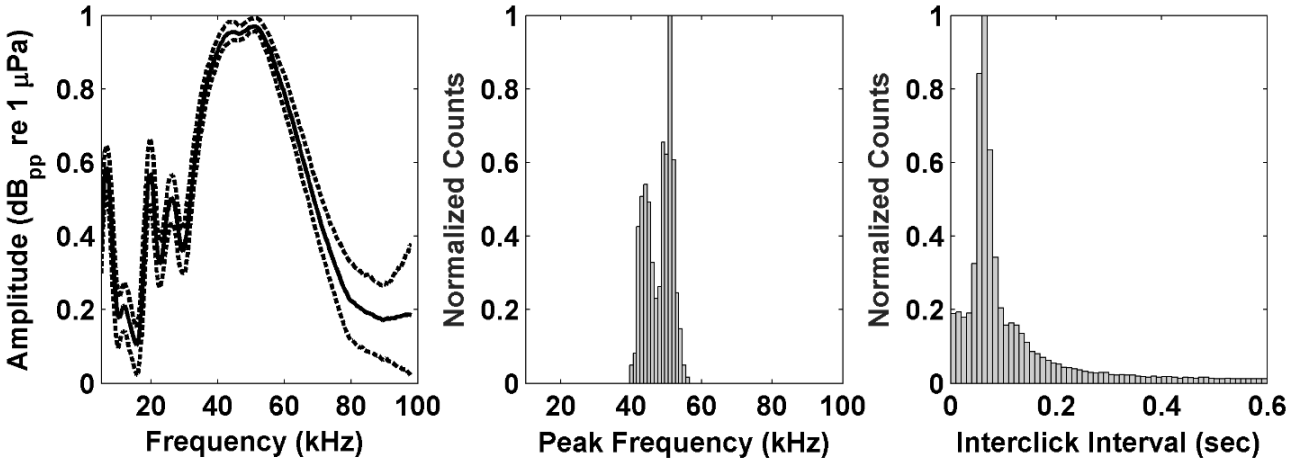

Figure 26. Left: Mean normalized received sound pressure spectrum level of click type 5 cluster (solid line) with 25th and 75th percentiles (dashed lines); Center: Distribution of click cluster peak frequencies with primary peak between 34 and 51 kHz; Right: Distribution of inter-click intervals within cluster with modal peak at 65 ms.

Click Type 7

Click type 7 clicks (Figure 27) have a peak frequency of 28 kHz and a modal ICI of 70 ms (Figure 28).

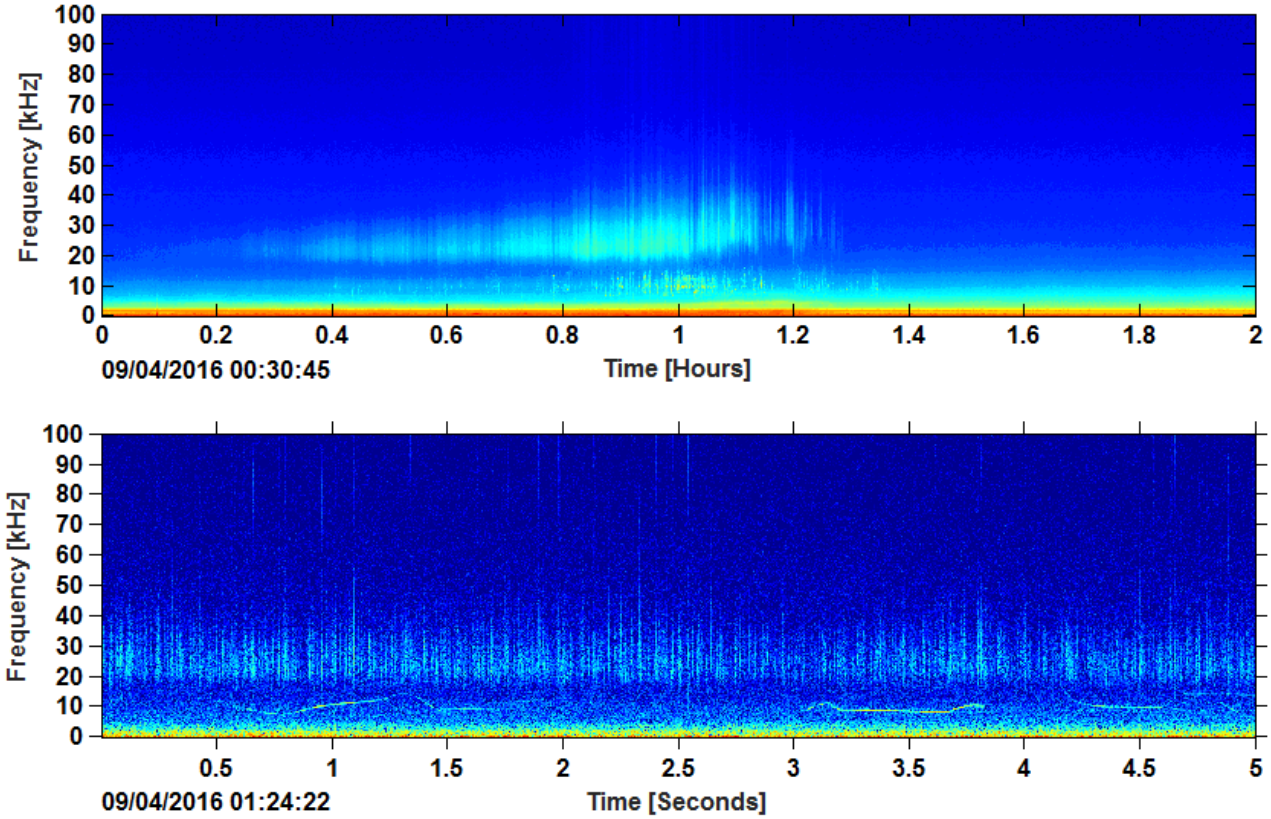

Figure 27. Click type 7 clicks in LTSA (top) and spectrogram (bottom) recorded at site HZ, September 2016.

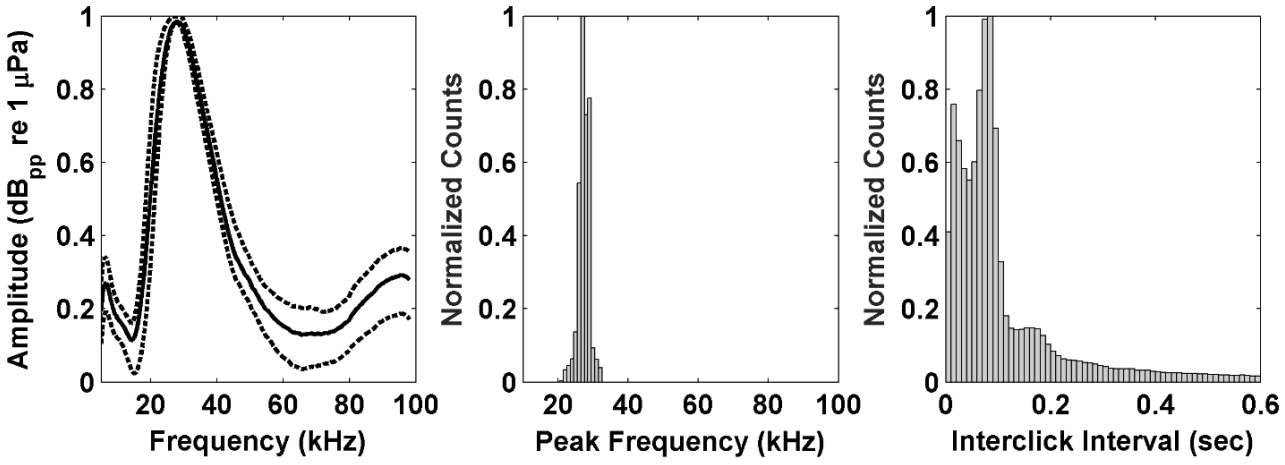

Figure 28. Left: Mean normalized received sound pressure spectrum level of click type 7 cluster (solid line) with 25th and 75th percentiles (dashed lines); Center: Distribution of click cluster peak frequencies with a peak at 28 kHz; Right: Distribution of inter-click-intervals within cluster with modal peak at 70 ms.

Click Type 8

Click type 8 clicks (Figure 29) have a main peak frequency at approximately 41 kHz (Figure 28). This click type has a modal ICI of 55 ms (Figure 30).

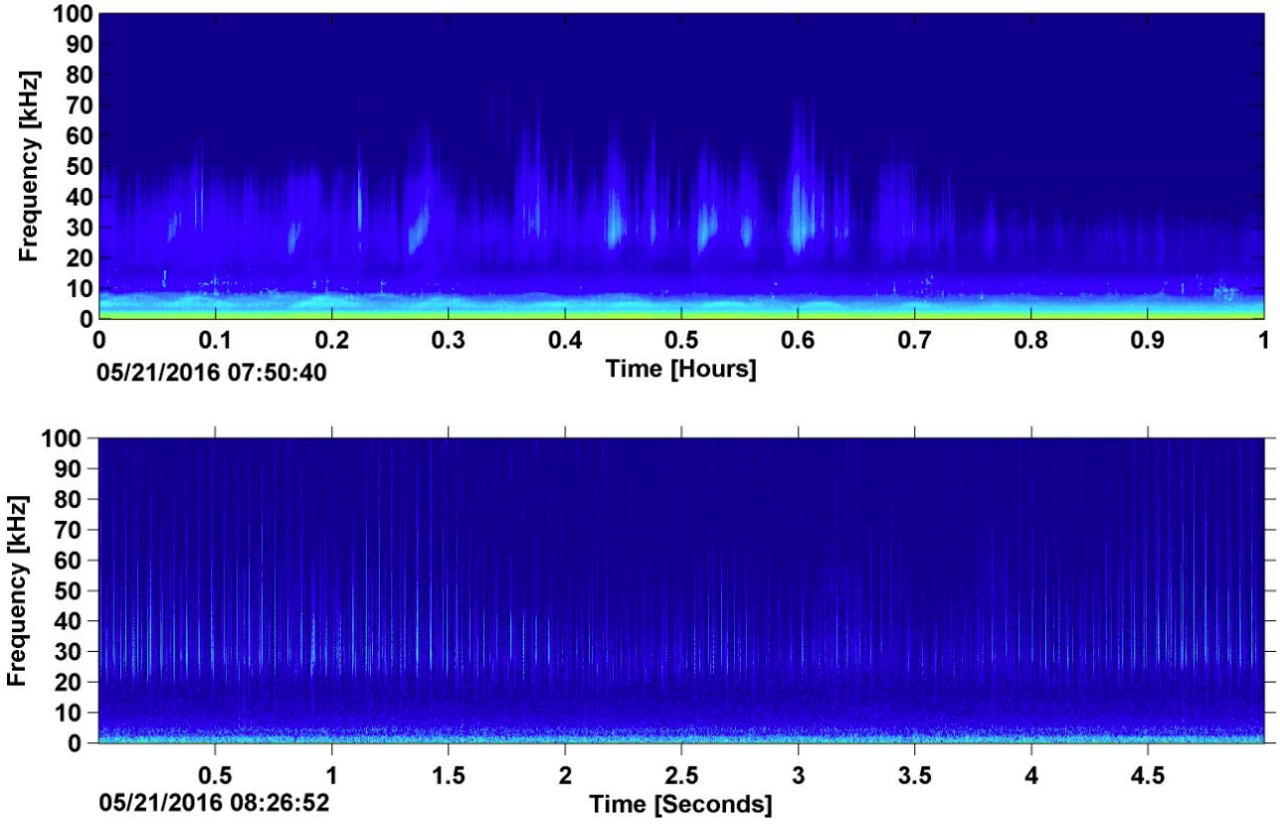

Figure 29. Click type 8 clicks in LTSA (top) and spectrogram (bottom) recorded at site WC, May 2016.

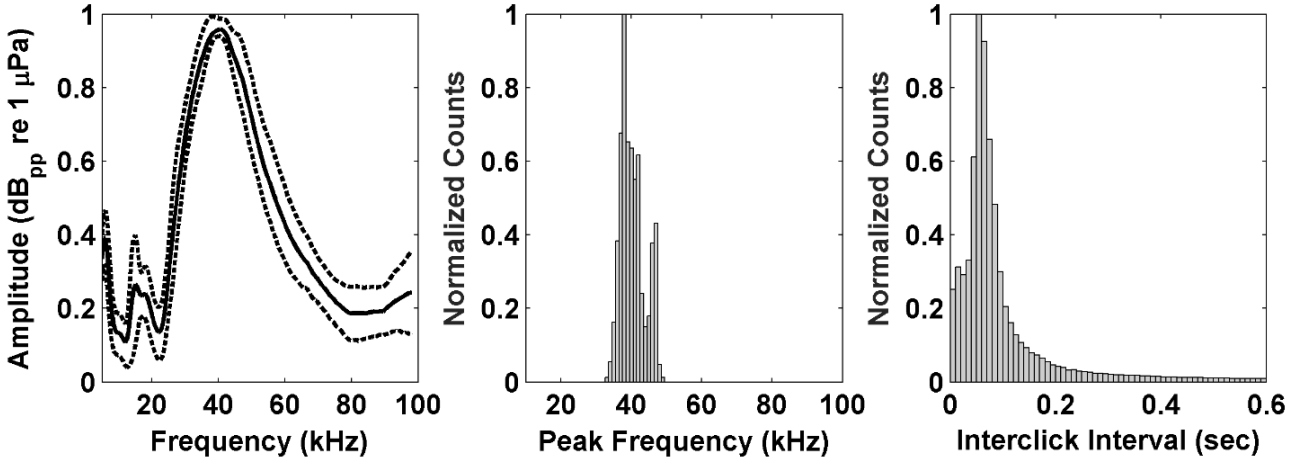

Figure 30. Left: Mean normalized received sound pressure spectrum level of click type 8 cluster (solid line) with 25th and 75th percentiles (dashed lines); Center: Distribution of click cluster peak frequencies with a peak at 41 kHz; Right: Distribution of inter-click-intervals within cluster with modal peak at 55 ms.

Click Type 9

Click type 9 clicks (Figure 31) have a main peak frequency at approximately 26 kHz, and a minor spectral peak at 16 kHz (Figure 32). This click type has a modal ICI of 175 ms (Figure 32).

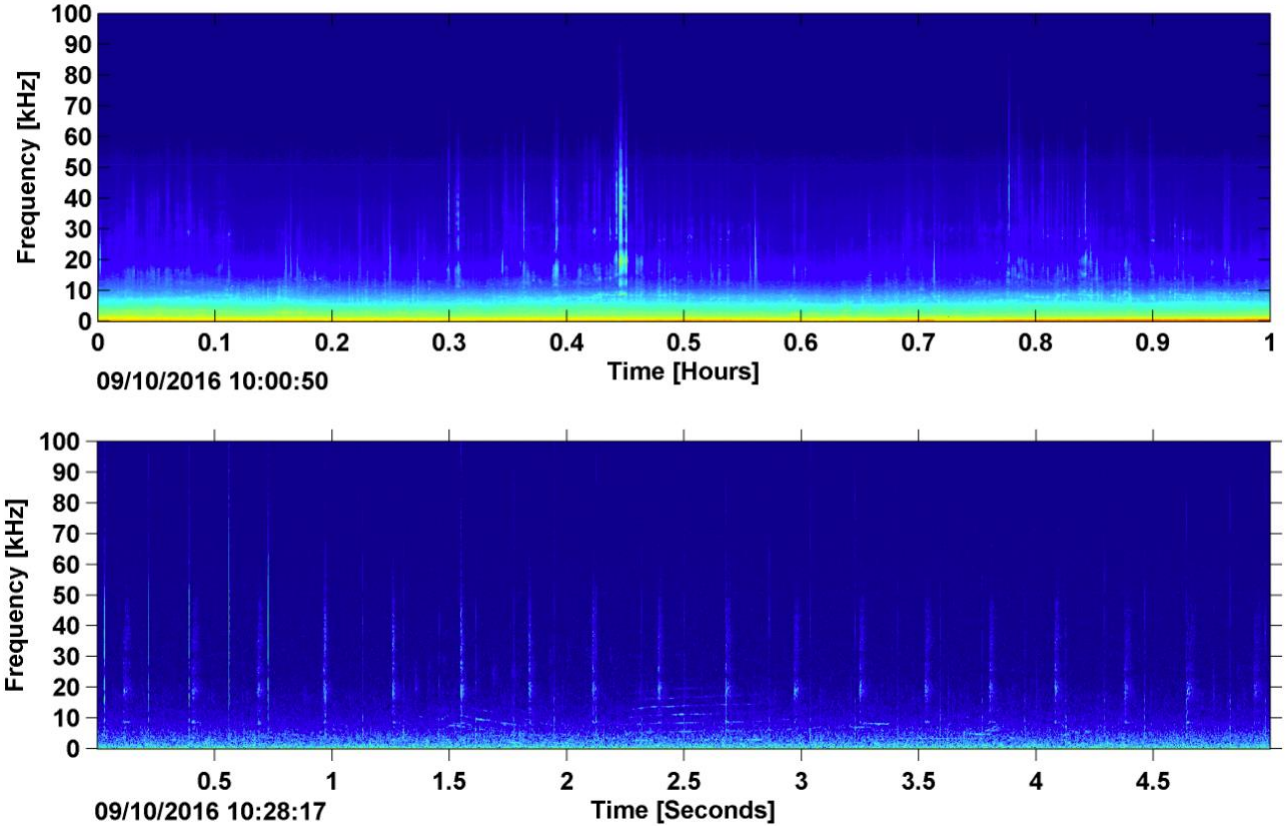

Figure 31. Click type 9 clicks in LTSA (top) and spectrogram (bottom) recorded at site WC, September 2016.

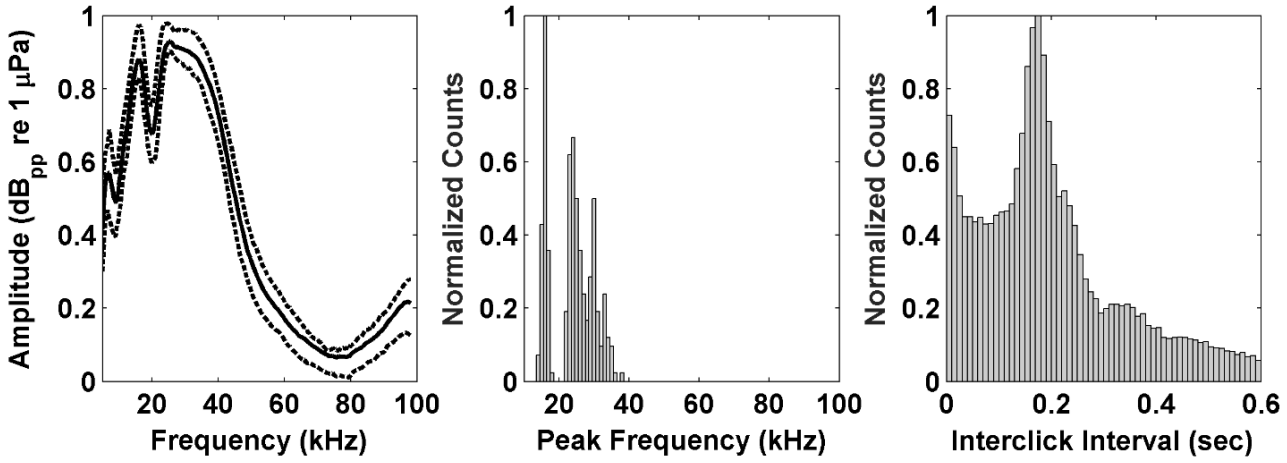

Figure 32. Left: Mean normalized received sound pressure spectrum level of click type 9 cluster (solid line) with 25th and 75th percentiles (dashed lines); Center: Distribution of click cluster peak frequencies with a peak at 26 kHz; Right: Distribution of inter-click-intervals within cluster with modal peak at 175 ms.

Click Type 10

Click type 10 clicks (Figure 33) have a peak frequency of approximately 26 kHz and a modal ICI of 200 ms (Figure 34).

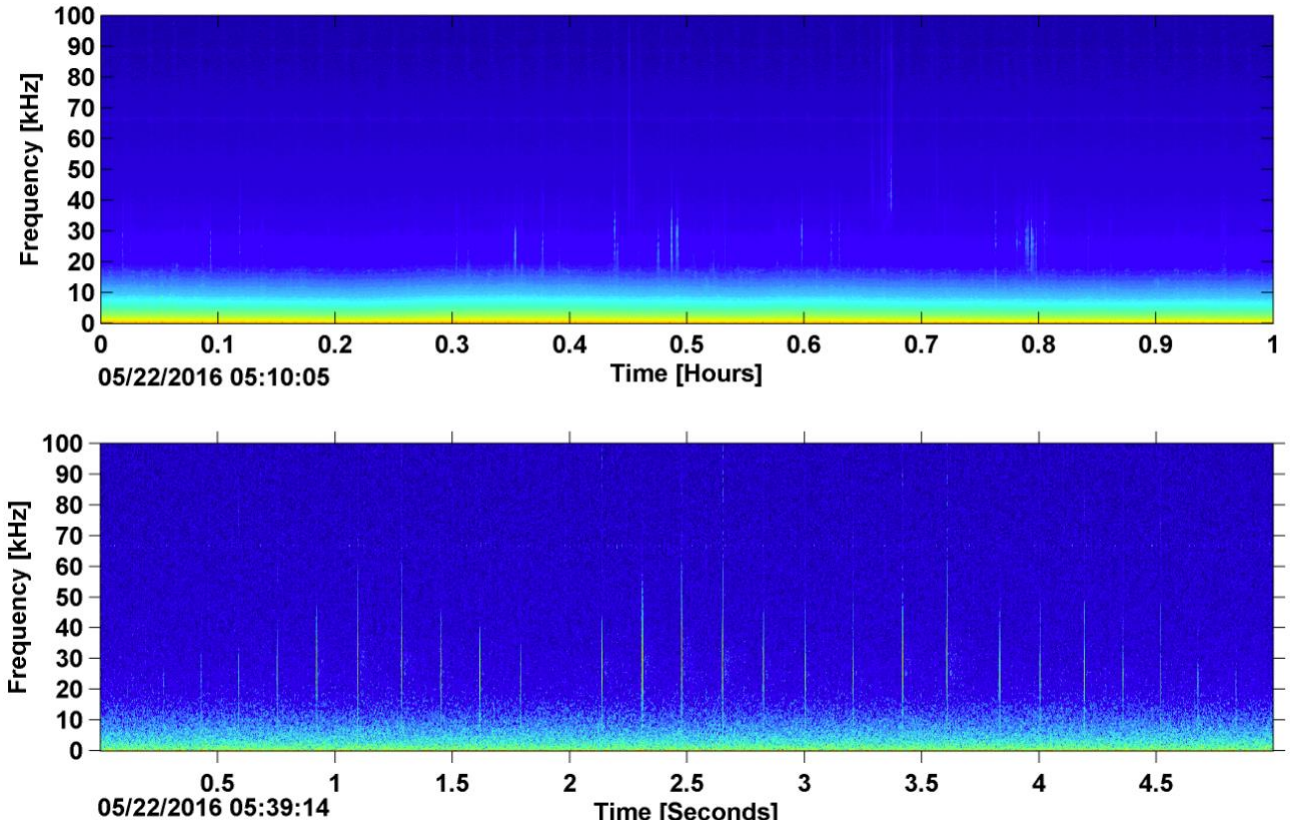

Figure 33. Click type 10 clicks in LTSA (top) and spectrogram (bottom) recorded at site GS, May 2016.

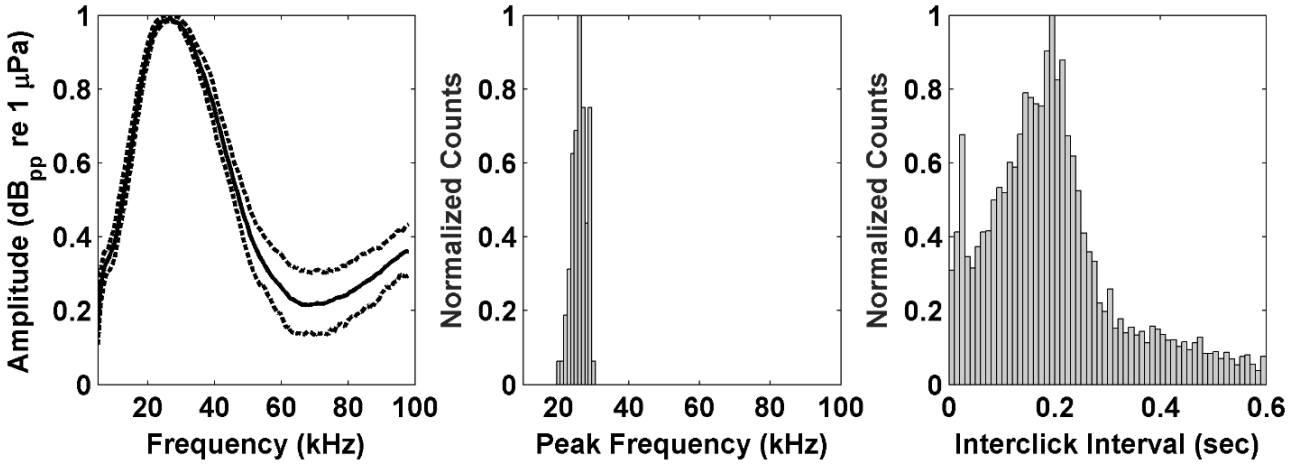

Figure 34. Left: Mean normalized received sound pressure spectrum level of click type 10 cluster (solid line) with 25th and 75th percentiles (dashed lines); Center: Distribution of click cluster peak frequencies with a peak at 26 kHz; Right: Distribution of inter-click-intervals within cluster with modal peak at 200 ms.

Anthropogenic Sounds

Several anthropogenic sounds were monitored for this report: broadband ship noise, explosions, airguns, and echosounders. The start and end of each individual sound or overall session was logged and their durations were added to estimate cumulative hours per week. An automated computer detector was used for the airgun and explosion analyses, all described below. Manual effort was expended for broadband ship noise and echosounders (Table 2).

Table 2. Anthropogenic sound data analysis parameters.

Sound Types	LTSA Search Parameters	
	Plot Length (hr)	Frequency Range (Hz)
Broadband Ship Noise	3	10 – 5,000
Explosions	0.75	10 – 1,000
Airguns	0.75	10 – 1,000
Echosounders	1	5,000 – 100,000

Broadband Ship Noise

Broadband ship sound occurs when a ship passes within a few kilometers of the hydrophone. Ship sound can occur for many hours at a time, but broadband ship sound typically lasts from 10 minutes up to 3 hours. Ship sound has a characteristic frequency-range dependent interference pattern in the LTSA (McKenna *et al.*, 2012). Combination of sound wave direct paths and surface reflected paths produce constructive and destructive interference (bright and dark bands) in the LTSA that varies by frequency and distance between the ship and the receiver (Figure 35, top). Noise can extend above 10 kHz, although its sound levels typically decrease rapidly above a few kHz. Broadband ship analysis effort consisted of manual scans of the LTSA set at 3 hours with a frequency range of 10 – 5,000 Hz.

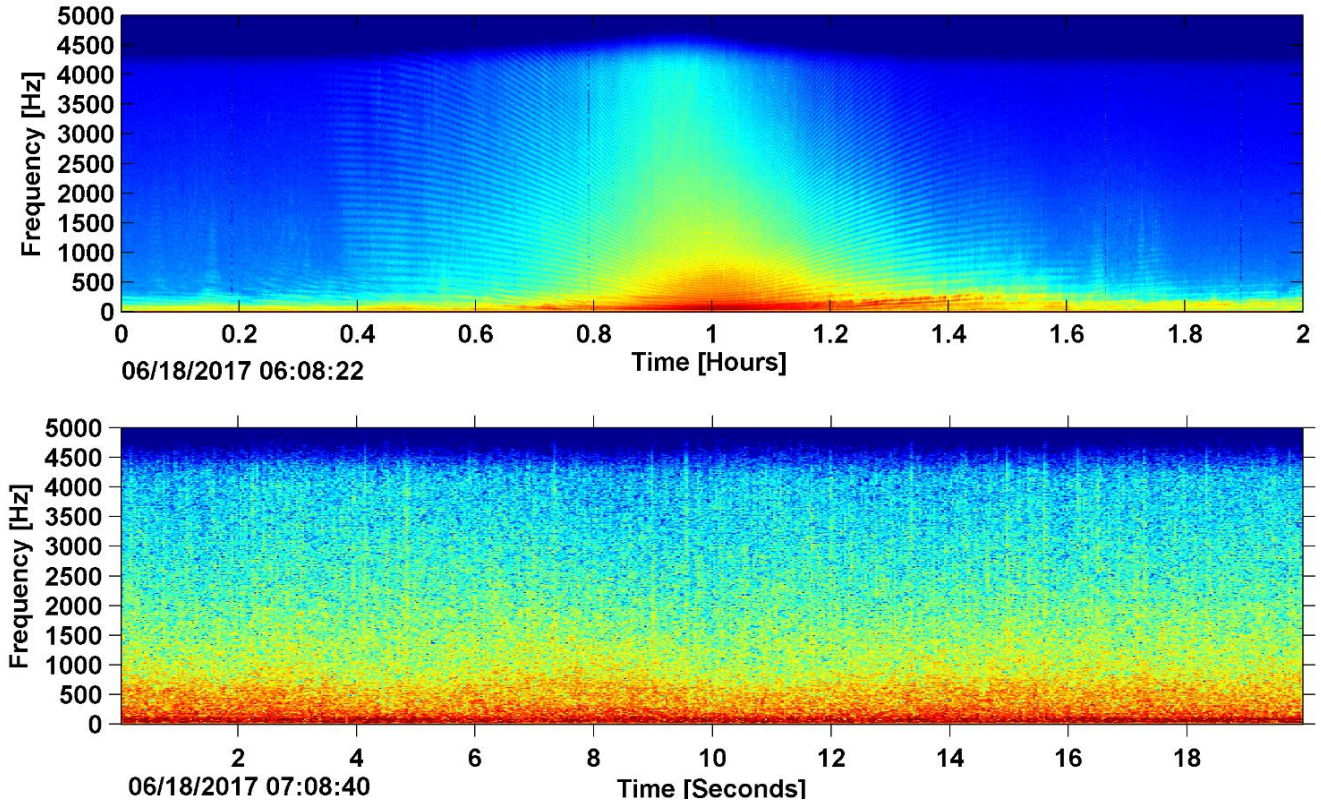

Figure 35. Broadband ship sound in the LTSA (top) and spectrogram (bottom) recorded at site BS, June 2017.

Explosions

Effort was directed toward detecting explosive sounds in the recordings including military explosions, shots from sub-seafloor exploration, and seal bombs used by the fishing industry. An explosion appears as a vertical spike in the LTSA that, when expanded in the spectrogram, has a sharp onset with a reverberant decay (Figure 36). Explosions were detected automatically using a matched filter detector on data decimated to 10 kHz sampling rate. The timeseries was filtered with a 10th order Butterworth bandpass filter between 200 and 2,000 Hz. Cross-correlation was computed between 75 seconds of the envelope of the filtered timeseries and the envelope of a filtered example explosion (0.7 s, Hann windowed) as the match filter signal. The cross-correlation was squared to 'sharpen' peaks of explosion detections. A floating threshold was calculated by taking the median cross-correlation value over the current 75 seconds of data to account for detecting explosions within noise, such as shipping. A cross-correlation threshold of 3*10-6 above the median was set. When the correlation coefficient reached above threshold, the timeseries was inspected more closely. Consecutive explosions were required to have a minimum time distance of 0.5 second to be detected. A 300-point (0.03 s) floating average energy across the detection was computed. The start and end times above the threshold were determined when the energy rose by more than 2 dB above the median energy across the detection. Peak-to-peak (pp) and root-mean-square (rms) received sound pressure levels (RL) were computed over the potential explosion period as well as a timeseries of the length of the explosion template before and after the explosion. The potential explosion was classified as a false detection and deleted if 1) the dB difference of pp and rms levels between signal and time AFTER the detection was less than 4 dB or 1.5 dB respectively; 2) the dB difference of pp and rms levels between signal and time BEFORE the signal was less than 3 dB or 1 dB, respectively; and 3) the detection was shorter than 0.03 or longer than 0.55 seconds of duration. The thresholds were evaluated based on the distribution of histograms of manually verified true and false detections. A trained analyst subsequently verified the remaining potential explosions for accuracy. Explosions have energy as low as 10 Hz and often extend up to 2,000 Hz or higher, lasting for a few seconds including the reverbation.

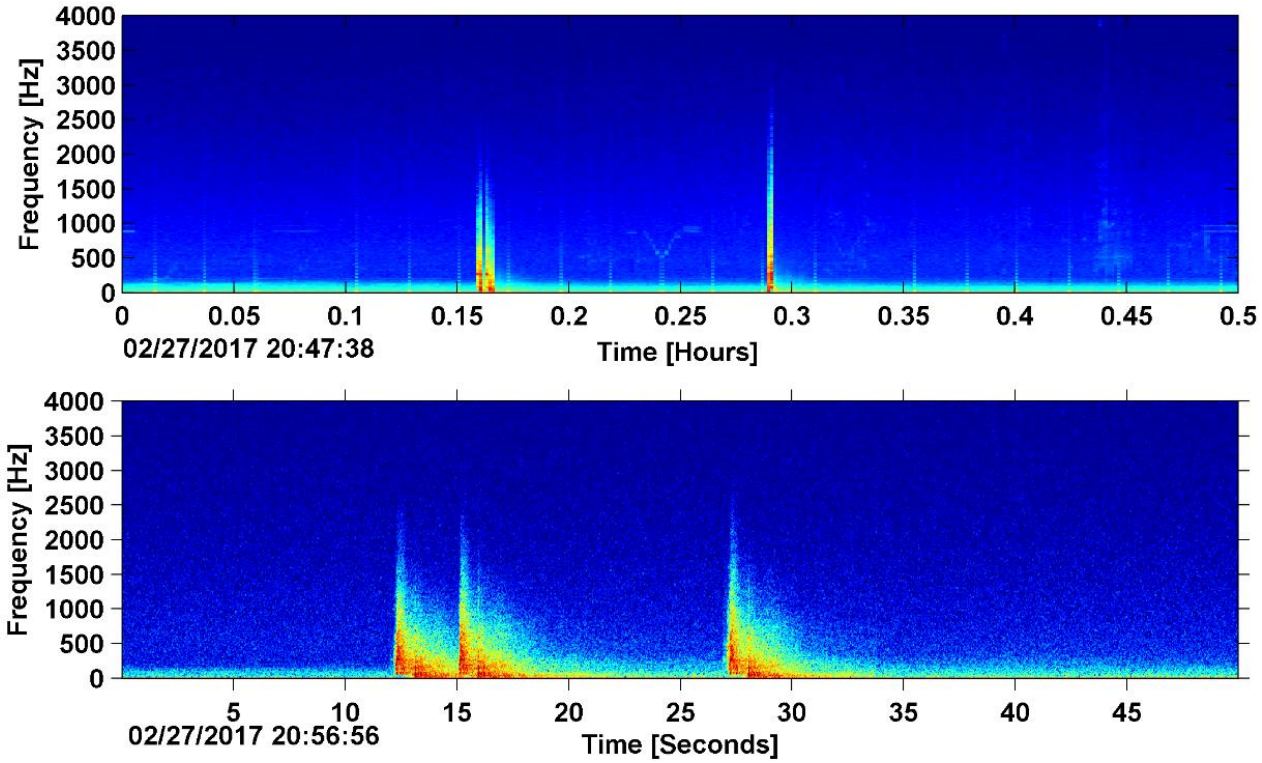

Figure 36. Explosion example in the LTSA (top) and spectrogram (bottom) recorded at site WC, February 2017.

Airguns

Airguns are regularly used in seismic exploration to investigate the ocean floor and what lies beneath it. A container of high-pressure air is momentarily vented to the surrounding water, producing an air-filled cavity which expands and contracts violently several times (Barger and Hamblen, 1980). While most of the energy produced by an airgun array falls below 250 Hz, airguns can produce significant energy at frequencies up to at least 1 kHz (Blackman *et al.*, 2004). Source levels tend to be over 200 dB re 1 µPa-m (Amundsen and Landro, 2010), and have been measured up to 260 dB rms re 1 µPa-m (Hildebrand, 2009). These blasts typically have an inter-pulse interval of approximately 10 seconds and can last from several hours to days (Figure 37). Airguns were detected automatically using a matched filter detector on data decimated to 10 kHz sampling rate. The timeseries was filtered with a 10th order Butterworth bandpass filter between 25 and 200 Hz. Cross correlation was computed between 75 seconds of the envelope of the filtered timeseries and the envelope of a filtered example explosion (0.7 s, Hann windowed) as the matched filter signal. The cross correlation was squared to 'sharpen' peaks of airgun blast detections. A floating threshold was calculated by taking the median cross correlation value over the current 75 seconds of data to account for detecting airguns within noise, such as shipping. A cross correlation threshold of $2*10^{-6}$ above the median was set. When the correlation coefficient reached above this threshold, the timeseries was inspected more closely. Consecutive airgun blasts were required to have a minimum start time difference of 2 seconds to be detected. A 300-point (0.03 s) floating average energy across the detection was computed. The start and end times above the threshold were marked when the energy rose by more than 2 dB above the median energy across the detection. Peak-to-peak (pp) and root mean-square (rms) received sound pressure levels (RL) were computed over the potential blast period as well as a timeseries of the length of the airgun blast template before and after the explosion. The potential airgun blast was classified as a false detection and deleted if 1) the signal dB difference of pp and rms during and AFTER the detection was less than 4 dB or 0.5 dB respectively; 2) the dB difference of pp and rms between signal and time BEFORE the signal was less than 3 dB or 0.5 dB, respectively; and 3) the detection was shorter than 0.03 or longer than 10 s. The thresholds were evaluated based on the distribution of histograms of manually verified true and false detections. Airgun blast interpulse intervals were used to discard potential airgun detections that were not part of a sequence. A trained analyst subsequently verified the remaining potential airgun detections for accuracy. Airgun blasts have energy as low as 10 Hz and can extend up to 250 Hz or higher, lasting for a few seconds including the reverberation.

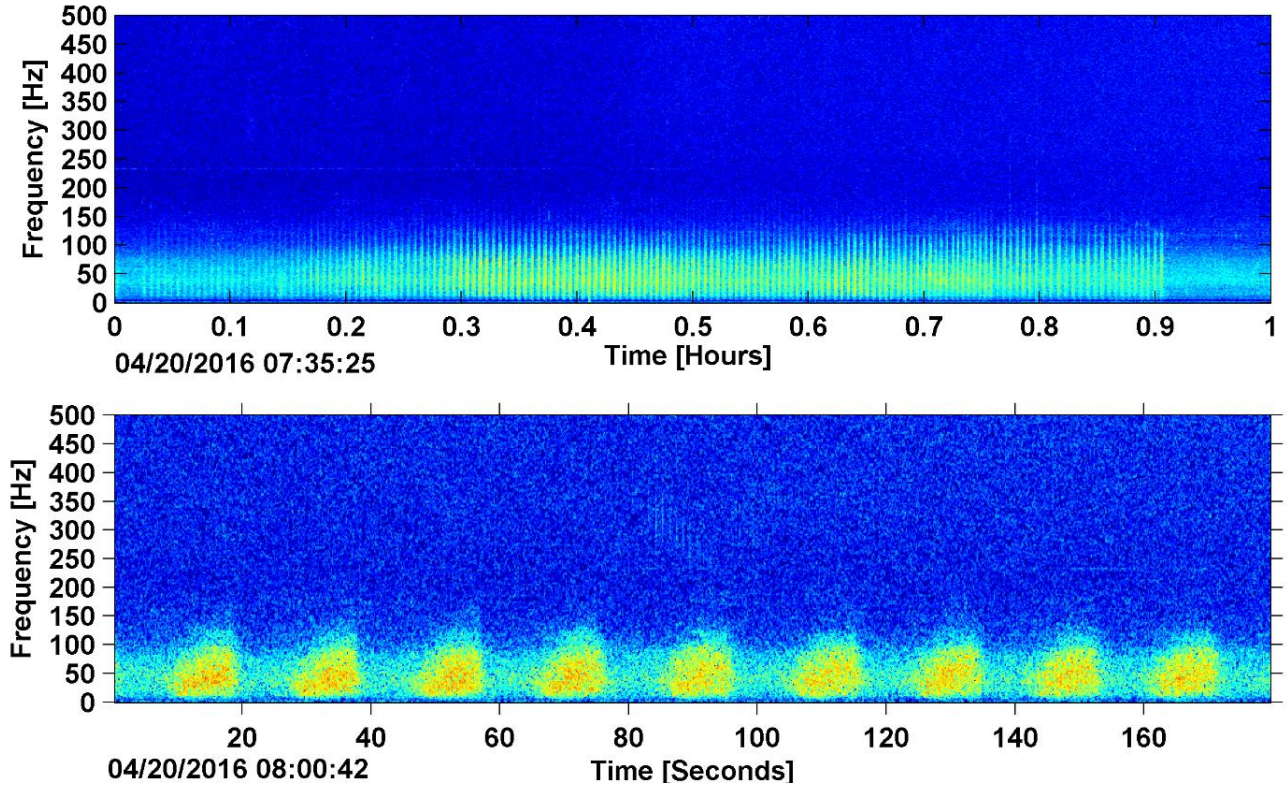

Figure 37. Airgun example in the LTSA (top), spectrogram (middle) and timeseries (bottom) recorded at site WC, April 2016.

Echosounders

Echosounding sonars transmit short pulses or frequency sweeps, typically in the high-frequency (above 5 kHz) band (Figure 38), although echosounders are occasionally found in the mid-frequency range (2-5 kHz). Many large and small vessels are equipped with echosounding sonar for water depth determination, fish detection, or other ocean sensing; typically these echosounders are operated much of the time a ship is at sea, as an aid for navigation and fishing operations. Presence of high-frequency echosounders was manually detected by analysts reviewing LTSA plots.

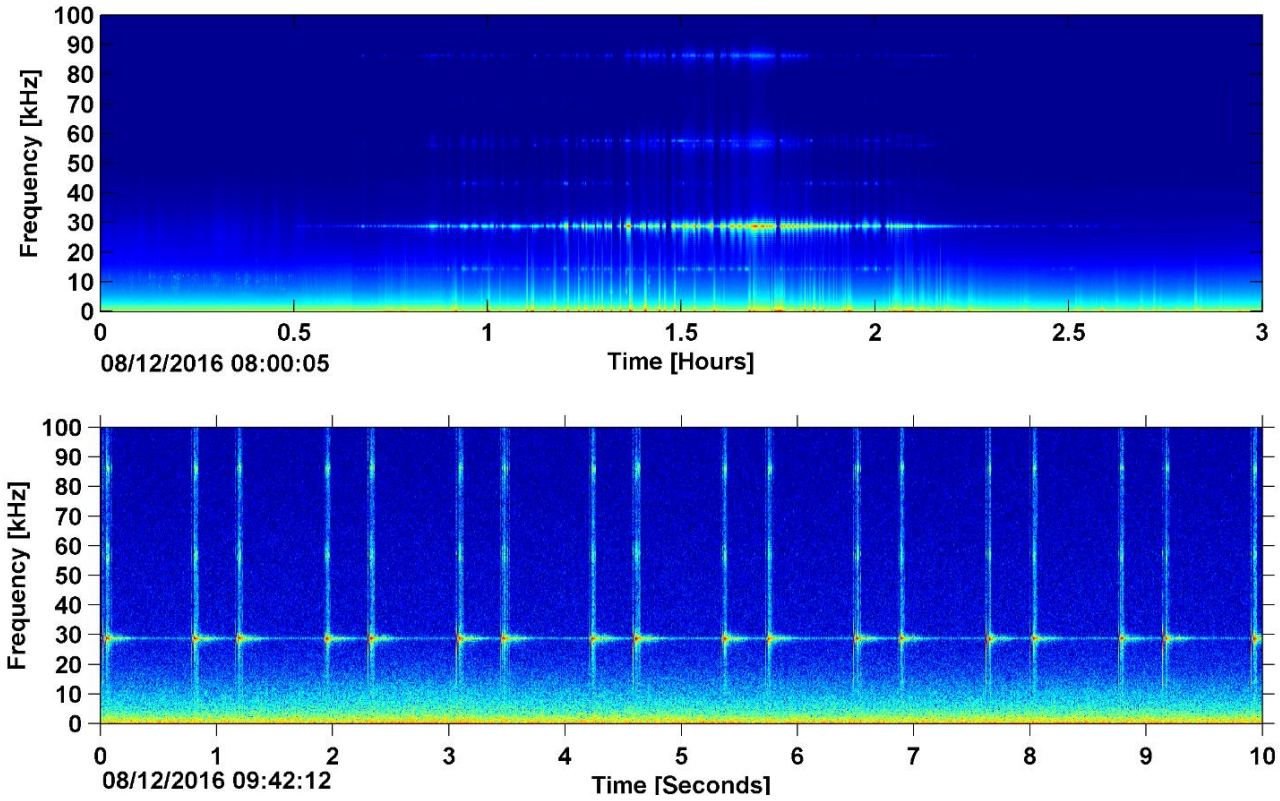

Figure 38. Echosounders in the LTSA (top) and spectrogram (bottom) recorded at site HZ, August 2016.

Results

The results of acoustic data analysis at all eight sites are summarized below. We describe the low-frequency ambient soundscape, the seasonal occurrence and relative abundance of several marine mammal acoustic signals, and detected anthropogenic sounds.

Ambient Soundscape

Daily-averaged ambient soundscape spectra were processed into monthly-averages and plotted using the same monthly color scheme for each of the deployments so that months from different sites and years can be compared. If more than a year of data is present, dashed lines are used for months in the second year. Partial months, those with less than 90% of total days recorded, include an asterisk (*) in the color legend.

- For all sites, levels between 10-100 Hz were dominated by anthropogenic sounds, primarily ship traffic and seismic exploration (Hildebrand, 2009). In this band, levels across all sites except BP are within ~10 dB of one another, with site BP showing levels 5-10 dB lower on average (Figure 45).
- Between 100-1000 Hz sound pressure spectrum levels are largely a function of wind and sea state. The highest levels are found at site HZ in March 2017 (Figure 39), and the lowest at site BP in September 2017 (Figure 45). In general, spectrum levels are highest during winter months, and lowest during summer months.
- A seasonal 20Hz fin whale signal is present at all seven sites. Highest levels were measured at site HZ in November 2016 (Figure 39).
- High levels in June/July 2016 at site BP may be due to strong currents that result in hydrophone cable strumming (Figure 45).
- High levels at low frequencies (10-20 Hz) at site BS may be due to strong currents that result in hydrophone cable strumming (Figure 46).
- There is a year-round presence of an unidentified down sweeping signal between ~800-400 Hz at site HZ that can be clearly seen in the summer and fall monthly sound pressure spectrum level averages (Figure 39). In July / August 2016, the signal has its highest signal-to-noise ratio (SNR) due to otherwise particularly low ambient sound levels, with signal levels in that band reaching ~2.5 dB above ambient levels.

Site	Month / Year	Days of Data / Days in Month
WAT_HZ_02	Apr-2016	08/30
	Jun-2017	18/30
WAT_OC_02	Apr-2016	06/30
	May-2017	17/31
WAT_NC_02	Apr-2016	09/30
	May-2017	23/31
WAT_BC_01	Apr-2016	10/30
	Jun-2017	10/30
WAT_WC_01	Apr-2016	10/30
WAT_GS_01	Jun-2017	26/30
WAT_BP_01	Apr-2016	02/30
	Jun-2017	26/30
WAT_BS_01	Apr-2016	03/30
	Aug-2016	27/31
	Jun-2017	25/30

Table 3. Incomplete months included in the ambient soundscape analysis during this recording period.

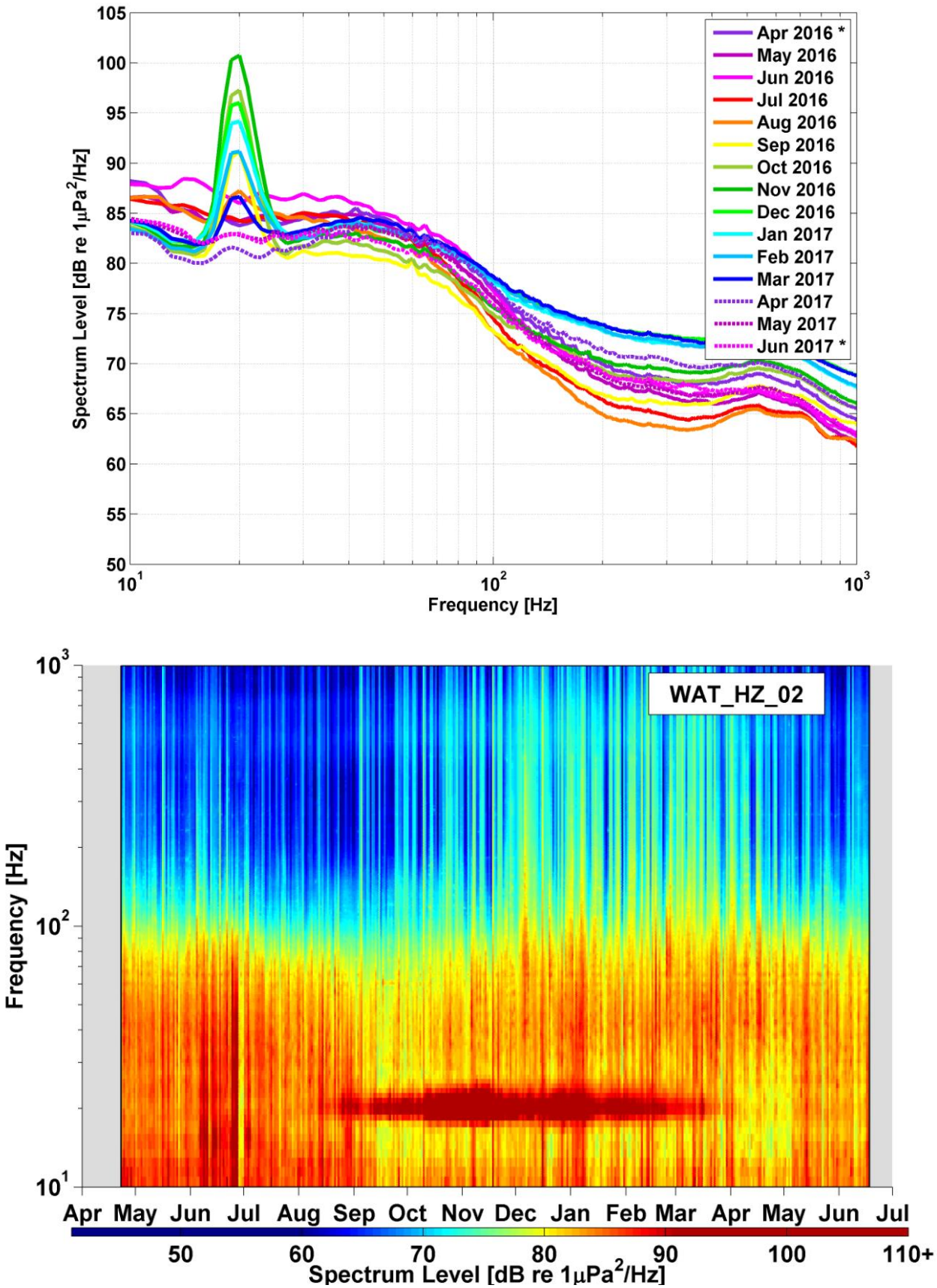

Figure 39. Low-frequency ambient soundscape at site HZ from April 2016 to May 2017 (top). Legend gives color-coding by month. Months with an asterisk (*) have partial recording effort. Long-term spectrograms using daily-averaged spectra for site HZ from April 2016 to June 2017 (bottom).

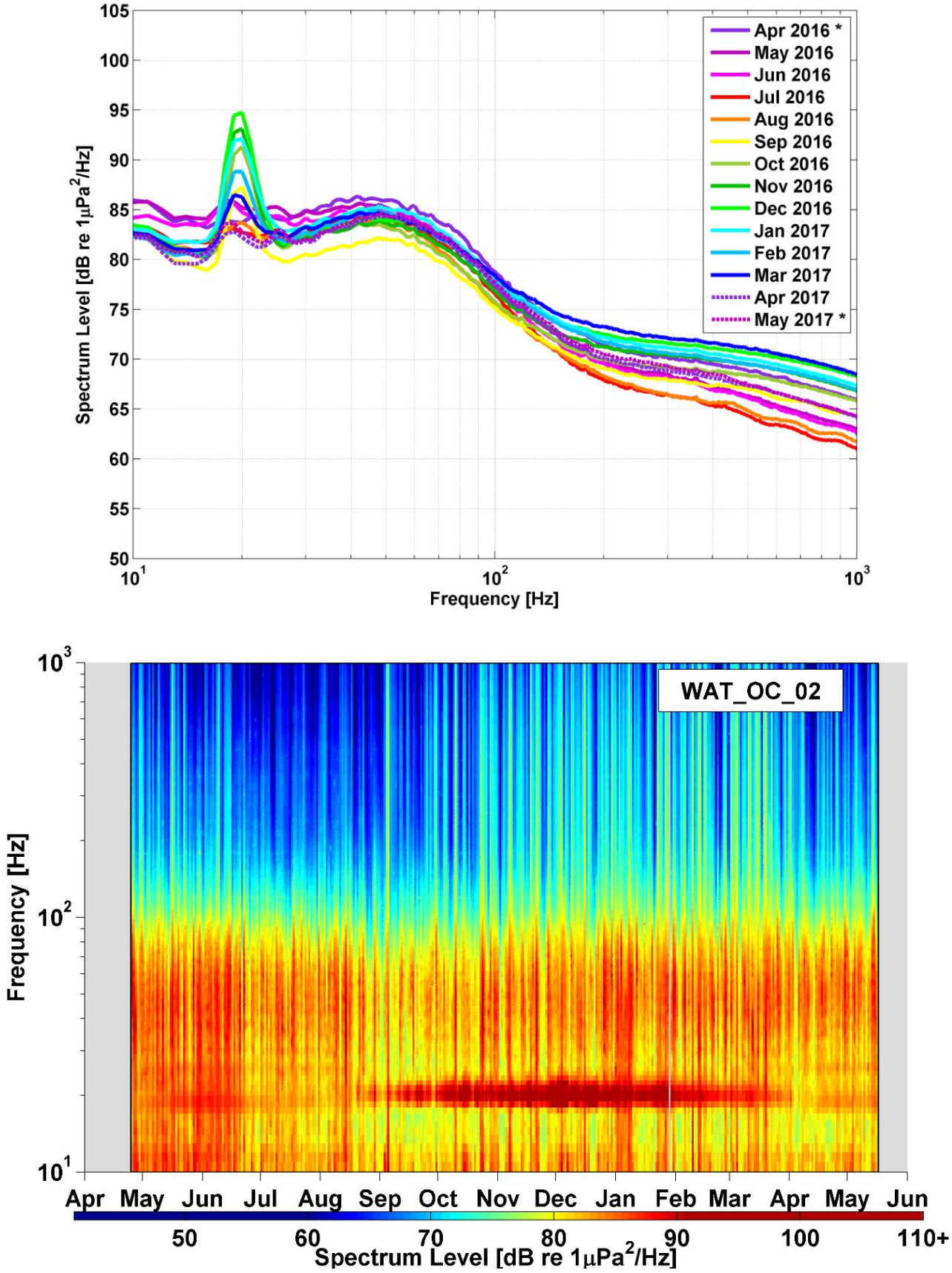

Figure 40. Low-frequency ambient soundscape at site OC from April 2016 to May 2017 (top). Legend gives color-coding by month. Months with an asterisk (*) have partial recording effort. Long-term spectrograms using daily-averaged spectra for site OC from April 2016 to June 2017 (bottom).

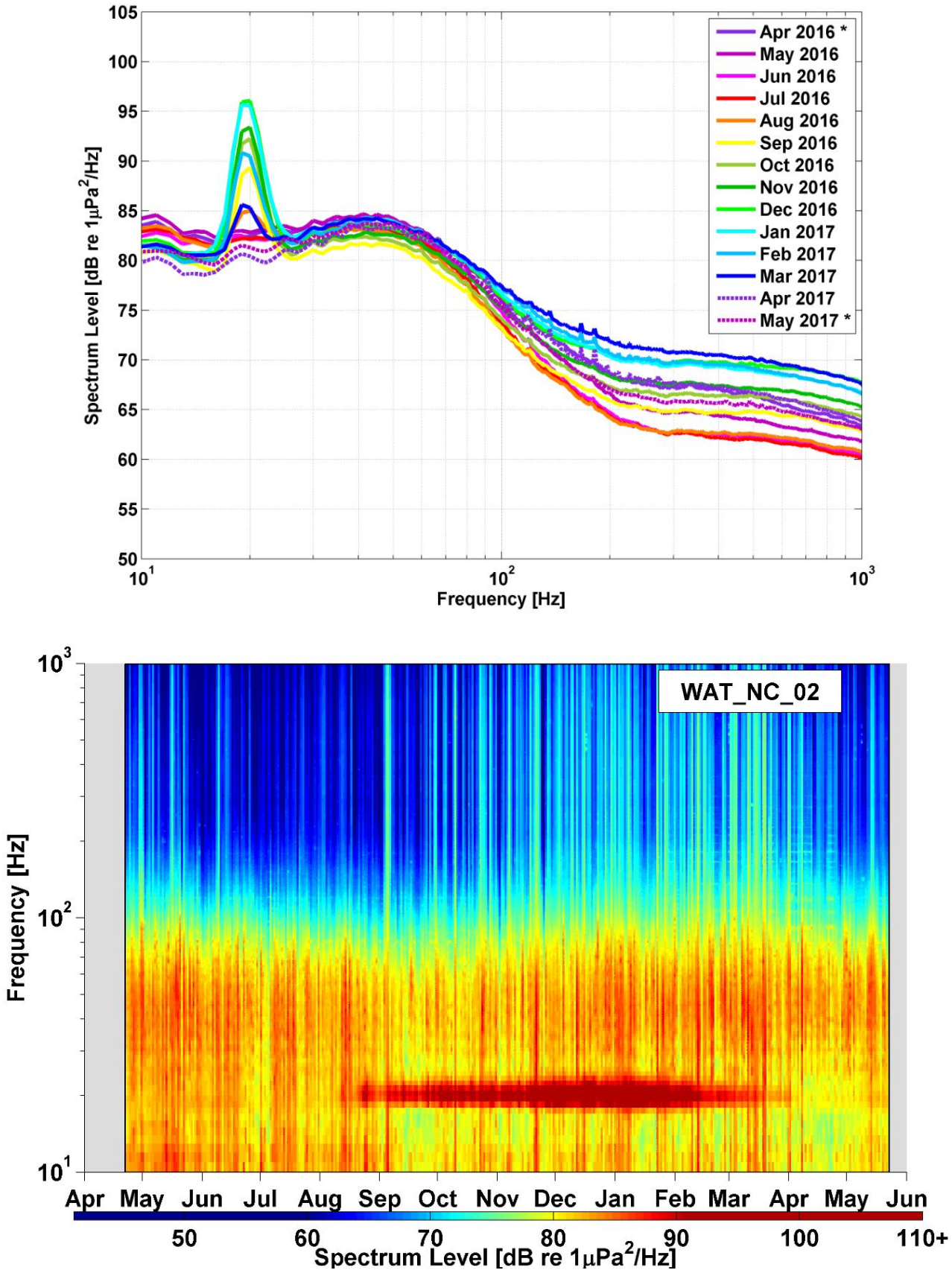

Figure 41. Low-frequency ambient soundscape at site NC from April 2016 to June 2017 (top). Legend gives color-coding by month. Months with an asterisk (*) have partial recording effort. Long-term spectrograms using daily-averaged spectra for site NC from April 2016 to June 2017 (bottom).

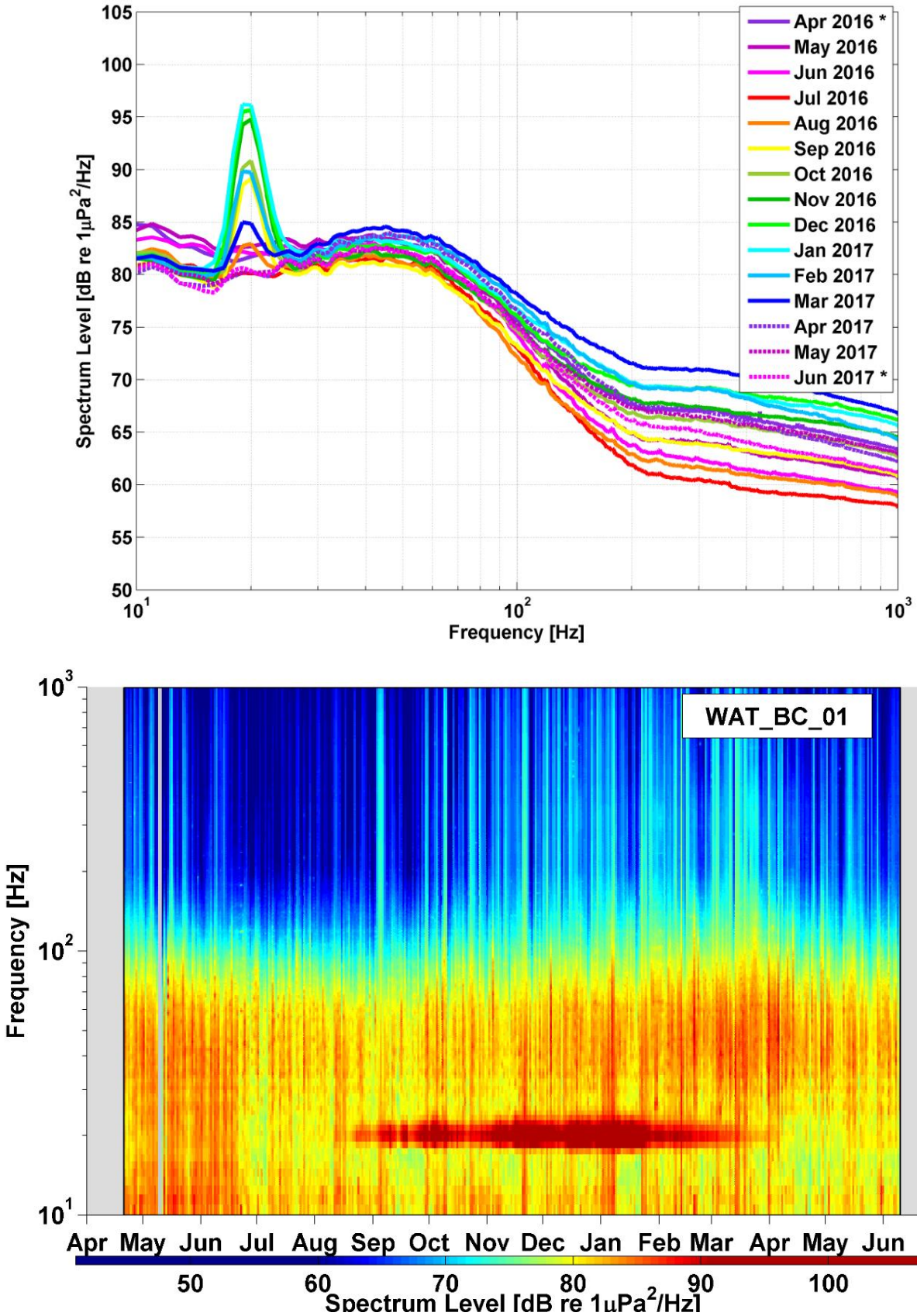

Figure 42. Low-frequency ambient soundscape at site BC from April 2016 to June 2017 (top). Legend gives color-coding by month. Months with an asterisk (*) have partial recording effort. Long-term spectrograms using daily-averaged spectra for site BC from April 2016 to June 2017 (bottom).

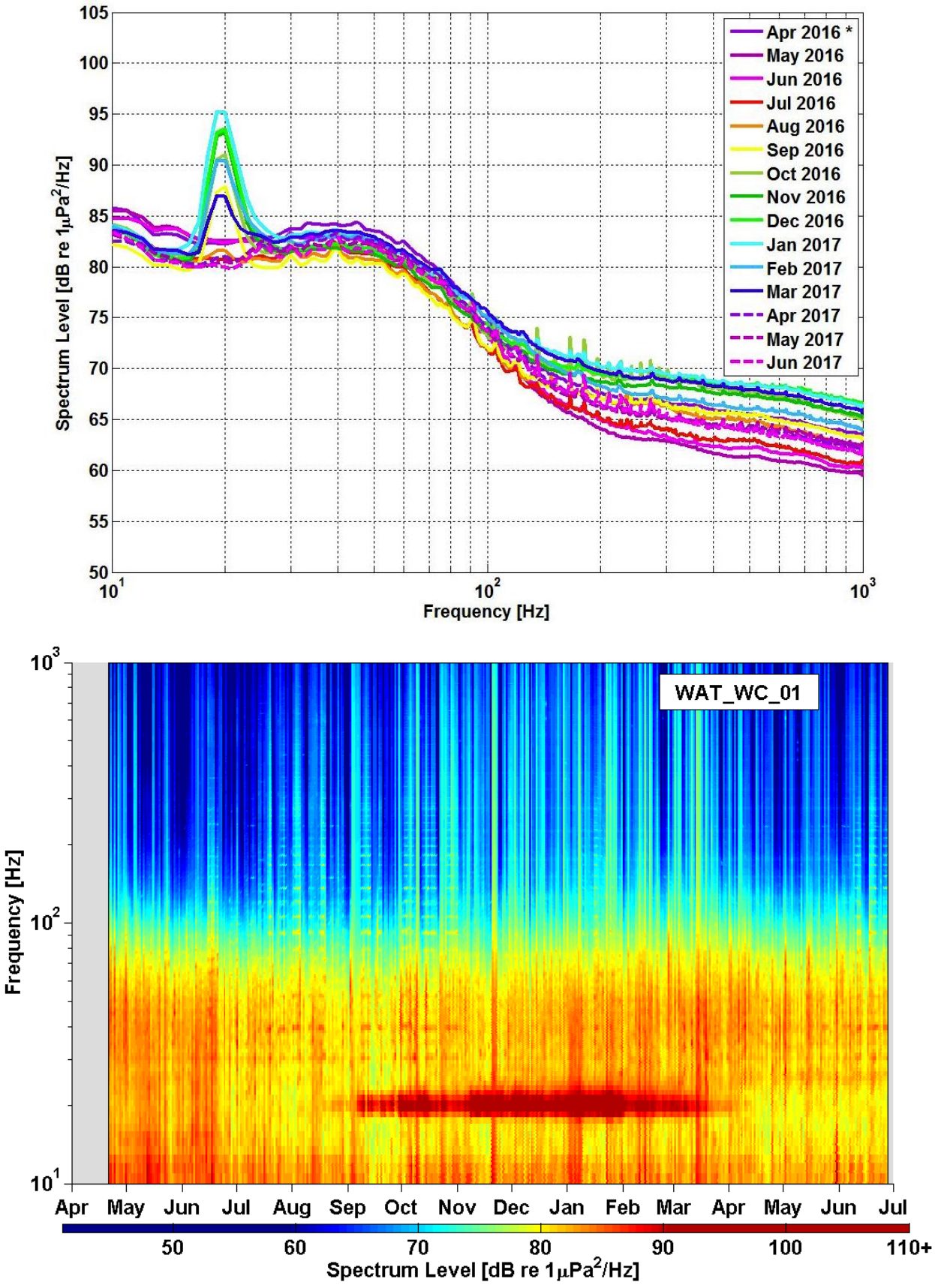

Figure 43. Low-frequency ambient soundscape at site WC from April 2016 to June 2017 (top). Legend gives color-coding by month. Months with an asterisk (*) have partial recording effort. Long-term spectrograms using daily-averaged spectra for site WC from April 2016 to June 2017 (bottom).

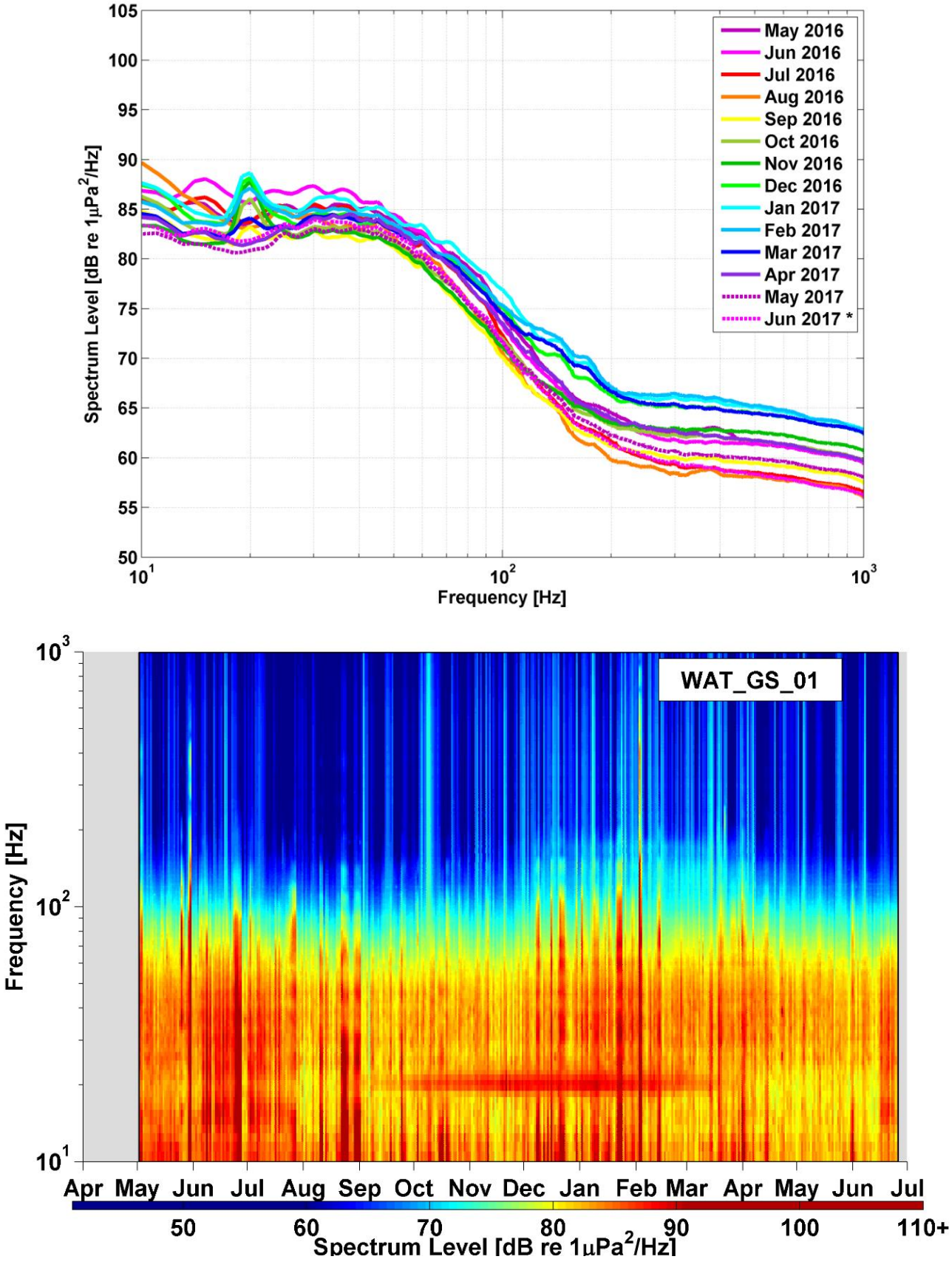

Figure 44. Low-frequency ambient soundscape at site GS from April 2016 to June 2017 (top). Legend gives color-coding by month. Months with an asterisk (*) have partial recording effort. Long-term spectrograms using daily-averaged spectra for site GS from April 2016 to June 2017 (bottom).

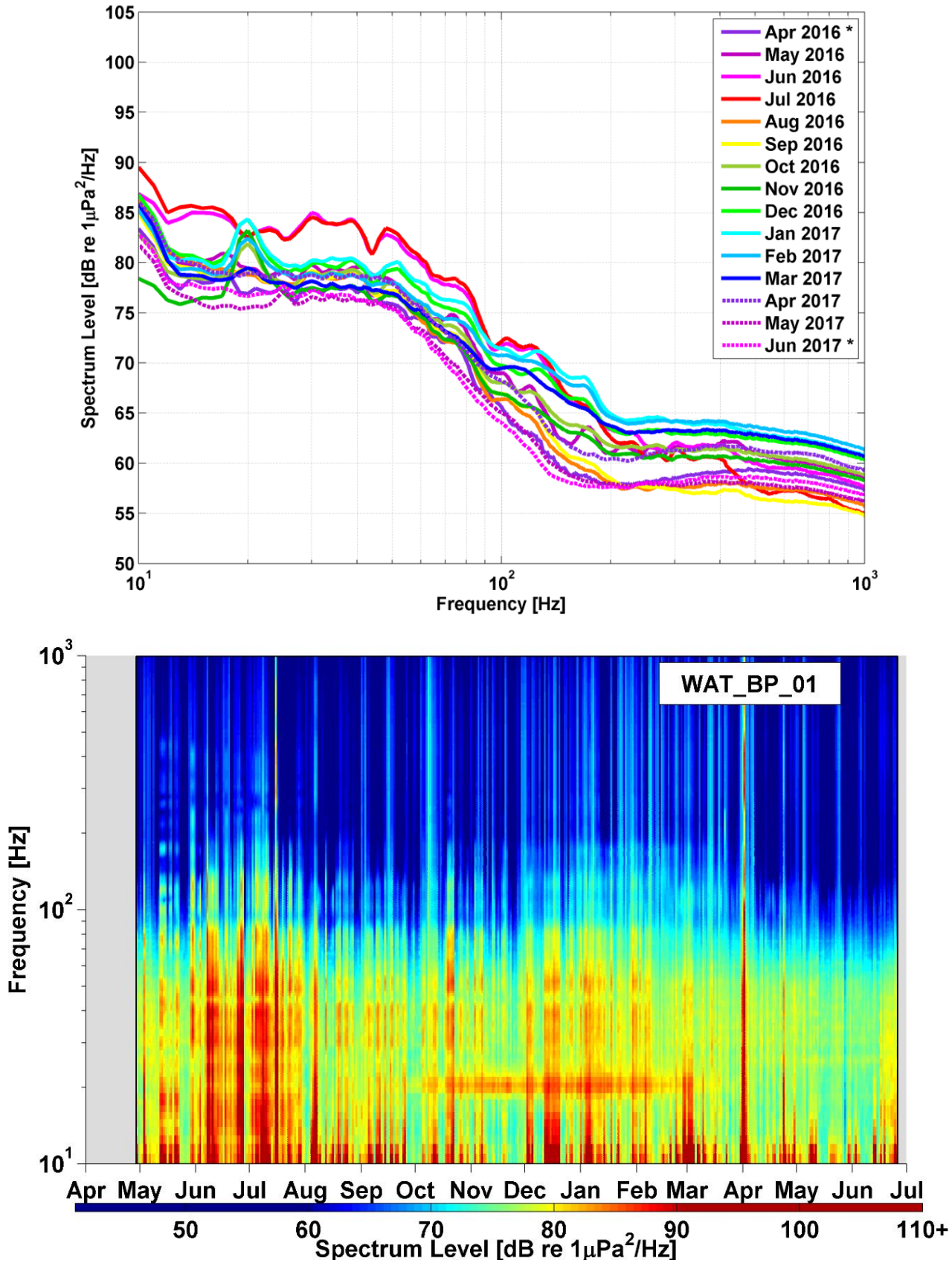

Figure 45. Low-frequency ambient soundscape at site BP from April 2016 to June 2017 (top). Legend gives color-coding by month. Months with an asterisk (*) have partial recording effort. Long-term spectrograms using daily-averaged spectra for site BP from April 2016 to June 2017 (bottom).

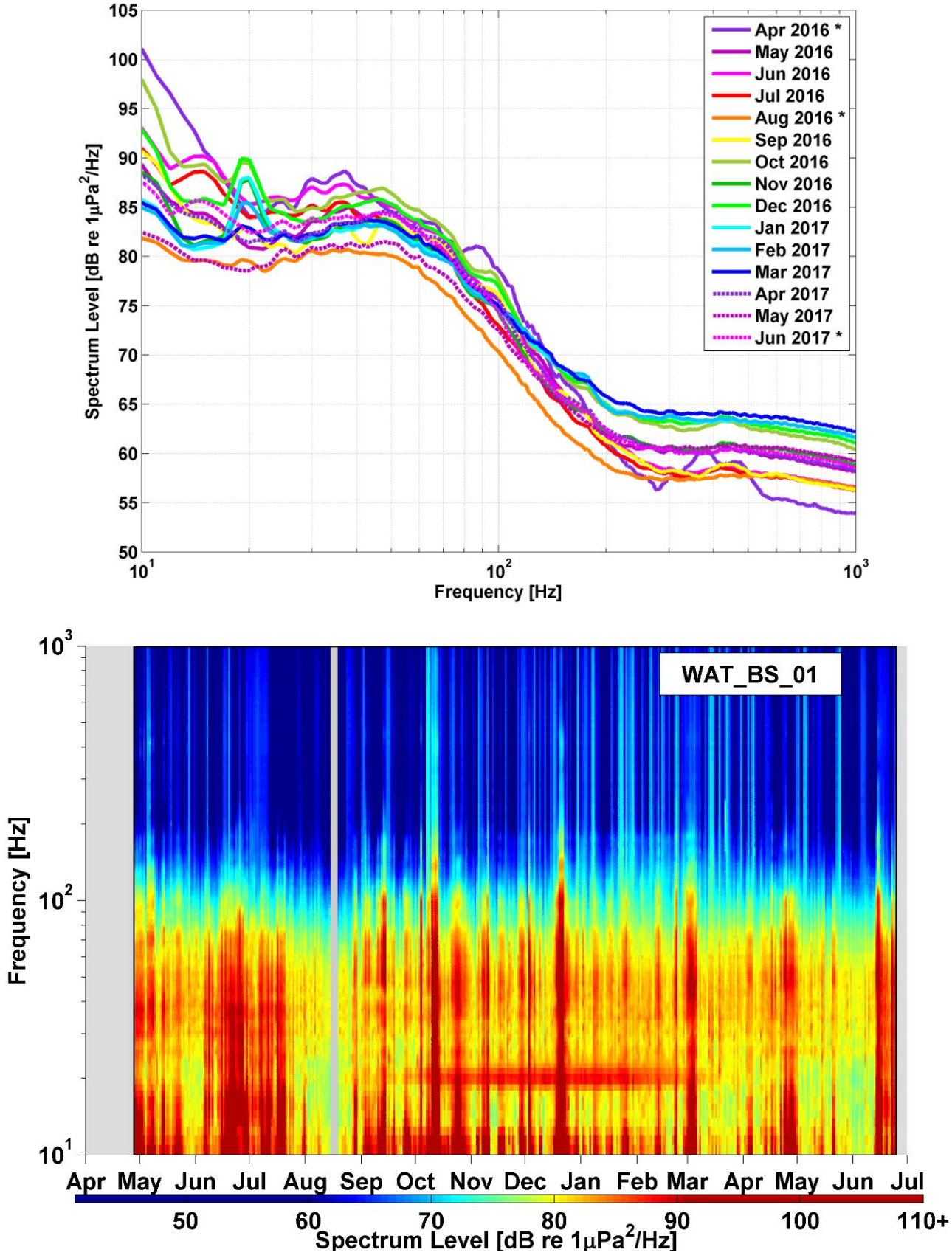

Figure 46. Low-frequency ambient soundscape at site BS from April 2016 to June 2017 (top). Legend gives color-coding by month. Months with an asterisk (*) have partial recording effort. Long-term spectrograms using daily-averaged spectra for site BS from April 2016 to June 2017 (bottom).

Odontocetes

Beaked Whales

Detections of Cuvier's, Gervais', Sowerby's, True's and Blainville's beaked whale echolocation clicks were detected at all eight sites, however if detections are very sparse for a particular specie and site combination, presence should be interpreted with caution prior to manual verification. More details of each species' presence at all eight sites are given below.

Cuvier's Beaked Whales

- Cuvier's beaked whale echolocation clicks were detected intermittently with highest detection rates from November to March at site HZ, and elevated year round presence at site WC (Figure 47, Figure 48).
- There was no diel pattern for Cuvier's beaked whale echolocation clicks (Figure 49, Figure 50).

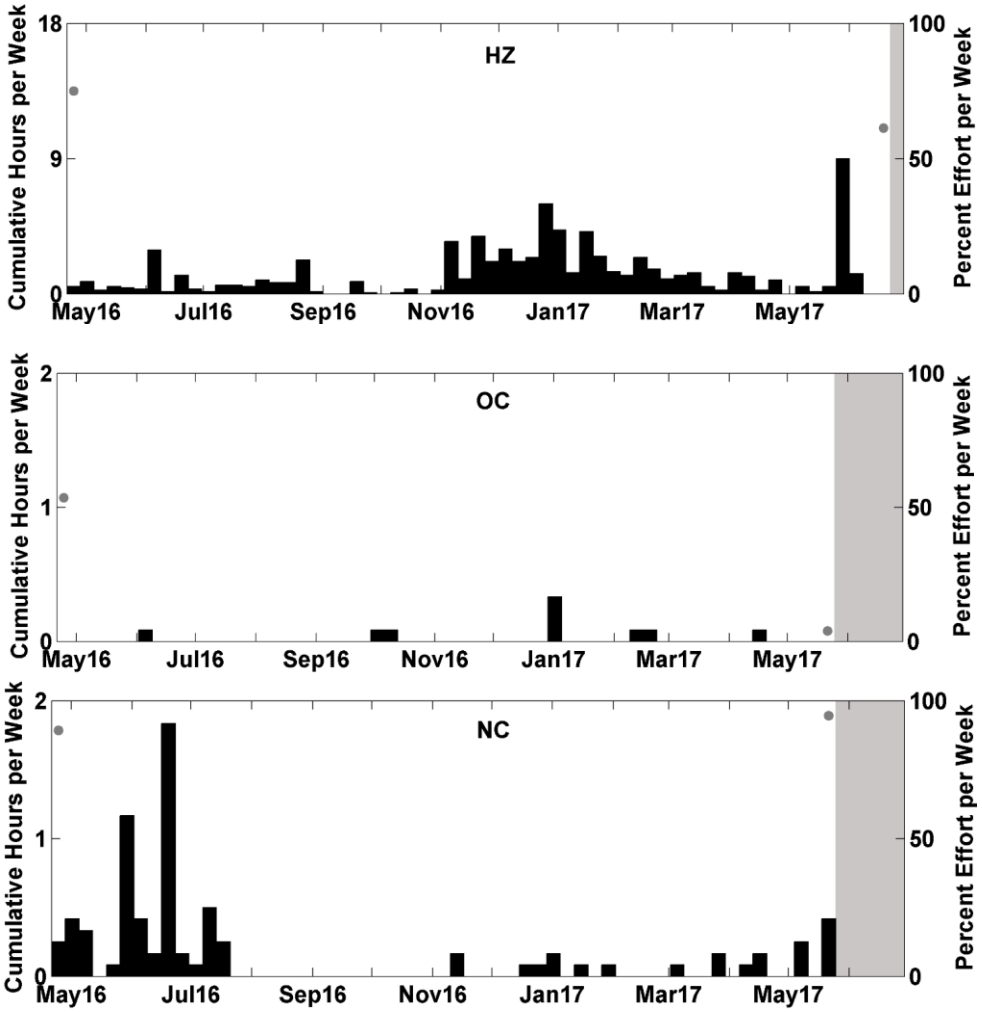

Figure 47. Weekly presence (black bars) of Cuvier's beaked whale echolocation clicks between April 2016 and June 2017 at sites NC, HZ, and OC. Gray dots represent percent of effort per week in weeks with less than 100% recording effort, and gray shading represents periods with no recording effort. Where gray dots or shading are absent, full recording effort occurred for the entire week. *Note: Axis change for site HZ due to a higher amount of Cuvier's beaked whale echolocation detections compared to the rest of the sites*.

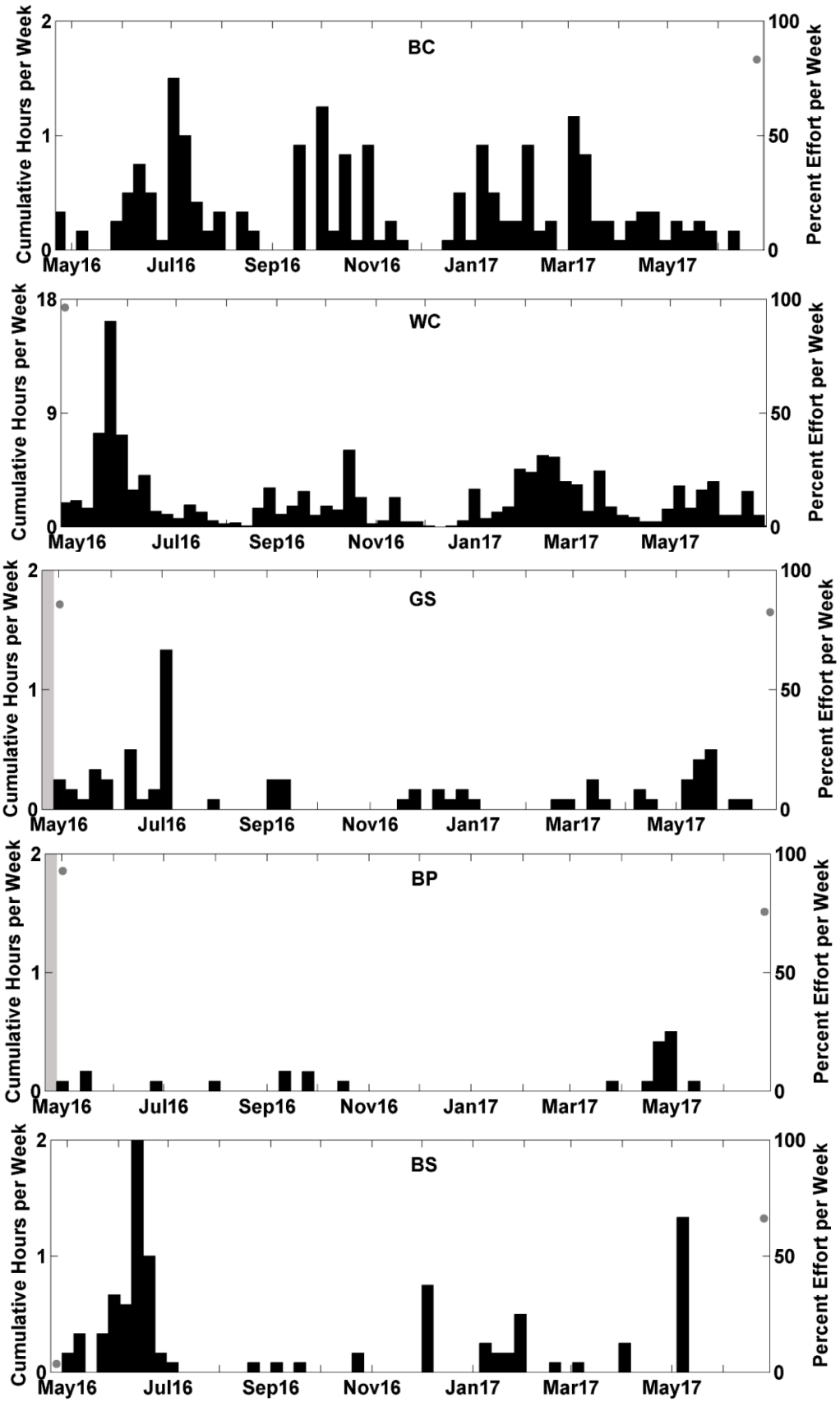

Figure 48. Weekly presence (black bars) of Cuvier's beaked whale echolocation clicks between April 2016 and June 2017 at sites BC, WC, GS, BP, and BS. Effort markings are described in Error! eference source not found. ***Note: Axis change for site WC due to a higher amount of Cuvier's beaked whale echolocation detections compared to the rest of the sites*.**

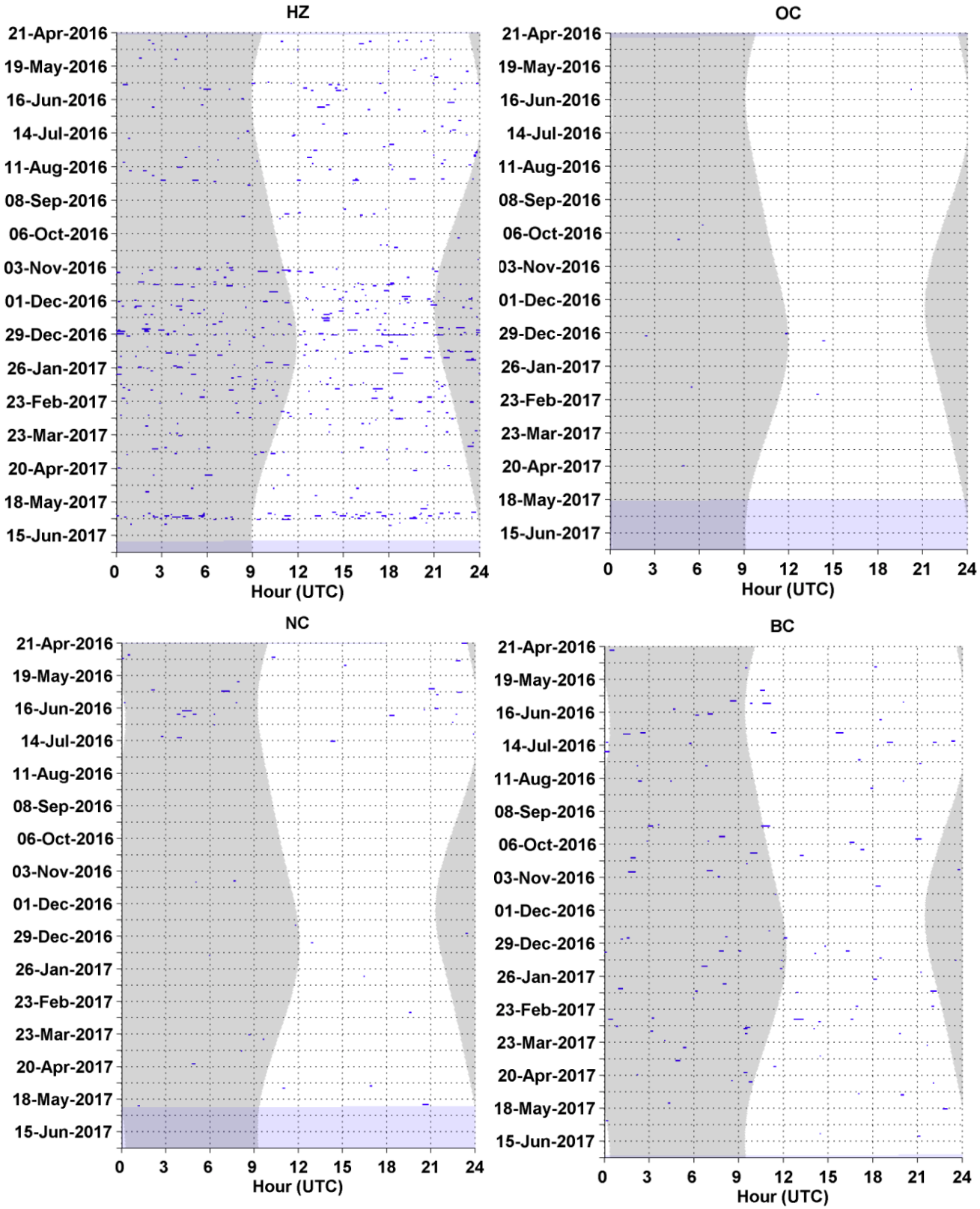

Figure 49. Cuvier's beaked whale echolocation clicks in five-minute bins (blue bars) at sites HZ, OC, NC, and BC. Gray vertical shading denotes nighttime, and light purple horizontal shading denotes absence of acoustic data.

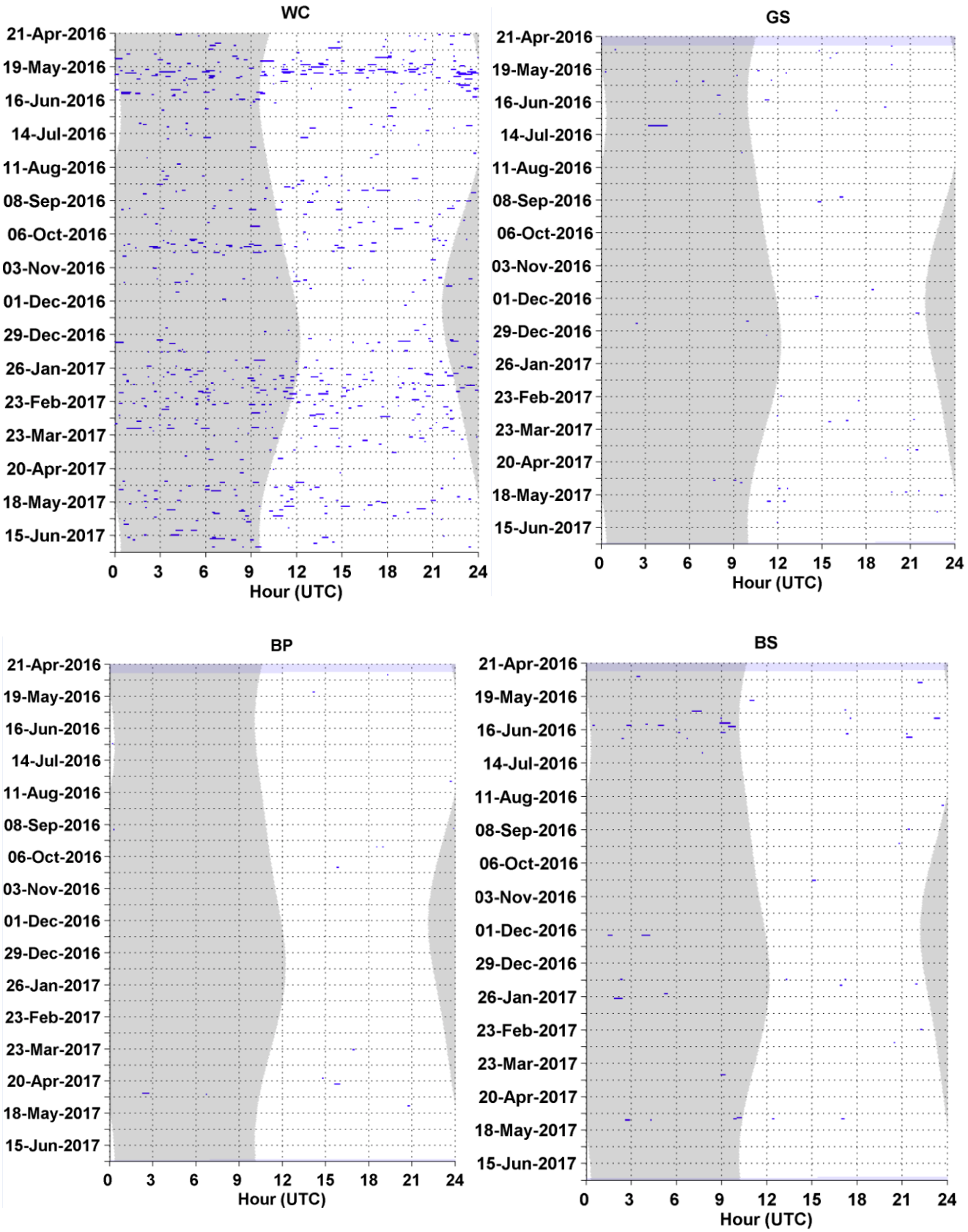

Figure 50. Cuvier's beaked whale echolocation clicks in five-minute bins (blue bars) at sites WC, GS, BP, and BS. Effort markings are described in Figure 49.

- Gervais' beaked whale echolocation clicks were primarily detected at the southernmost sites, BP and GS, between June 2016 and March 2017 (Figure 52).
- There was no diel pattern for Gervais' beaked whale echolocation clicks (Figure 53, Figure 54).

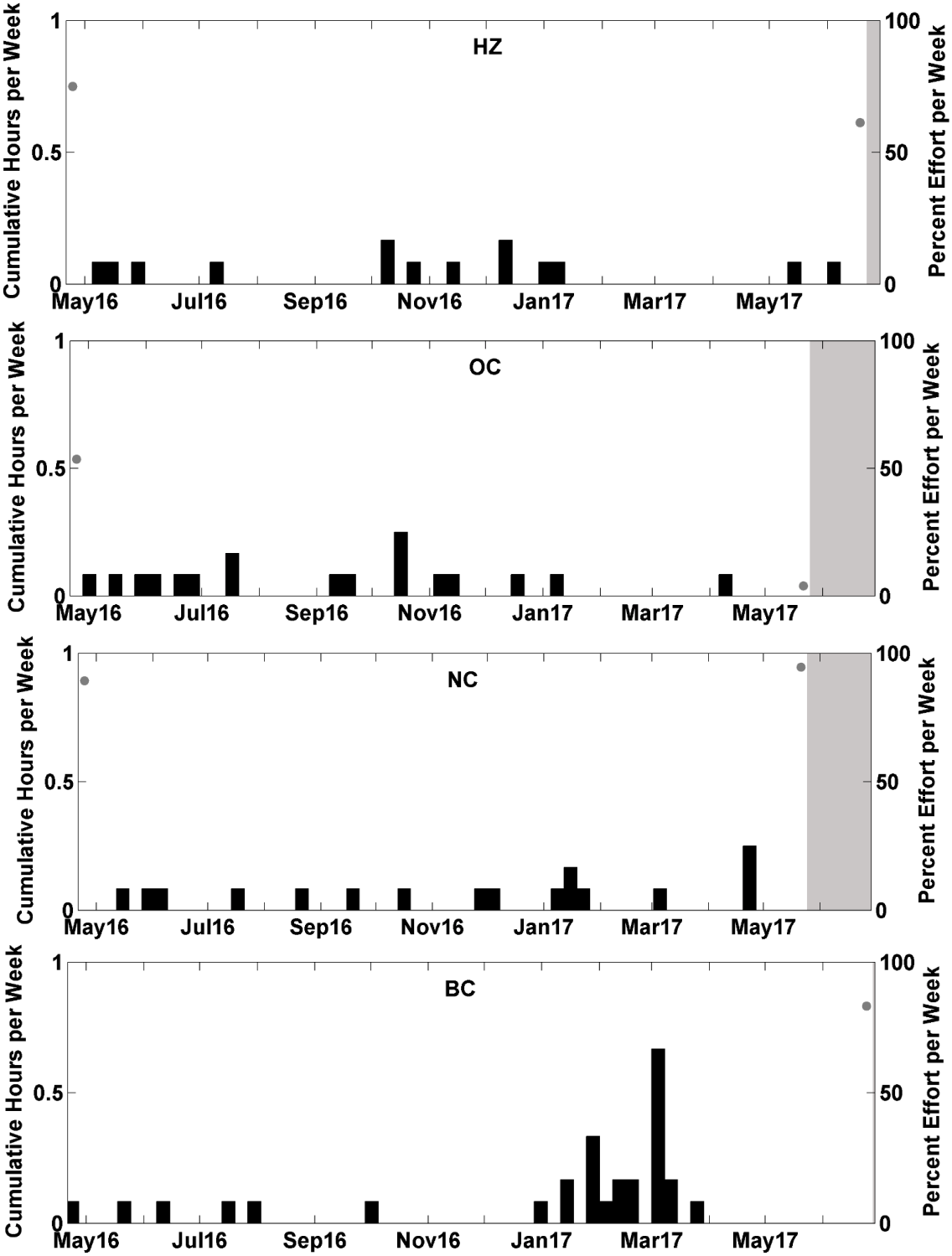

Figure 51. Weekly presence (black bars) of Gervais' beaked whale echolocation clicks between April 2016 and June 2017 at sites HZ, OC, NC, and BC. Effort markings are described in Figure 47.

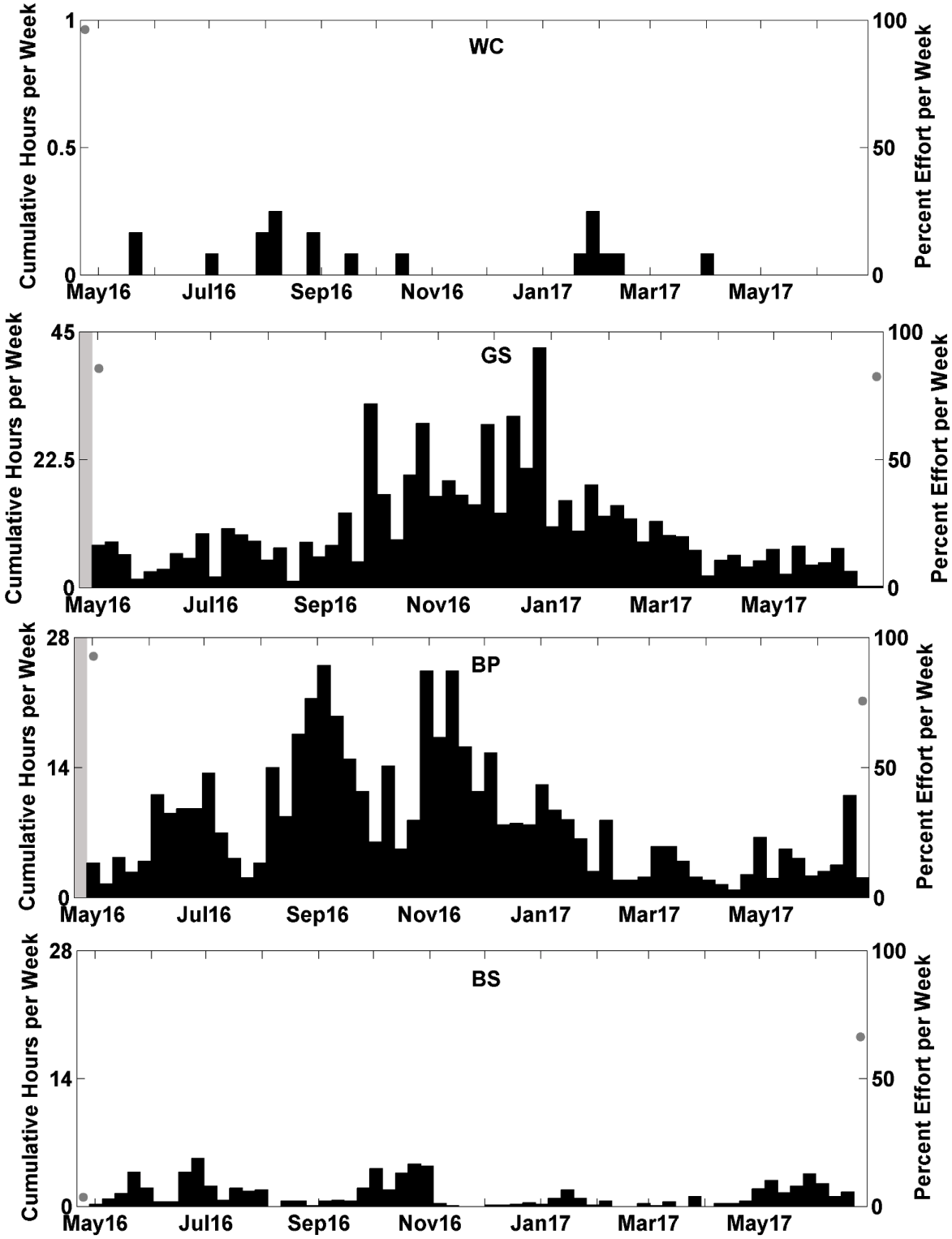

Figure 52. Weekly presence (black bars) of Gervais' beaked whale echolocation clicks between April 2016 and June 2017 at sites WC, GS, BP, and BS. Effort markings are described in Figure 47 ***Note: Axis change for sites BS, BP, and GS due to a higher amount of Gervais' beaked whale echolocation detections compared to the rest of the sites.***

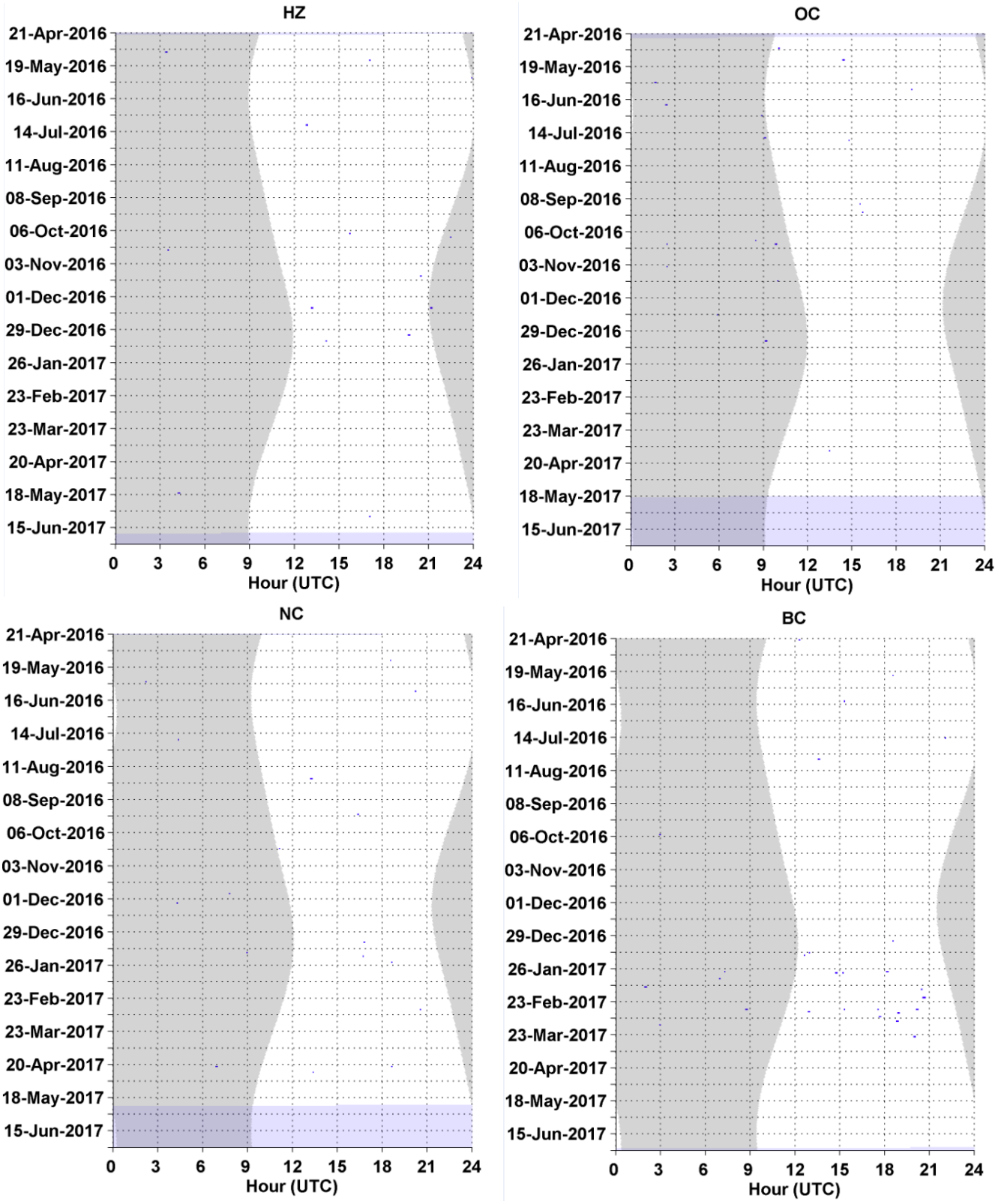

Figure 53. Gervais' beaked whale echolocation clicks in five-minute bins (blue bars) at sites HZ, OC, NC, and BC. Effort markings are described in Figure 49.

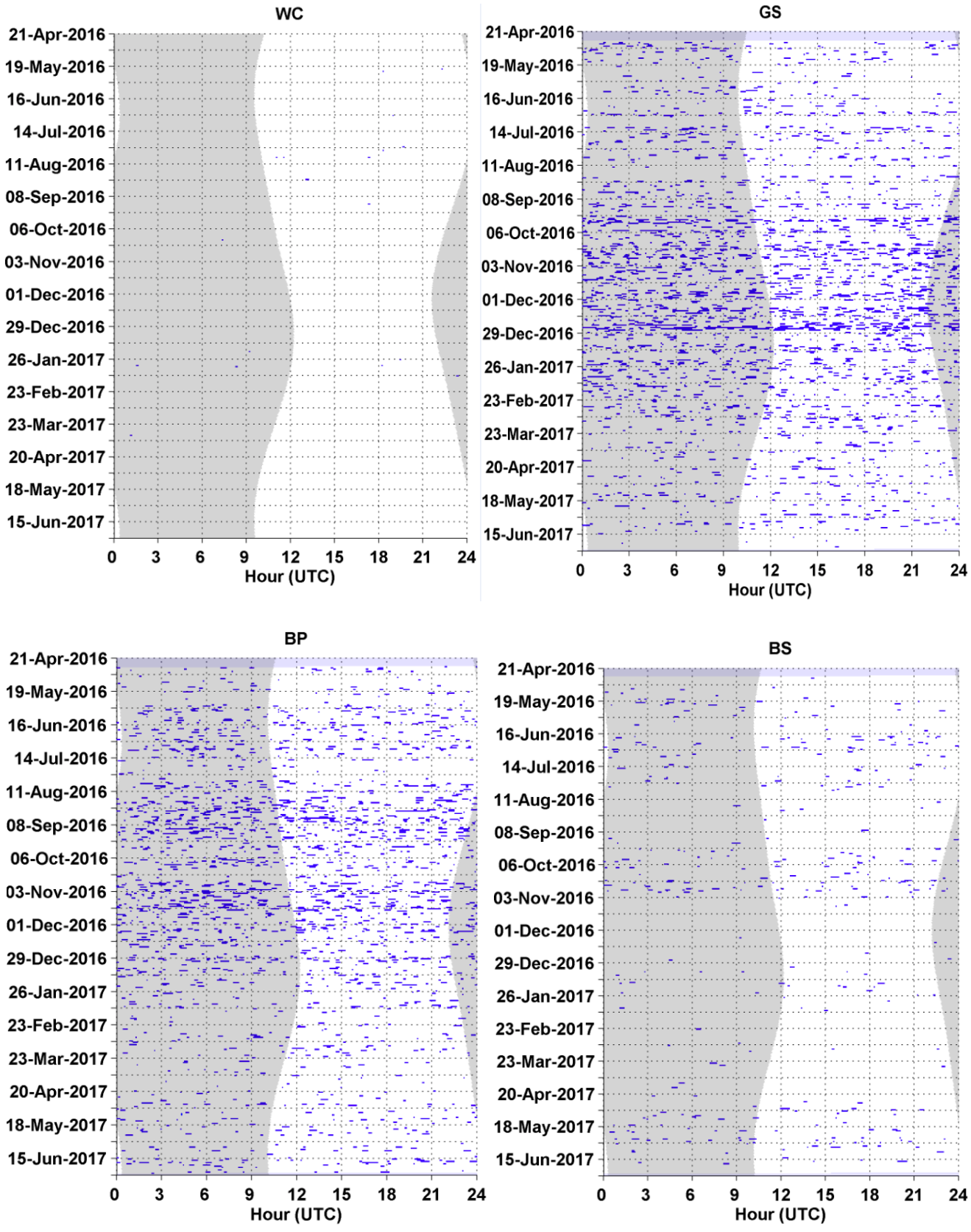

Figure 54. Gervais' beaked whale echolocation clicks in five-minute bins (blue bars) at sites WC, GS, BP, and BS. Effort markings are described in Figure 49.

- Sowerby's beaked whale echolocation clicks were primarily detected at the five northernmost sites, HZ, OC, NC, BC, and WC (Figure 55, Figure 56). At site NC, detections peaked in May 2017. There was no clear seasonal pattern at other sites (Figure 56).
- There was no diel pattern for Sowerby's beaked whale echolocation clicks (Figure 57, Figure 58).

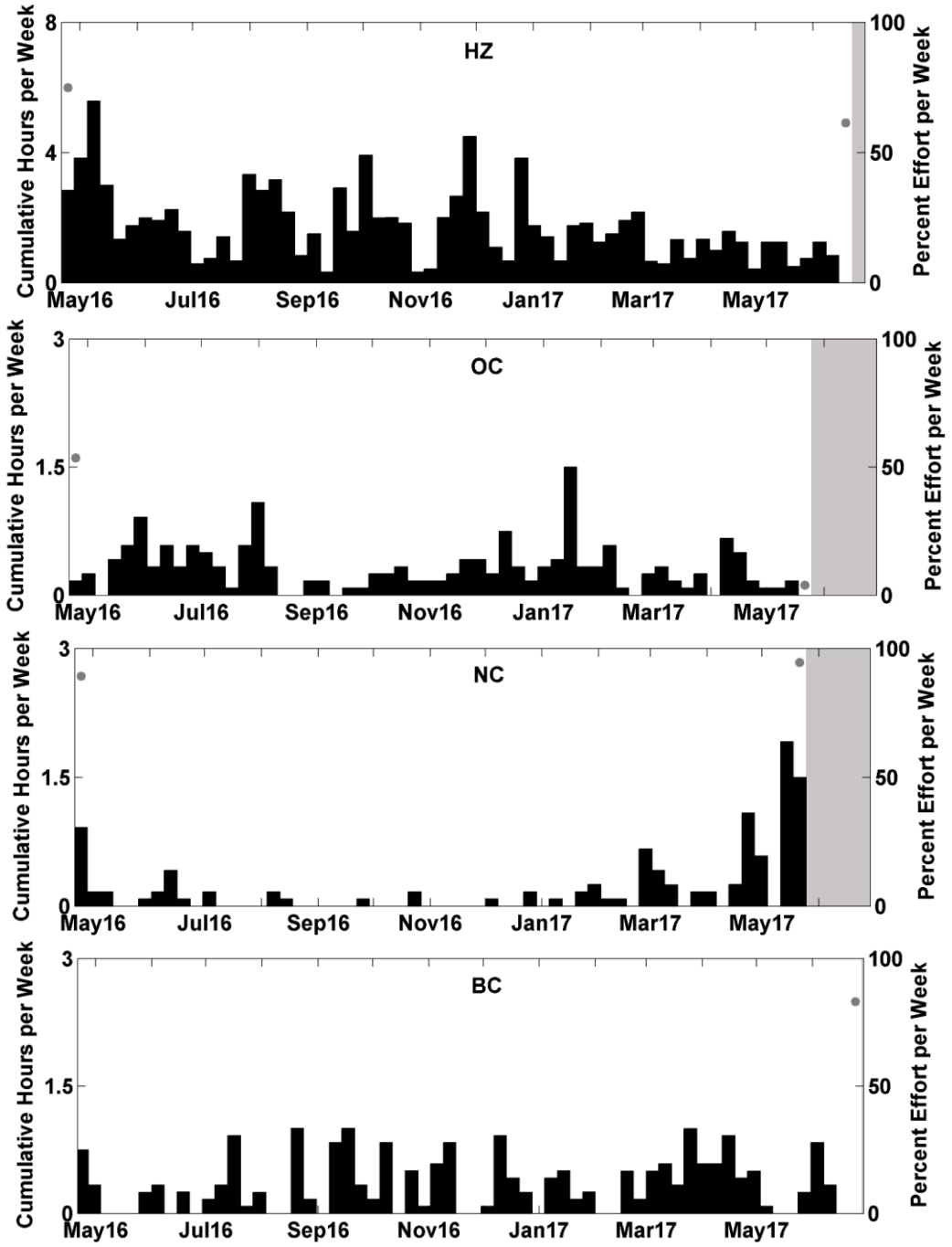

Figure 55. Weekly presence (black bars) of Sowerby's beaked whale echolocation clicks between April 2016 and June 2017 at sites HZ, OC, NC, and BC. Effort markings are described in Figure 47. *Note: Axis change for site HZ due to a higher amount of Sowerby's beaked whale echolocation detections compared to the rest of the sites*.

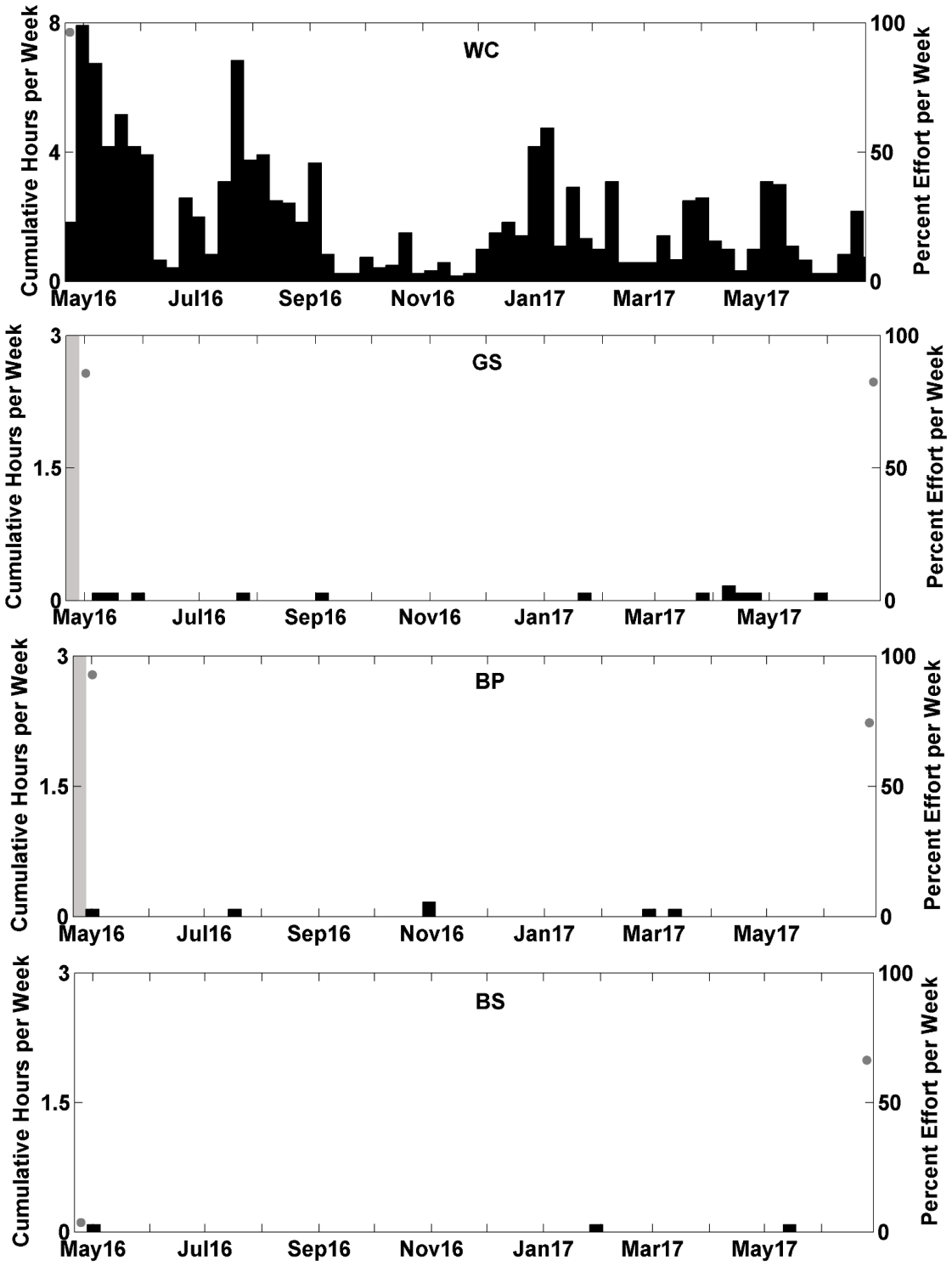

Figure 56. Weekly presence (black bars) of Sowerby's beaked whale echolocation clicks between April 2016 and June 2017 at sites WC, GS, BP, and BS. Effort markings are described in Figure 47. ***Note: Axis change for site WC due to a higher amount of Sowerby's beaked whale echolocation detections compared to the rest of the sites*****.**

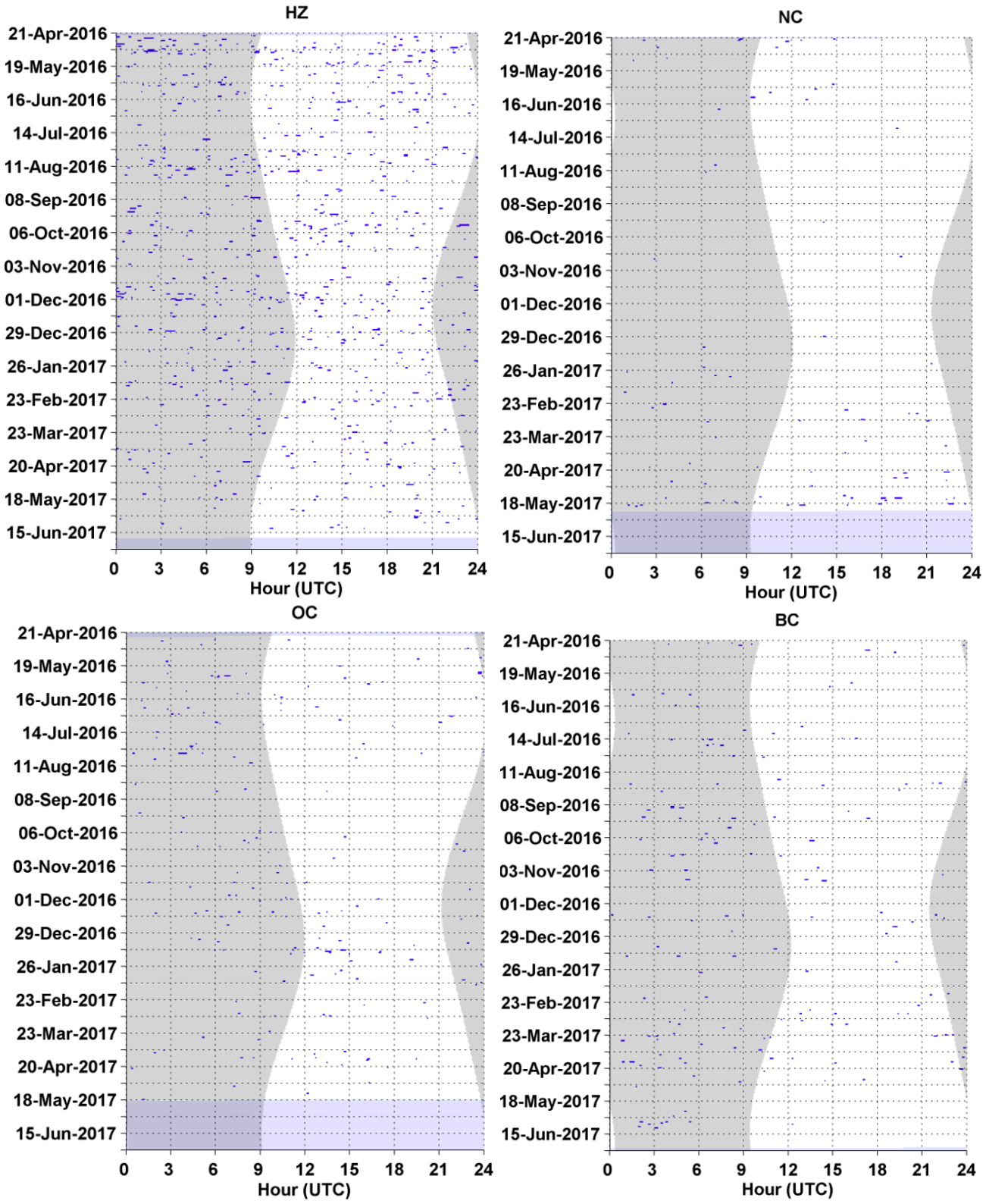

Figure 57. Sowerby's beaked whale echolocation clicks in five-minute bins (blue bars) at sites HZ, OC, NC, and BC. Effort markings are described in Figure 49.

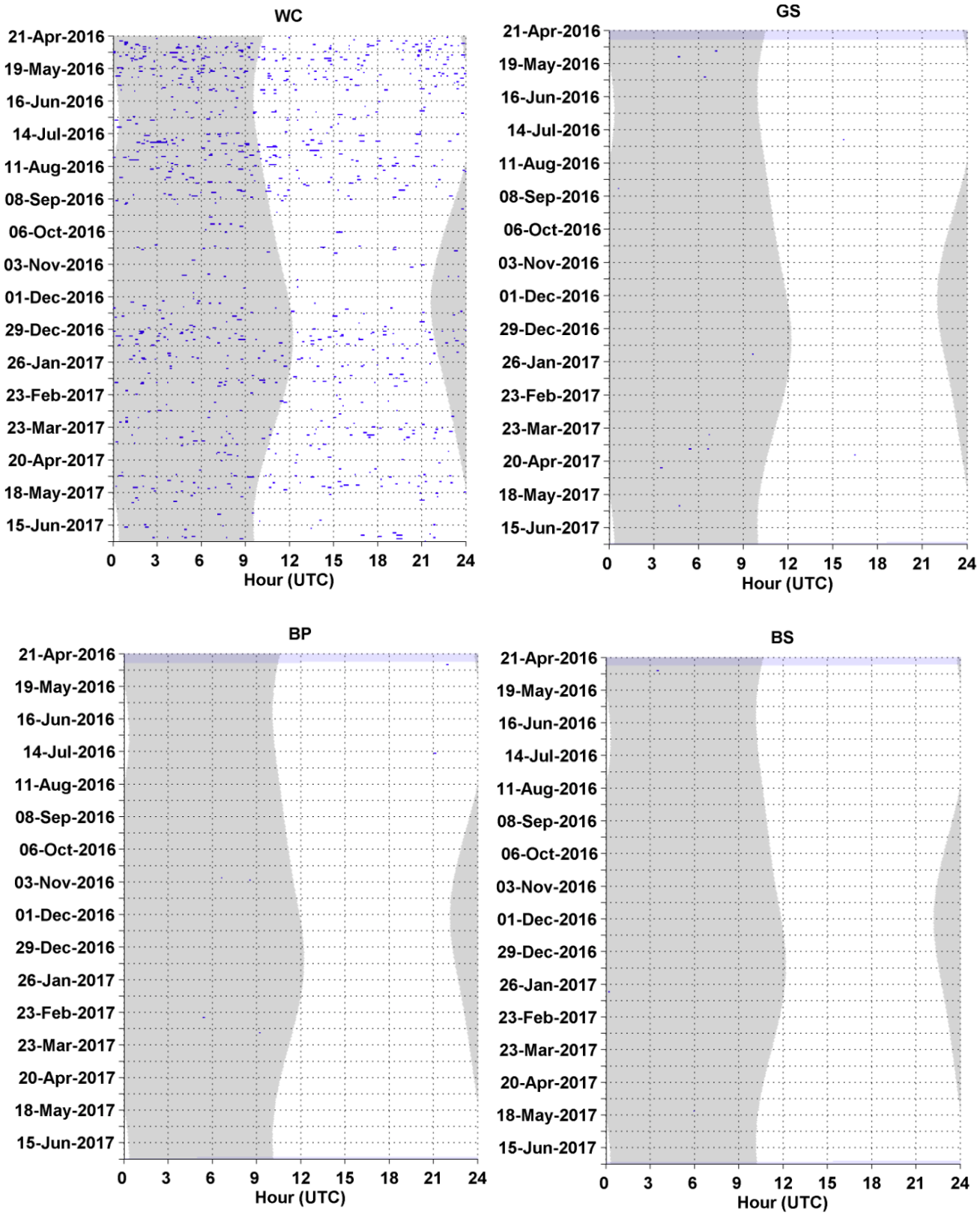

Figure 58. Sowerby's beaked whale echolocation clicks in five-minute bins (blue bars) at sites WC, GS, BP, and BS. Effort markings are described in Figure 49.

- True's beaked whales echolocation clicks were primarily detected at site NC between May and July 2016 (Figure 59). Detections at southern sites may be misclassified Gervais' detections (Figure 60).
- There was no diel pattern for True's beaked whale echolocation clicks (Figure 61, Figure 62).

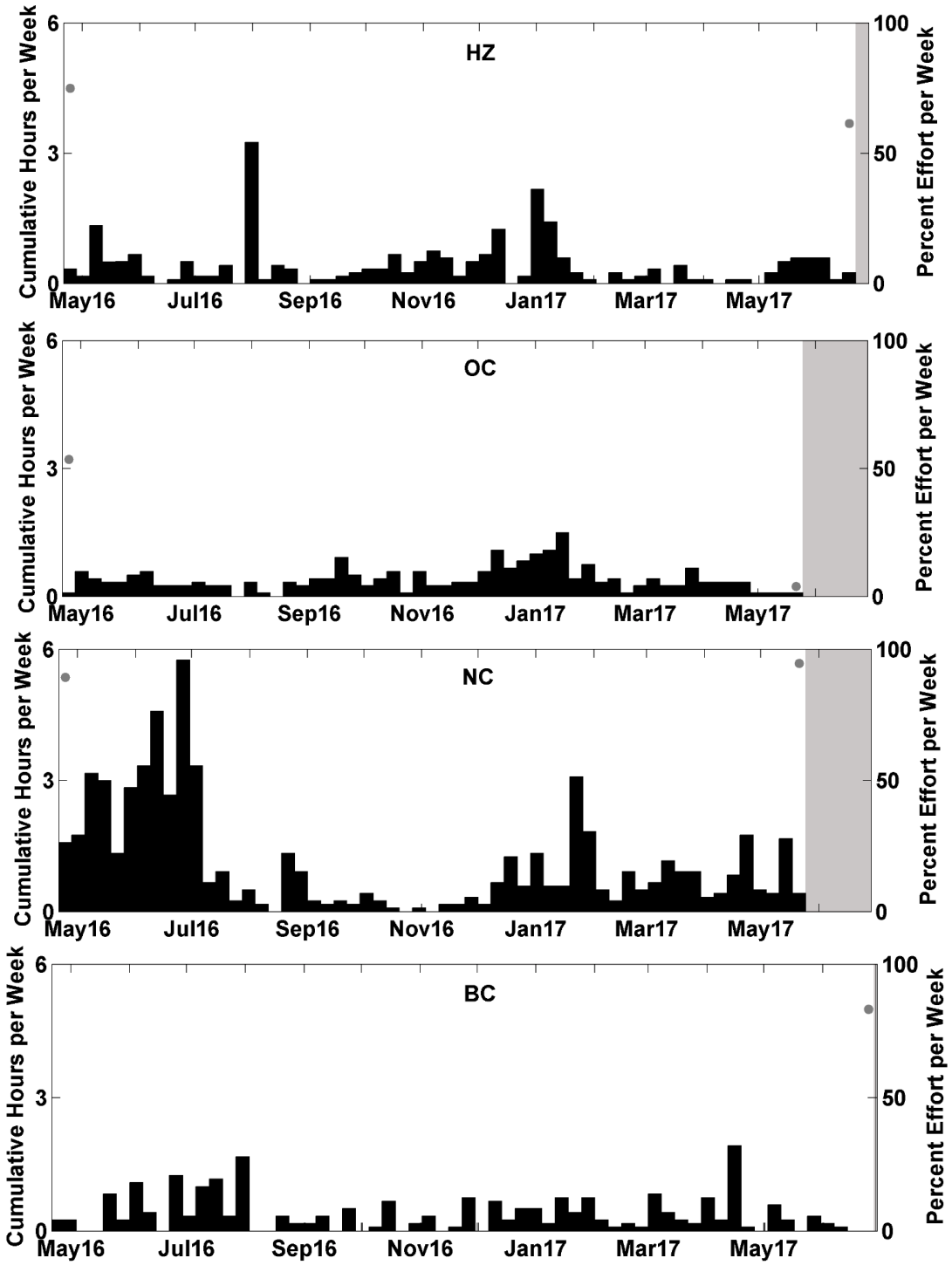

Figure 59. Weekly presence (black bars) of True's beaked whale echolocation clicks between April 2016 and June 2017 at sites HZ, OC, NC, and BC. Effort markings are described in Figure 47.

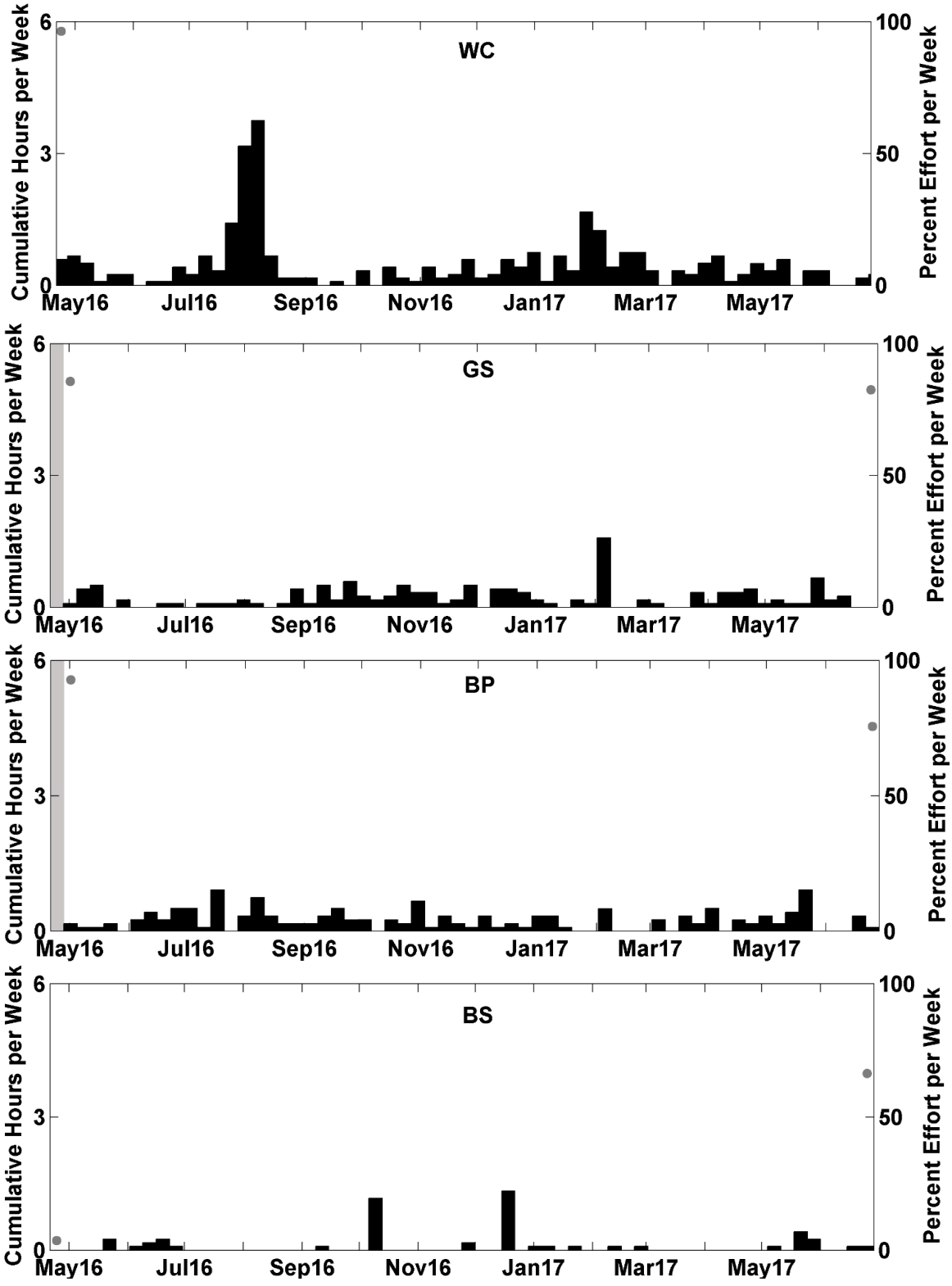

Figure 60. Weekly presence (black bars) of True's beaked whale echolocation clicks between April 2016 and June 2017 at sites WC, GS, BP, and BS. Effort markings are described in Figure 47.

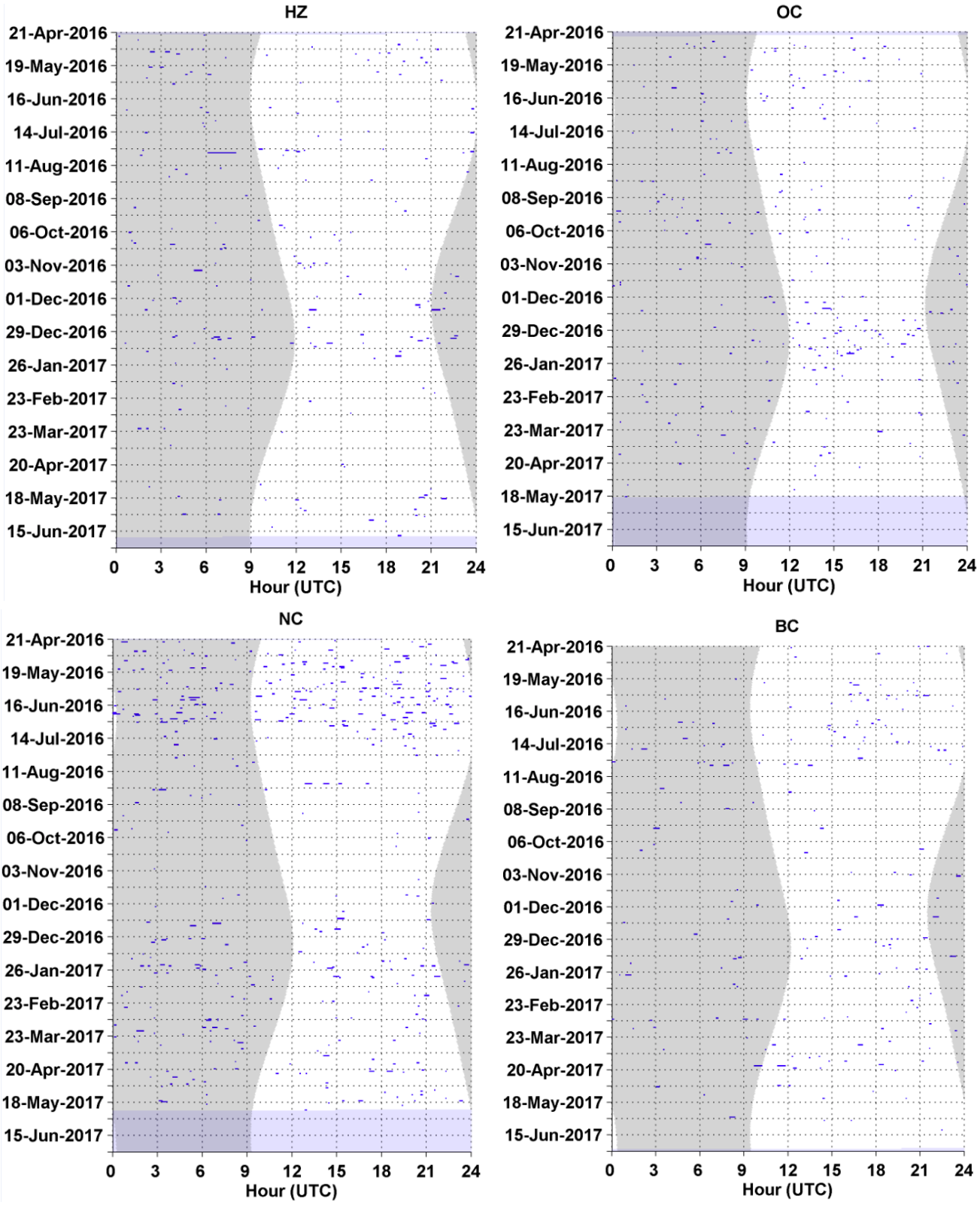

Figure 61. True's beaked whale echolocation clicks in five-minute bins (blue bars) at sites HZ, OC, NC, and BC. Effort markings are described in Figure 49.

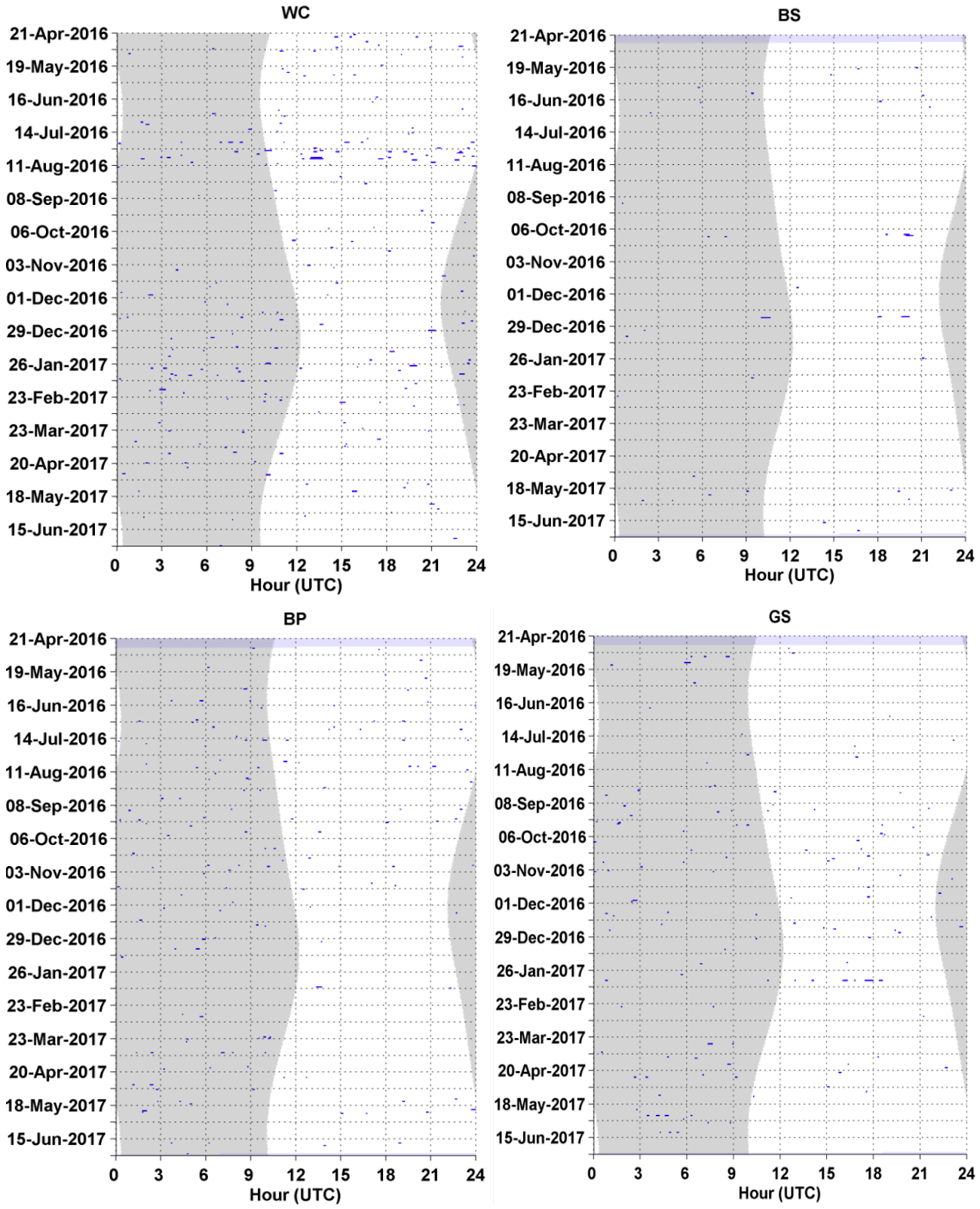

Figure 62. True's beaked whale echolocation clicks in five-minute bins (blue bars) at sites WC, GS, BP, and BS. Effort markings are described in Figure 49.

- Blainville's beaked whale echolocation clicks were primarily detected at site BS, with high detection rates from November 2016 to July 2017. (Figure 63, Figure 64).
- There was no diel pattern for Blainville's beaked whale echolocation clicks (Figure 65, Figure 66).

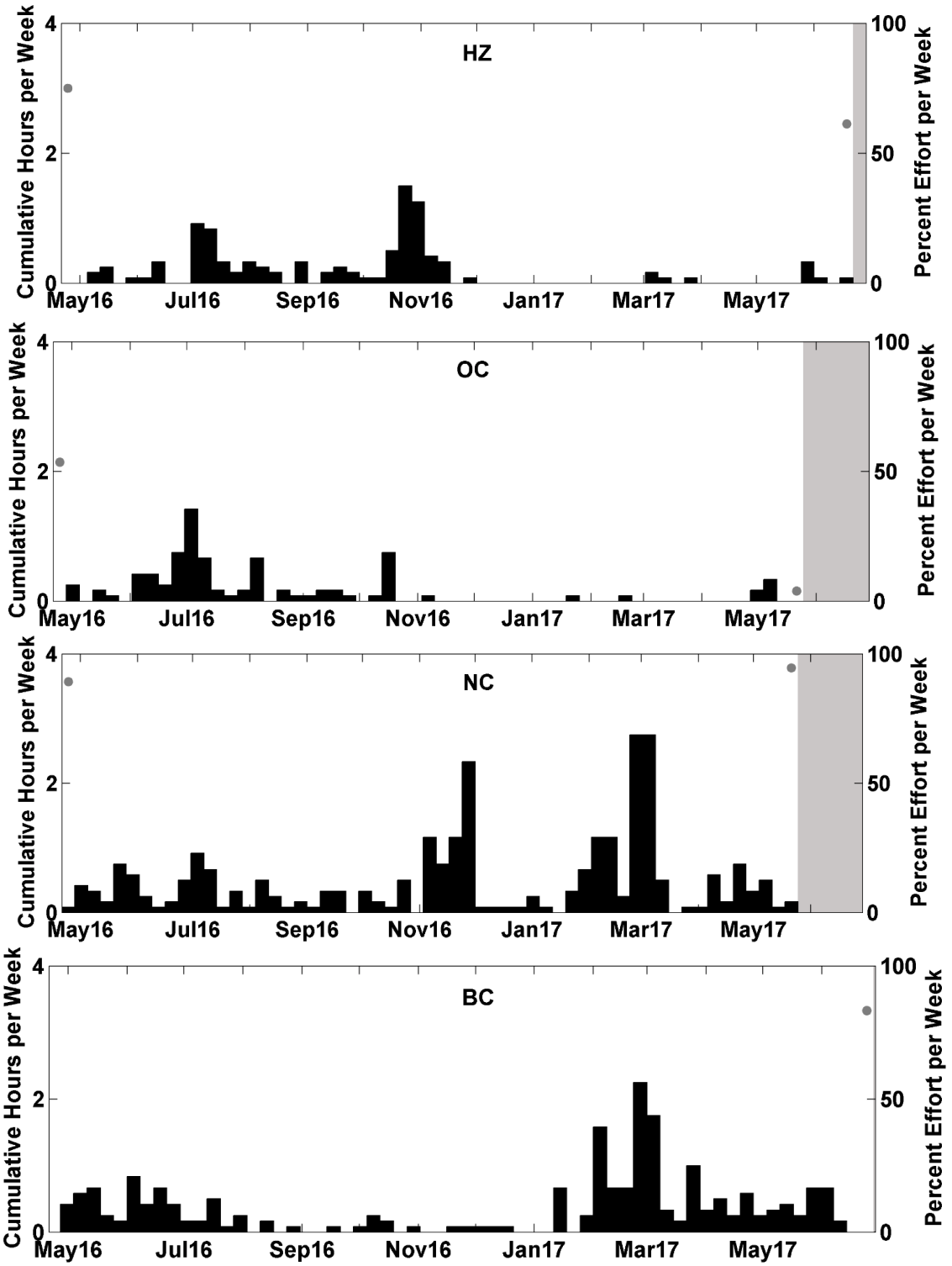

Figure 63. Weekly presence (black bars) of Blainville's beaked whale echolocation clicks between April 2016 and June 2017 at sites HZ, OC, NC, and BC. Effort markings are described in Figure 47.

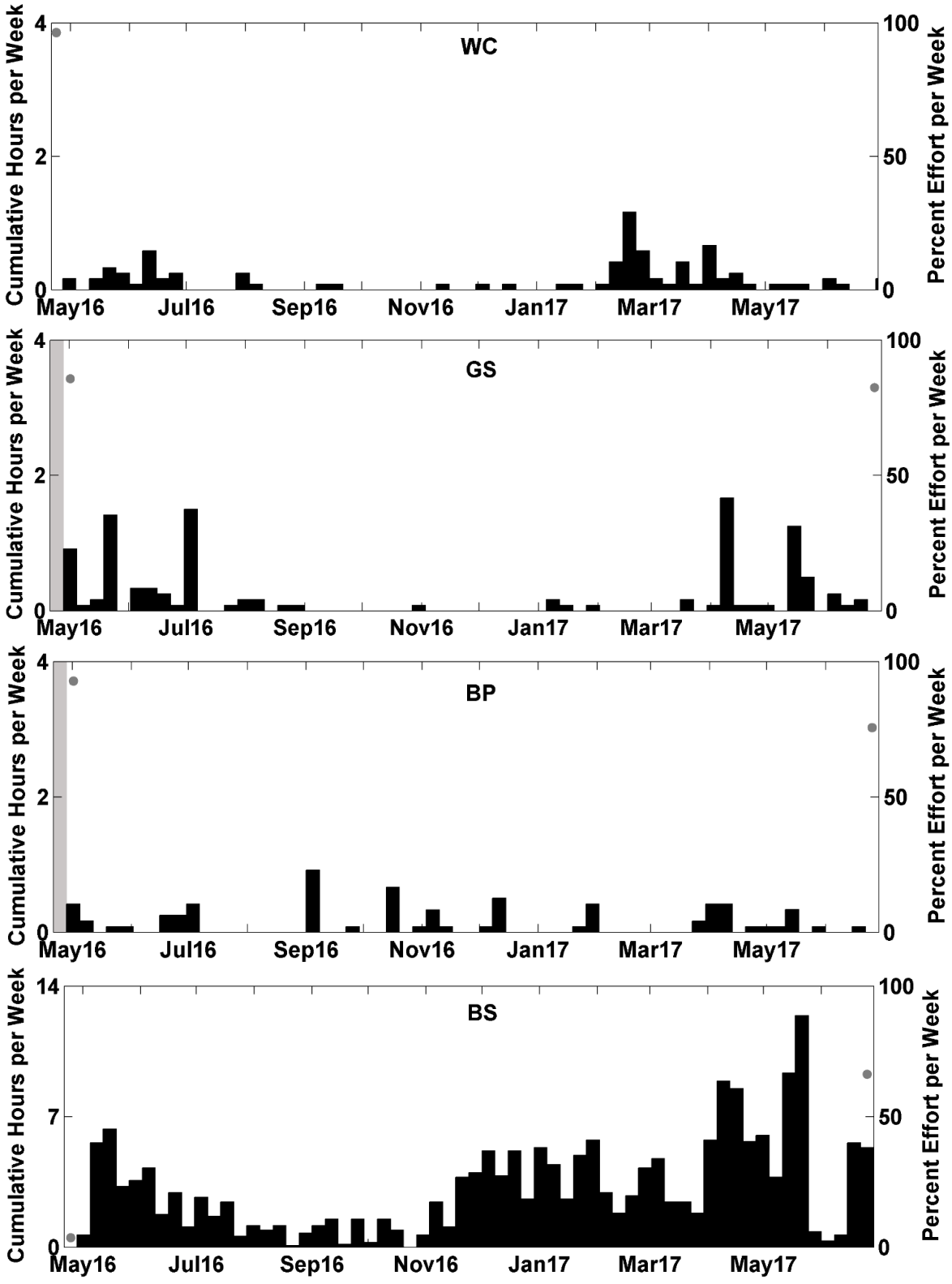

Figure 64. Weekly presence (black bars) of Blainville's beaked whale echolocation clicks between April 2016 and June 2017 at sites WC, GS, BP, and BS. Effort markings are described in Figure 47. ***Note: Axis change for site BS due to a higher amount of Blainville's beaked whale echolocation detections compared to the rest of the sites*****.**

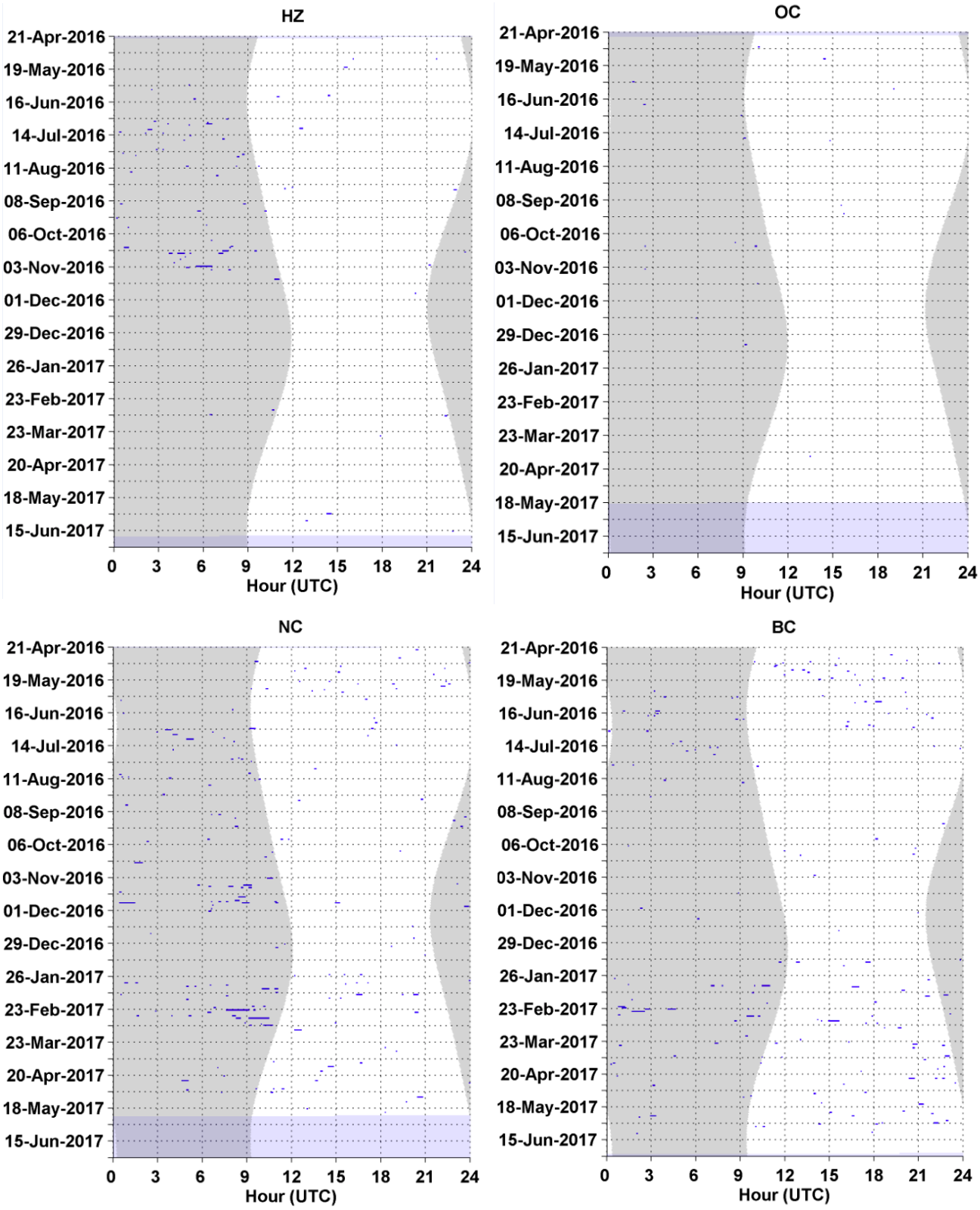

Figure 65. Blainville's beaked whale echolocation clicks in five-minute bins (blue bars) at sites HZ, OC, NC, and BC. Effort markings are described in Figure 49.

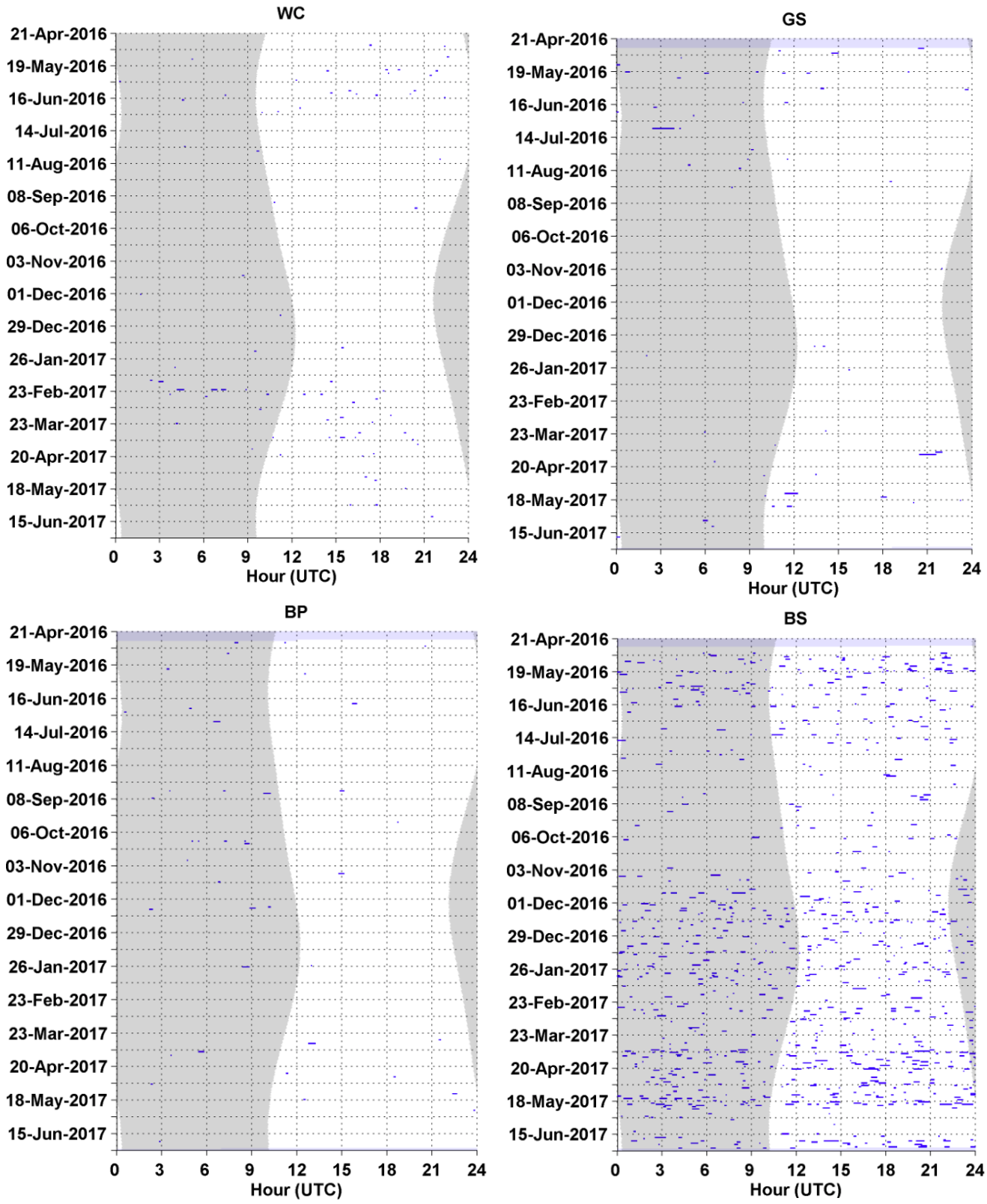

Figure 66. Blainville's beaked whale echolocation clicks in five-minute bins (blue bars) at sites WC, GS, BP, and BS. Effort markings are described in Figure 49.

Sperm Whales

- Sperm whale clicks detections occurred at all sites (Figure 67, Figure 68) with highest detection rates at sites NC and HZ (Figure 67). Detections were considerably lower at site BP compared to all the other sites (Figure 68).
- There was no diel pattern for sperm whale clicks at any of the sites (Figure 69, Figure 70).

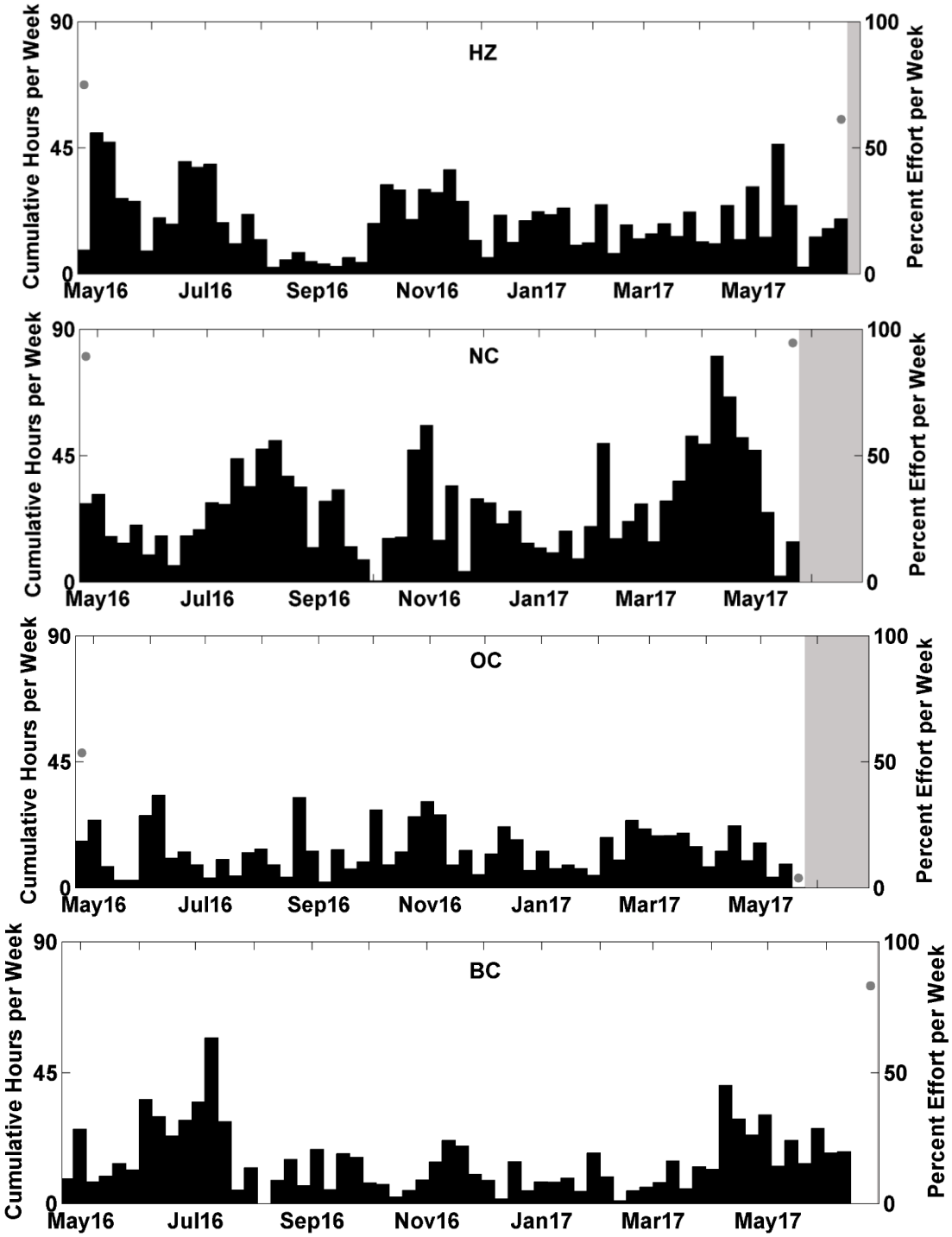

Figure 67. Weekly presence (black bars) of sperm whale echolocation clicks between April 2016 and June 2017 at sites NC, HZ, OC, and WC. Effort markings are described in Figure 47.

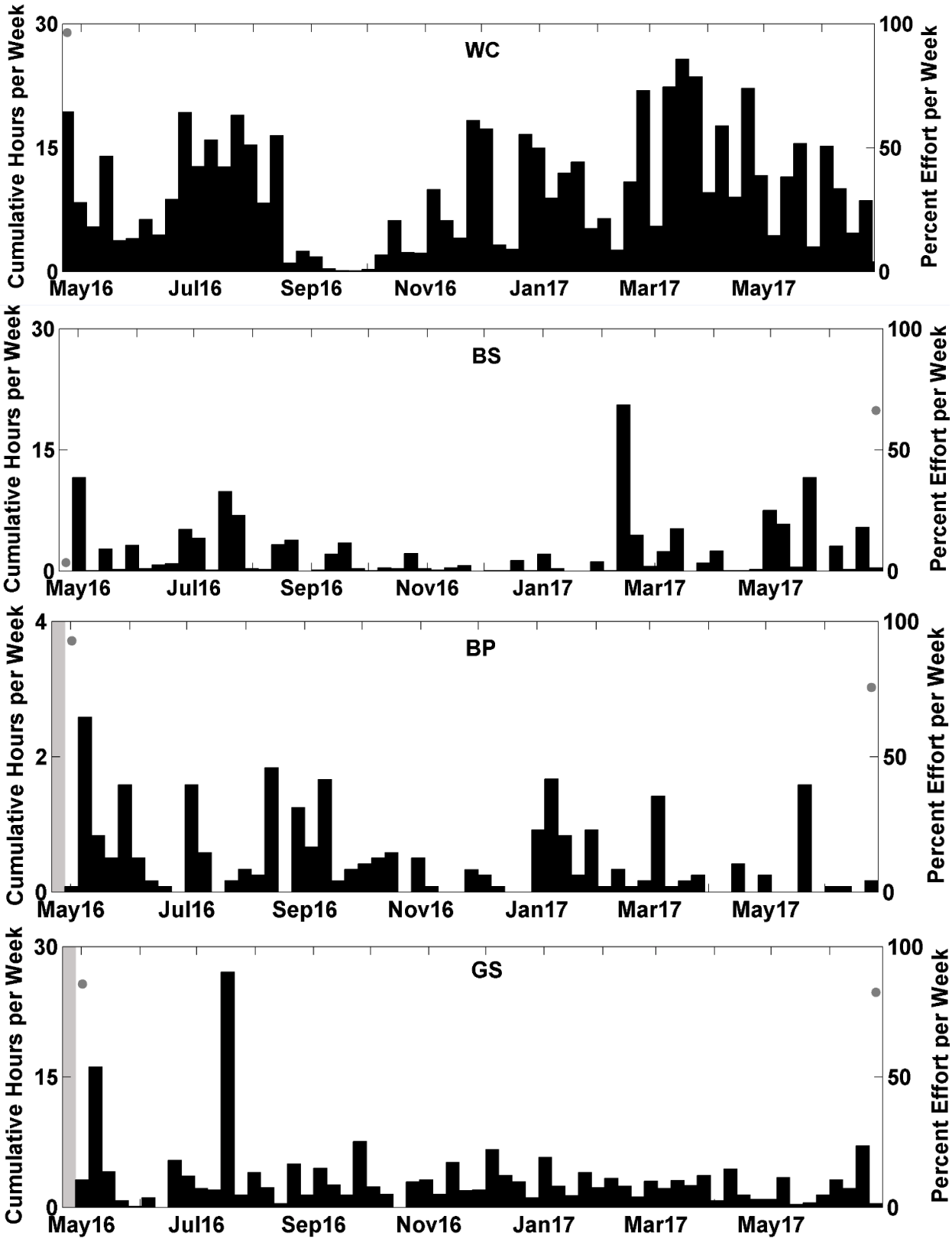

Figure 68. Weekly presence (black bars) of sperm whale echolocation clicks between April 2016 and June 2017 at sites WC, GS, BP, and BS. Effort markings are described in Figure 47. ***Note: Axis change for sites WC, GS, BP, and BS due to a lower amount of sperm whale echolocation detections compared to the rest of the sites*****.**

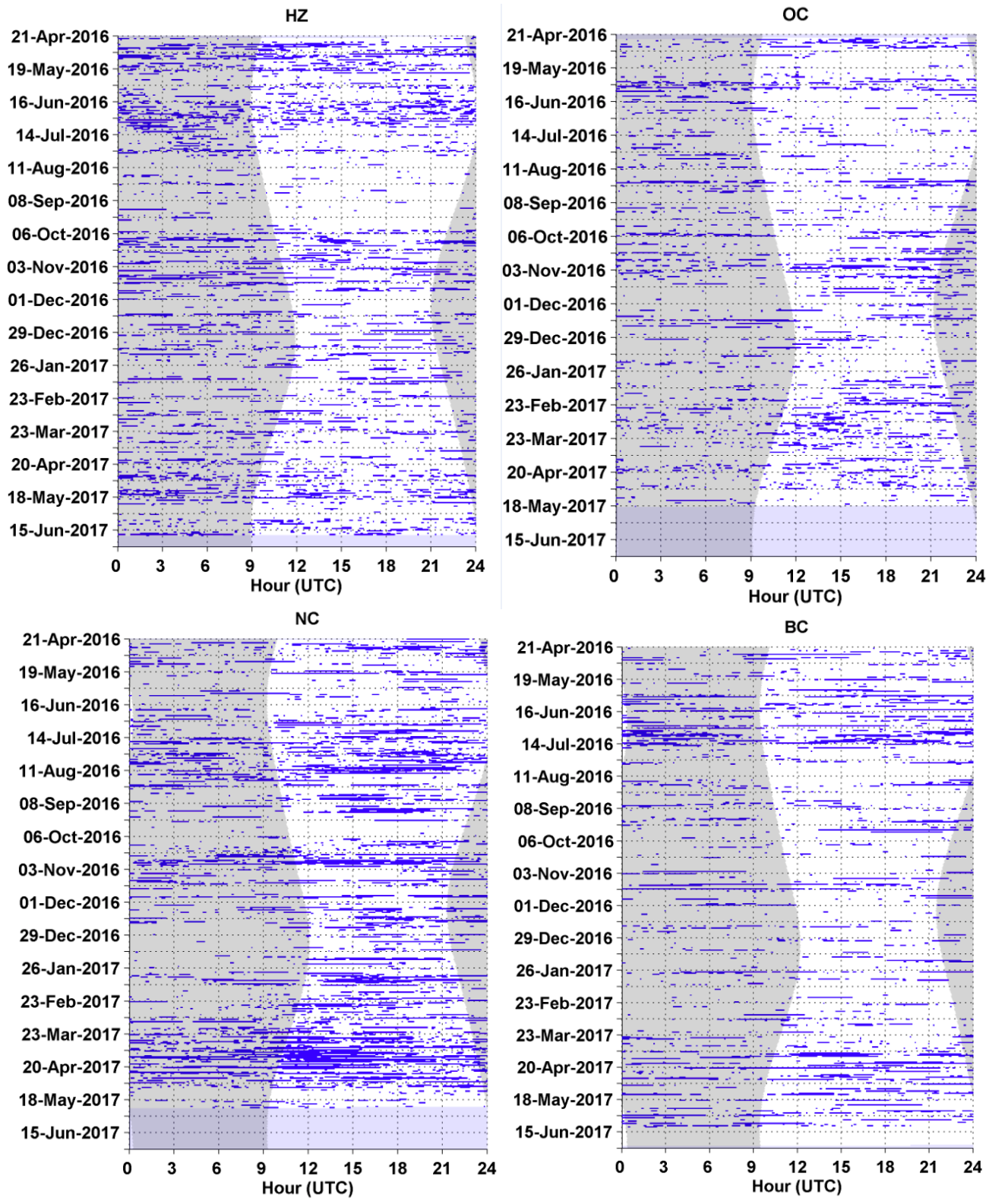

Figure 69. Sperm whale echolocation clicks in five-minute bins (blue bars) at sites HZ, OC, NC, and BC. Effort markings are described in Figure 49.

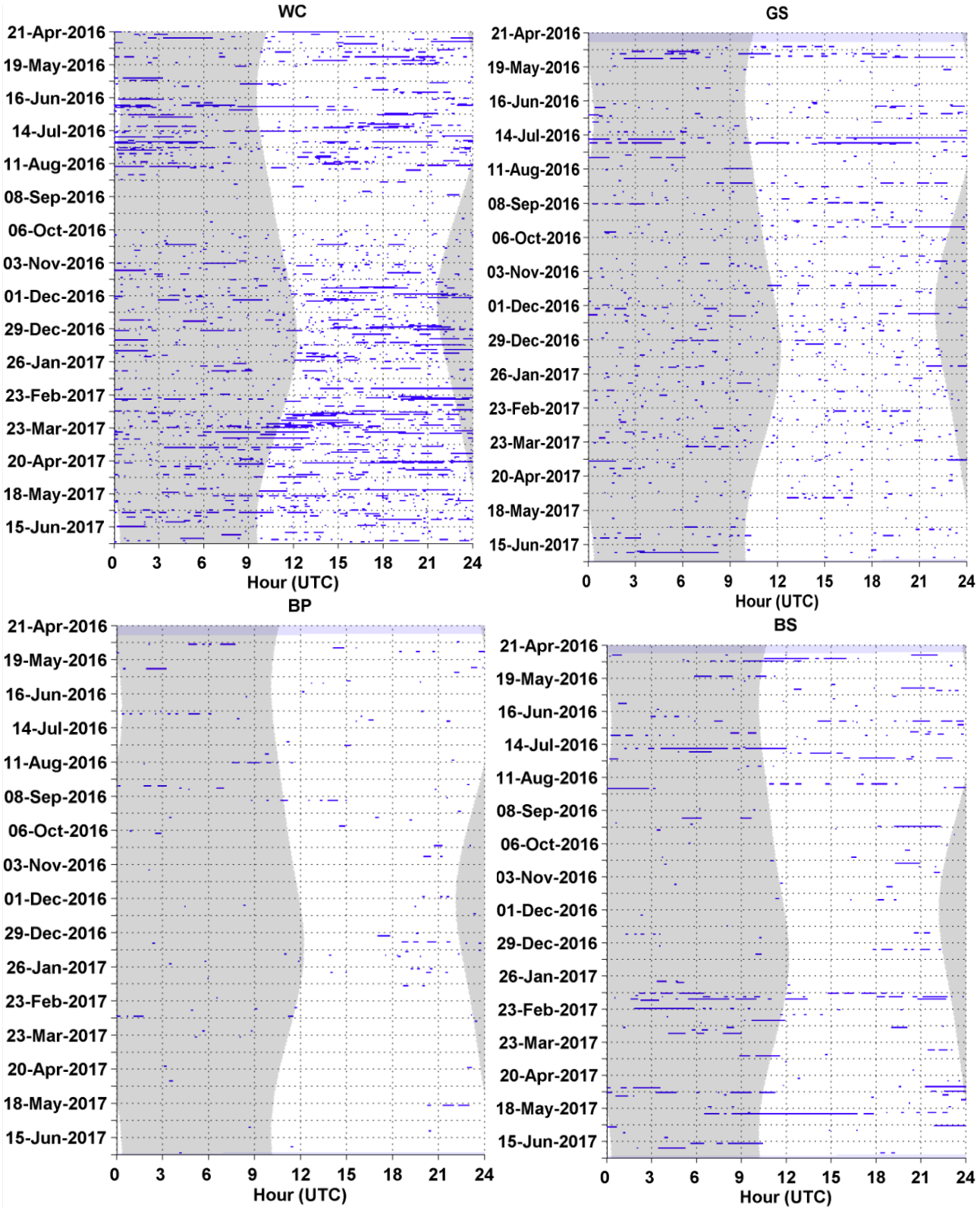

Figure 70. Sperm whale echolocation clicks in five-minute bins (blue bars) at sites WC, GS, BP, and BS. Effort markings are described in Figure 49.

***Kogia* spp.**

- *Kogia* spp. clicks were detected intermittently at seven of the eight sites (Figure 71, Figure 72) and were highest at the southernmost sites, BS, BP and GS (Figure 72). No detections occurred at site OC.
- There was no diel pattern for *Kogia* spp. clicks (
- Figure 73, Figure 74).

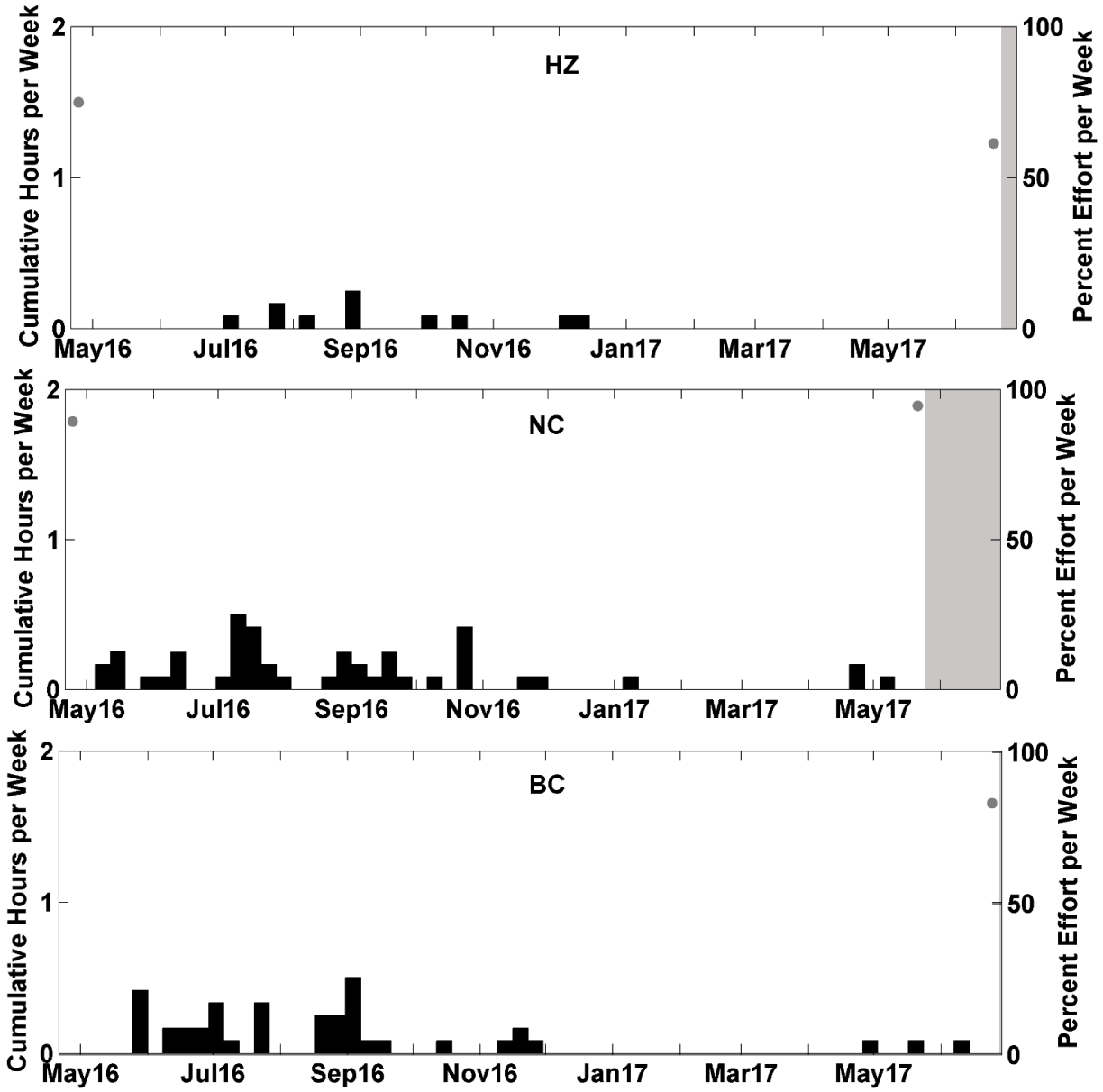

Figure 71. Weekly presence (black bars) of *Kogia* spp. echolocation clicks between April 2016 and June 2017 at sites HZ, NC, and BC. Effort markings are described in Figure 47.

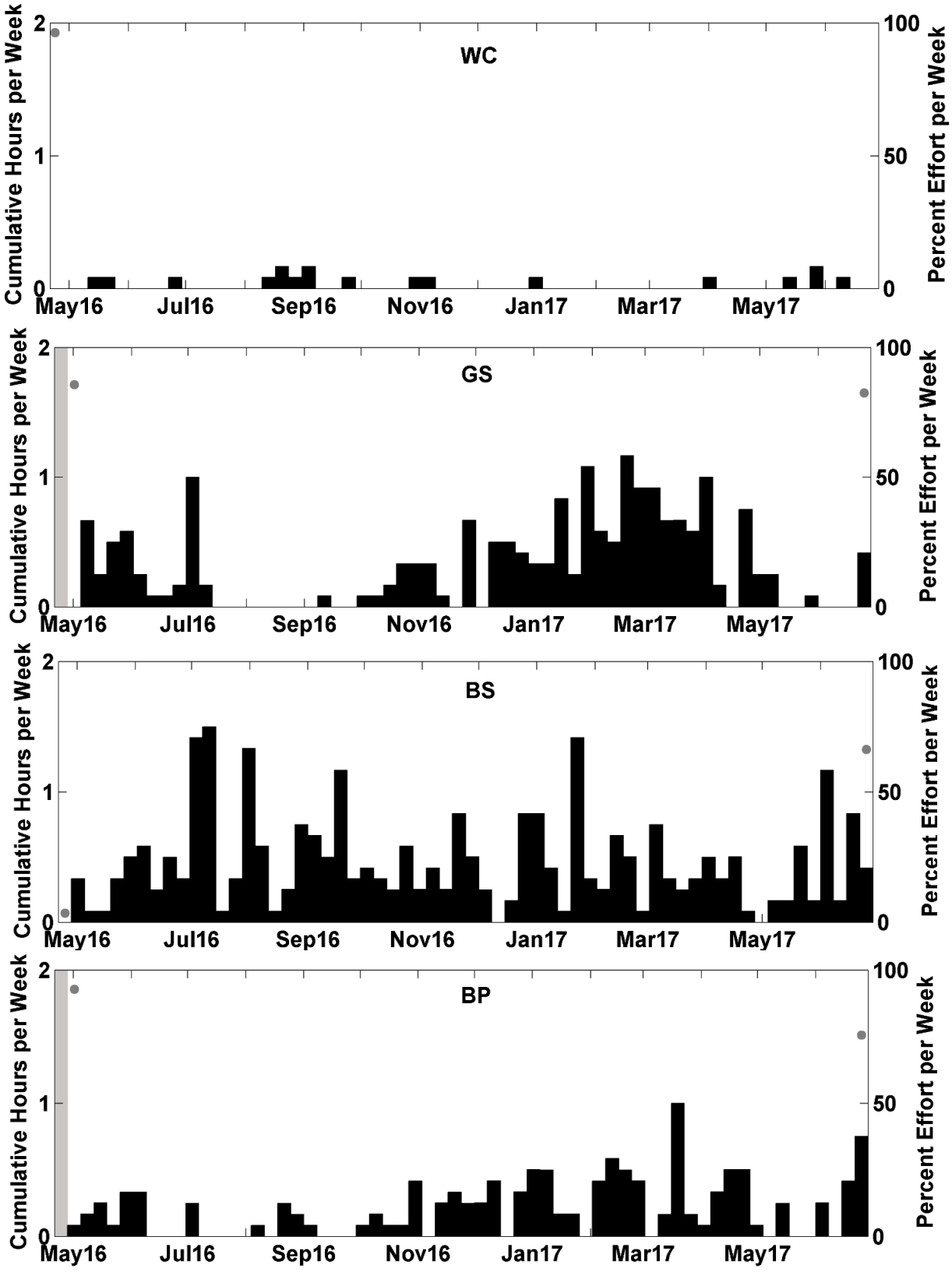

Figure 72. Weekly presence (black bars) of *Kogia* spp. echolocation clicks between April 2016 and June 2017 at sites WC, GS, BP, and BS. Effort markings are described in Figure 47.

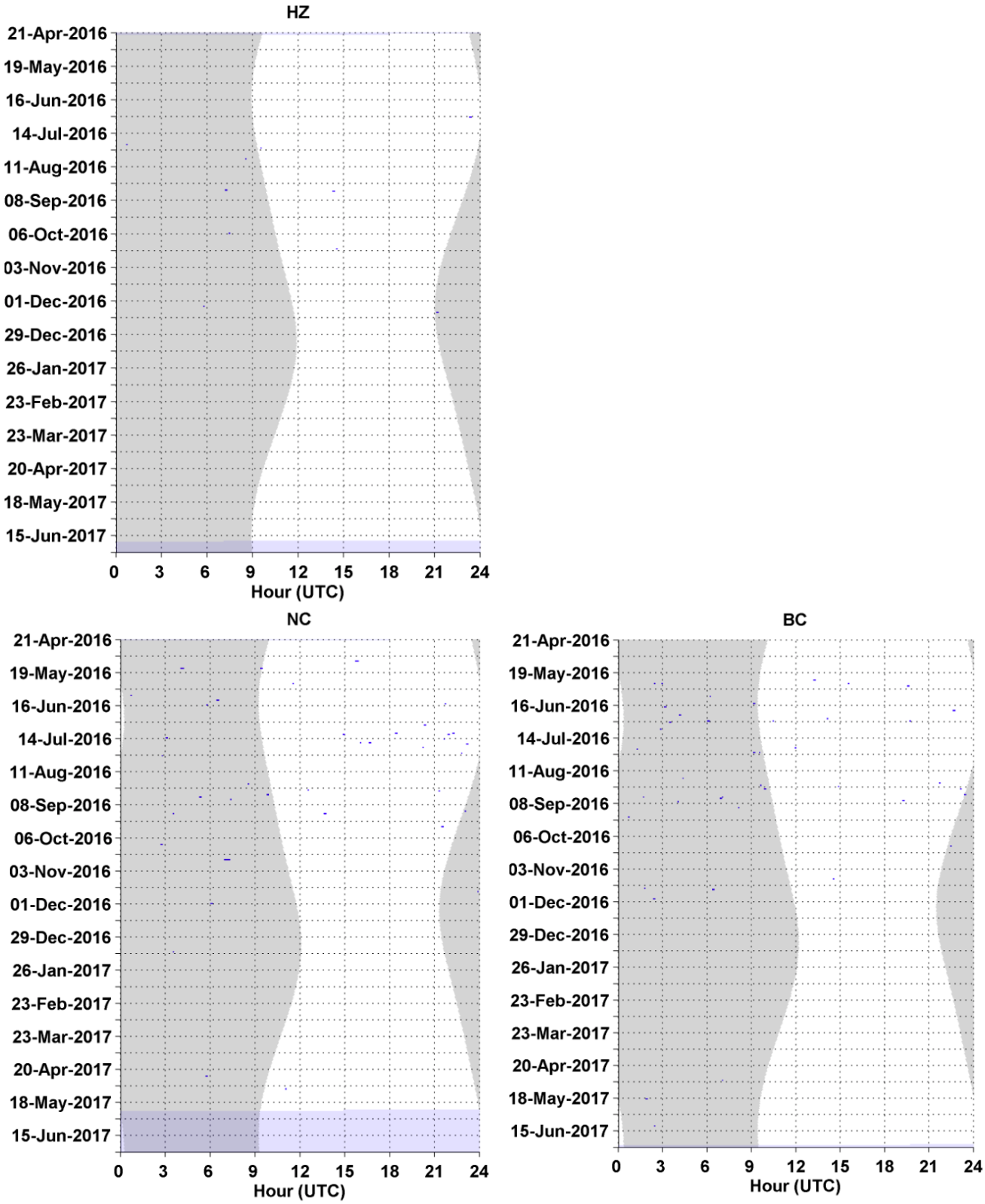

Figure 73. *Kogia* spp. echolocation clicks in five-minute bins (blue bars) at sites HZ, NC and BC. Effort markings are described in Figure 49.

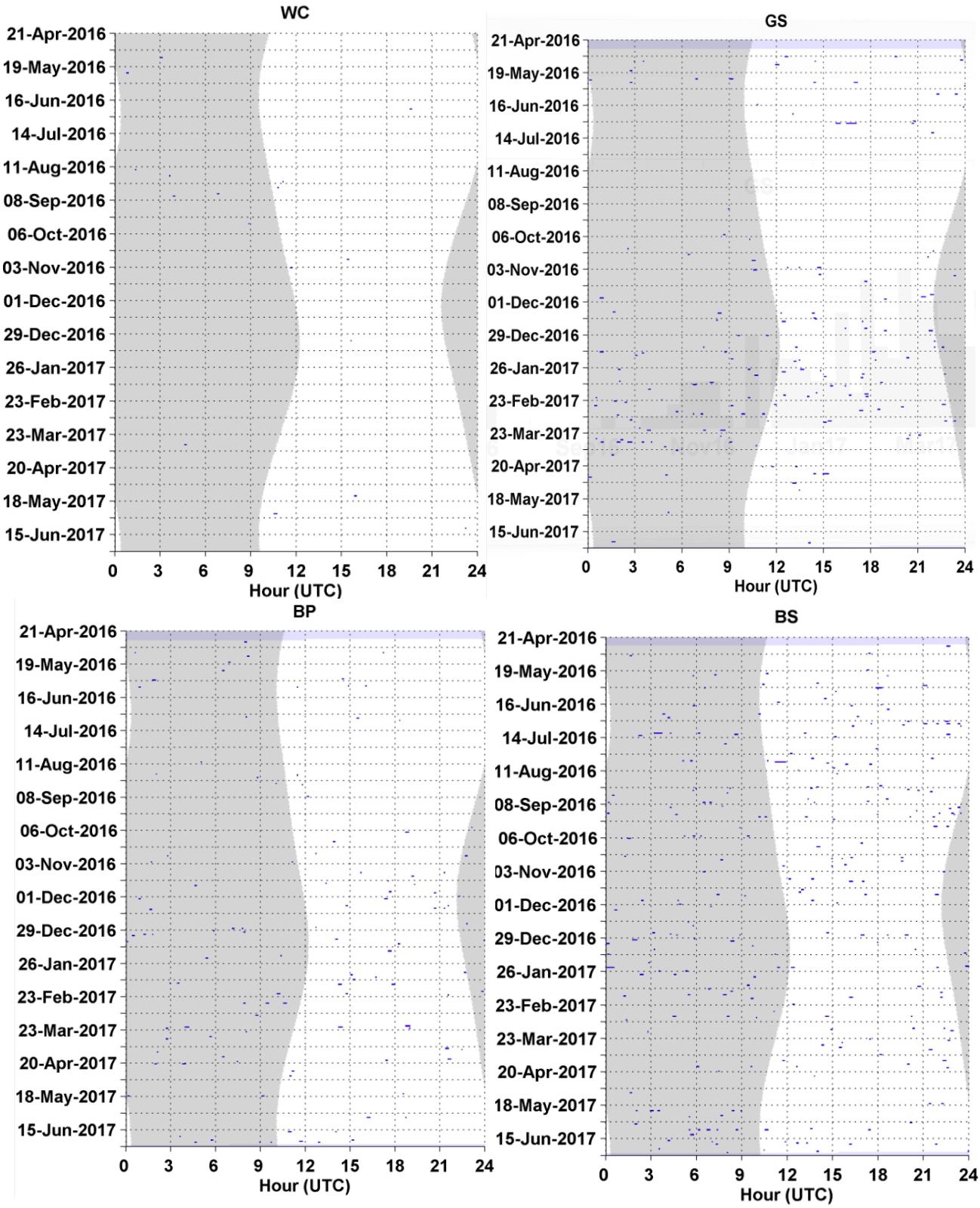

Figure 74. *Kogia* spp. echolocation clicks in five-minute bins (blue bars) at sites WC, GS, BP, and BS. Effort markings are described in Figure 49.

Delphinid Click Types

Risso's Dolphins

- Risso's dolphins were detected at all eight sites (Figure 75, Figure 76) with highest detections rates at sites NC and BC. Detections peaked from May to August 2016 and from March to July 2017.
- There were distinct diel patterns for Risso's dolphins with detections occurring primarily during daytime from approximately April to June, and switching to primarily during nighttime in July at sites NC, WC, and BC (Figure 77, Figure 78). At sites HZ, BS, BP and GS detections occurred primarily during the night time (Figure 77, Figure 78).

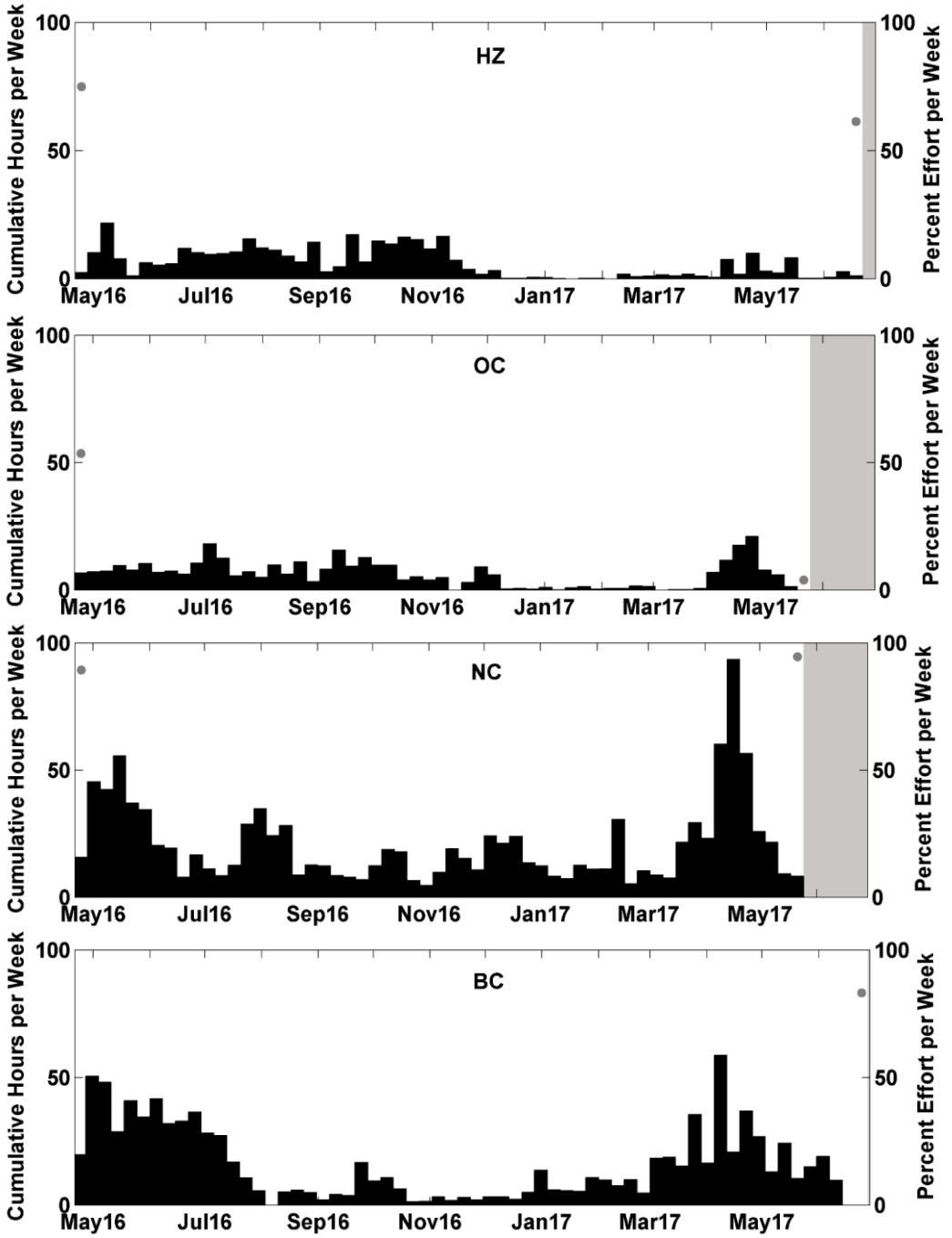

Figure 75. Weekly presence (black bars) of Risso's dolphin clicks between April 2016 and June 2017 at sites HZ, OC, NC, and BC. Effort markings are described in Figure 47.

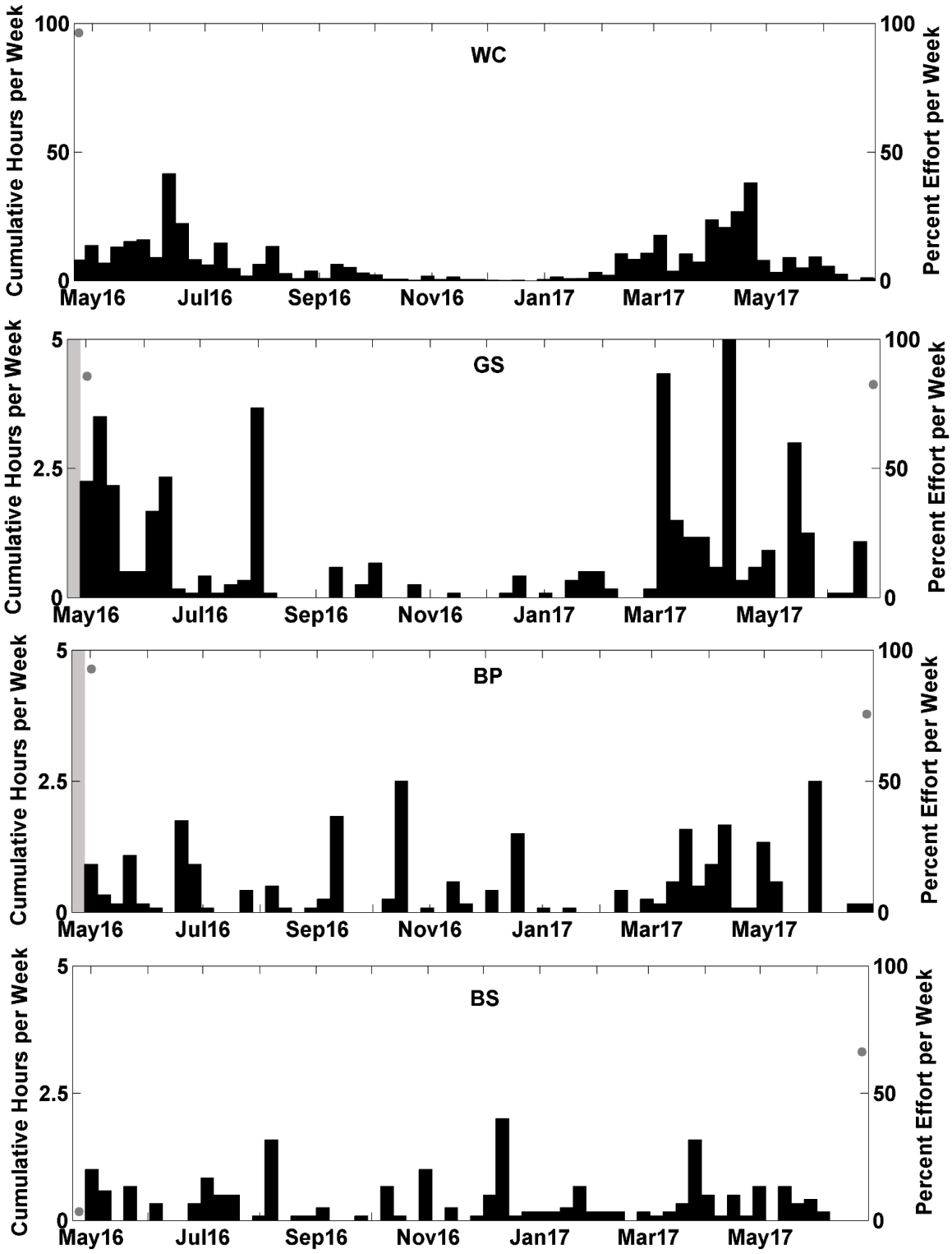

Figure 76. Weekly presence (black bars) of Risso's dolphin clicks between April 2016 and June 2017 at sites WC, GS, BP, and BS. Effort markings are described in Figure 47. ***Note: Axis change for sites GS, BP, and BS due to a lower amount of Risso's dolphin click detections compared to the rest of the sites.***

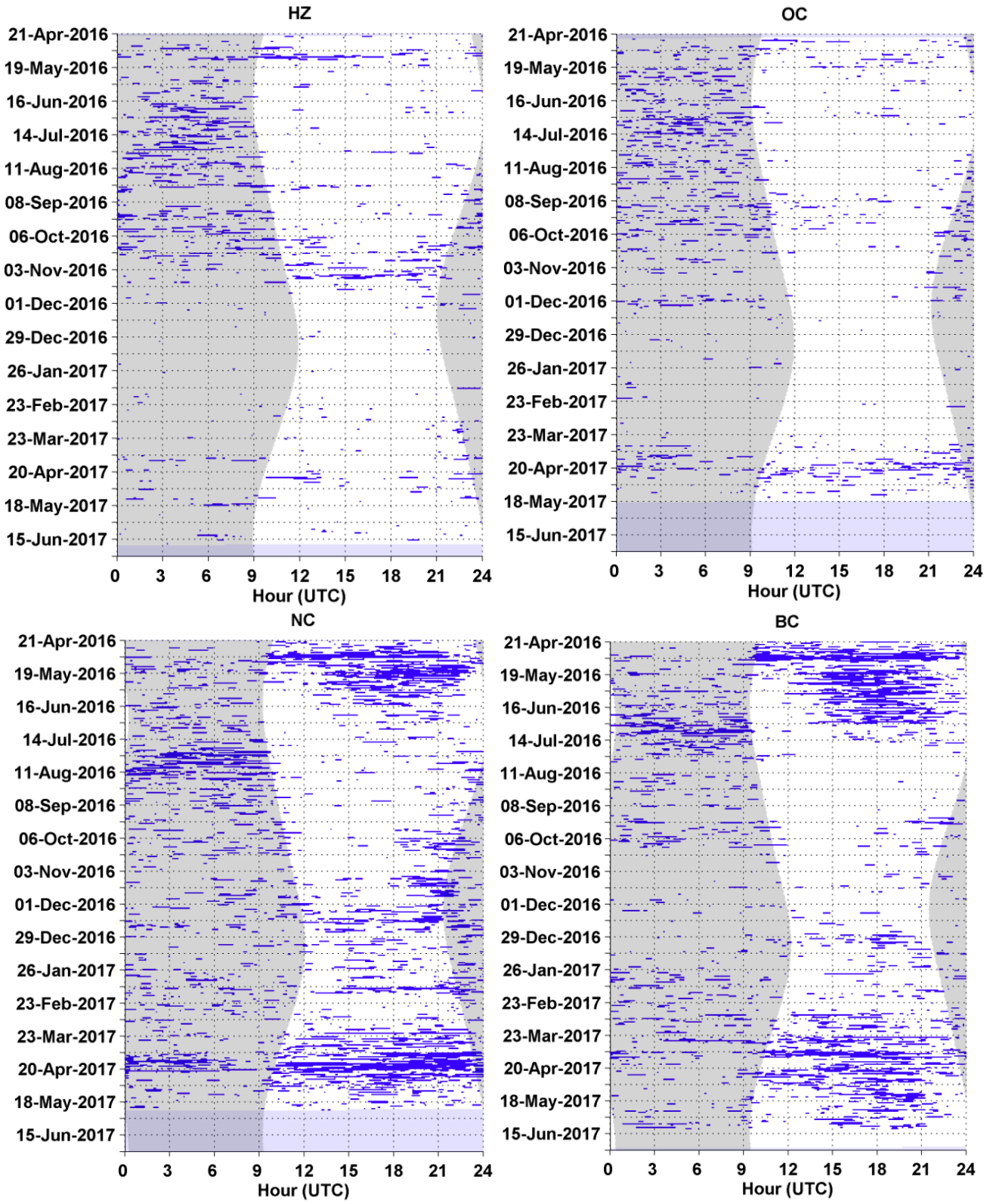

Figure 77. Risso's dolphin clicks in five-minute bins (blue bars) at sites HZ, OC, NC, and BC. Effort markings are described in Figure 49.

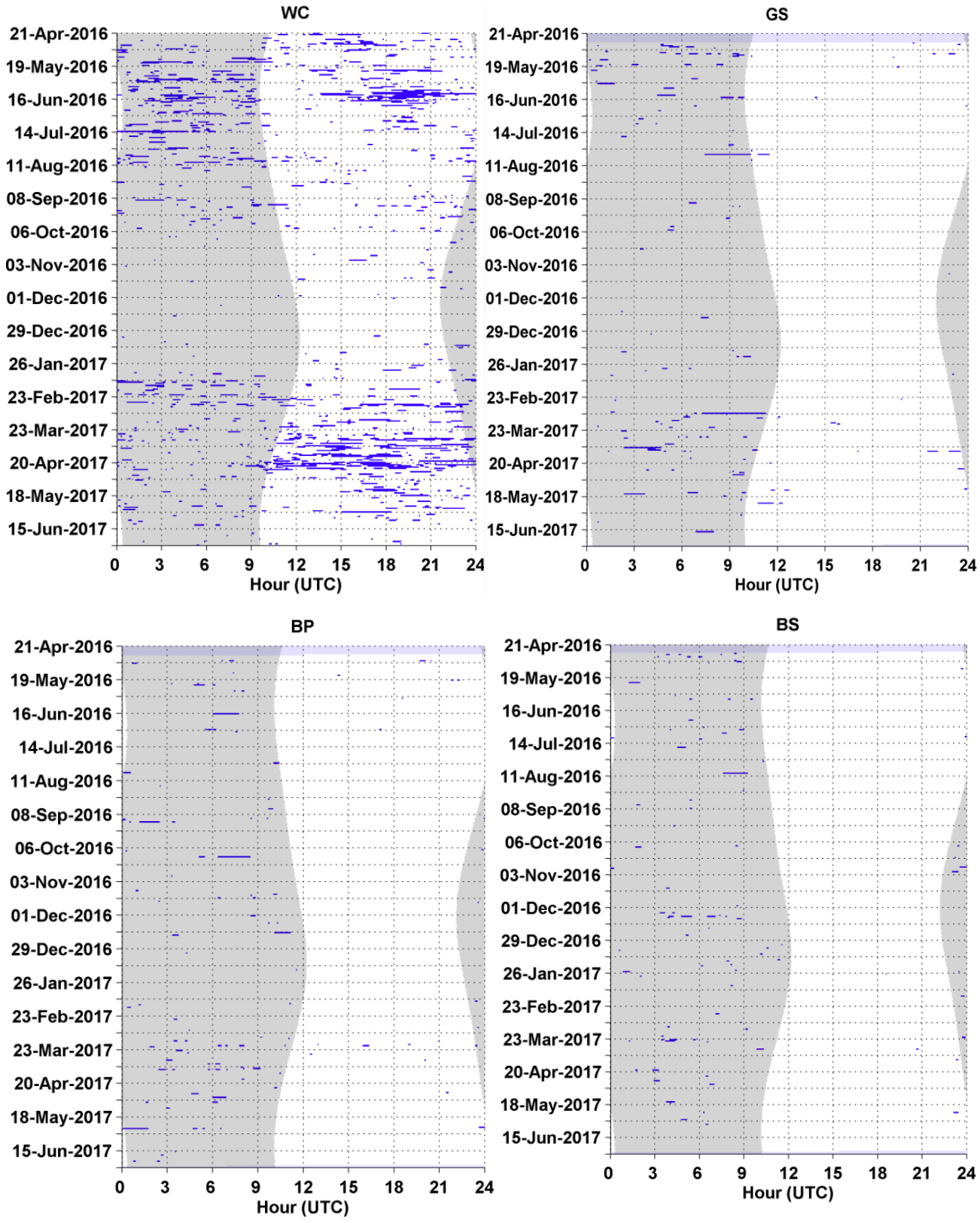

Figure 78. Risso's dolphin clicks in five-minute bins (blue bars) at sites WC, GS, BP, and BS. Effort markings are described in Figure 49.

Click Type 2

- Click type 2 was detected intermittently at sites NC, HZ, WC and BC (Figure 79, Figure 80) with higher detection counts from May to October 2016. No detections occurred at site BS.
- The majority of click type 2 detections occurred during the daytime hours (Figure 81, Figure 82).

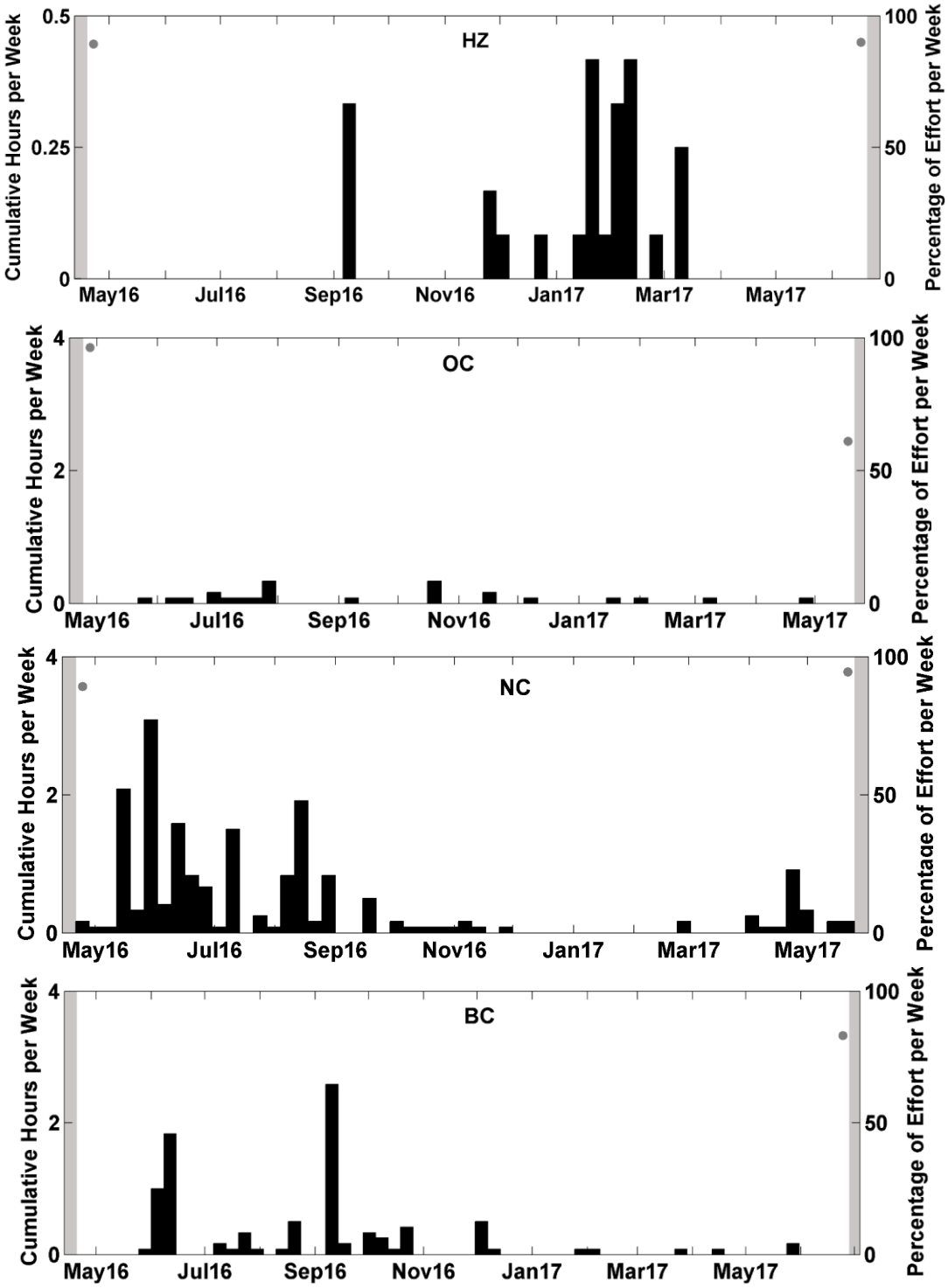

Figure 79. Weekly presence (black bars) of click type 2 detections between April 2016 and June 2017 at sites HZ, OC, NC, and BC. Effort markings are described in Figure 47.

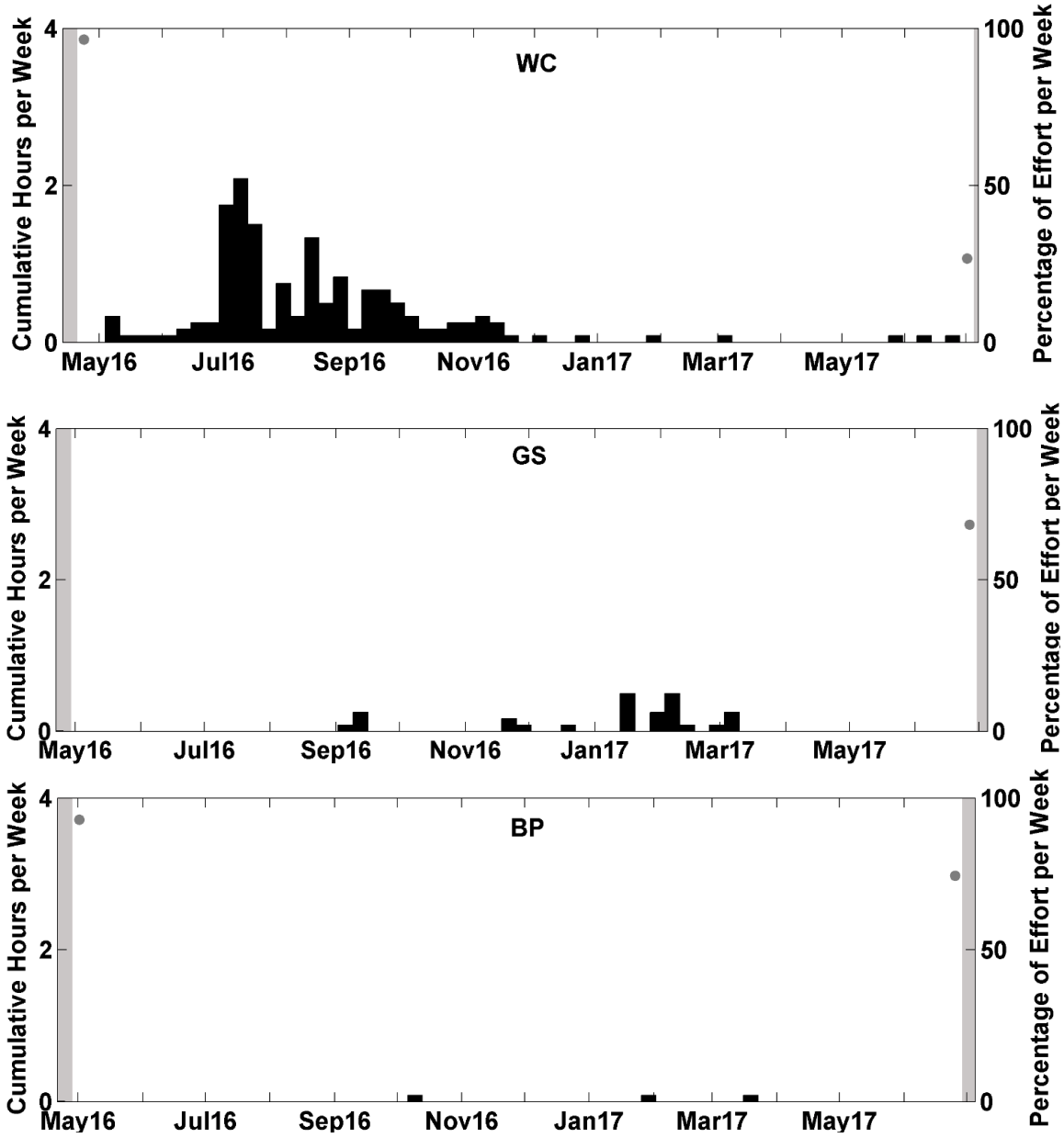

Figure 80. Weekly presence (black bars) of click type 2 detections between April 2016 and June 2017 at sites WC, BP, and GS. Effort markings are described in Figure 47.

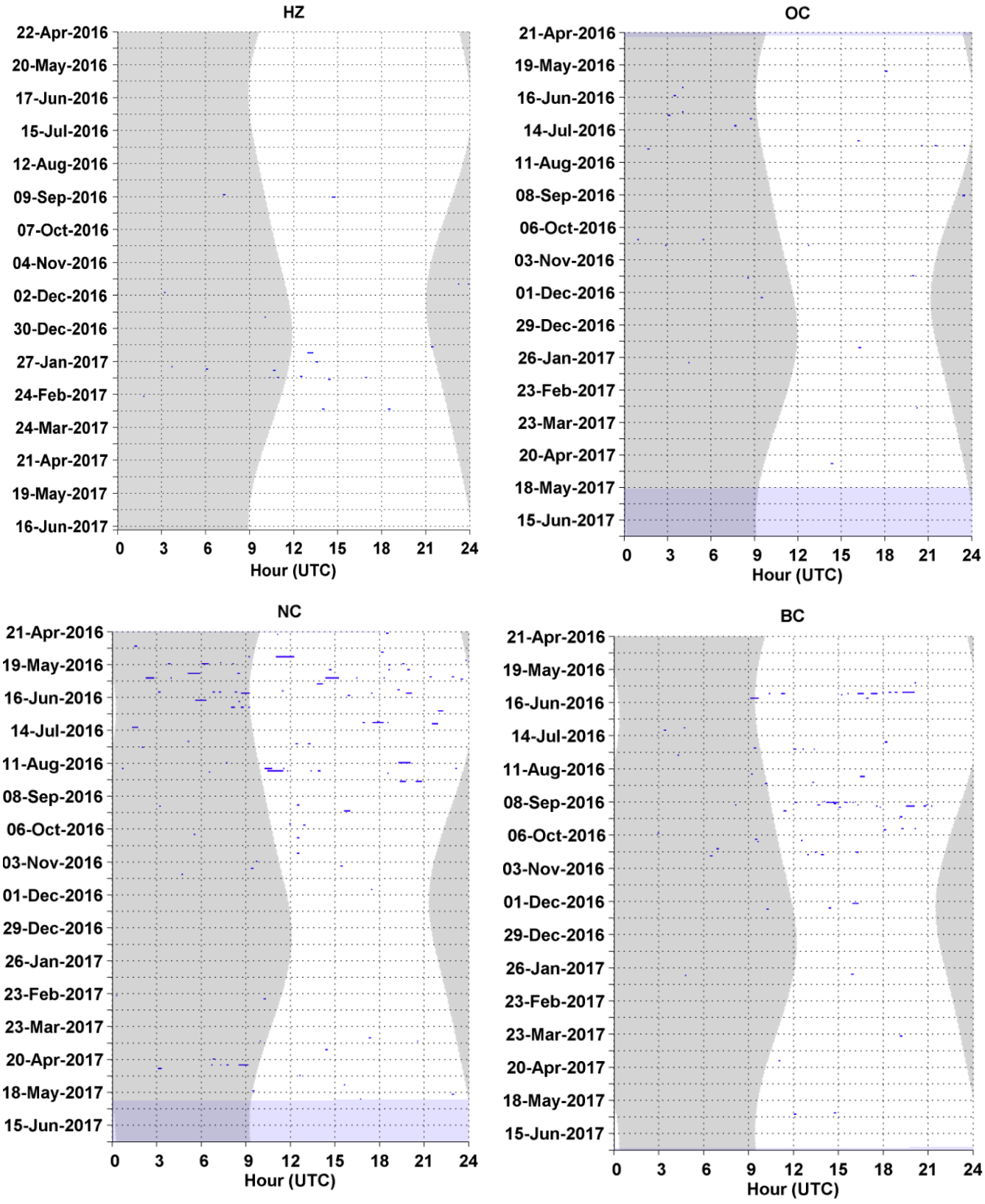

Figure 81. Click type 2 detections in five-minute bins (blue bars) at sites HZ, OC, NC, and BC. Effort markings are described in Figure 49.

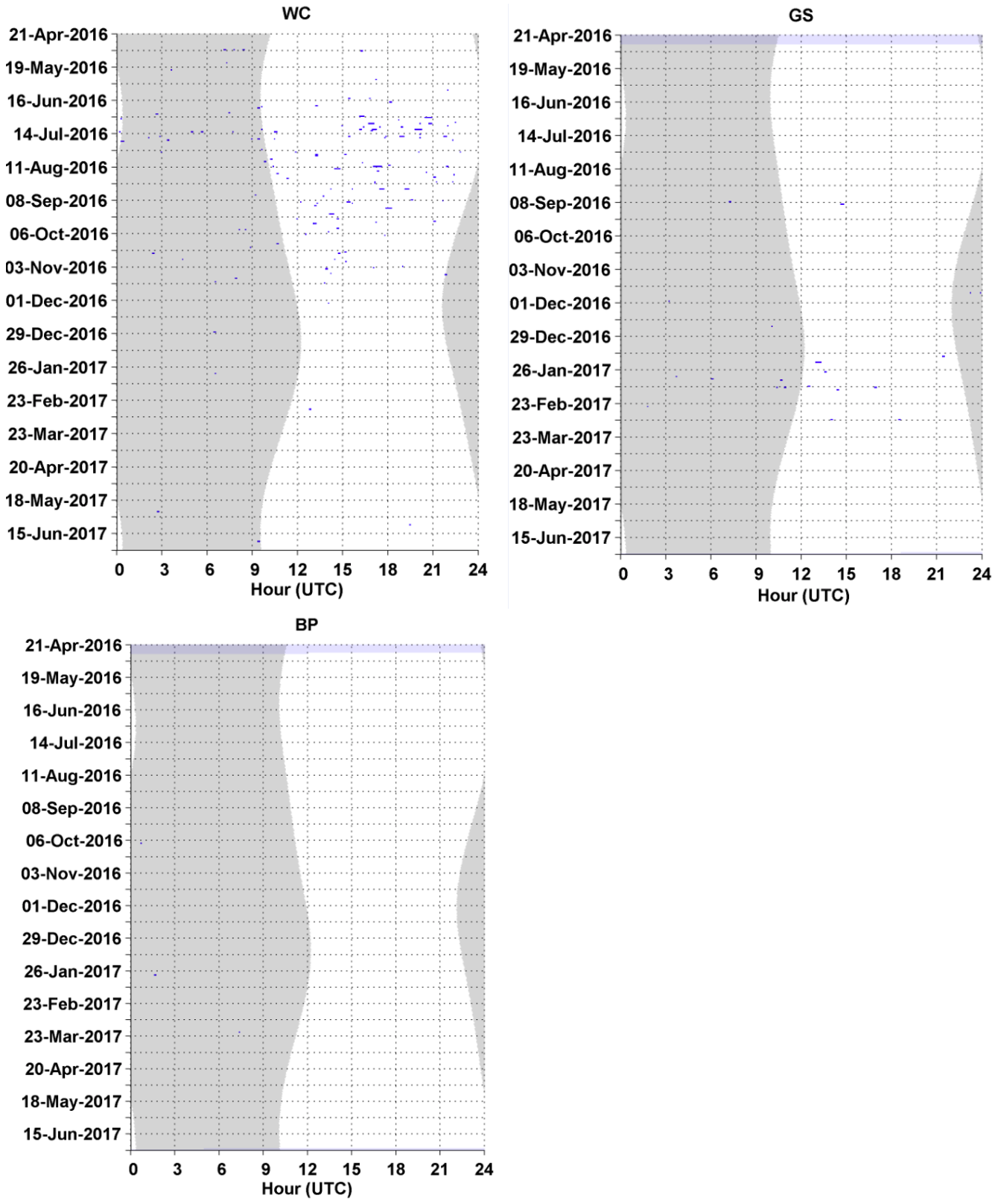

Figure 82. Click type 2 detections in five-minute bins (blue bars) at sites WC, GS, and BP. Effort markings are described in Figure 49.

Click Type 3

- Click type 3 was detected in high numbers across all eight sites (Figure 83, Figure 84) but was highest at sites NC, WC, and BC. Detections peaked from May to July 2016 and December 2016 to July 2017.
- The majority of click type 3 occurred during the nighttime hours (Figure 85, Figure 86).

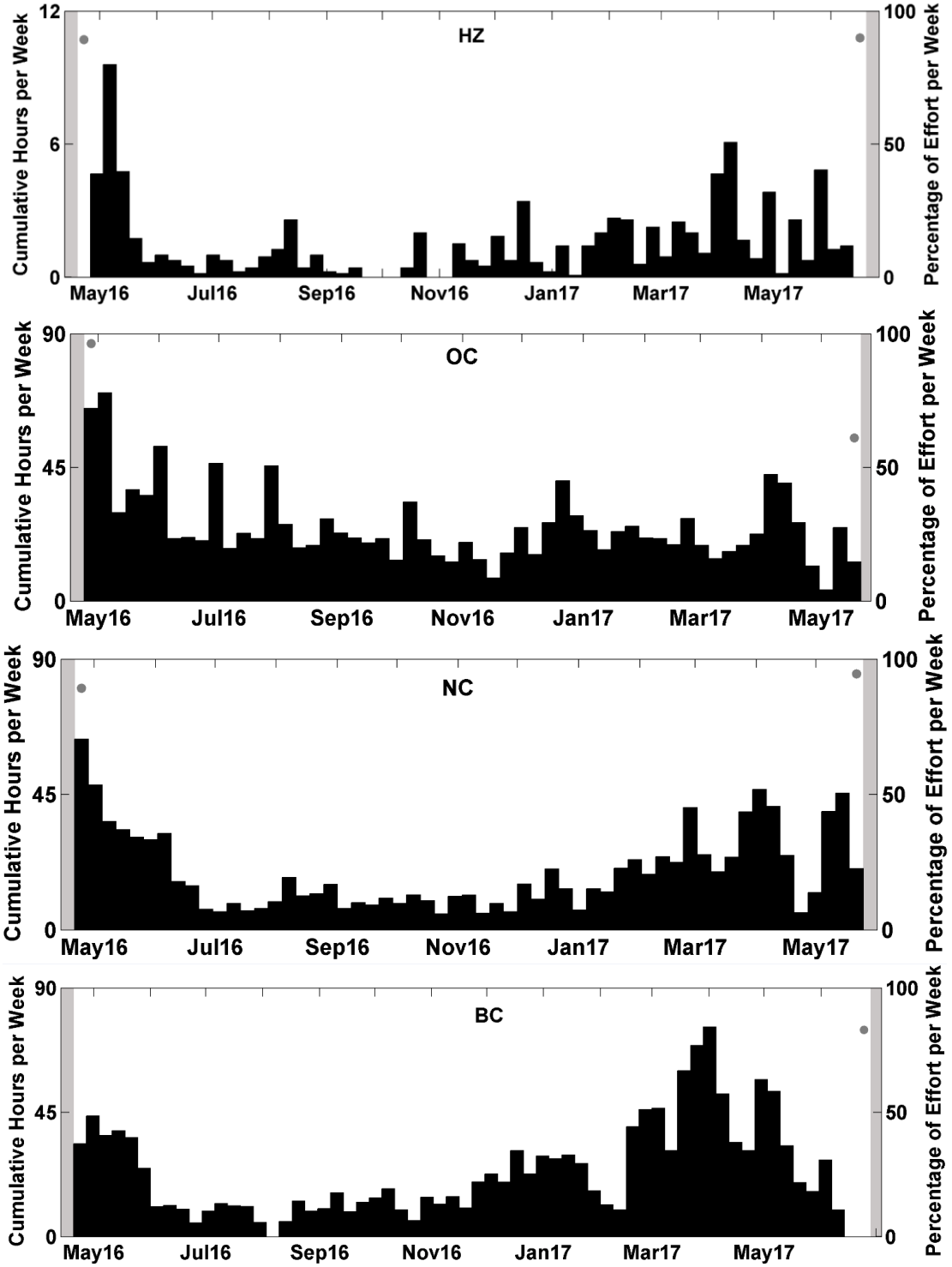

Figure 83. Weekly presence (black bars) of click type 3 detections between April 2016 and June 2017 at sites HZ, OC, NC, and BC. Effort markings are described in Figure 47.

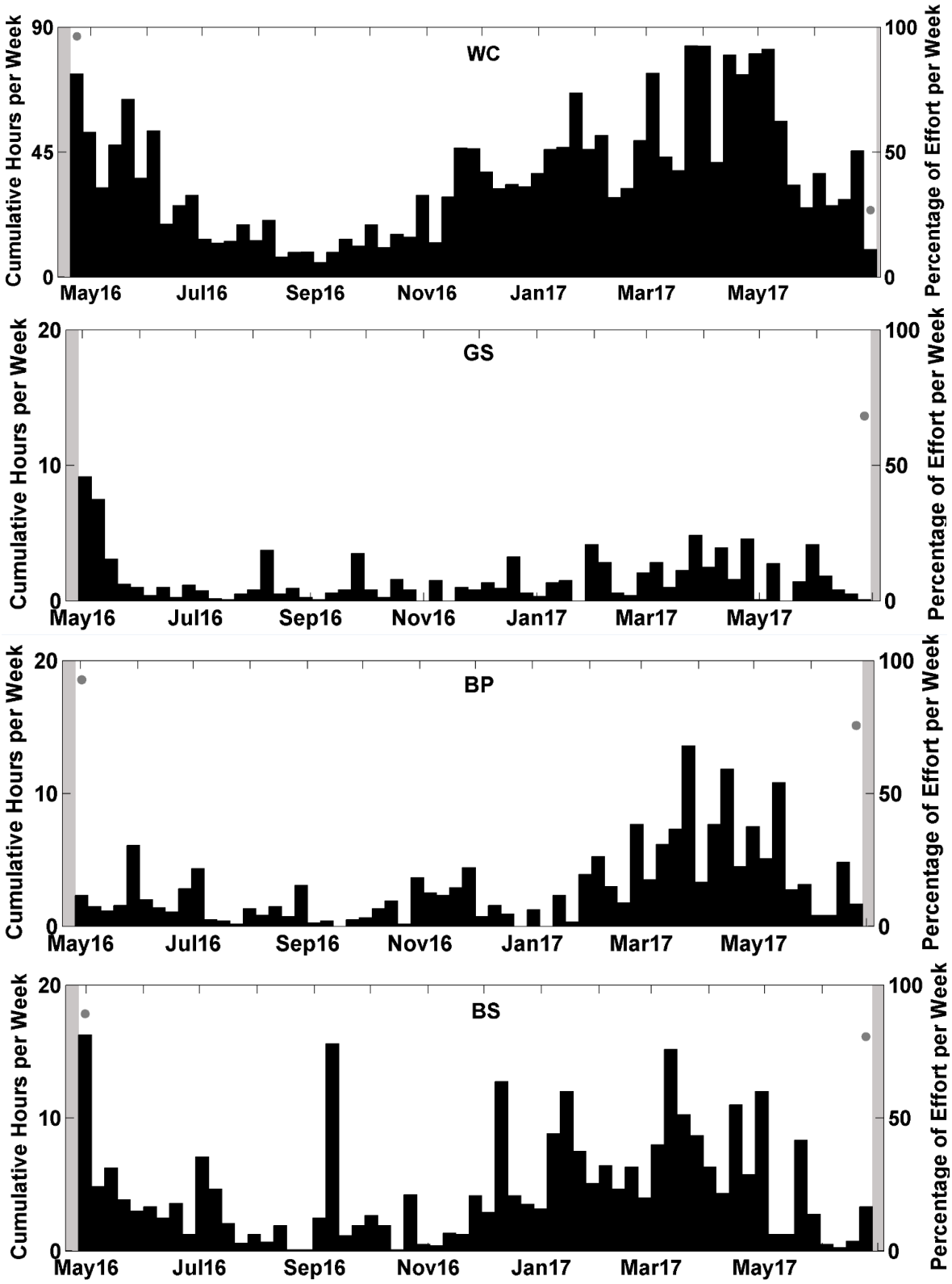

Figure 84. Weekly presence (black bars) of click type 3 detections between April 2016 and June 2017 at site WC, GS, BP, and BS. Effort markings are described in Figure 47. *Note: Axis change for site BS, BP, and GS due to a lower amount of click type 3 detections compared to the rest of the sites*.

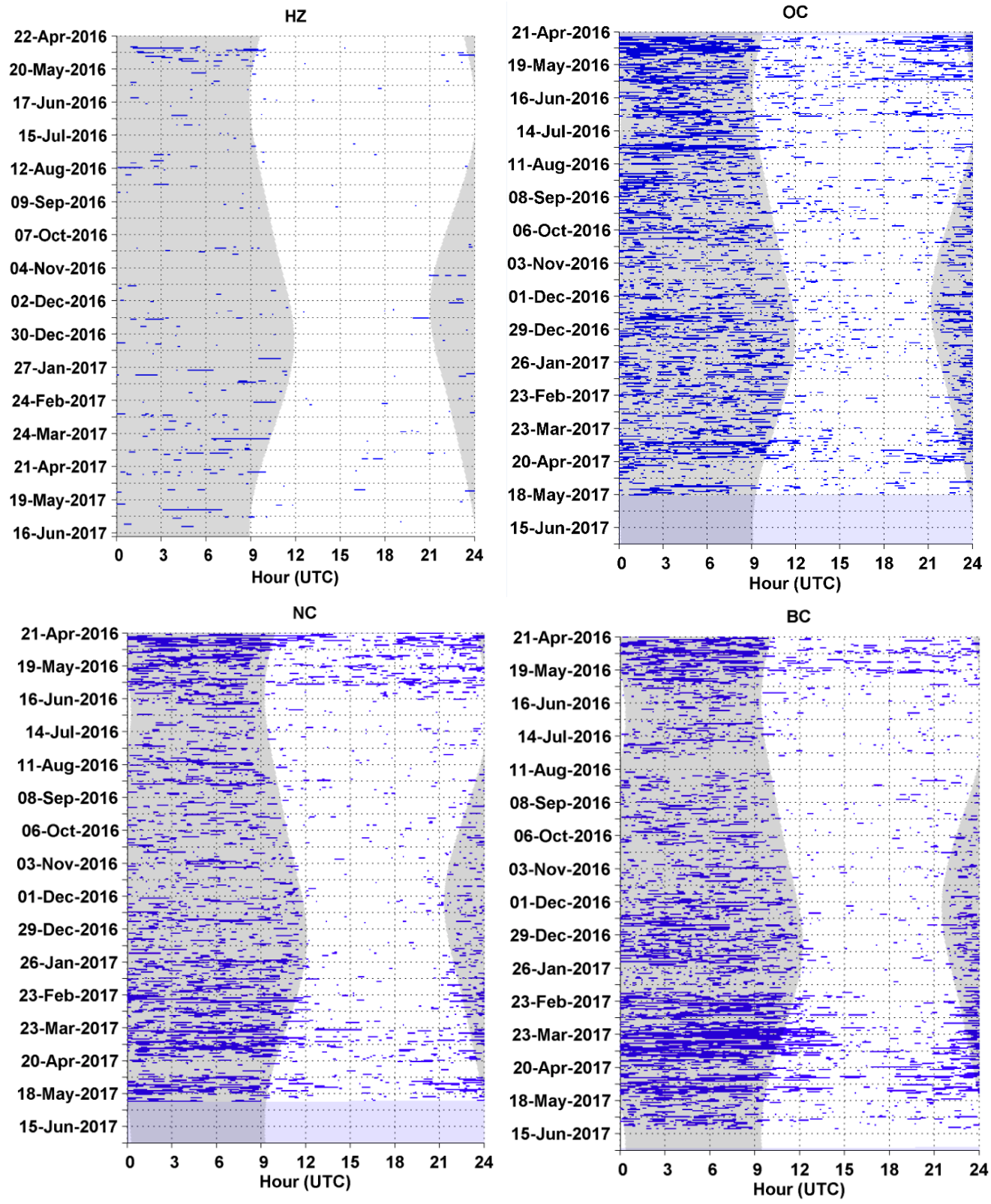

Figure 85. Click type 3 detections in five-minute bins (blue bars) at sites HZ, OC, NC, and BC. Effort markings are described in Figure 49.

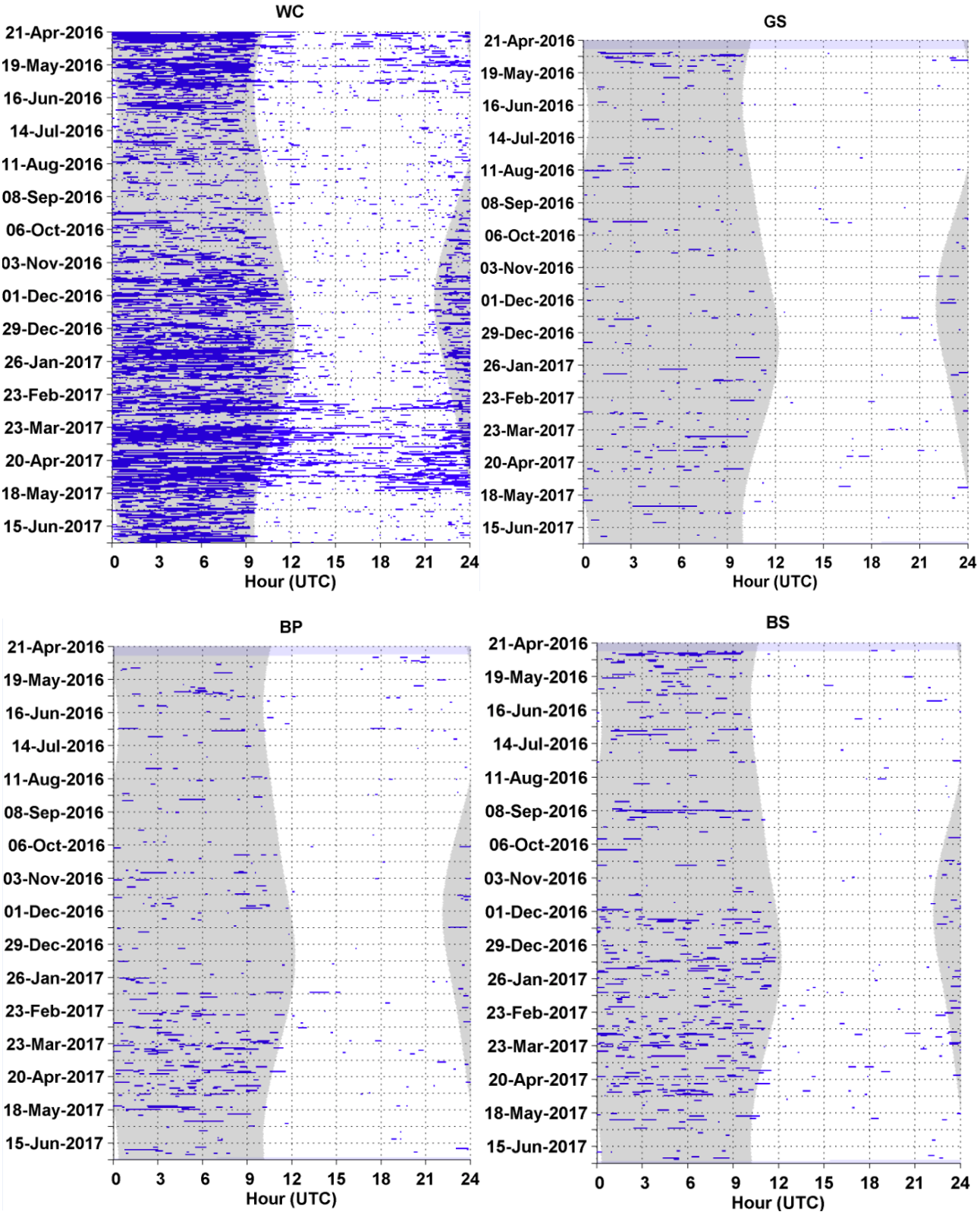

Figure 86. Click type 3 detections in five-minute bins (blue bars) at sites WC, GS, BP, and BS. Effort markings are described in Figure 49.

Click Type 4 / 6

- Click type 4 / 6 was detected intermittently at all eight sites (Figure 87, Figure 88) but was detected in very high numbers at site WC with high detection rates from July to November 2016 (Figure 88).
- There was no diel pattern for click type 4 / 6 (Figure 89, Figure 90).

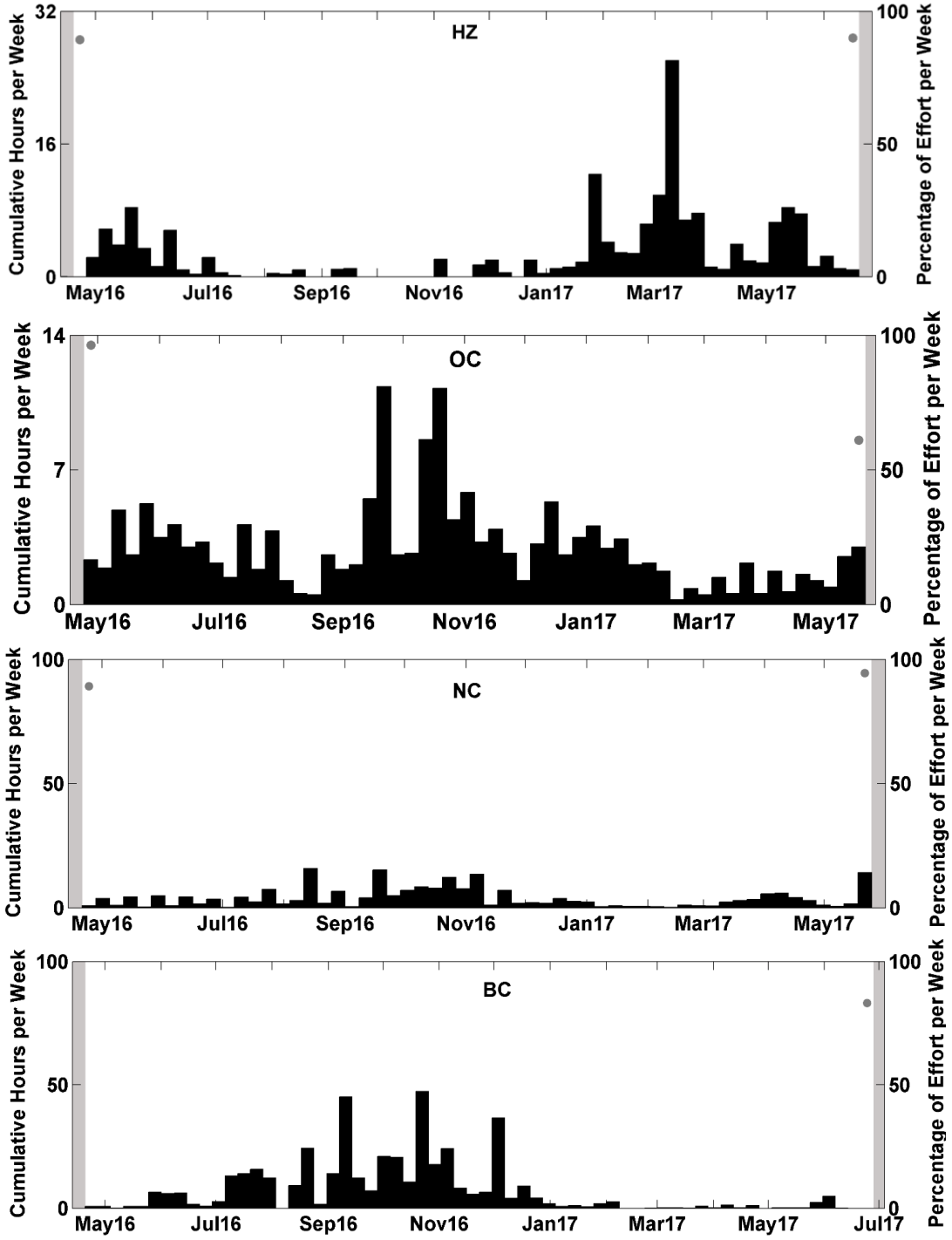

Figure 87. Weekly presence (black bars) of click type 4 / 6 detections between April 2016 and June 2017 at sites HZ, OC, NC, and BC. Effort markings are described in Figure 47. *Note: Axis change for site OC due to a lower amount of click type 4 & 6 detections compared to the rest of the sites*.

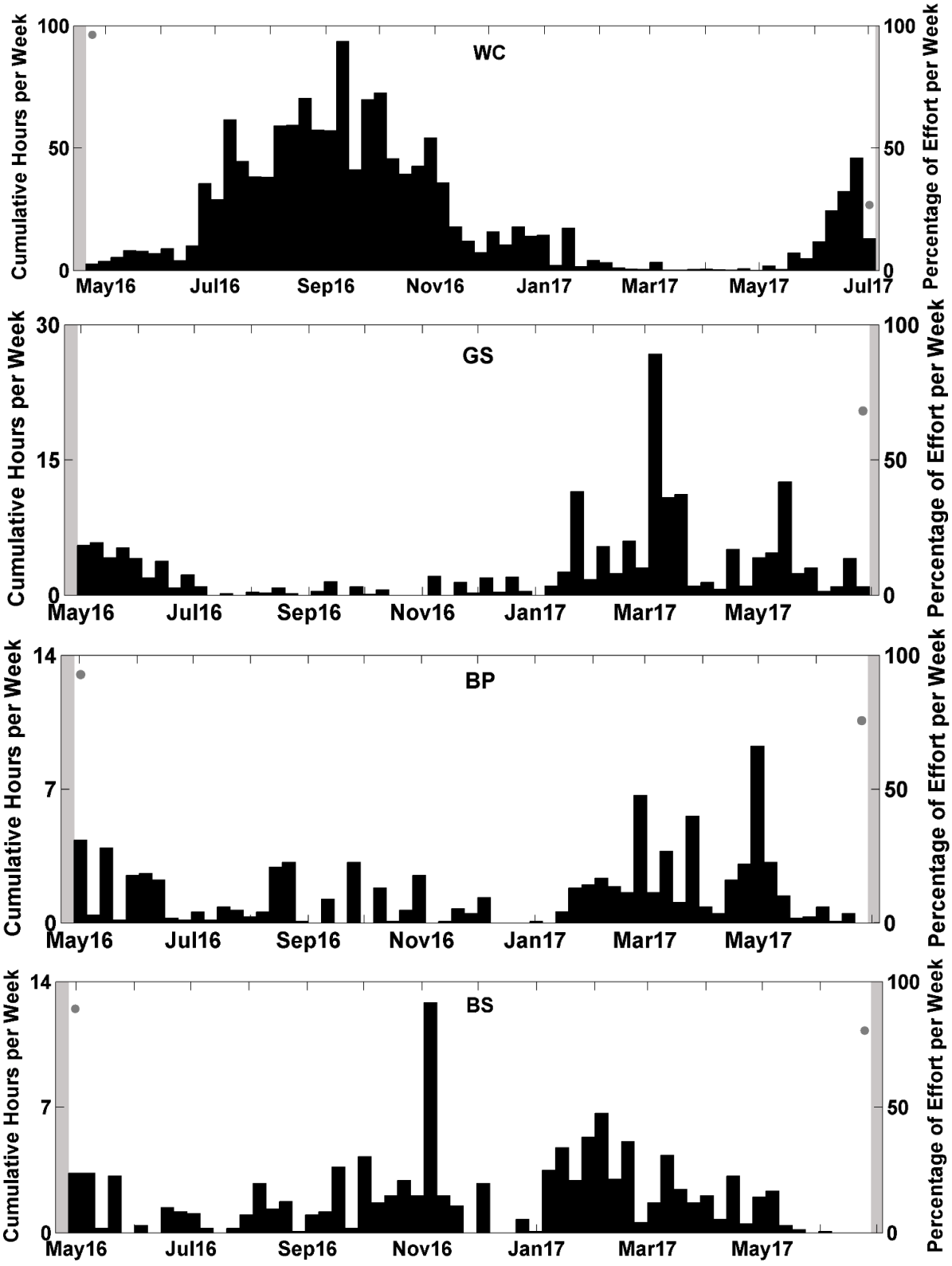

Figure 88. Weekly presence (black bars) of click type 4 / 6 detections between April 2016 and June 2017 at sites WC, GS, BP, and BS. Effort markings are described in Figure 47. *Note: Axis change for sites GS, BP, and BS due to a lower amount of click type 4 & 6 detections compared to the rest of the sites*.

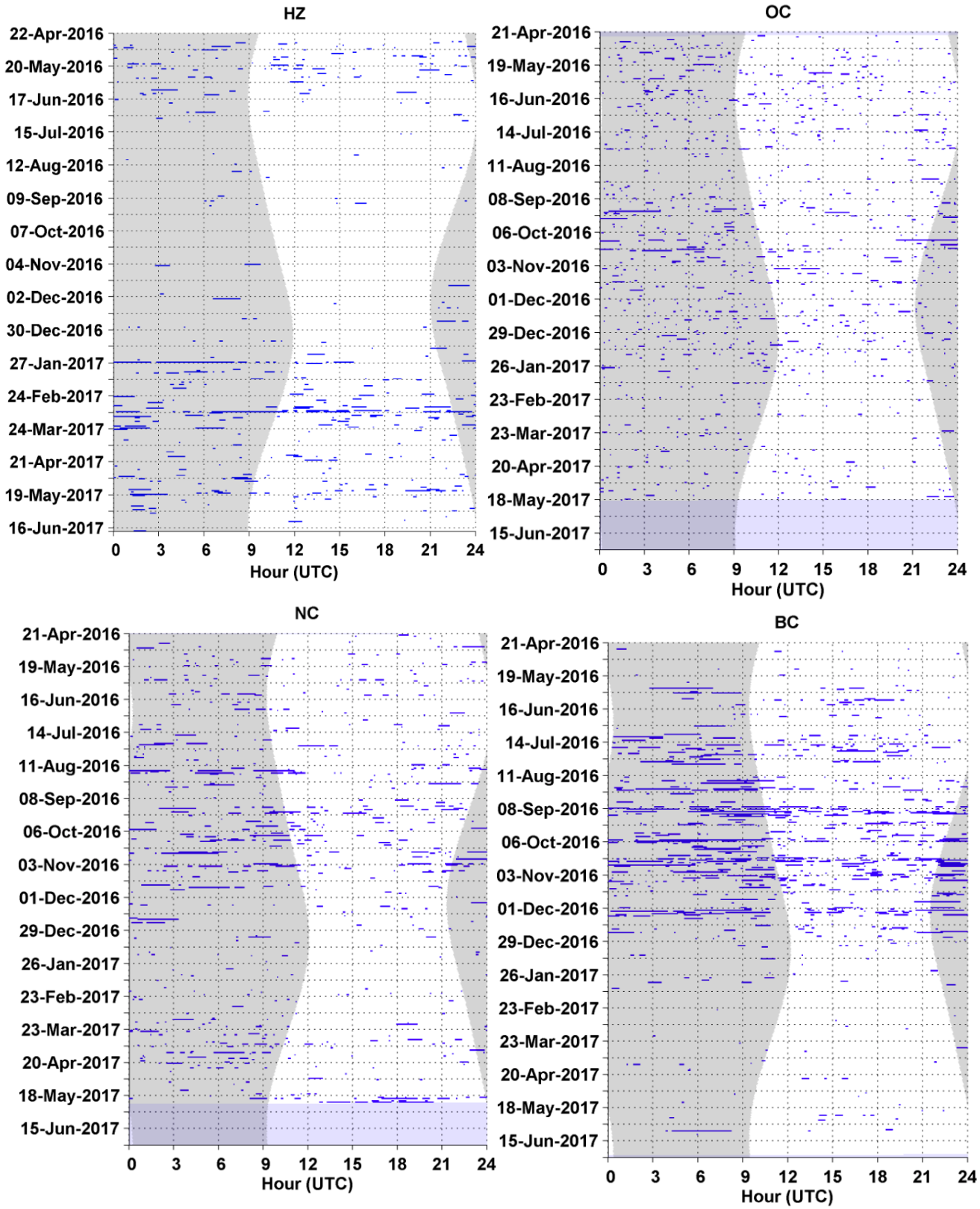

Figure 89. Click type 4 / 6 detections in five-minute bins (blue bars) at sites HZ, OC, NC, and BC. Effort markings are described in Figure 49.

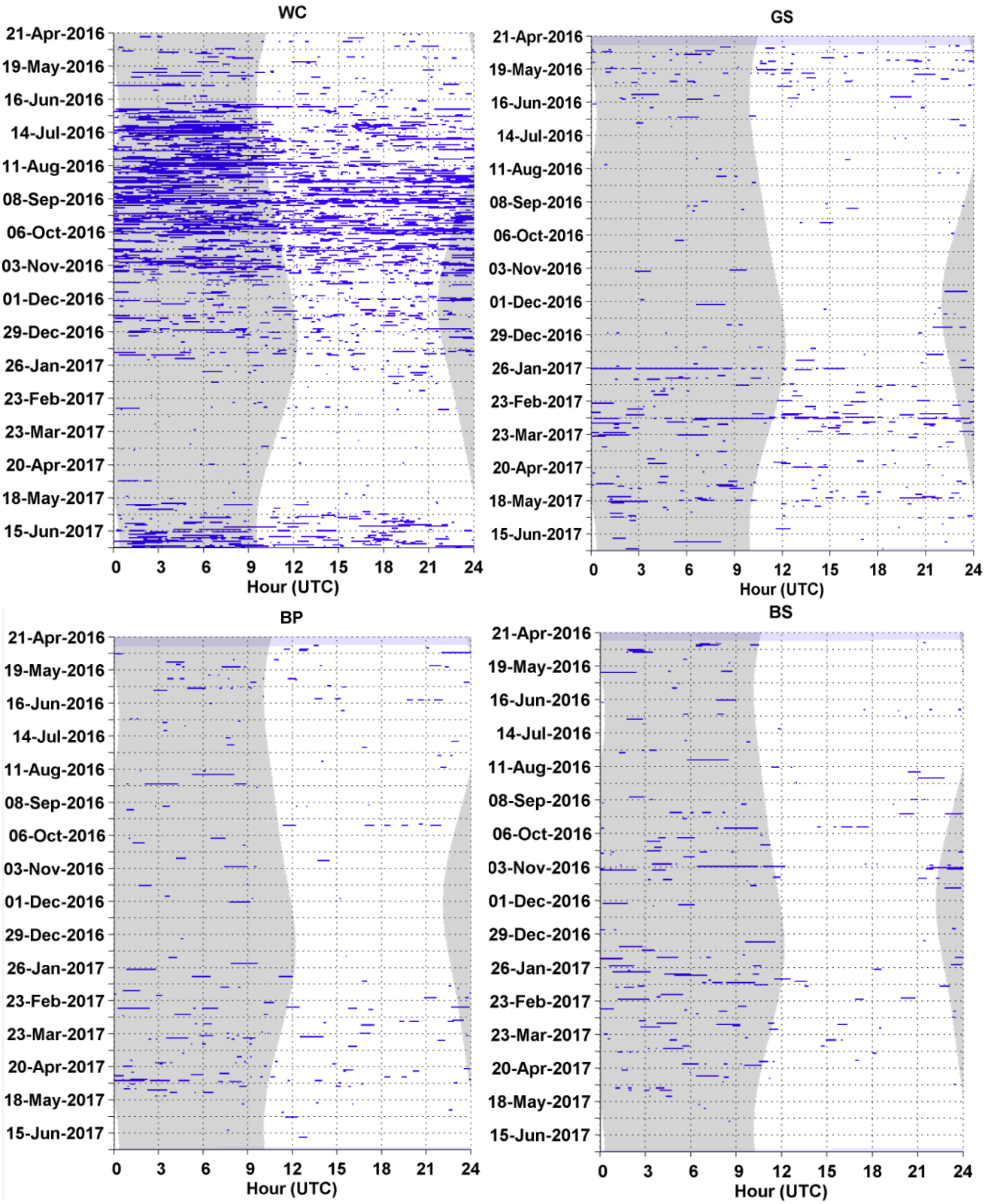

Figure 90. Click type 4 / 6 detections in five-minute bins (blue bars) at sites WC, GS, BP, and BS. Effort markings are described in Figure 49.

Click Type 5

- Click type 5 was detected intermittently with higher detection rates at the northern sites, NC, OC, BC, and WC (Figure 91, Figure 92).
- Click type 5 occurred primarily during nighttime hours (Figure 93, Figure 94).

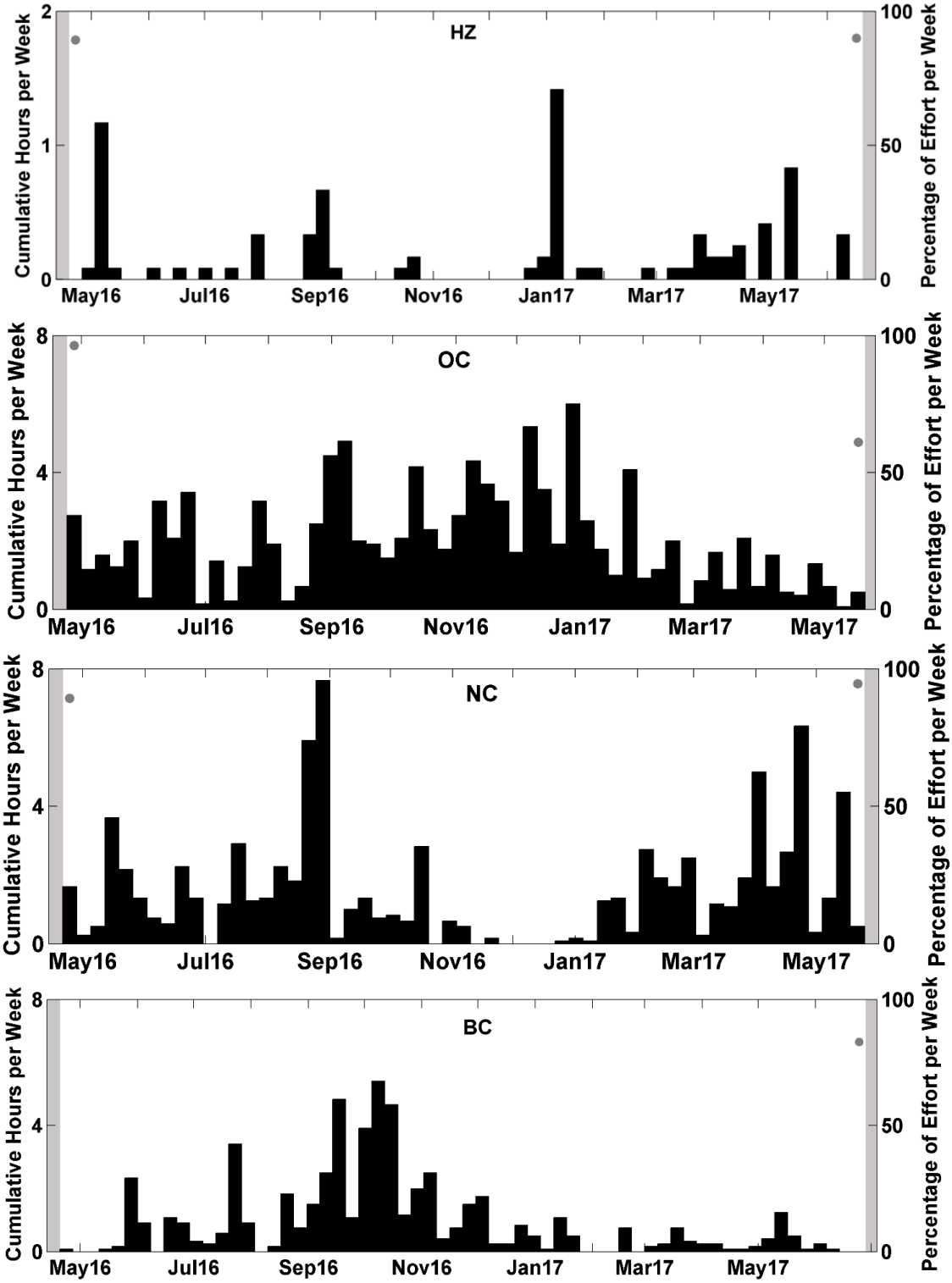

Figure 91. Weekly presence (black bars) of click type 5 detections between April 2016 and June 2017 at sites HZ, OC, NC, and BC. Effort markings are described in Figure 47.

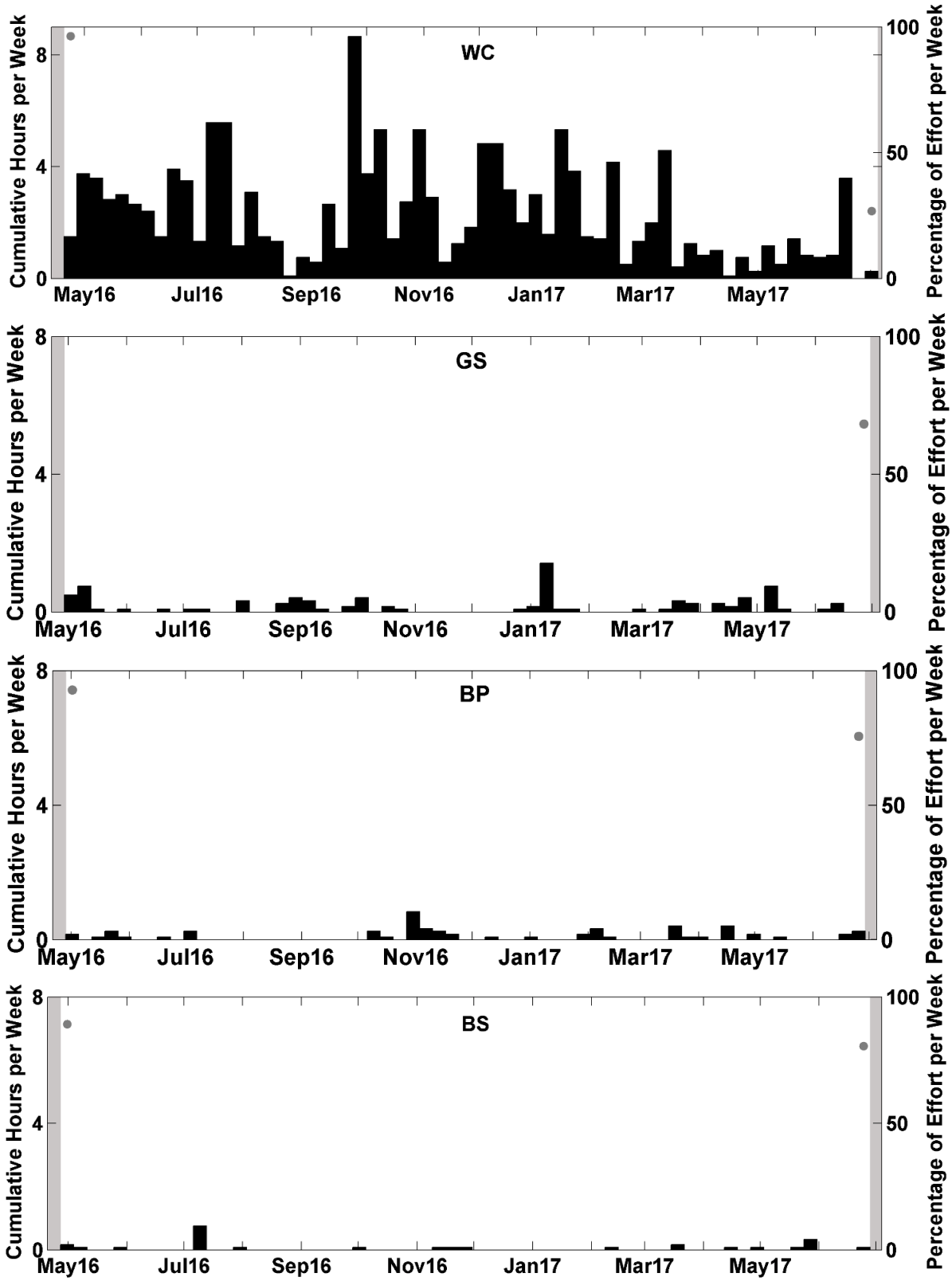

Figure 92. Weekly presence (black bars) of click type 5 detections between April 2016 and June 2017 at sites WC, GS, BP, and BS. Effort markings are described in Figure 47.

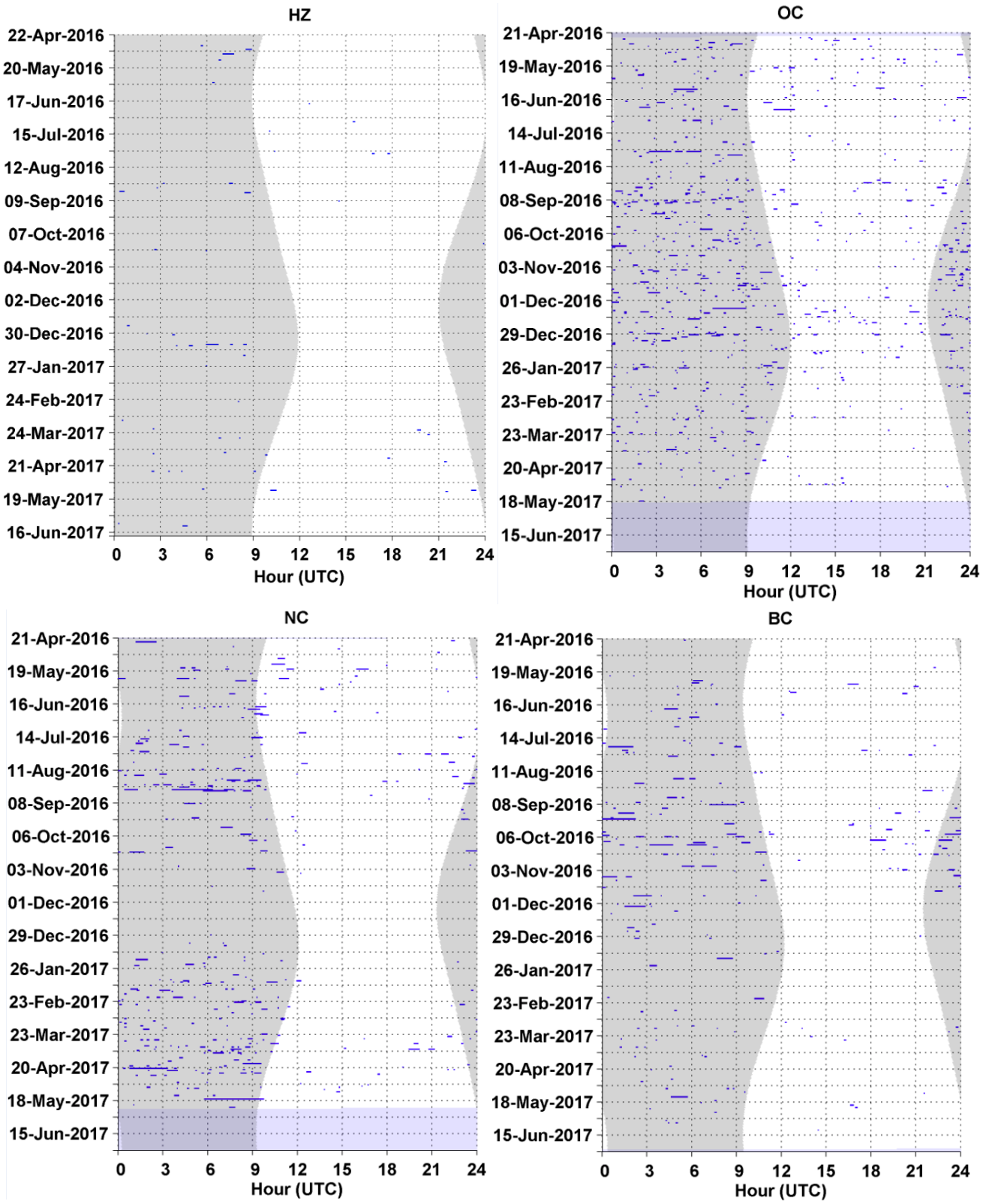

Figure 93. Click type 5 detections in five-minute bins (blue bars) at sites HZ, OC, NC, and BC. Effort markings are described in Figure 49.

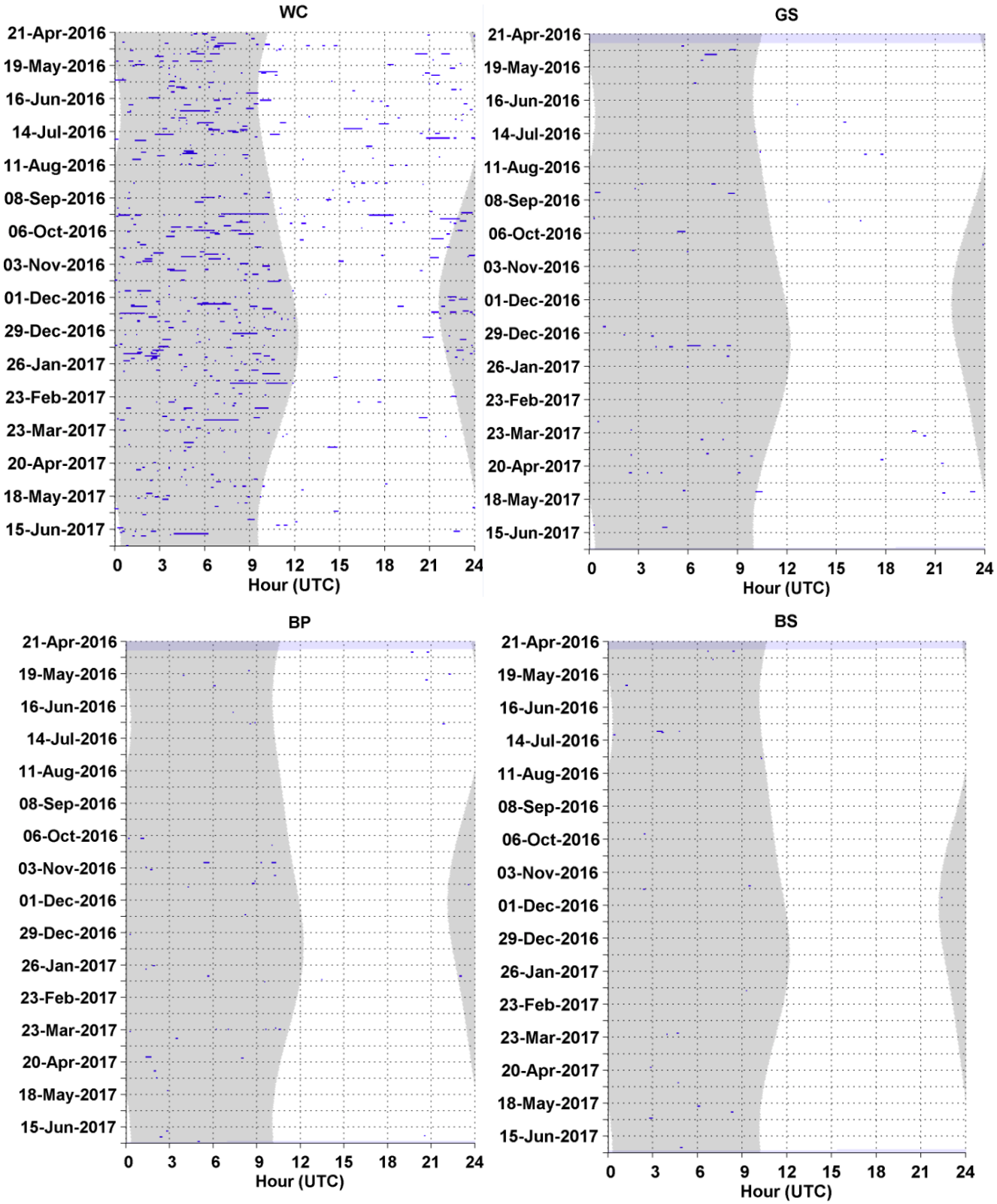

Figure 94. Click type 5 detections in five-minute bins (blue bars) at sites WC, GS, BP, and BS. Effort markings are described in Figure 49.

Click Type 7

- Click type 7 was detected at all eight sites (Figure 95, Figure 96). Detections were high from November 2016 to March 2017 at sites NC, WC, and BC (Figure 95, Figure 96). Detections were lowest at sites HZ, BS, BP, and GS (Figure 96).
- Click type 7 occurred almost exclusively during the nighttime hours (Figure 97, Figure 98).

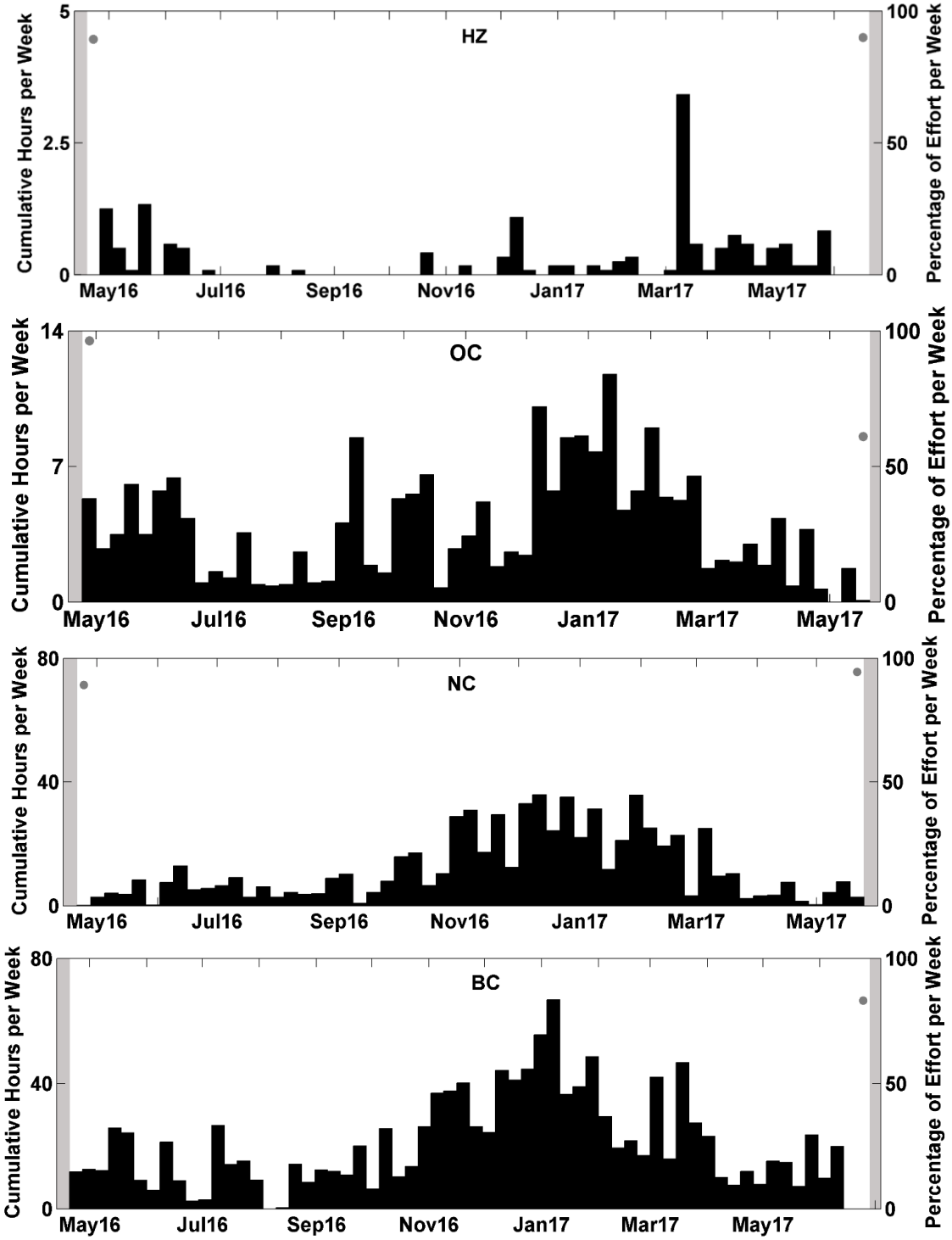

Figure 95. Weekly presence (black bars) of click type 7 detections between April 2016 and June 2017 at sites HZ, OC, NC, and BC. Effort markings are described in Figure 47. ***Note: Axis change for site HZ and OC due to a lower amount of click type 7 detections compared to the rest of the sites*****.**

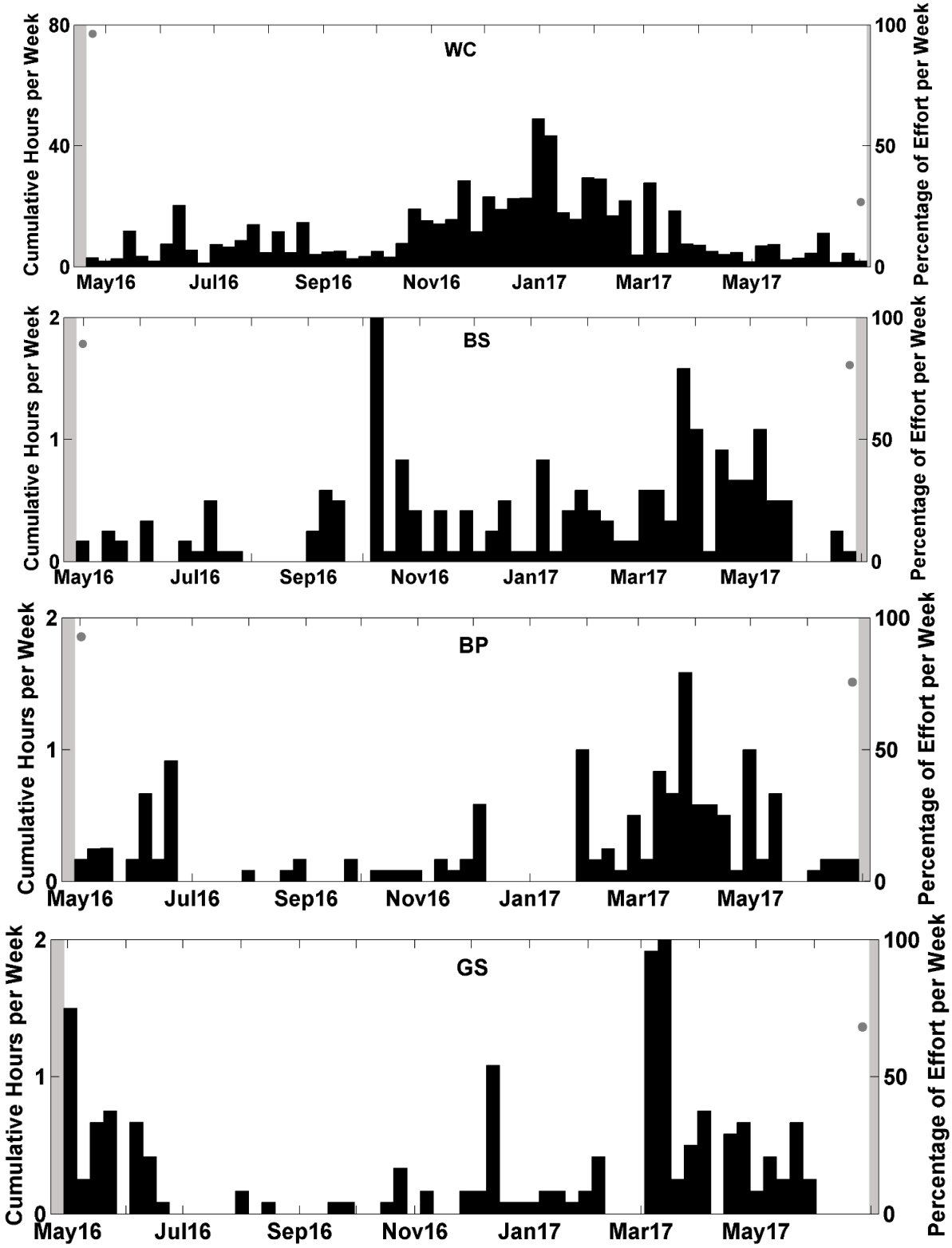

Figure 96. Weekly presence (black bars) of click type 7 detections between April 2016 and June 2017 at sites WC, GS, BP, and BS. Effort markings are described in Figure 47. *Note: Axis change for sites BS, BP, and GS due to a lower amount of click type 7 detections compared to the rest of the sites*.

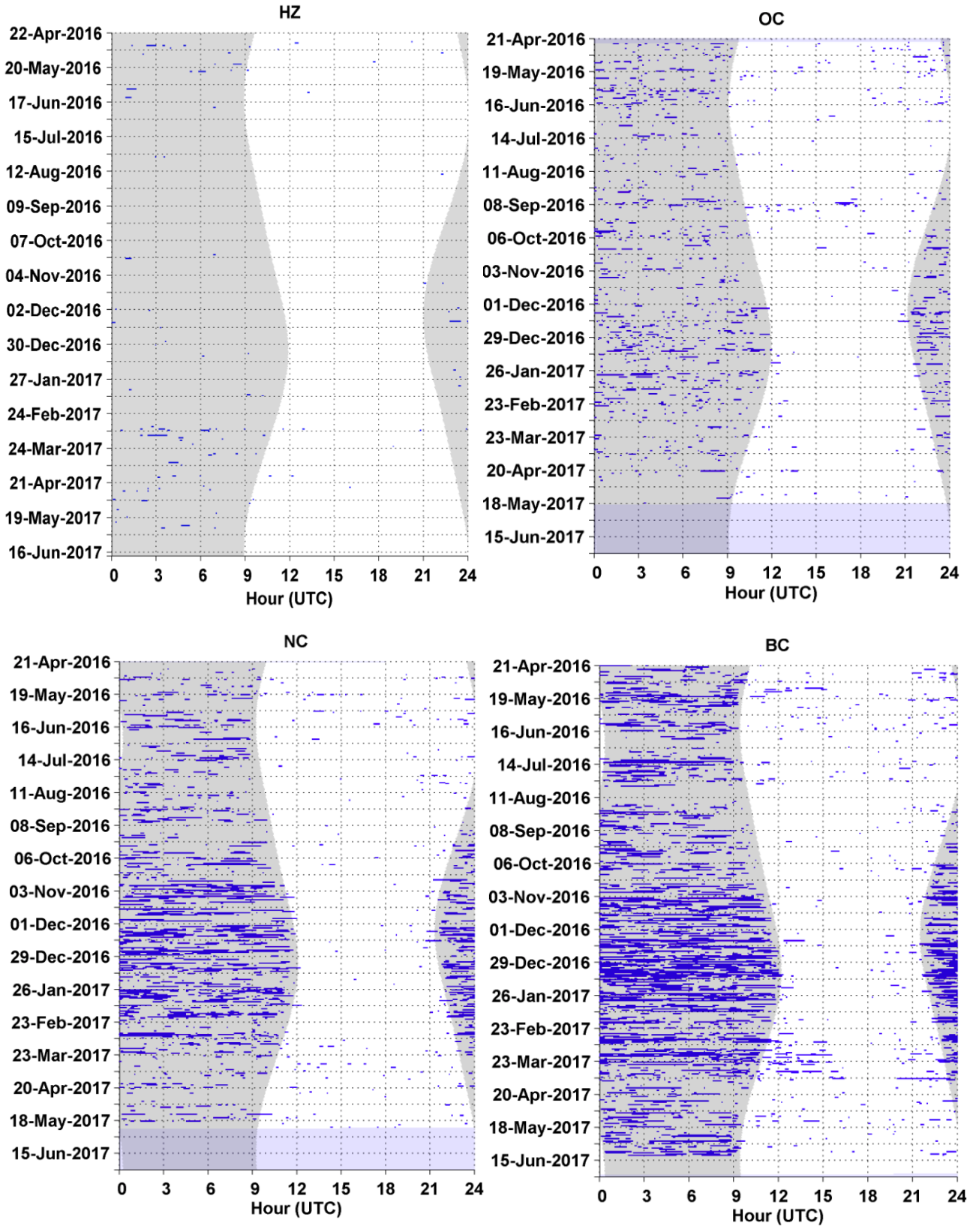

Figure 97. Click type 7 detections in five-minute bins (blue bars) at sites HZ, OC, NC, and BC. Effort markings are described in Figure 49.

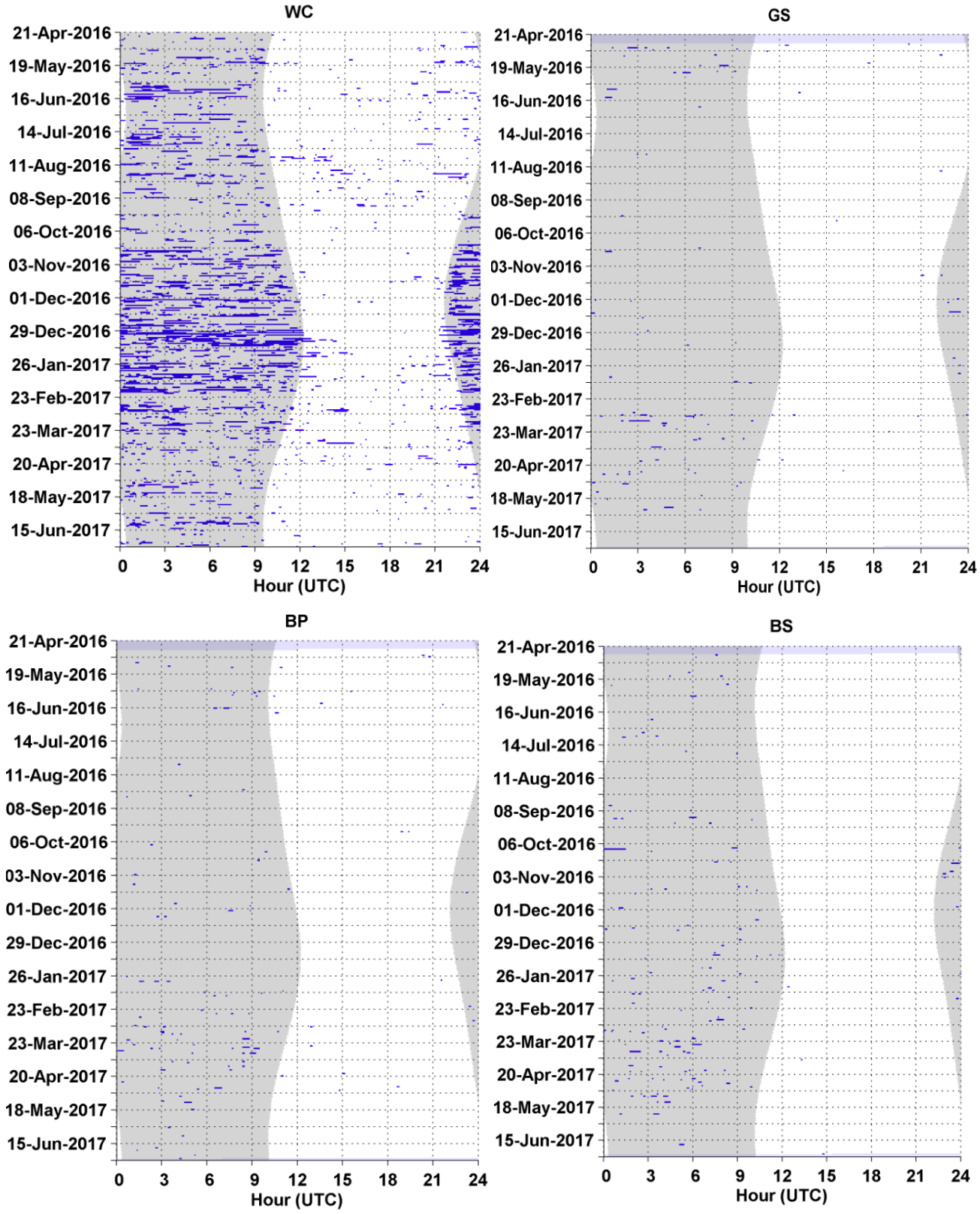

Figure 98. Click type 7 detections in five-minute bins (blue bars) at sites WC, GS, BP, and BS. Effort markings are described in Figure 49.

Click Type 8

- Click type 8 was detected regularly at all eight sites (Figure 99, Figure 100) with the highest detections occurring at sites NC, WC, and BC. Sites BS, BP, and GS had the lowest amount of detections.
- Click type 8 clicks occurred primarily during nighttime hours (Figure 101, Figure 102).

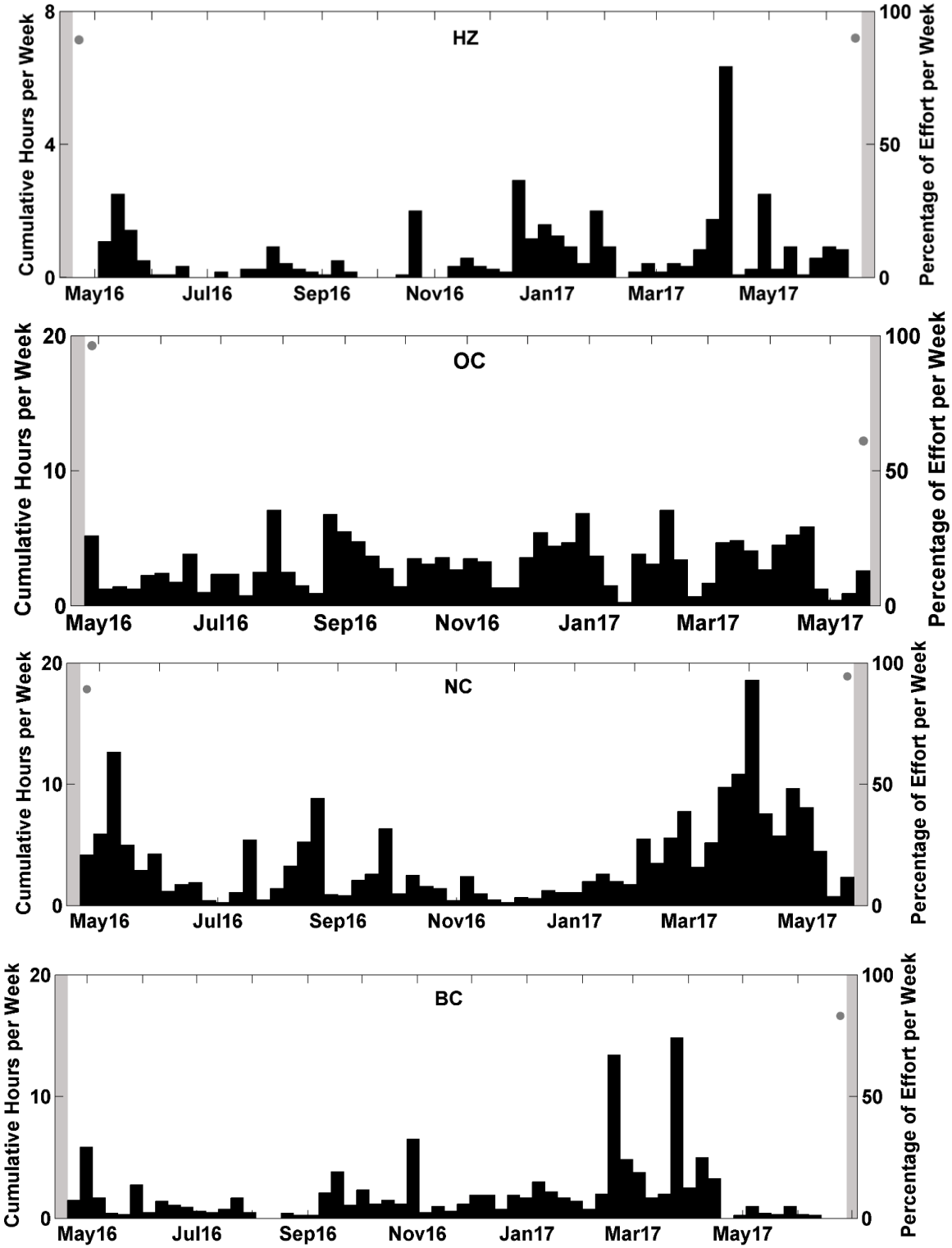

Figure 99. Weekly presence (black bars) of click type 8 detections between April 2016 and June 2017 at sites HZ, OC, NC, and BC. Effort markings are described in Figure 47. ***Note: Axis change for sites HZ due to a lower amount of click type 8 detections compared to the rest of the sites*****.**

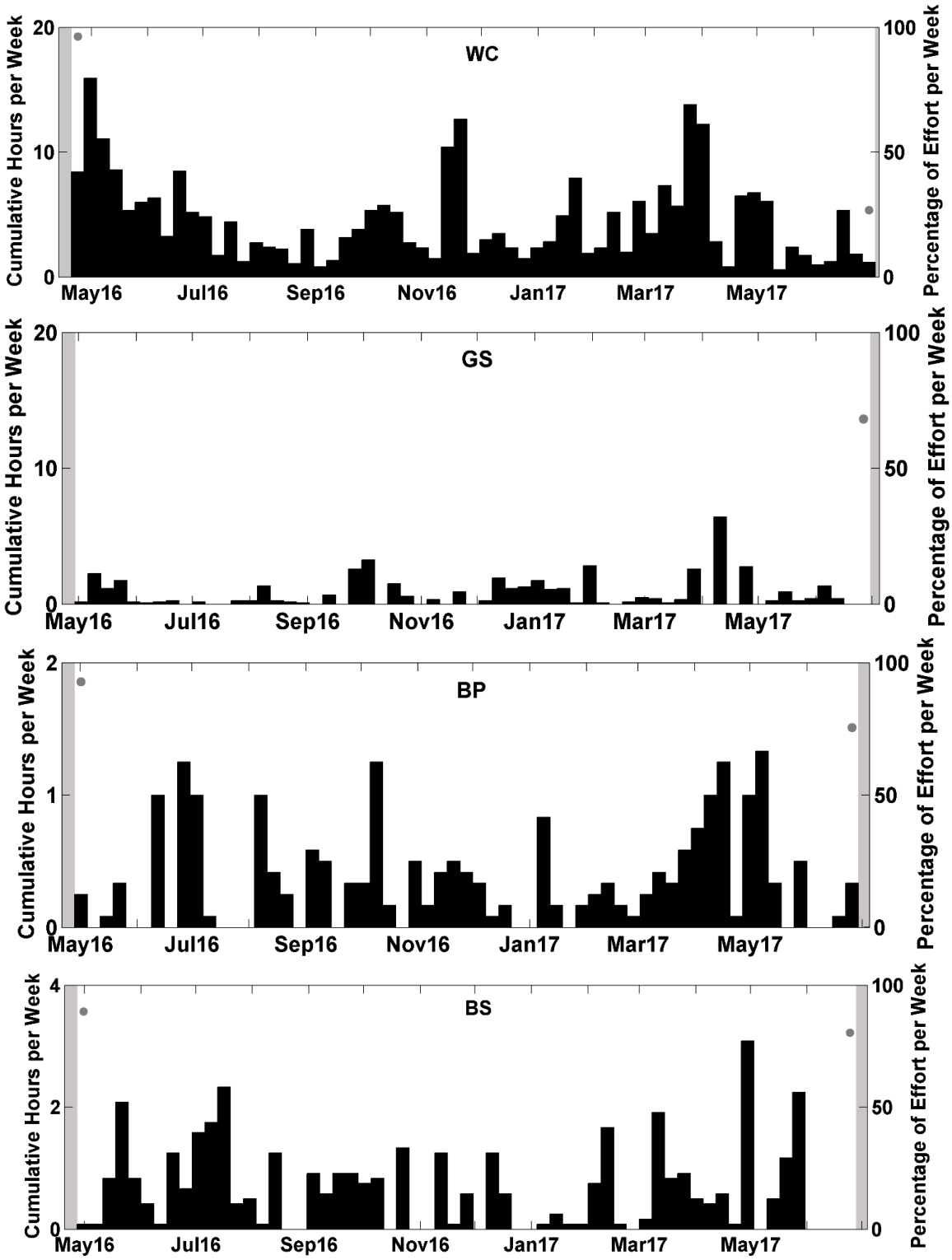

Figure 100. Weekly presence (black bars) of click type 8 detections between April 2016 and June 2017 at sites WC, GS, BP, and BS. Effort markings are described in Figure 47. *Note: Axis change for sites BS and BP due to a lower amount of click type 8 detections compared to the rest of the sites.*

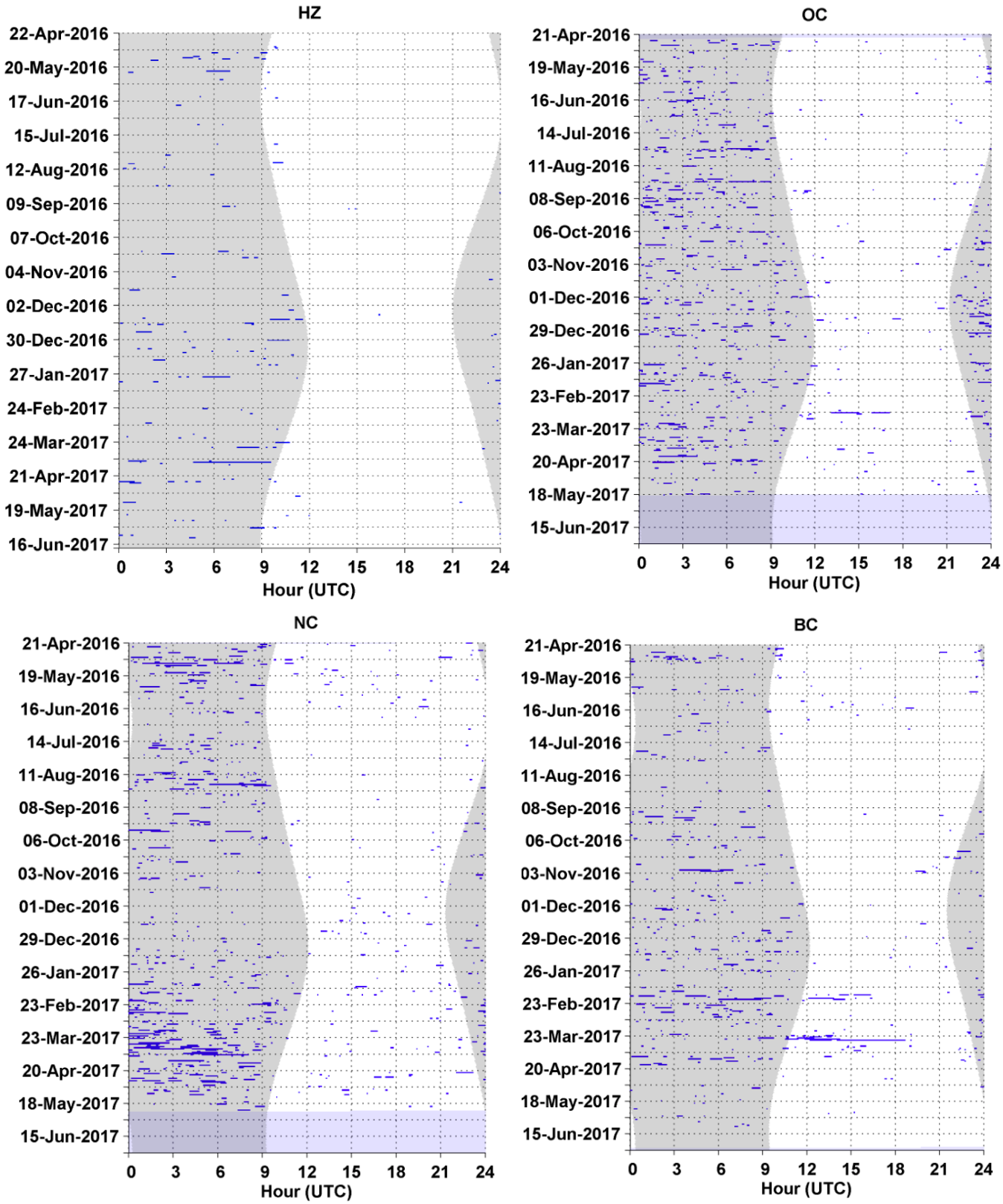

Figure 101. Click type 8 detections in five-minute bins (blue bars) at sites HZ, OC, NC, and BC. Effort markings are described in Figure 49.

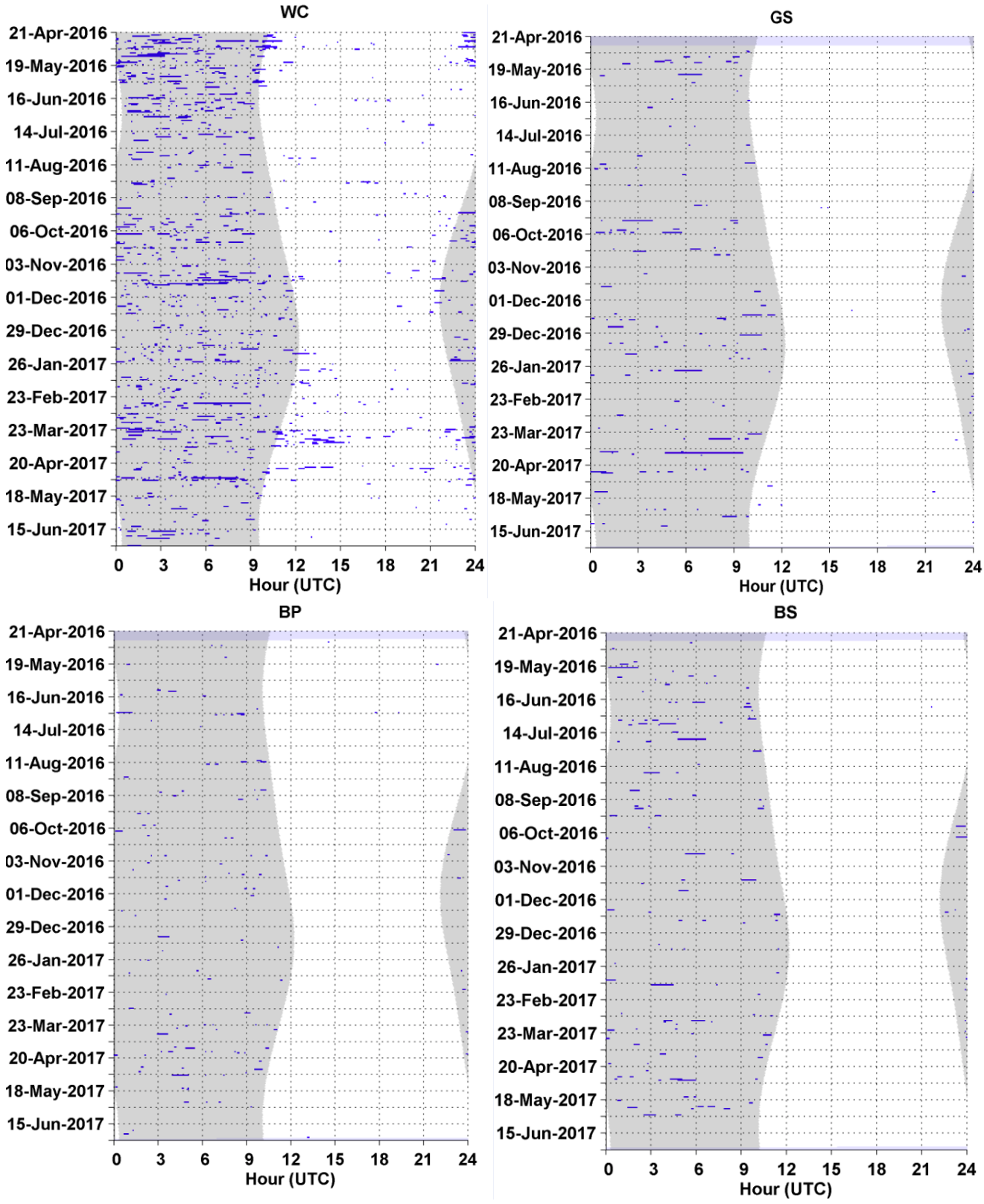

Figure 102. Click type 8 detections in five-minute bins (blue bars) at sites WC, GS, BP, and BS. Effort markings are described in Figure 49.

Click Type 9

- Click type 9 was detected regularly across all eight sites (Figure 103, Figure 104). Detections were highest at sites HZ, WC, and BC (Figure 103, Figure 104).
- Click type 9 occurred primarily during the daytime hours (Figure 105, Figure 106).

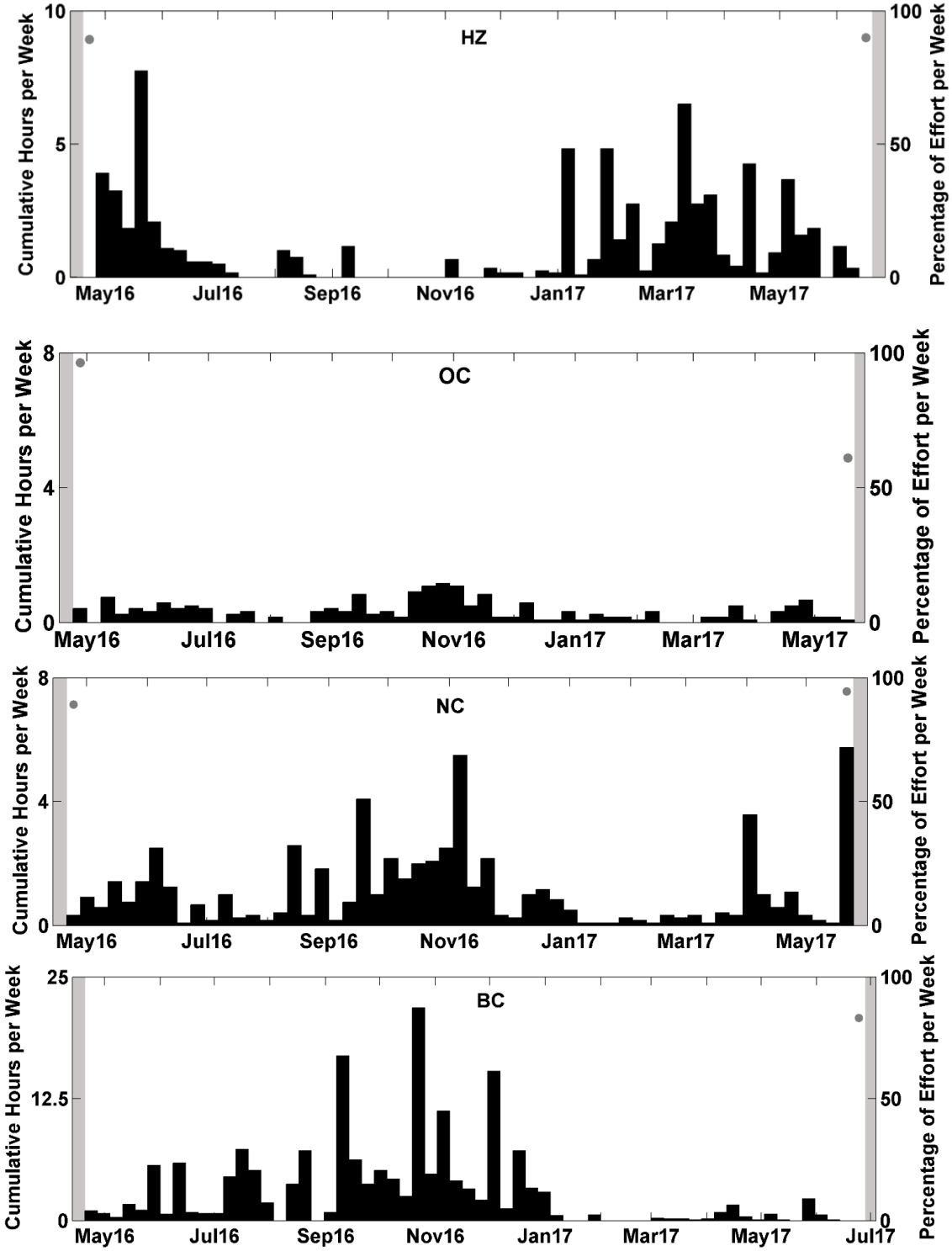

Figure 103. Weekly presence (black bars) of click type 9 detections between April 2016 and June 2017 at sites HZ, OC, NC, and BC. Effort markings are described in Figure 47. *Note: Axis change for sites HZ and BC due to a higher amount of click type 9 detections compared to the rest of the sites*.

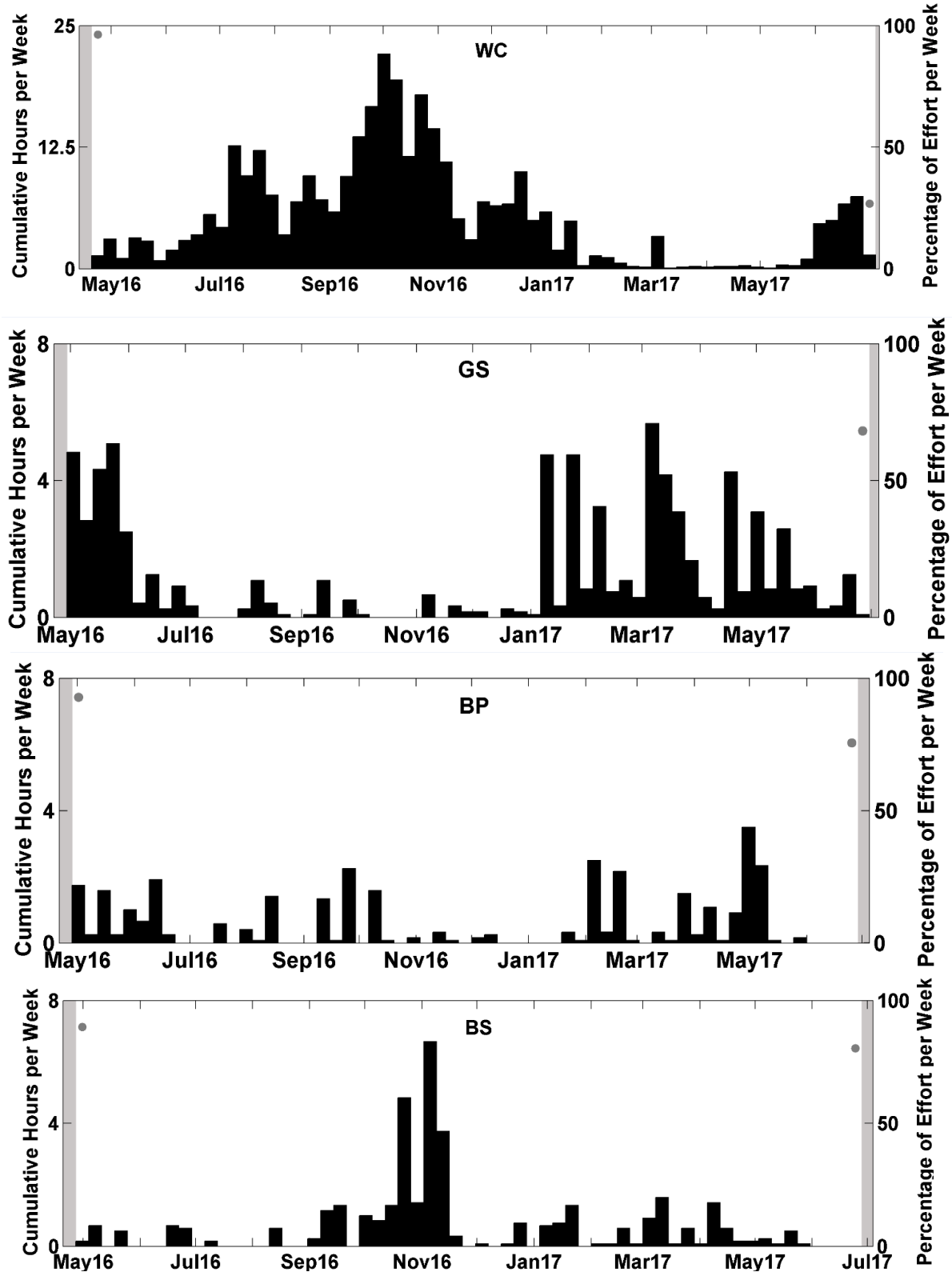

Figure 104. Weekly presence (black bars) of click type 9 detections between April 2016 and June 2017 at sites WC, GS, BP, and BS. Effort markings are described in Figure 47. ***Note: Axis change for site WC due to a higher amount of click type 9 detections compared to the rest of the sites*****.**

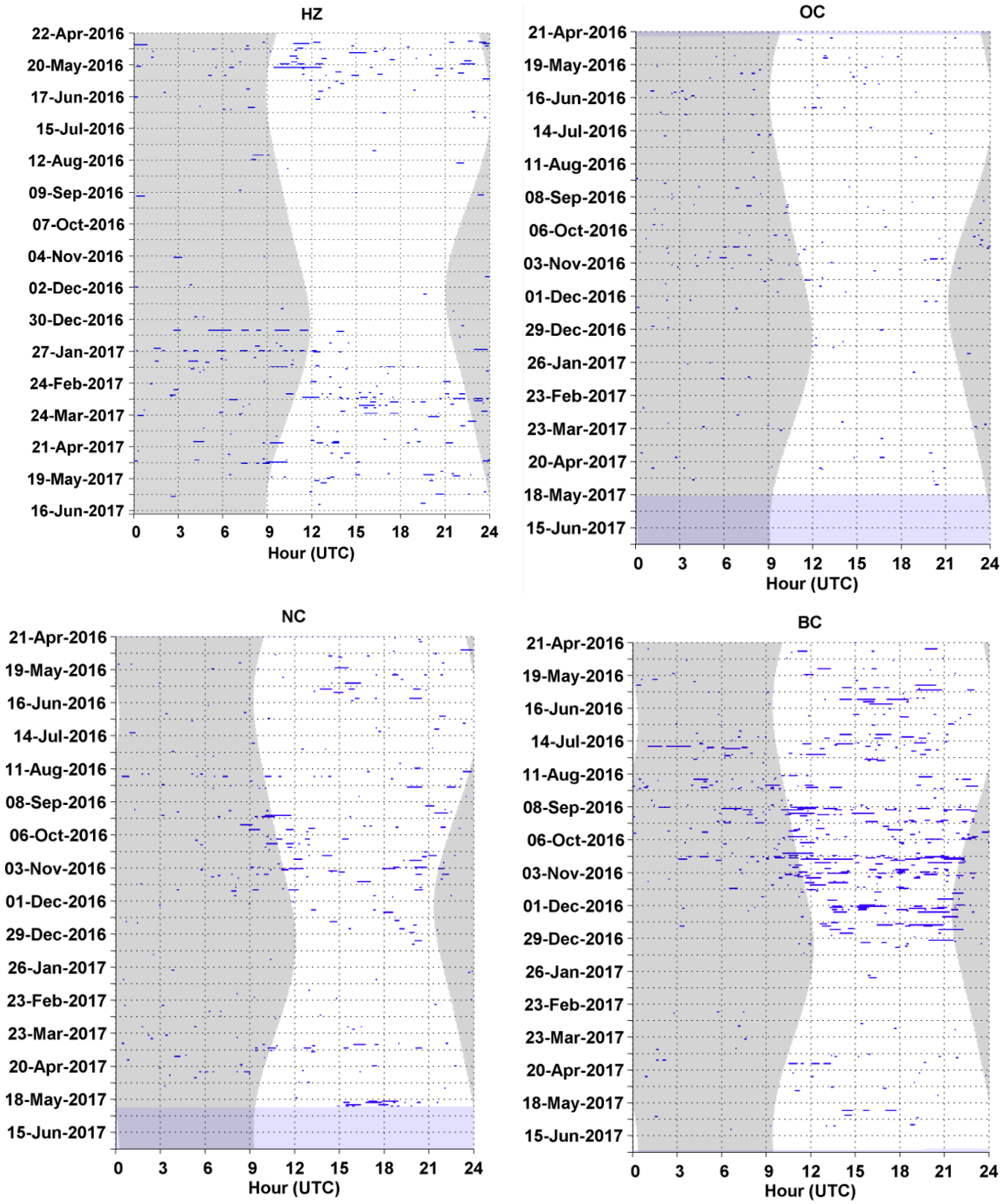

Figure 105. Click type 9 detections in five-minute bins (blue bars) at sites HZ, OC, NC, and BC. Effort markings are described in Figure 49.

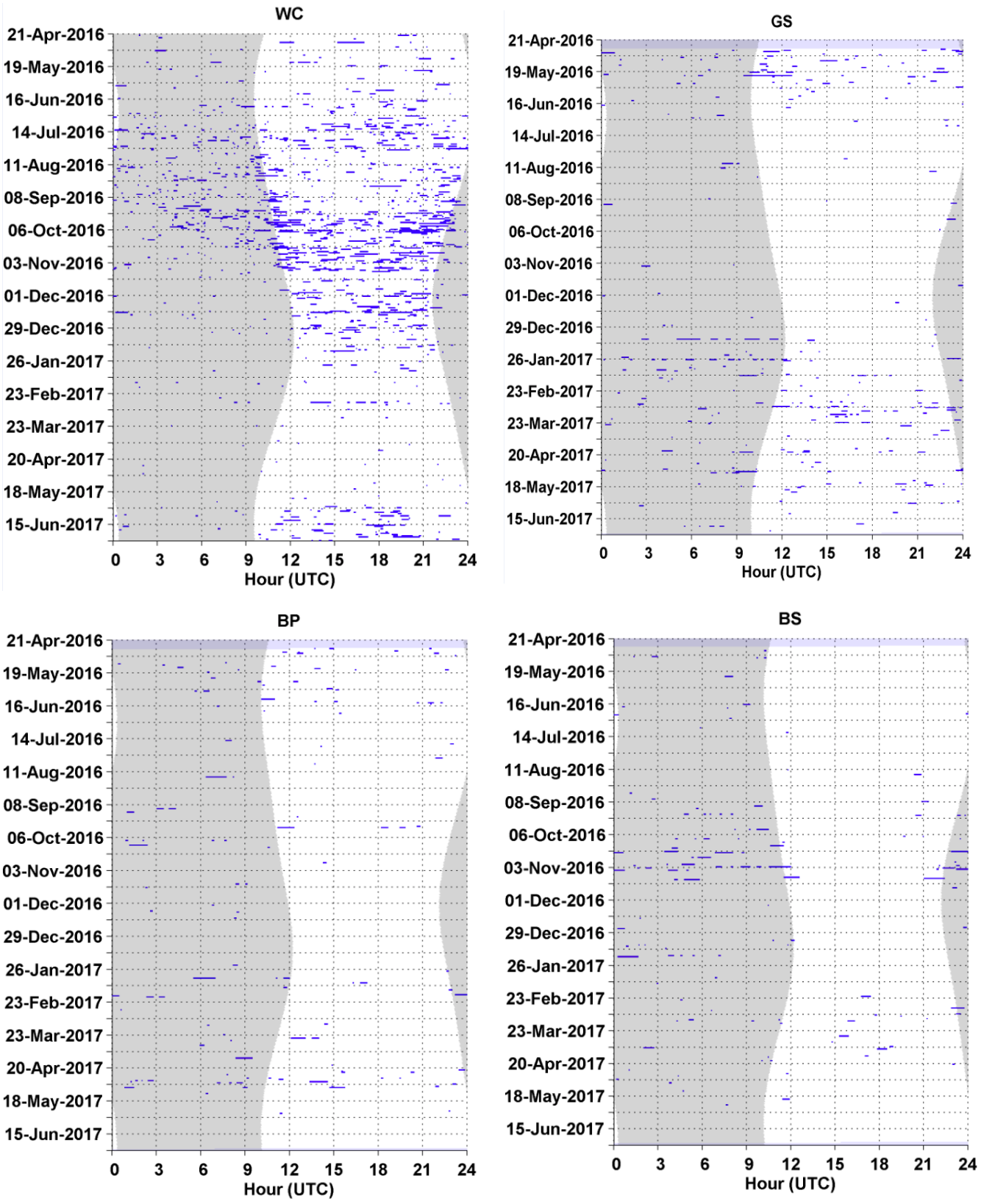

Figure 106. Click type 9 detections in five-minute bins (blue bars) at sites WC, GS, BP, and BS. Effort markings are described in Figure 49.

Click Type 10

- Click type 10 occurred regularly across all eight sites (Figure 107, Figure 108) with detections highest between July and November 2016 at sites NC, WC, and BC (Figure 107, Figure 108).
- There was no diel pattern for click type 10 (Figure 109, Figure 110).

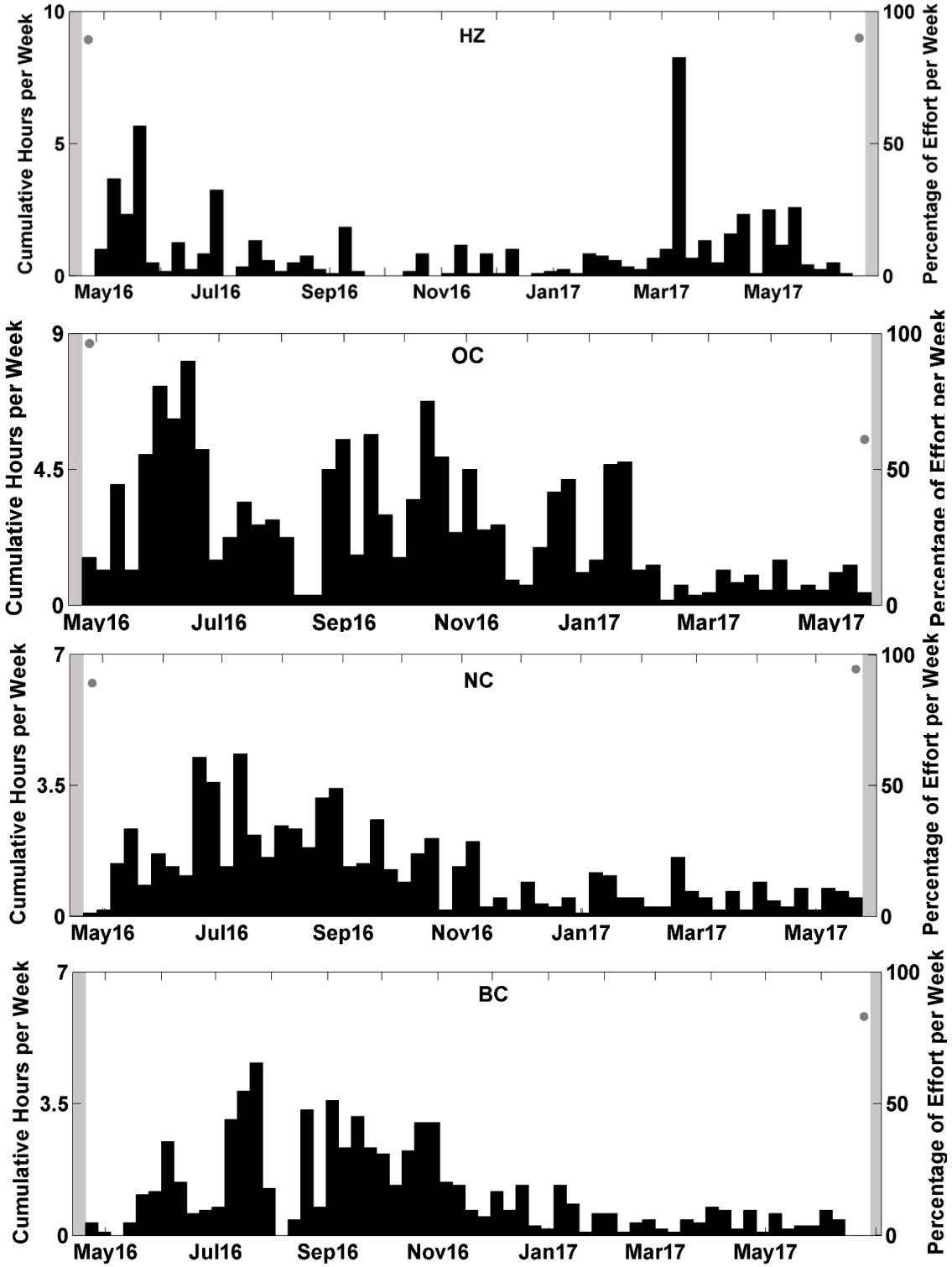

Figure 107. Weekly presence (black bars) of click type 10 detections between April 2016 and June 2017 at sites HZ, OC, NC, and BC. Effort markings are described in Figure 47. ***Note: Axis change for site HZ and OC due to a higher amount of click type 10 detections compared to the rest of the sites*****.**

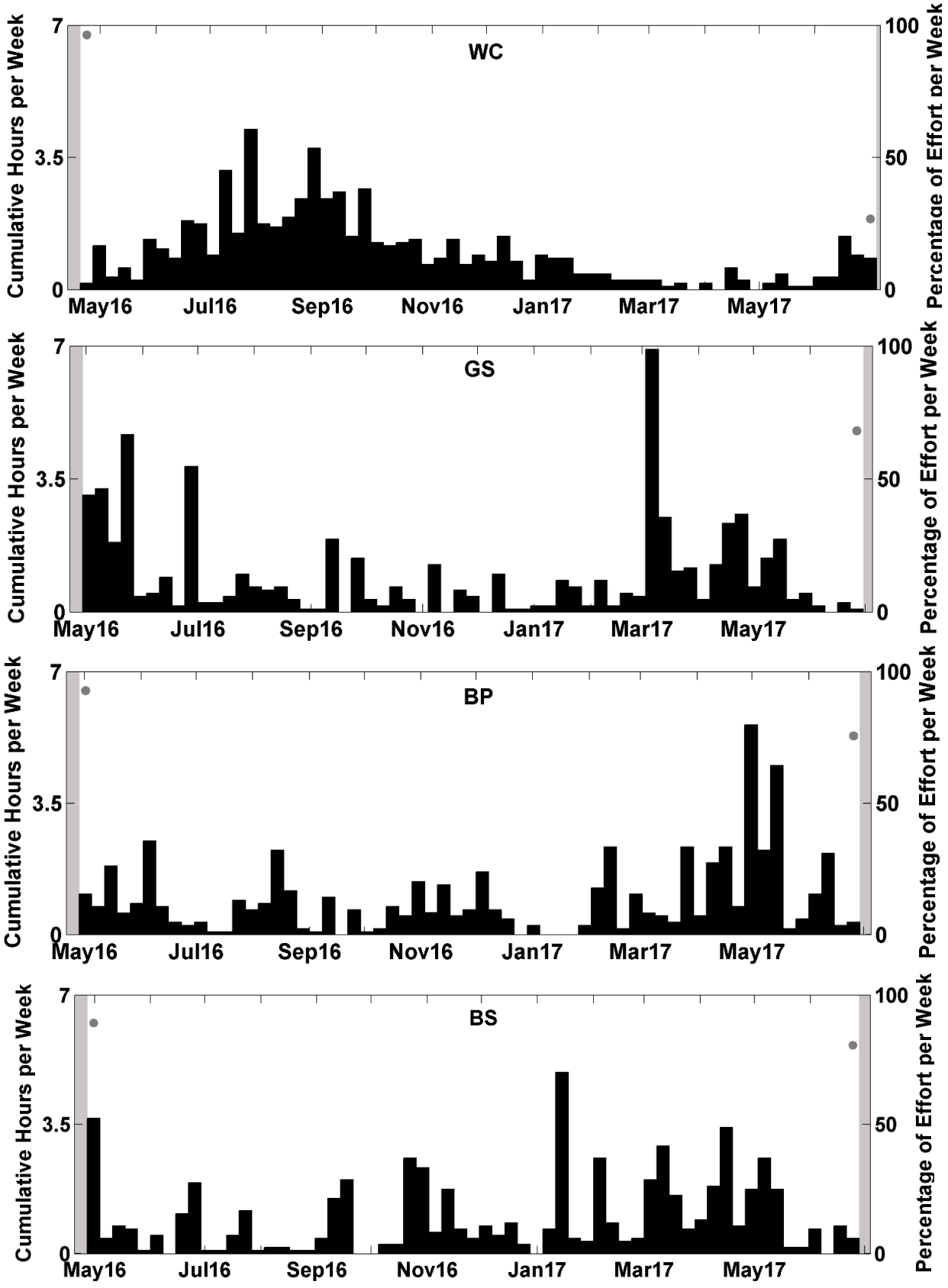

Figure 108. Weekly presence (black bars) of click type 10 detections between April 2016 and June 2017 at sites WC, GS, BP, and BS. Effort markings are described in Figure 47.

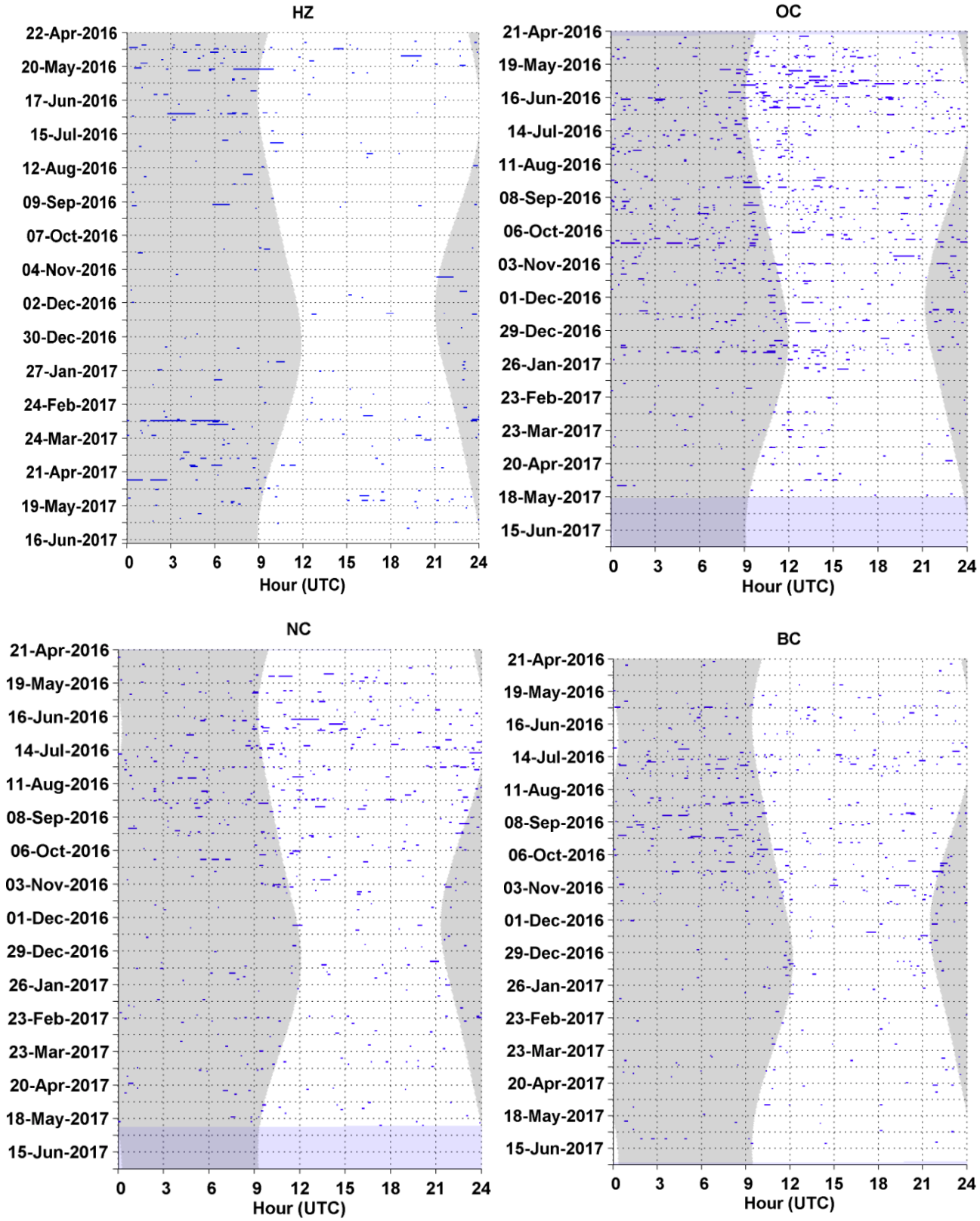

Figure 109. Click type 10 detections in five-minute bins (blue bars) at sites HZ, OC, NC, and BC. Effort markings are described in Figure 49.

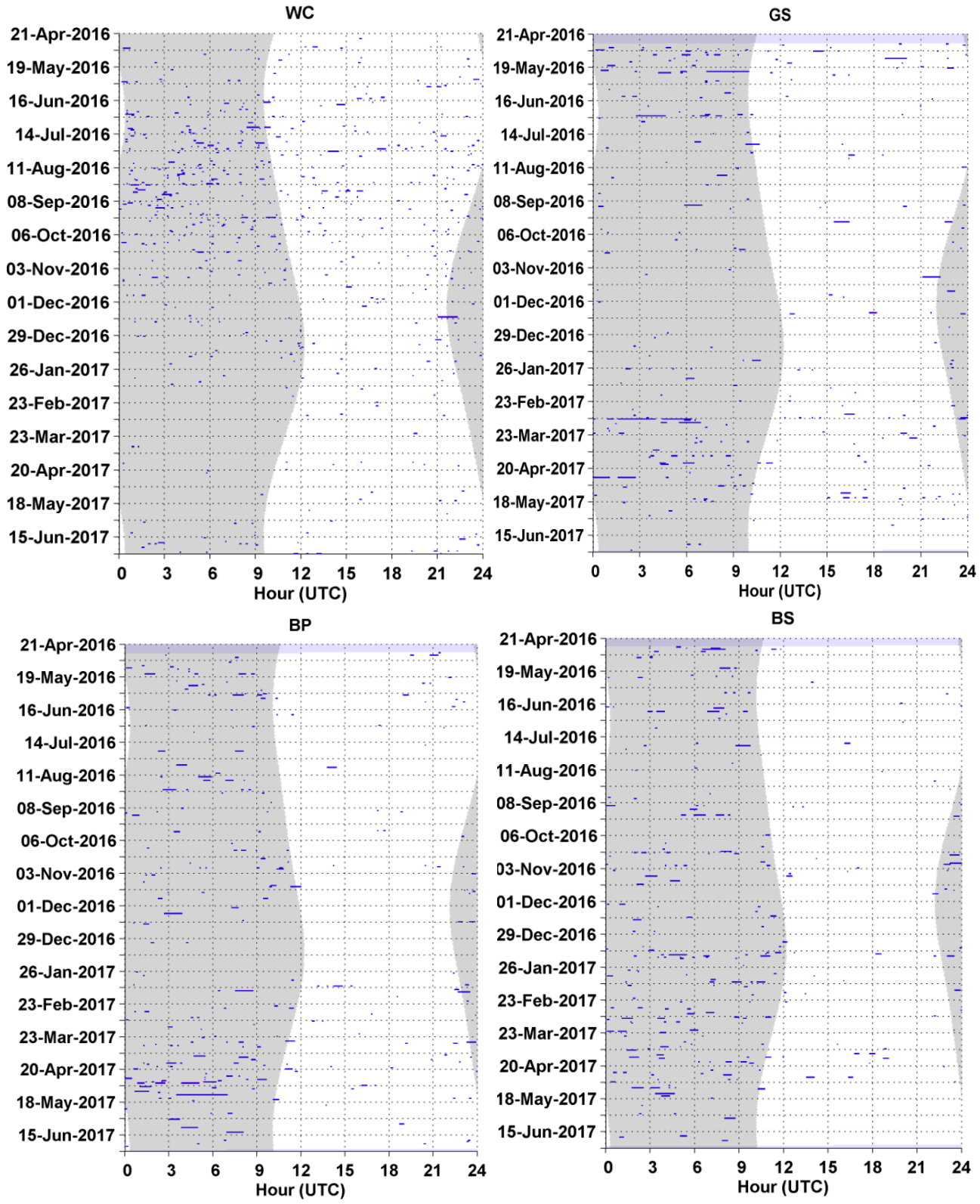

Figure 110. Click type 10 detections in five-minute bins (blue bars) at sites WC, GS, BP, and BS. Effort markings are described in Figure 49.

Unclassified Odontocete Clicks

Signals that had characteristics of odontocete clicks, but could not be classified to species were labeled as unclassified odontocetes. Clicks were left unclassified if too few clicks were detected in a time bin (< 20 clicks / minute), if they did not match documented click type, or if detected clicks were of poor quality (e.g. low amplitude or masked).

- Unclassified clicks were detected throughout the recording period at all eight sites (Figure 111, Figure 112).
- There was no discernible diel pattern for unclassified clicks (Figure 113, Figure 114).

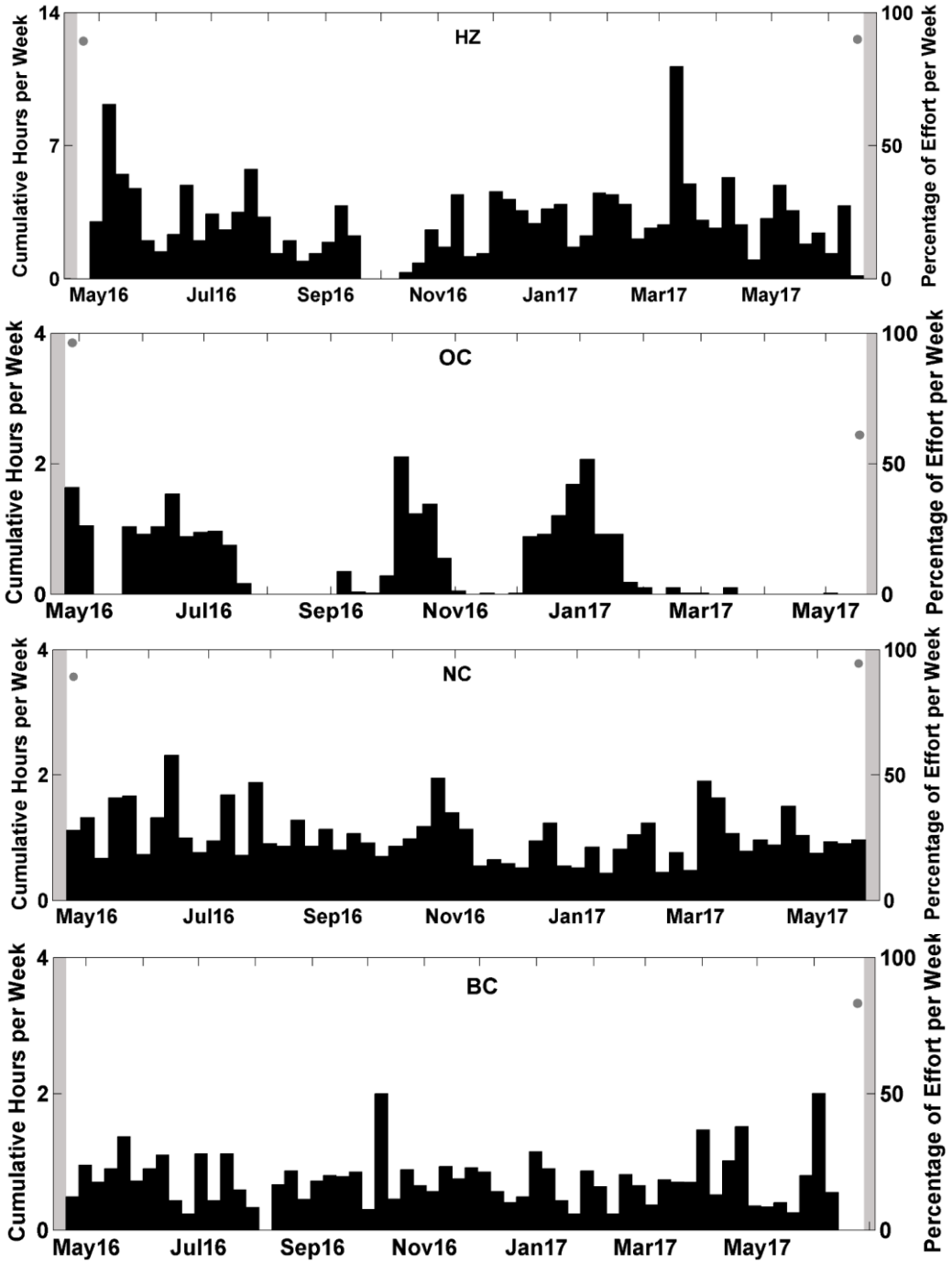

Figure 111. Weekly presence (black bars) of unclassified click detections between April 2016 and June 2017 at sites HZ, OC, NC, and BC. Effort markings are described in Figure 47.

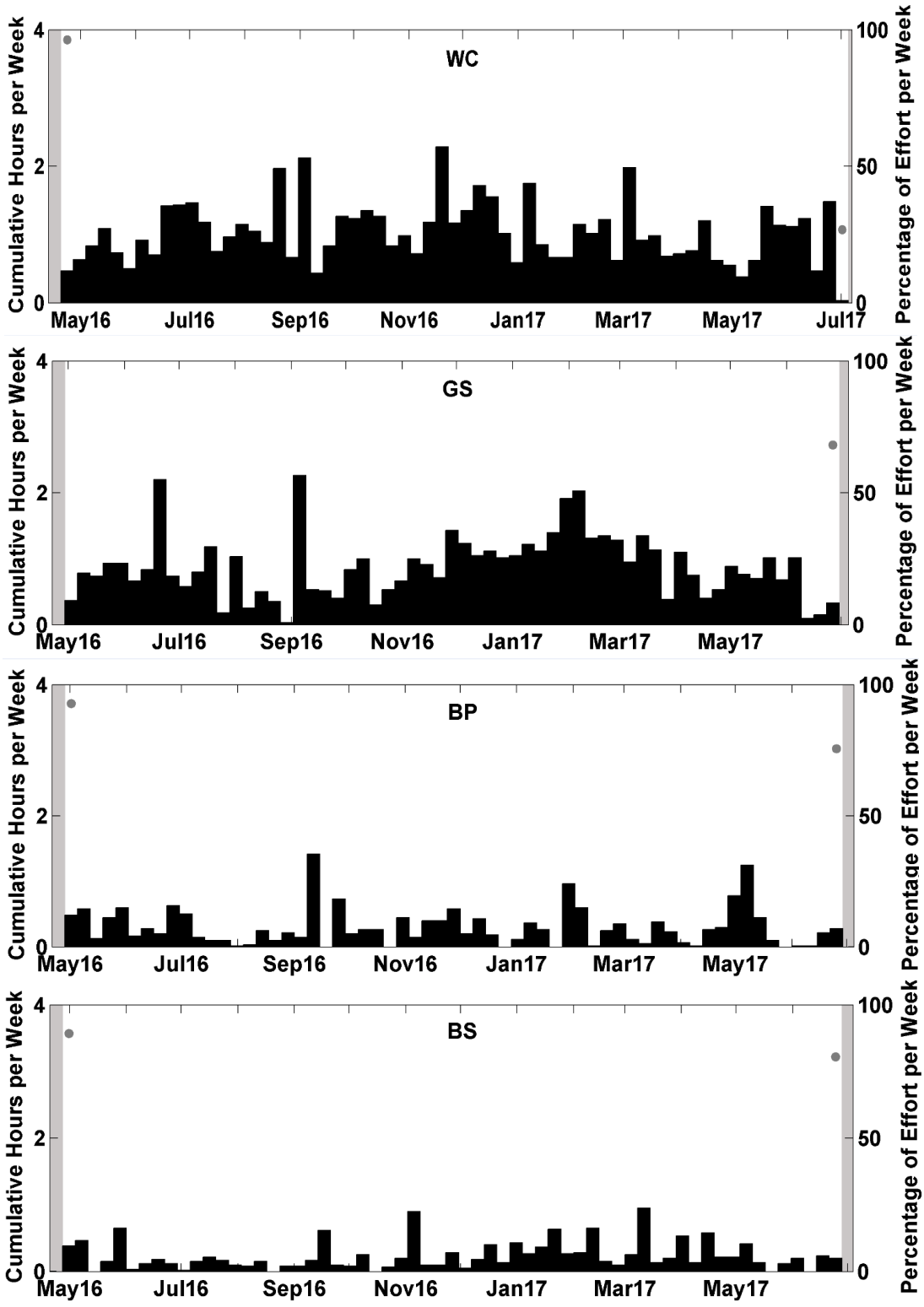

Figure 112. Weekly presence (black bars) of unclassified click detections between April 2016 and June 2017 at sites WC, GS, BP, and BS. Effort markings are described in Figure 47.

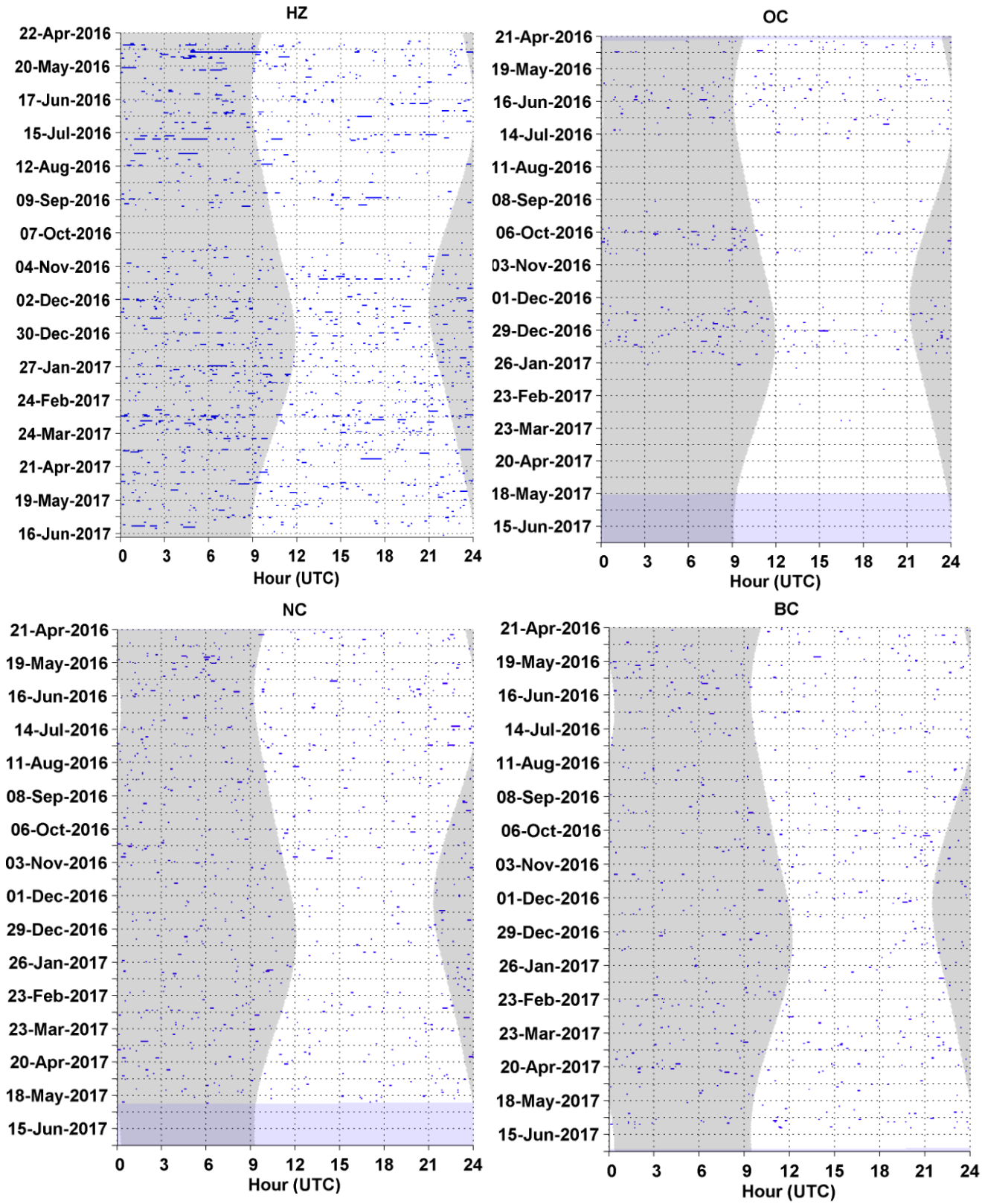

Figure 113. Unclassified lick detections in five-minute bins (blue bars) at sites HZ, OC, NC, and BC. Effort markings are described in Figure 49.

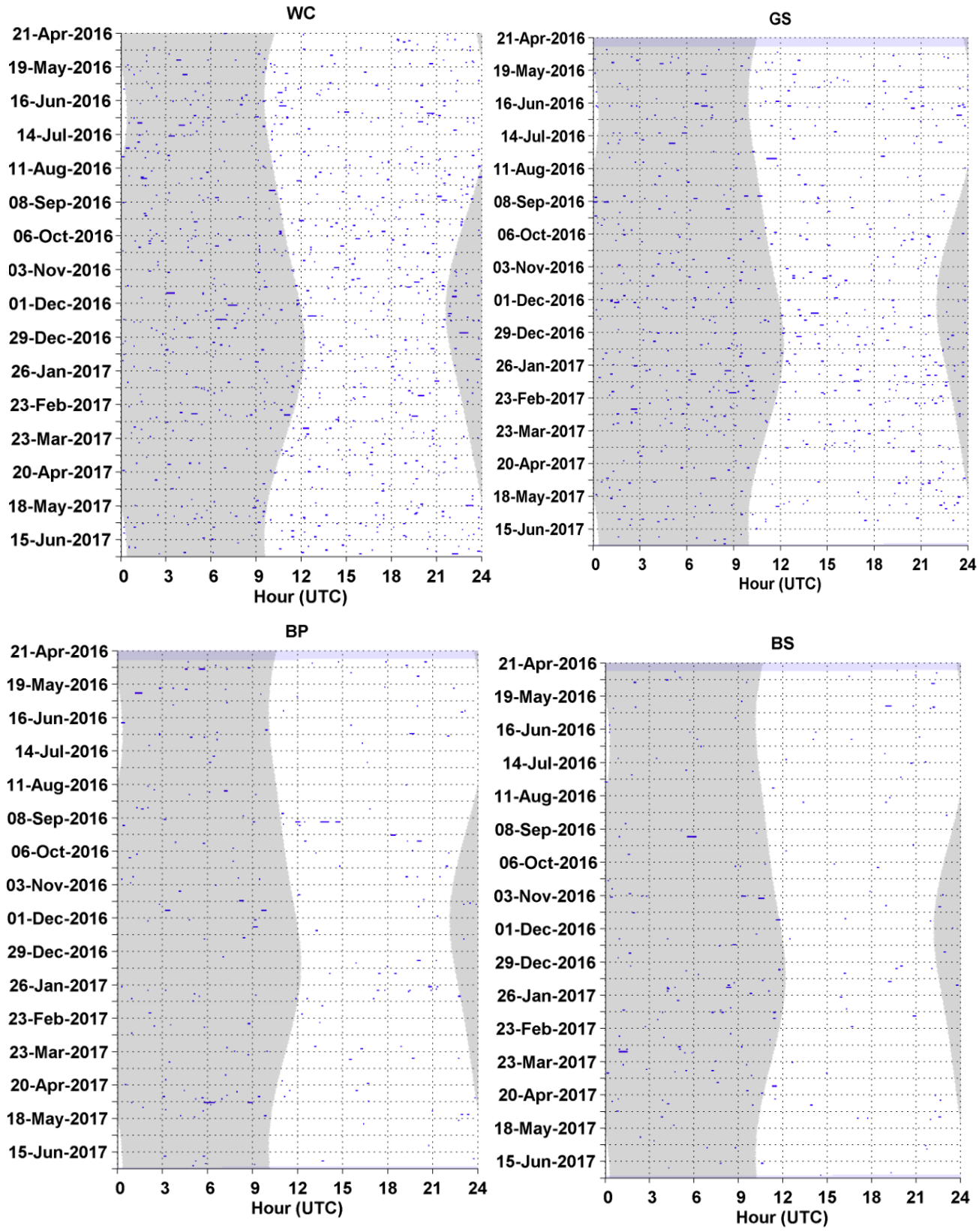

Figure 114. Unclassified click detections in five-minute bins (blue bars) at sites WC, GS, BP, and BS. Effort markings are described in Figure 49.

Anthropogenic Sounds

Four types of anthropogenic sounds were detected: broadband ship noise, explosions, airguns, and echosounders.

Broadband Ship Noise

- Broadband ship sounds were detected at all eight sites (Figure 115, Figure 116) during the recording period. Site WC and BC had the highest amount of ship detections.
- There was no diel pattern for broadband ship sounds at the eight sites (Figure 117, Figure 118).

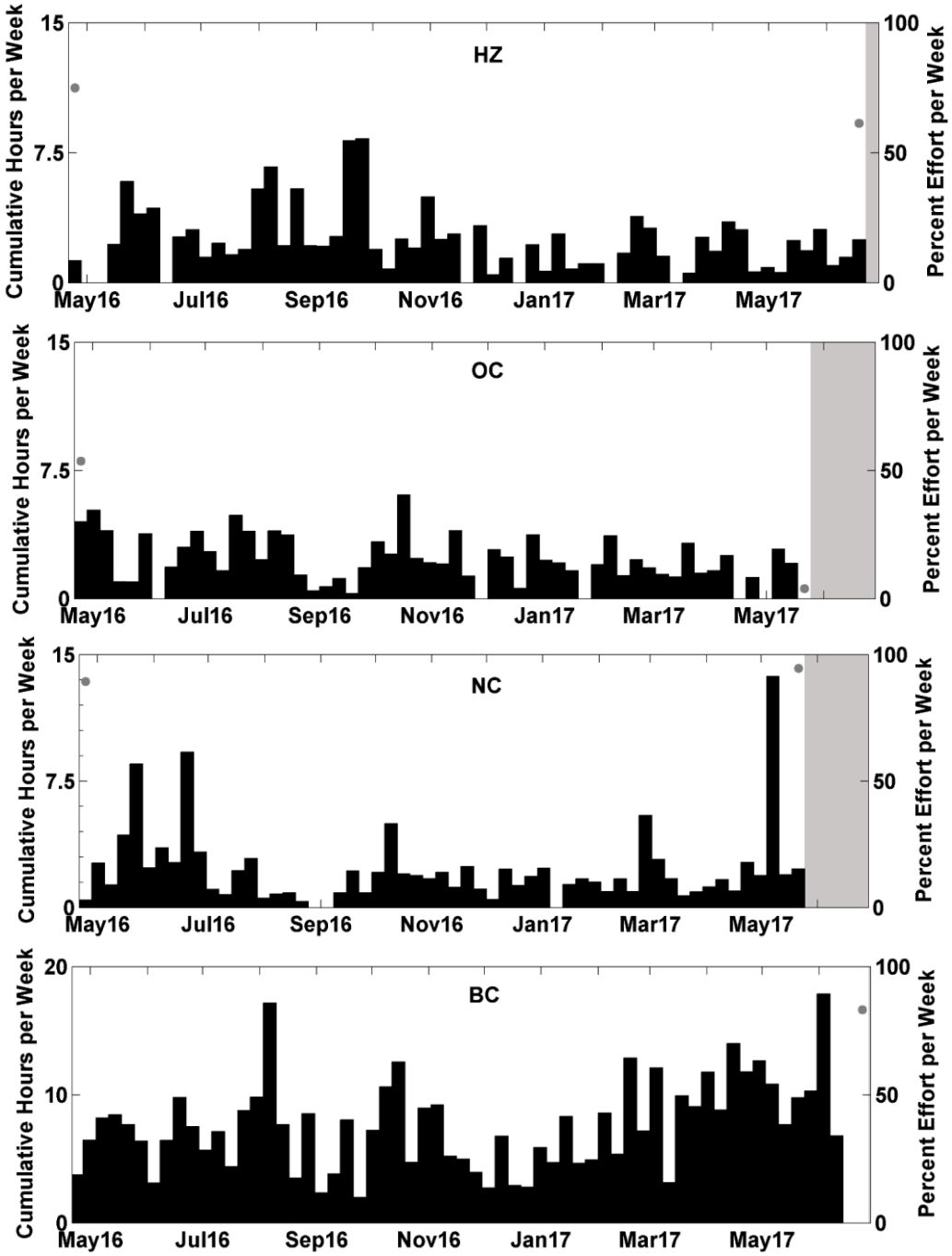

Figure 115. Weekly presence (black bars) of broadband ship sounds between April 2016 and June 2017 at sites HZ, OC, NC, and BC. Effort markings are described in Figure 47. ***Note: Axis change for site BC due to a higher amount of broadband ship detections compared to the rest of the sites.***

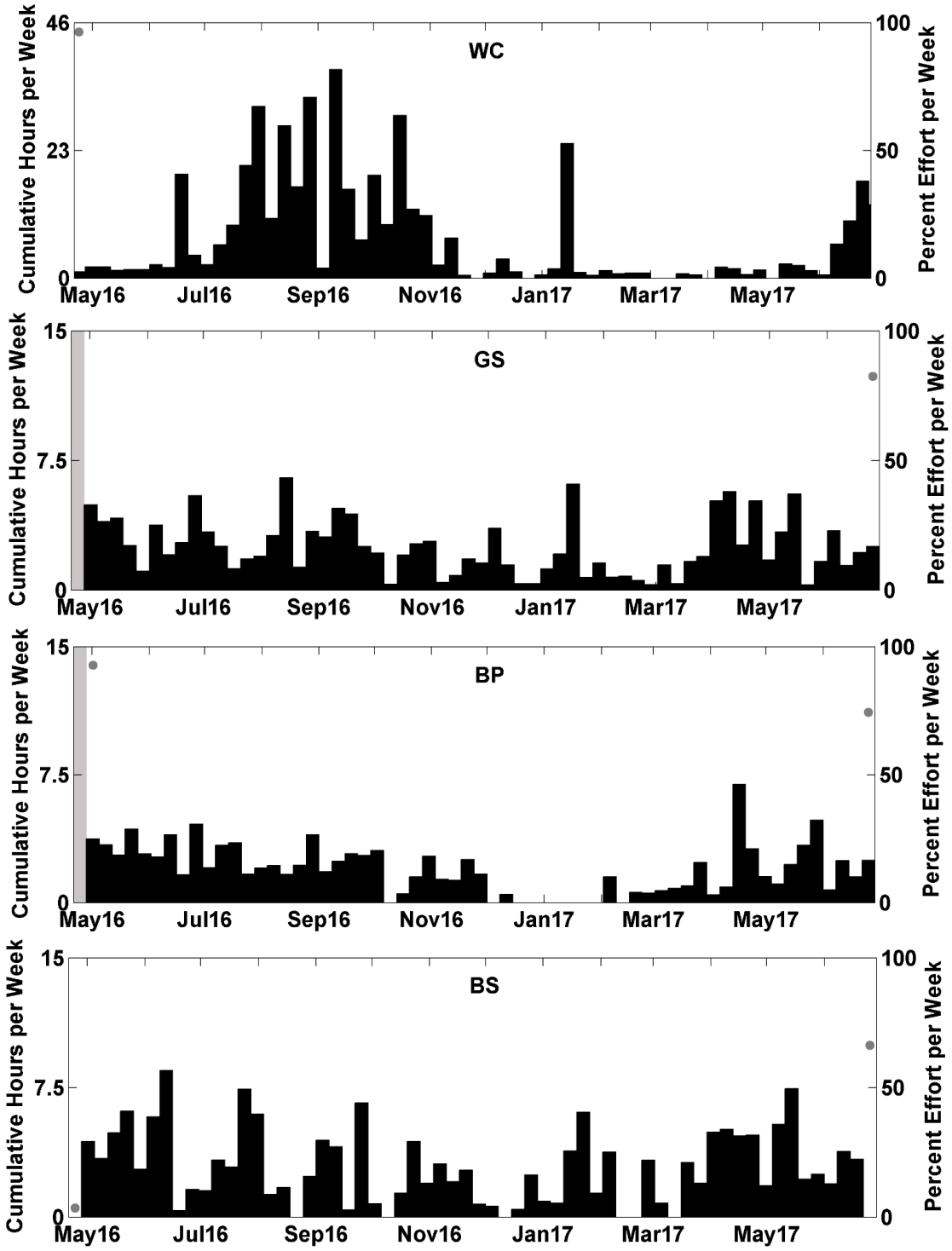

Figure 116. Weekly presence (black bars) of broadband ship sounds between April 2016 and June 2017 at sites WC, GS, BP, and BS. Effort markings are described in Figure 47. ***Note: Axis change for site WC due to a higher amount of broadband ship detections compared to the rest of the sites.***

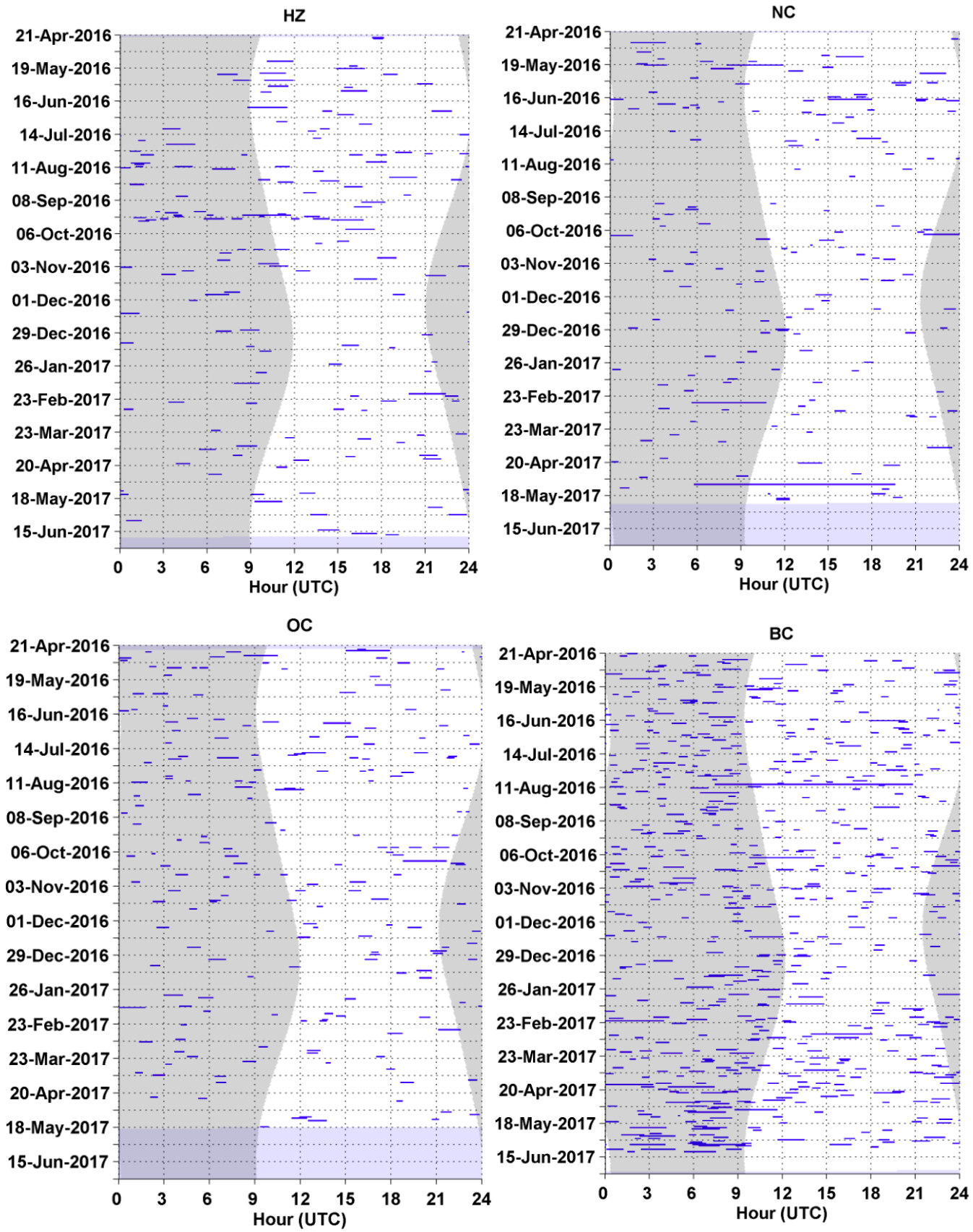

Figure 117. Broadband ship sounds in five-minute bins (blue bars) at sites HZ, OC, NC, and BC. Effort markings are described in Figure 49.

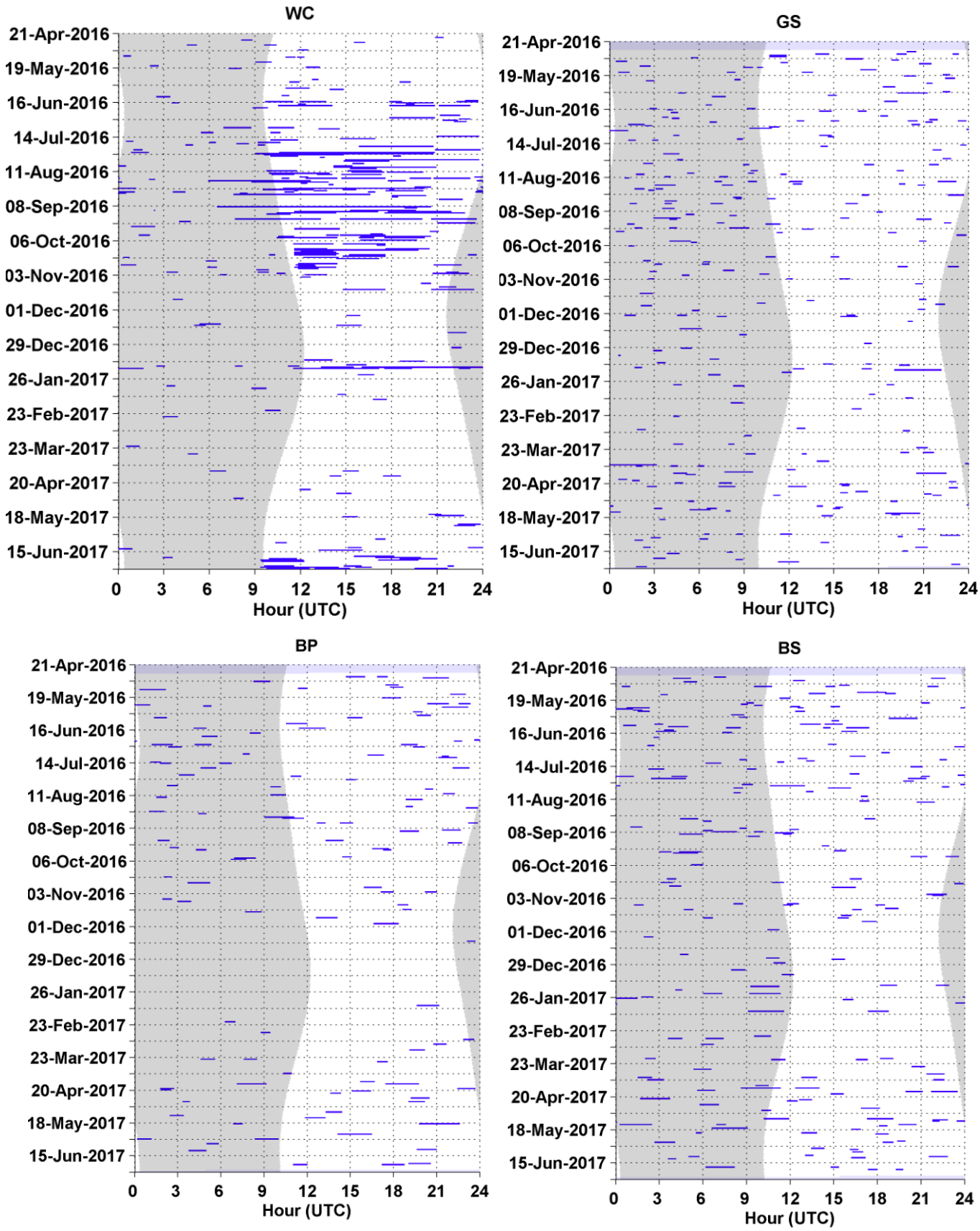

Figure 118. Broadband ship sounds in five-minute bins (blue bars) at sites WC, GS, BP, and BS. Effort markings are described in Figure 49.

Explosions

- There were explosions detected at four of the sites throughout the recording period (Figure 119). 34 explosions were detected between at site NC, six explosions were detected at site WC, six explosions were detected at site BC, and two explosions were detected at site BP.
- There were no detections at sites HZ, OC, BS, or GS (Figure 120).

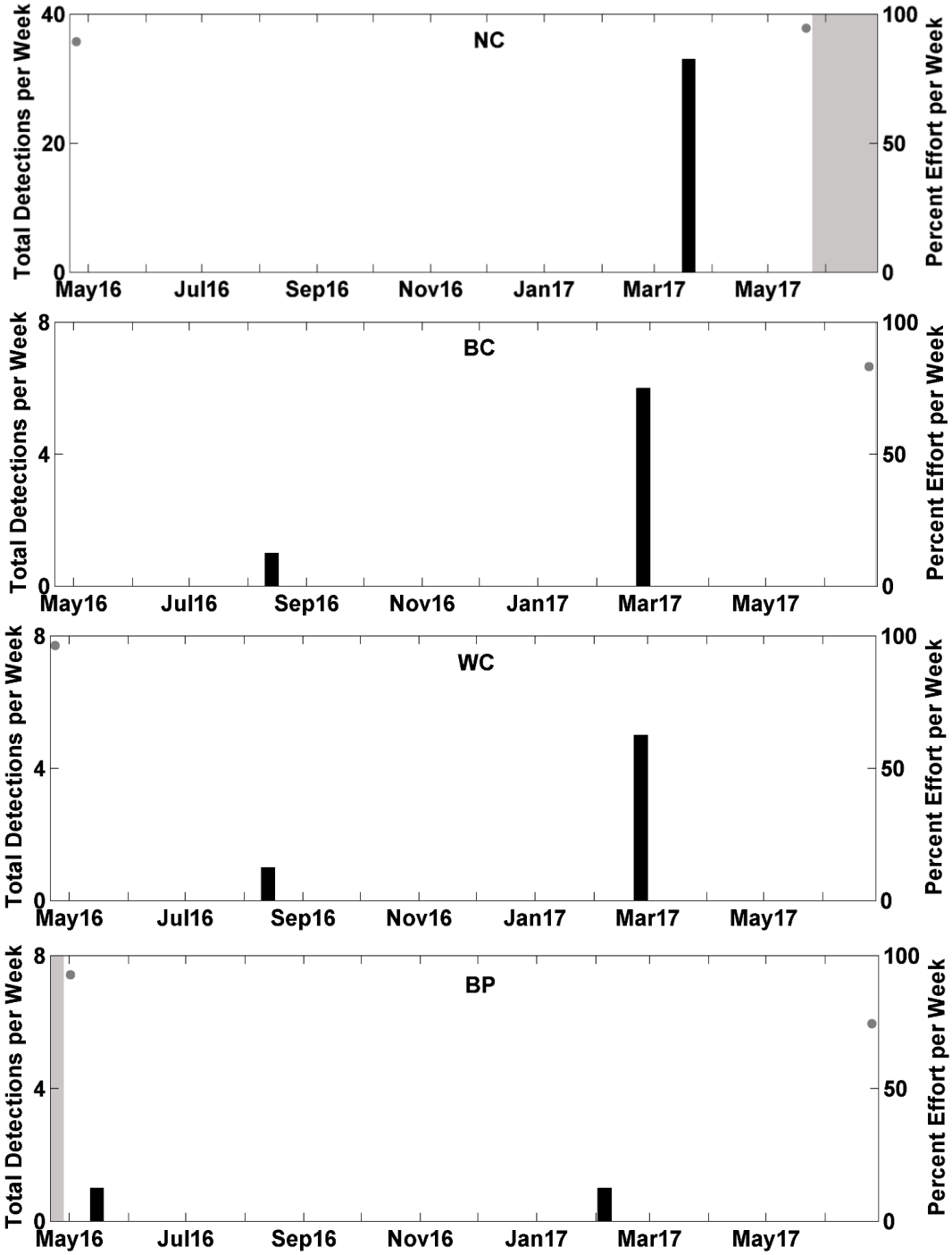

Figure 119. Weekly presence (black bars) of explosions between April 2016 and June 2017 at sites NC, BC, WC, and BP. Effort markings are described in Figure 47. ***Note: Axis change for site NC due to a higher amount of explosion detections compared to the rest of the sites.***

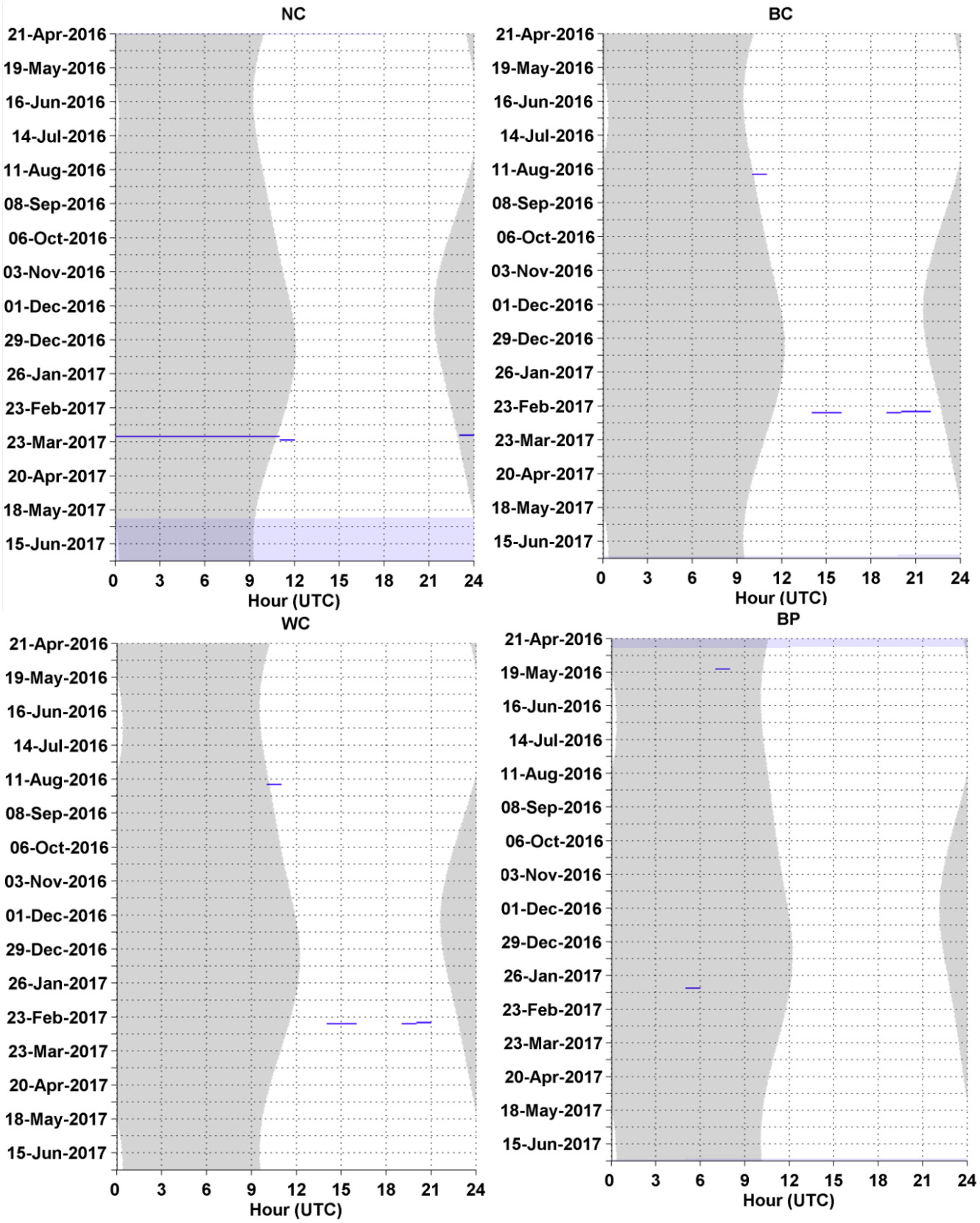

Figure 120. Explosion detections in five-minute bins (blue bars) at sites NC, BC, WC, and BP. Effort markings are described in Figure 49.

Airguns

- Airguns were detected at all eight of the sites over the recording period (Figure 121, Figure 122). At all eight sites, detections primarily occurred between April and September 2016 in high numbers. Site NC had detections intermittently throughout the recording period (Figure 121).
- There was no diel pattern for airgun detections at any of the eight sites.

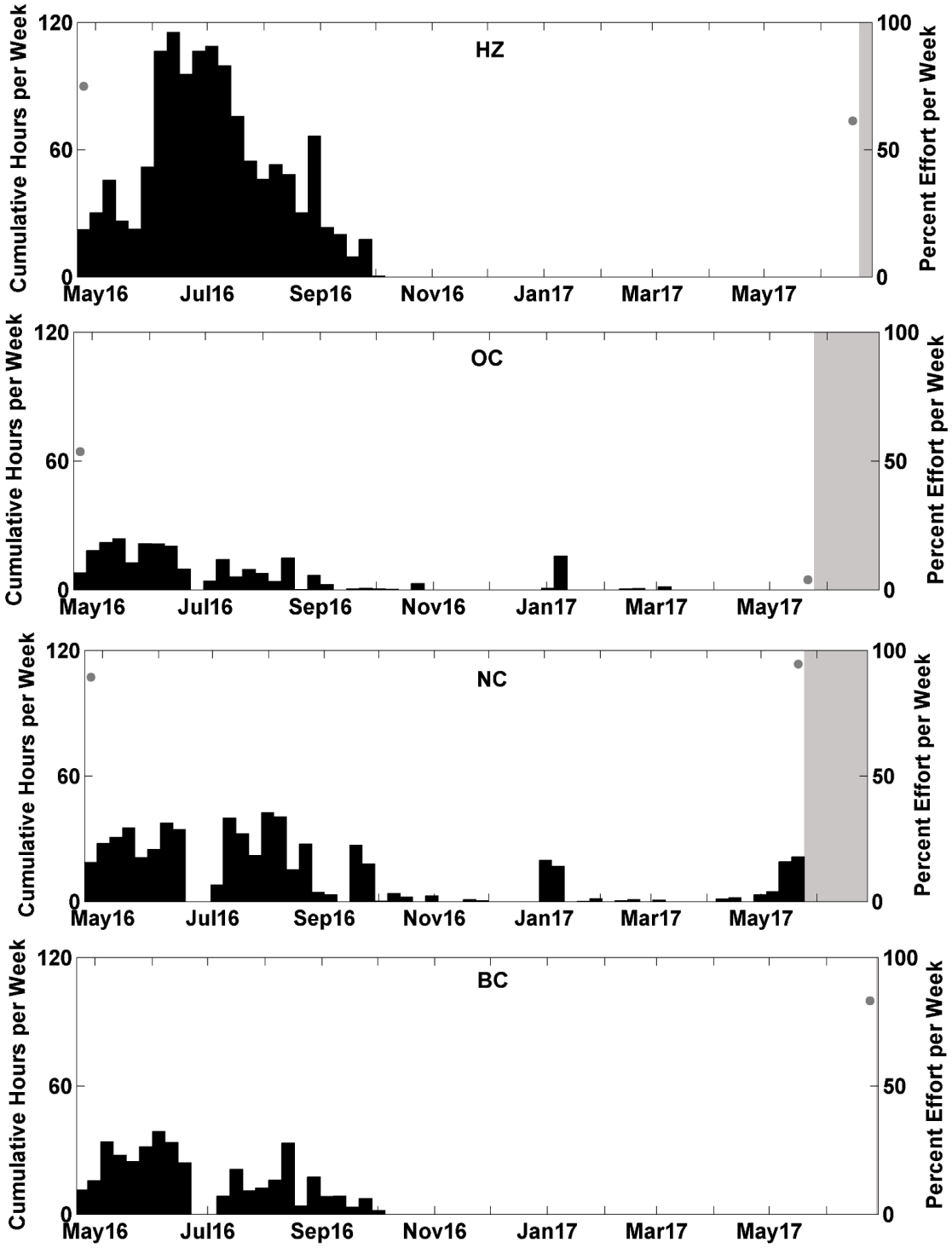

Figure 121. Weekly presence (black bars) of airguns between April 2016 and June 2017 at sites HZ, OC, NC, and BC. Effort markings are described in Figure 47.

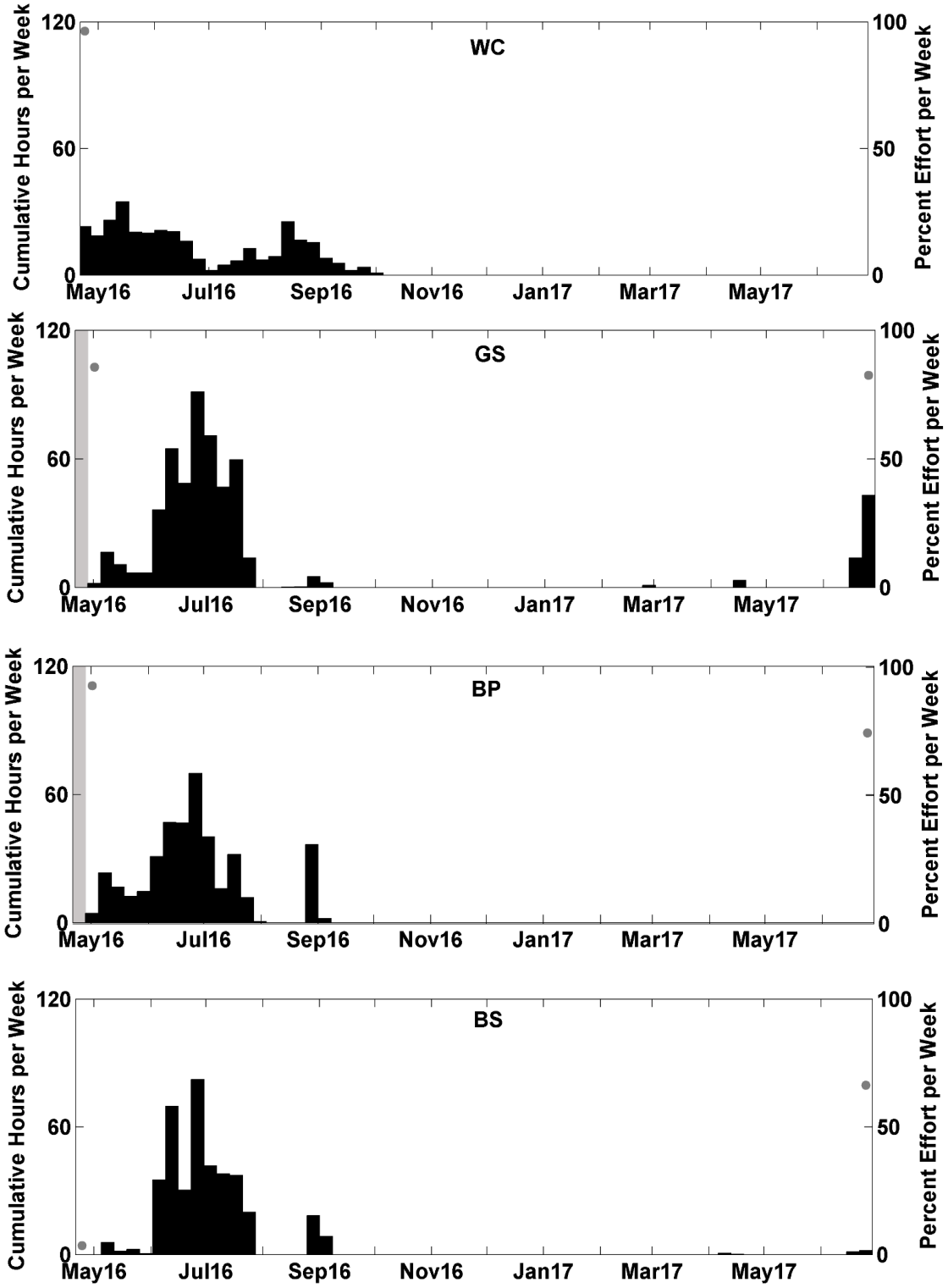

Figure 122. Weekly presence (black bars) of airguns between April 2016 and June 2017 at sites WC, GS, BP, and BS. Effort markings are described in Figure 47.

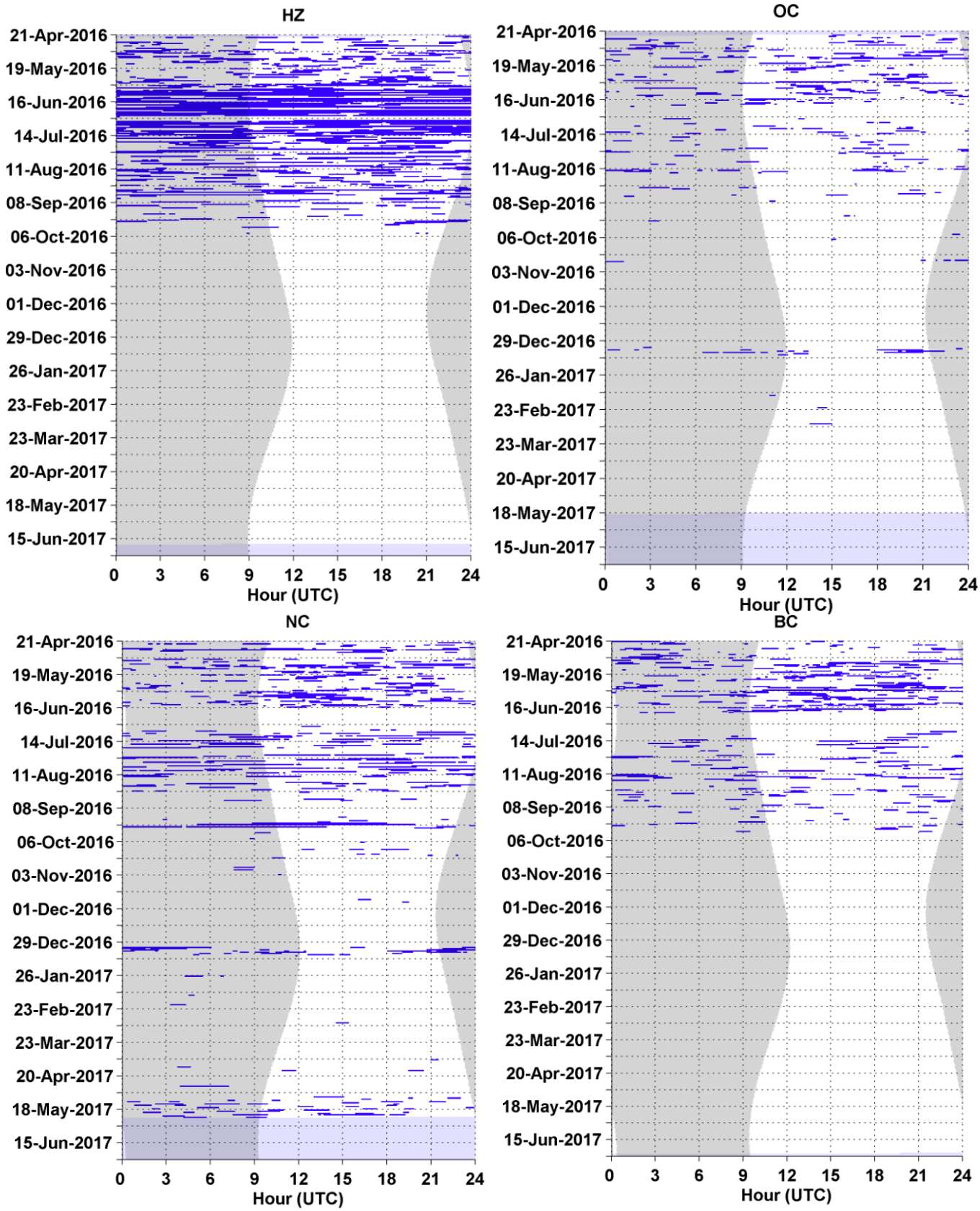

Figure 123. Airgun detections in five-minute bins (blue bars) at sites HZ, OC, NC, and BC. Effort markings are described in Figure 49.

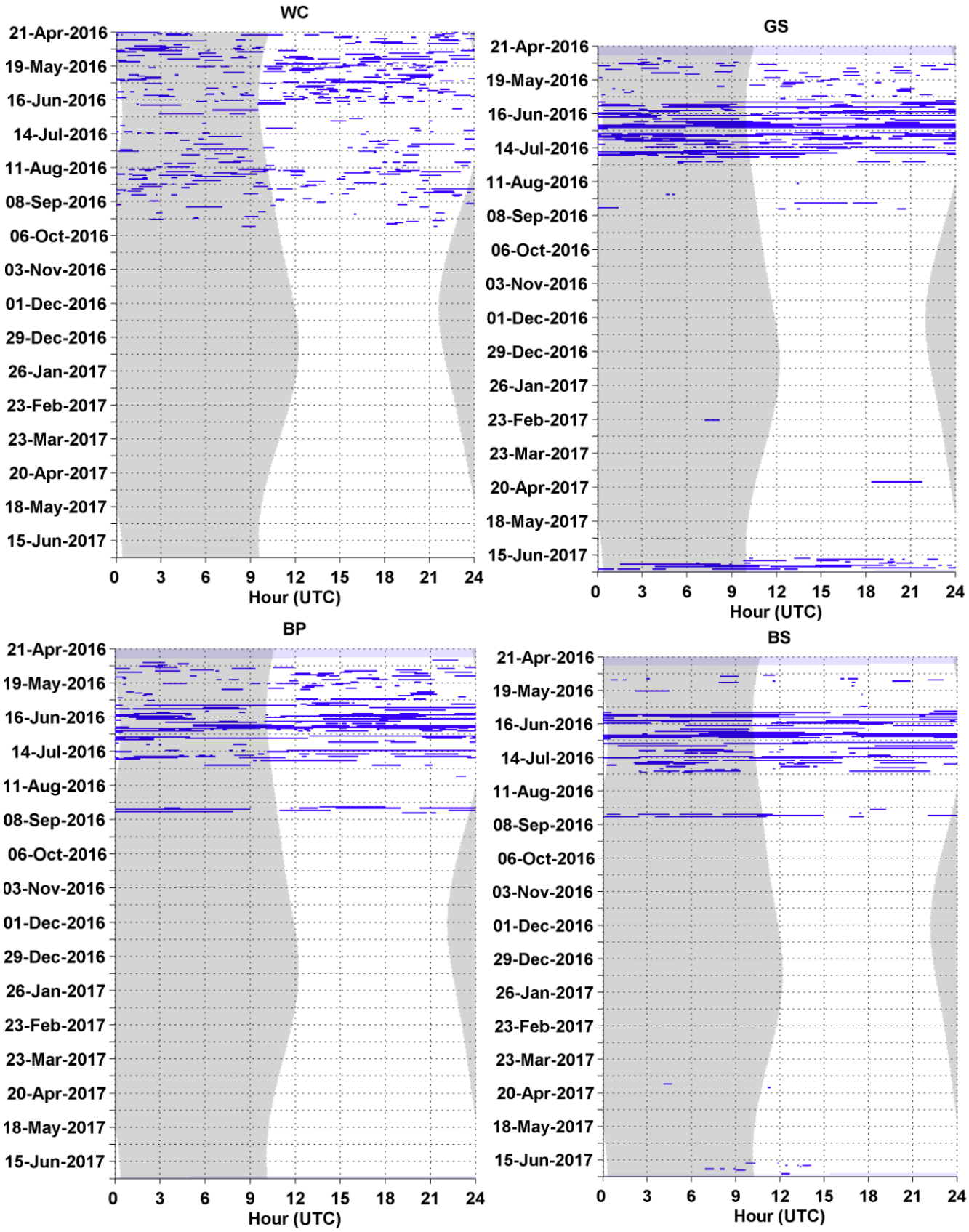

Figure 124. Airgun detections in five-minute bins (blue bars) at sites WC, GS, BP, and BS. Effort markings are described in Figure 49.

Echosounders

- Echosounders were detected sporadically at all eight sites (Figure 125, Figure 126).
- Site WC had the largest number of detections occurring from June to November 2016 (Figure 126).
- There was no diel pattern for echosounder detections (Figure 127,
- Figure 128).

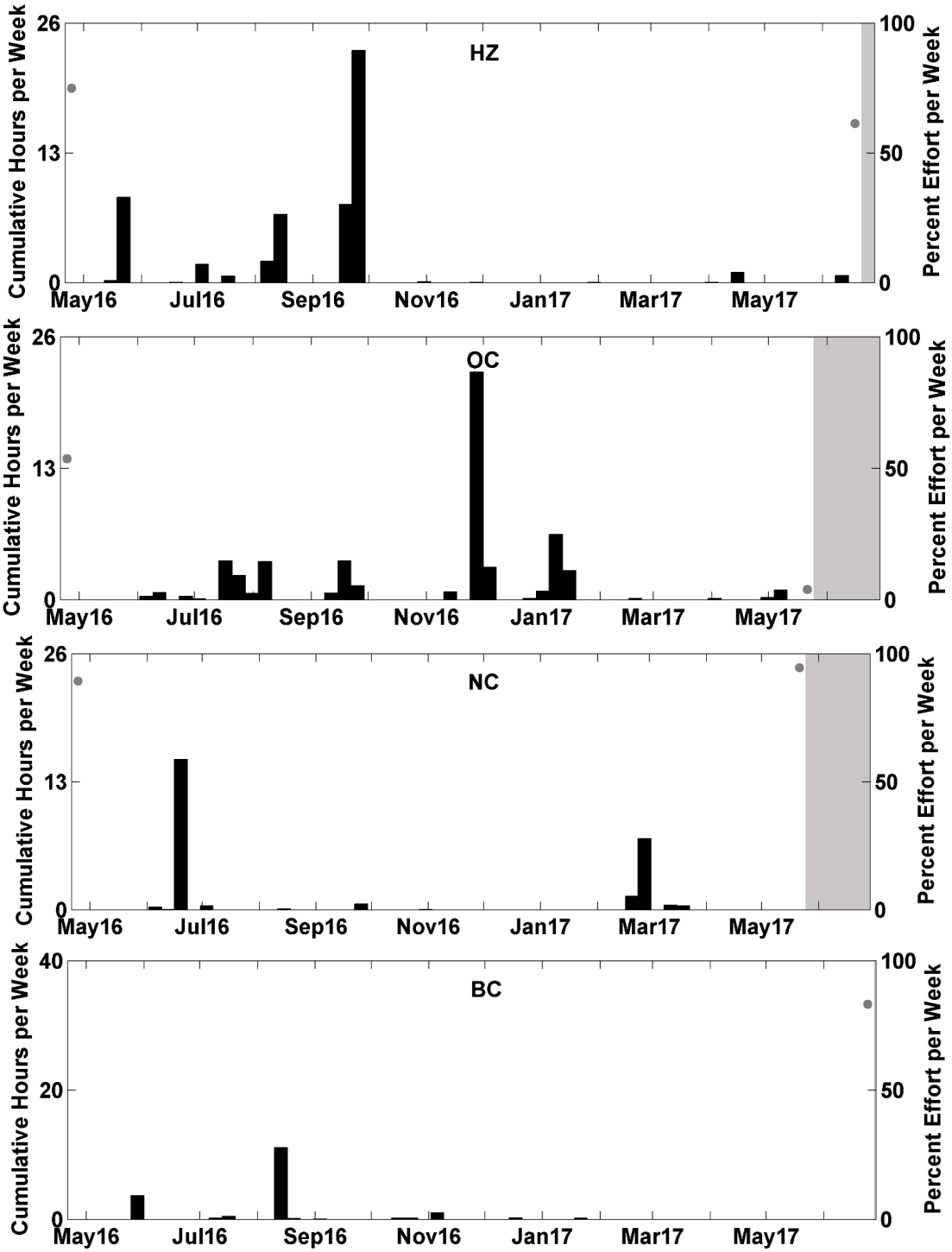

Figure 125. Weekly presence (black bars) of echosounders between April 2016 and June 2017 at site HZ, NC, OC, and BC. Effort markings are described in Figure 47. ***Note: Axis change for site BC due to a higher amount of echosounder detections compared to the rest of the sites*****.**

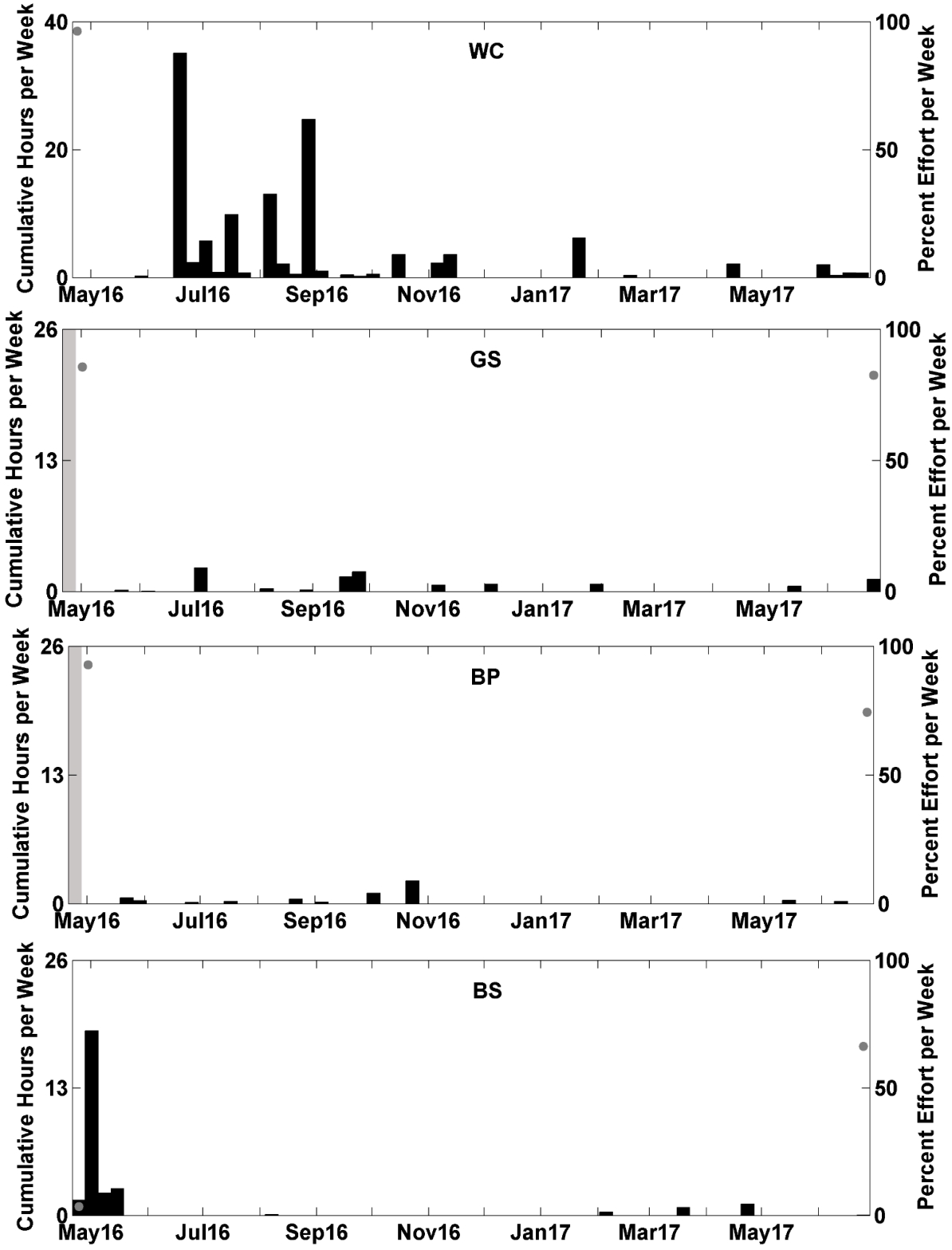

Figure 126. Weekly presence (black bars) of echosounders between April 2016 and June 2017 at site WC, GS, BP, and BS. Effort markings are described in Figure 47. ***Note: Axis change for site WC due to a higher amount of echosounder detections compared to the rest of the sites*****.**

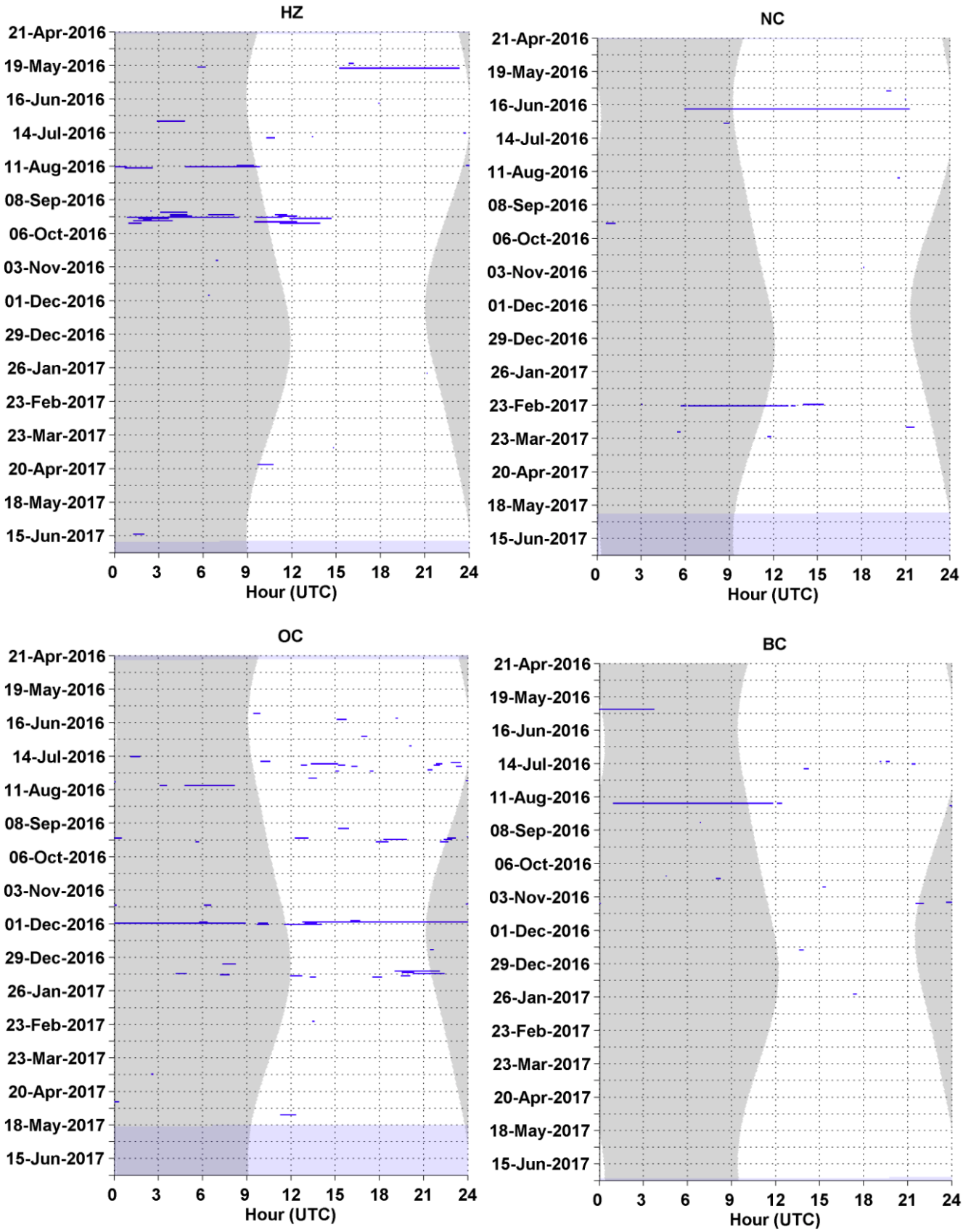

Figure 127. Echosounder detections in five-minute bins (blue bars) at sites HZ, OC, NC, and BC. Effort markings are described in Figure 49.

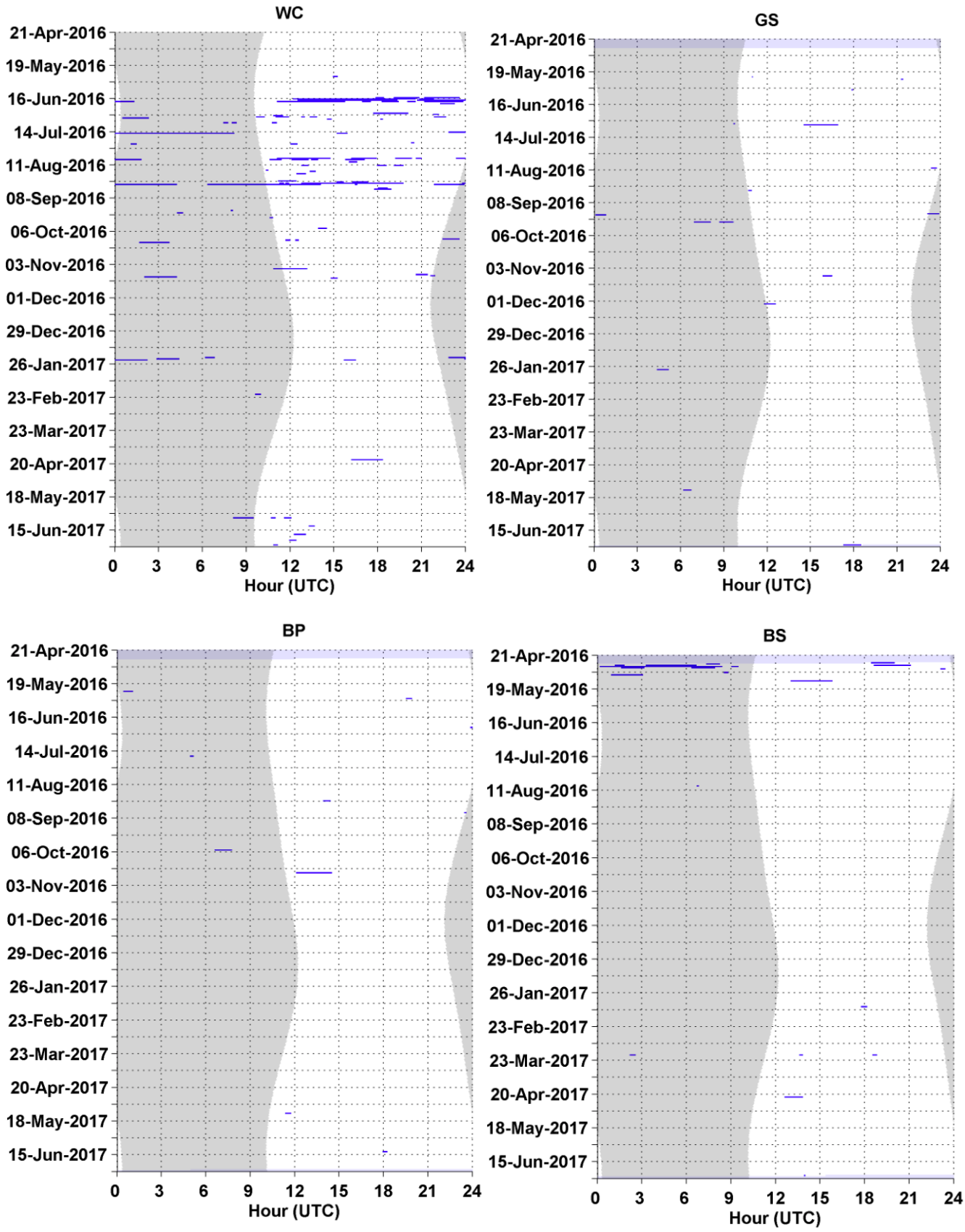

Figure 128. Echosounder detections in five-minute bins (blue bars) at sites WC, GS, BP, and BS. Effort markings are described in Figure 49.

References

Amundsen, L., and Landro, M. (**2010**). "Marine Seismic Sources, Part 1 - Air-guns for no experts," (Geo ExPro), pp. 32-34.

Au, W. W. L. (**1993**). *The Sonar of Dolphins* (Springer).

Barger, J. E., and Hamblen, W. R. (**1980**). "The air gun impulsive underwater transducer," The Journal of the Acoustical Society of America **68**, 1038-1045.

Baumann-Pickering, S., McDonald, M. A., Simonis, A. E., Berga, A. S., Merkens, K. P. B., Oleson, E. M., Roch, M. A., Wiggins, S. M., Rankin, S., Yack, T. M., and Hildebrand, J. A. (**2013**). "Species-specific beaked whale echolocation signals," The Journal of the Acoustical Society of America **134**, 2293-2301.

Baumann-Pickering, S., Roch, M. A., Brownell Jr, R. L., Simonis, A. E., McDonald, M. A., Solsona-Berga, A., Oleson, E. M., Wiggins, S. M., and Hildebrand, J. A. (**2014**). "Spatio Temporal Patterns of Beaked Whale Echolocation Signals in the North Pacific," PLOS ONE **9**, e86072.

Blackman, D. K., Groot-Hedlin, C. d., Harben, P., Sauter, A., and Orcutt, J. A. (**2004**). "Testing low/very low frequency acoustic sources for basin-wide propagation in the Indian Ocean," The Journal of the Acoustical Society of America **116**, 2057-2066.

Cholewiak, D., Baumann-Pickering, S., and Parijs, S. V. (**2013**). "Description of sounds associated with Sowerby's beaked whales (Mesoplodon bidens) in the western North Atlantic Ocean," The Journal of the Acoustical Society of America **134**, 3905-3912.

DeAngelis, A. I., Stanistreet, J., Baumann-Pickering, S., and Cholewiak, D. A description of echolocation clicks recorded in the presence of True's beaked whale (*Mesoplodon mirus*). JASA, *in review*.

Frasier, K. E. (**2015**). "Density estimation of delphinids using passive acoustics: A case study in the Gulf of Mexico," (University of California San Diego, Scripps Institution of Oceanography, La Jolla, CA, USA), p. 321.

Frasier, K. E., Roch, M. A., Soldevilla, M. S., Wiggins, S. M., Garrison, L. P., Hildebrand, J. A. (**2017**). Automated classification of dolphin echolocation click types from the Gulf of Mexico. PLOS Computational Biology **13**, e1005823.

Gillespie, D., Dunn, C., Gordon, J., Claridge, D., Embling, C., and Boyd, I. (**2009**). "Field recordings of Gervais' beaked whales *Mesoplodon europaeus* from the Bahamas," The Journal of the Acoustical Society of America **125**, 3428-3433.

Goold, J. C., and Jones, S. E. (**1995**). "Time and frequency domain characteristics of sperm whale clicks," The Journal of the Acoustical Society of America **98**, 1279-1291.

Hildebrand, J. A. (**2009**). "Anthropogenic and natural sources of ambient noise in the ocean," Marine Ecology Progress Series **395**, 5-20.

Johnson, M., Madsen, P. T., Zimmer, W. M. X., de Soto, N. A., and Tyack, P. L. (**2004**). "Beaked whales echolocate on prey," Proceedings of the Royal Society B: Biological Sciences **271**, S383-S386.

Johnson, M., Madsen, P. T., Zimmer, W. M. X., de Soto, N. A., and Tyack, P. L. (**2006**). "Foraging Blainville's beaked whales (*Mesoplodon densirostris*) produce distinct click types matched to different phases of echolocation," Journal of Experimental Biology **209**, 5038.

Madsen, P. T., Payne, R., Kristiansen, N. U., Wahlberg, M., Kerr, I., and Møhl, B. (**2002a**). "Sperm whale sound production studied with ultrasound time/depth-recording tags," Journal of Experimental Biology **205**, 1899.

Madsen, P. T., Wahlberg, M., and Møhl, B. (**2002b**). "Male sperm whale (*Physeter macrocephalus*) acoustics in a high-latitude habitat: implications for echolocation and communication," Behavioral Ecology and Sociobiology **53**, 31-41.

McKenna, M. F., Ross, D., Wiggins, S. M., and Hildebrand, J. A. (**2012**). "Underwater radiated noise from modern commercial ships," The Journal of the Acoustical Society of America **131**, 92-103.

Møhl, B., Wahlberg, M., Madsen, P. T., Heerfordt, A., and Lund, A. (**2003**). "The monopulsed nature of sperm whale clicks," The Journal of the Acoustical Society of America **114**, 1143 1154.

Roch, M. A., Klinck, H., Baumann-Pickering, S., Mellinger, D. K., Qui, S., Soldevilla, M. S., and Hildebrand, J. A. (**2011**). "Classification of echolocation clicks from odontocetes in the Southern California Bight," The Journal of the Acoustical Society of America **129**, 467 475.

Soldevilla, M. S., Henderson, E. E., Campbell, G. S., Wiggins, S. M., Hildebrand, J. A., and Roch, M. A. (**2008**). "Classification of Risso's and Pacific white-sided dolphins using spectral properties of echolocation clicks," The Journal of the Acoustical Society of America **124**, 609-624.

Soldevilla, M. S. Baumann-Pickering S, Cholewiak, D., Hodge, L. E. W., Oleson, E. M., Rankin, S. (**2017**). "Geographic variation in Risso's dolphin echolocation click spectra." The Journal of the Acoustical Society of America. **142**, 599-617.

Watkins, W. A., and Schevill, W. E. (**1977**). "Sperm whale codas," The Journal of the Acoustical Society of America **62**, 1485-1490.

Watwood, S. L., Miller, P. J. O., Johnson, M., Madsen, P. T., and Tyack, P. L. (**2006**). "Deep-diving foraging behaviour of sperm whales (Physeter macrocephalus)," Journal of Animal Ecology **75**, 814-825.

Wiggins, S. M., and Hildebrand, J. A. (**2007**). "High-frequency Acoustic Recording Package (HARP) for broad-band, long-term marine mammal monitoring," (IEEE, Tokyo, Japan, International Symposium on Underwater Technology and Workshop on Scientific Use of Submarine Cables and Related Technologies), pp. 551-557.

Zimmer, W. M. X., Johnson, M. P., Madsen, P. T., and Tyack, P. L. (**2005**). "Echolocation clicks of free-ranging Cuvier's beaked whales (*Ziphius cavirostris*)," The Journal of the Acoustical Society of America **117**, 3919-3927.